



**HAL**  
open science

# Nutrient input from seamounts and hydrothermal vents in the Southern Ocean: impacts on the pelagic ecosystems and implications for conservation

Sara Sergi

► **To cite this version:**

Sara Sergi. Nutrient input from seamounts and hydrothermal vents in the Southern Ocean: impacts on the pelagic ecosystems and implications for conservation. Oceanography. Sorbonne Université, 2021. English. NNT: 2021SORUS508 . tel-03719580

**HAL Id: tel-03719580**

**<https://theses.hal.science/tel-03719580v1>**

Submitted on 11 Jul 2022

**HAL** is a multi-disciplinary open access archive for the deposit and dissemination of scientific research documents, whether they are published or not. The documents may come from teaching and research institutions in France or abroad, or from public or private research centers.

L'archive ouverte pluridisciplinaire **HAL**, est destinée au dépôt et à la diffusion de documents scientifiques de niveau recherche, publiés ou non, émanant des établissements d'enseignement et de recherche français ou étrangers, des laboratoires publics ou privés.



**SORBONNE UNIVERSITY**

Laboratoire d'Océanographie et du Climat LOCEAN

ED129: Science de l'Environnement d'Ile de France

**Nutrient input from seamounts and hydrothermal vents in  
the Southern Ocean: impacts on the pelagic ecosystems and  
implications for conservation**

by

**Sara SERGI**

PhD thesis in Meteorology, Physical Oceanography and Environmental Physics

Under the supervision of Francesco D'OVIDIO

Presented and publicly defended on 27th, September 2021.

**Jury:**

<b>Pascale BOURET-AUBERTOT</b>	Professeur LOCEAN/Sorbonne Université	President
<b>Andrea DOGLIOLI</b>	Maître de Conférences MIO/Université Aix-Marseille	Reviewer
<b>Hélène PLANQUETTE</b>	Directrice de recherche CNRS LEMAR/Université Bretagne Occidentale	Reviewer
<b>Marc ELEAUME</b>	Maître de Conférences ISYEB/MNHN	Examiner
<b>Sara LABROUSSE</b>	Chargée de recherche CNRS LOCEAN/Sorbonne Université	Examiner
<b>Francesco D'OVIDIO</b>	Directeur de recherche CNRS LOCEAN/Sorbonne Université	Supervisor







*Ancora un'alba sul mondo:  
altra luce, un giorno  
mai vissuto da nessuno,  
ancora qualcuno è nato:  
con occhi e mani  
e sorride.*

D. M. Turollo



# *Abstract*

Bottom-up forces control a large fraction of marine ecosystem variability. In the Southern Ocean, iron limitation generates intense contrasts in the biological productivity affecting the distribution of pelagic ecosystems. In particular, the iron input close to islands and continental shelves fuels phytoplankton blooms stretching for hundreds of kilometres along the intense Antarctic Circumpolar Current and sustaining large trophic chains. In recent years, the role of deep nutrient sources in biogeochemical cycles, such as hydrothermal iron, and the intensity of vertical connectivity pathways in the off-shore Southern Ocean have been reconsidered. However, the biological impact of such deep nutrient sources on the pelagic production have not been evaluated yet (e.g. hydrothermal iron) or their contribution appears to be negligible (e.g. seamounts). As a consequence, the waters of the Antarctic Circumpolar Currents are often described as a high nutrient low phytoplankton desert, punctuated by massive blooms in the wake of islands. Conservation efforts are in line with this description, with subantarctic Marine Protected Areas only occurring around islands. Two questions are then addressed in this thesis. The first one investigates the ecological role of deep bottom-up processes and their influence on open ocean trophic hotspots. The second one evaluates how the analysis of deep bottom-up forcings on pelagic ecosystems can be used to inform marine conservation policies.

The first question is addressed under the lens of the structuring effect of the Antarctic Circumpolar Current on the pelagic ecosystems. The Lagrangian analysis of geostrophic currents is used for reproducing the surface expression of phytoplankton biomasses in the off-shore Southern Ocean driven by previously unknown deep iron supplies. Firstly, two studies present the first observational evidences of hydrothermal iron impact on surface primary production in the iron-depleted Southern Ocean. Intense biological responses are observed with *in-situ* profiling floats (maximum depth-integrated biomass superior to  $80 \text{ mgChla.m}^{-2}$ ) and satellite-derived estimations of Net Primary Production (up to  $\text{gC.m}^{-2}.\text{yr}^{-1}$ ). My specific contribution in these studies was to connect the intense phytoplankton signals to hydrothermal iron with a Lagrangian analysis of the altimetry-derived geostrophic fields.

Secondly, I revisited the ecological role of seamounts by studying a region consistently targeted by multiple predators even though no significant iron input seems to fertilize it.

By combining high resolution bathymetric data, multi-satellite data, Lagrangian analyses of the velocity field and Biogeochemical Argo floats, this study identifies phytoplankton blooms associated to the water masses that transited over topographic highs and spreading over huge distances, similarly to islands' blooms. Despite its moderate intensity, this phytoplankton production appears to provide a similar ecological function of the biologically-rich islands' systems. The presence of foraging grounds for megafauna species, inferred by animal tracking data, is supported by the satellite-based evaluation of phytoplankton dominant communities which are more likely to support pelagic ecosystems that include large predators.

In the second part of the thesis, I analyse how the analysis of deep bottom-up forcings on pelagic ecosystems can be used to inform marine conservation policies. In this aim I firstly evaluate the inclusion of bottom-up processes studied in the first part of the thesis in the conservation strategy established by the Convention for the Conservation of Antarctic Marine Living Resources, an international body responsible for the management of the marine ecosystems in the international seas of the Southern Ocean. The literature review highlights the need to include analyses of biophysical mechanisms unravelled by circulation connectivity patterns at regional scale for developing a Marine Protected Areas' system representative of habitats, species and ecosystems' processes.

Secondly, I provide a more comprehensive study case of the scientific contribution to a conservation policy: the extension of the French National Natural Reserve of Saint-Paul and Amsterdam Islands. This region hosts several seabirds and marine mammal colonies and is targeted by numerous migratory species. However, the productivity at the basis of the pelagic food-web and its drivers have been little investigated. In this thesis, I address this pelagic knowledge gap by evaluating the variability patterns of phytoplankton biomass in this region and their biophysical drivers. These analyses and the subsequential identification of bioregions structuring the distributions of different compartments of the trophic chain are official contributions to the scientific basis supporting the project of extension of the National Natural Reserve of the Southern French Territories.

The findings of this thesis highlight bottom-up controls driven by deep nutrient sources and shaping the pelagic seascape at large scales ( $O(10^3 \text{ km})$ ) in the off-shore Southern Ocean. Understanding of physical drivers of pelagic ecosystems is an important way forward to address future vulnerabilities of ecosystems under climate changes' threats.

On the other side management frameworks require to develop instruments and practices able to integrate climate change information in all the steps of conservation actions and confirm the political commitments showed in international conservation targets (e.g., High Ambition Coalition for Nature and People). This shall apply both to existing and future management frameworks, such the one that will be implemented after the Implementing Agreement on Biodiversity Beyond National Jurisdiction.

## *Résumé détaillé en français*

Les processus bottom-up contrôlent une portion importante de la variabilité des écosystèmes marins. Dans l’océan Austral, la carence en fer limite la croissance phytoplanctonique et génère des contrastes intenses en production primaire, ce qui affecte la distribution des écosystèmes pélagiques. En particulier, les apports en fer émanant des îles et des plateaux continentaux alimentent des blooms phytoplanctoniques intenses. Ceux-ci s’étendent en aval des reliefs topographiques sur des centaines de kilomètres le long du Courant Circumpolaire Antarctique et entretiennent des vastes réseaux trophiques.

Dans les dernières années, le rôle des sources profondes en éléments nutritifs, tels le fer hydrothermal, dans les cycles biogéochimiques et l’intensité des mécanismes de connexion verticale près des reliefs sous-marins de l’océan hauturier ont été examinés. Cependant, l’effet de ces apports profonds en fer sur la production pélagique n’a toujours pas été observé (e.g., fer hydrothermal) et ses apports ont été considérés comme négligeables (e.g., monts sous-marins). Les eaux du Courant Circumpolaire Antarctique sont de ce fait souvent décrites comme un milieu “désertique” du point de vue biologique, riche en macronutriments (nitrate, phosphate et silicate) et appauvri en chlorophylle-*a*, marqué par des blooms phytoplanctoniques massifs en aval des îles. Les programmes de conservation vont de pair avec cette description, avec des Aires Marines Protégées subantarctiques définies autour des îles. Cette thèse traite donc deux sujets. Premièrement, elle explore le rôle écologique des processus bottom-up liés aux apports profonds en fer et leur influence sur les hotspots trophiques dans l’océan hauturier. Deuxièmement, elle examine comment l’étude des forçages profonds bottom-up sur les écosystèmes pélagiques peut contribuer aux politiques de conservation des ressources marines. Ces deux questions sont traitées dans deux Parties distinctes de la thèse (respectivement II et III), chacune constituée de deux Chapitres et chacun portant sur une ou deux études différentes.

Afin de répondre à ces objectifs, cette thèse considère des outils d’observation couvrant un large spectre d’échelles spatiales et temporelles. Les informations sur l’écosystème pélagique sont obtenues à partir d’observations *in-situ* et satellites de la biomasse phytoplanctonique ainsi que des estimations des communautés phytoplanctoniques dominantes obtenues par satellite. À ceci s’ajoutent les observations issues de la télémétrie animale, qui permettent d’identifier les habitats pélagiques ciblés par les grands prédateurs à grande

échelle. Ces informations biologiques sont contextualisées à partir des données environnementales satellites et des modèles numériques. Le rôle clé du transport horizontal sur le paysage pélagique est considéré à travers l'analyse des champs de vitesses géostrophiques obtenus par altimétrie satellite. Le cadre d'analyse Lagrangien est ainsi appliqué aux courants géostrophiques pour reproduire l'expression de surface des biomasses phytoplanktoniques dans l'océan Austral hauturier. Par analogie à l'étude des blooms phytoplanktoniques en aval des îles, ces méthodes d'analyse reproduisent l'advection de nutriments en aval de leur sources et évaluent ainsi leur éventuel effet biologique. En particulier, les études développées ciblent des signaux biologiques qui ne peuvent pas être expliqués par les apports en fer connus. Ces outils d'analyse, décrits en détail dans la Partie I, sont ainsi employés afin de répondre à la première question de thèse: *Quel est le rôle écologique des apports de nutriments profonds et comment ceux-ci influencent le paysage pélagique dans l'océan Austral ?*

Au cours des dernières années, l'apport du fer hydrothermal au stock océanique de fer a été considérablement ré-évalué, en particulier dans l'océan Austral. Cela fait suite aux découvertes scientifiques effectuées le long trois axes de recherche. Tout d'abord, la modélisation a permis de démontrer que les observations en fer dissous dans l'océan Austral ne peuvent être répliquées dans des simulations que lorsque les sources hydrothermales y sont incluses [Tagliabue et al., 2010]. Deuxièmement, des observations ont mis en évidence la stabilisation des panaches de fer hydrothermal sur de grandes distances (milliers de kilomètres) dans plusieurs bassins océaniques [Bennett et al., 2008; Tagliabue et al., 2010; Wu et al., 2011; Resing et al., 2015; Fitzsimmons et al., 2017; Tagliabue and Resing, 2016]. Enfin, ces découvertes sont corroborées par les progrès récents de la biogéochimie océanique démontrant la complexation et la stabilisation du fer d'origine hydrothermale dans la colonne d'eau [Sander and Koschinsky, 2011; Bennett et al., 2008; Yücel et al., 2011]. Par conséquent, le rôle du fer hydrothermal dans l'activité biologique est soupçonné d'être largement sous-estimé, en particulier dans l'océan Austral, fortement limité en fer [Tagliabue et al., 2010].

Le premier Chapitre de la Partie II comprend deux études évaluant de l'effet du fer d'origine hydrothermale sur la production primaire de surface dans l'océan Austral à partir d'observations. Ces études portent sur deux blooms, l'un situé en aval de vents hydrothermaux de la dorsale sud-ouest indienne, et l'autre près des vents hydrothermaux



de la dorsale australo-antarctique. Dans ces deux zones, des réponses biologiques intenses sont observées par estimation de la Production Primaire Nette à partir d'observations satellites (jusqu'à  $\text{gC}\cdot\text{m}^{-2}\cdot\text{yr}^{-1}$ ) et/ou par flotteurs *in-situ* (biomasse maximale intégrée sur la couche de mélange supérieure à  $80 \text{ mgChla}\cdot\text{m}^{-2}$ ). La présence de fer, potentiellement d'origine hydrothermale, est corroborée par les distributions historiques de  $\delta^3\text{He}$ , un traceur conservatif du fer hydrothermal, et par la présence de masses d'eaux enrichies en fer dissous sur l'ensemble de la colonne d'eau soujacent le bloom phytoplanctonique. Les remontées verticales des isolignes de densité, les valeurs intenses en énergie cinétique turbulente profonde, ainsi les valeurs de diffusivité verticale accrues, corroborent la présence de mécanismes verticaux permettant d'introduire le fer profond dans la couche océanique de surface. Dans les deux études, j'ai adopté une analyse Lagrangienne des champs de vitesses géostrophiques dérivés par altimétrie afin d'évaluer si la présence des vents hydrothermaux pouvait expliquer les biomasses phytoplanctoniques observées. Ces analyses ont permis de relier les intenses signaux phytoplanctoniques soit aux eaux profondes influencées par le fer hydrothermal (étude parue dans [Ardyna et al. \[2019\]](#)), soit directement au vents hydrothermaux (étude parue dans [Schine et al. \[2021\]](#)).

À notre connaissance, les études présentées dans ce chapitre de thèse sont les premières observations de connexions directes entre le fer hydrothermal et la production primaire de surface. Ces observations ouvrent des perspectives importantes tant pour notre compréhension de la pompe biologique du carbone que pour des questions écologiques. Par exemple, la campagne océanographique Phantastic I a mesuré un flux moyen de  $\text{CO}_2$  air-mer de  $-32 \text{ mmol}\cdot\text{m}^{-2}\cdot\text{d}^{-1}$  dans le bloom phytoplanctonique associé à la dorsale australo-antarctique [[Schine et al., 2021](#)]. Ce flux est trois fois supérieur au flux maximal de  $\text{CO}_2$  air-mer mesuré dans le bloom de Kerguelen [[Merlivat et al., 2015](#)]. Par ailleurs, les blooms phytoplanctoniques ici étudiés se situent dans des régions identifiées comme importantes pour les grands prédateurs (oiseaux de mer et mammifères marins) [par exemple voir [Nel et al., 2001](#); [Andrews-Goff et al., 2018](#), pour les régions ciblées dans le secteur indien et pacifique, respectivement]. Le fer hydrothermal apparaît donc comme une nouvelle source de fer pour l'océan de surface qui façonne le paysage marin pélagique de l'océan Austral.

Alors que le premier Chapitre de thèse s'intéresse à des blooms phytoplanctoniques intenses inexpliqués par les apports en fer connus dans l'océan Austral et évalue leurs possibles origines, le deuxième Chapitre de la Partie II de la thèse s'intéresse, lui, à des

niveaux trophiques supérieurs. Les grands prédateurs pélagiques sont largement utilisés par les écologistes comme indicateurs biologiques dans l’océan ouvert. En effet, les régions ciblées par plusieurs espèces de prédateurs peuvent être indicatives de la présence élevée de biomasse et de biodiversité des niveaux trophiques inférieurs [Thiers et al., 2017; Lascelles et al., 2012; Hindell et al., 2020]. L’étude contenue dans ce chapitre considère une région éloignée des îles mais identifiée comme hotspot pélagique par les suivis télémétriques de cinq espèces de prédateurs supérieurs (phoques et manchots) observés entre 2003 et 2014 à partir des îles sud-africaines du Prince-Édouard. Les individus de ces cinq colonies ciblent en effet une région éloignée des apports majeurs en fer (atmosphérique, continental, hydrothermal ou par la fonte des glaces) mais en aval de nombreux monts sous-marins. Ces reliefs topographiques sont connus pour induire une augmentation de la biomasse phytoplanctonique, y compris dans l’océan Austral [Sokolov and Rintoul, 2007]; cependant aucun effet de ces reliefs sur l’activité primaire de surface n’a été détecté dans la région d’étude jusqu’à présent [Graham et al., 2015; Ardyna et al., 2017].

L’étude contenue dans le deuxième chapitre de la Partie II ré-évalue deux conclusions héritées des travaux du passé. Il s’agit de l’apparente nature oligotrophe de la région d’étude et du rôle du mont sous-marin dans le maintien de sa productivité. L’approche adoptée présente deux nouveautés principales : (1) l’utilisation d’une base de données récente à haute résolution répertoriant les monts sous-marins, (2) l’adoption d’une perspective écologique, différemment à la perspective biogéochimique adoptée dans Graham et al. [2015] et Ardyna et al. [2017]. Cette perspective écologique nous amène à considérer des échelles spatiales et temporelles plus réduites par rapport aux échelles circumpolaires et climatologiques considérées par le passé.

L’apparente nature oligotrophe de la zone d’étude, considérée dans les cartes climatologiques à faible teneur en chlorophylle *a*, est ainsi ré-évaluée dans ces travaux. Tout d’abord deux flotteurs Biogeochemical-Argo montrent une augmentation en chlorophylle *a* et rétrodiffusion en aval des monts sous-marins (environ  $1 \text{ mg/m}^3$  et  $3.0 \cdot 10^{-3} \text{ m}^{-1}$  respectivement) comparé aux masses d’eaux en amont de ceux-ci (environ  $0.6 \text{ mg/m}^3$  et  $2.0 \cdot 10^{-3} \text{ m}^{-1}$  respectivement). Par ailleurs, des efflorescences de phytoplancton (chlorophylle *a* supérieure à  $0,6 \text{ mg.m}^{-3}$ , le double des eaux environnantes) s’étendant sur des milliers de kilomètres en aval des monts sous-marins sont identifiées dans les cartes mensuelles de couleur de l’eau. En adoptant une approche Lagrangienne, l’analyse démontre que ces

efflorescences modérées ont pour origine des sites spécifiques où le Courant Circumpolaire Antarctique interagit avec les monts sous-marins. Ces résultats ouvrent des nouvelles perspectives sur l'effet biologique des monts sous-marins dans l'océan Austral, qui était auparavant considéré comme négligeable [Graham et al., 2015; Ardyna et al., 2017] ou très localisé [Oliveira et al., 2016; Lemos et al., 2018].

Malgré sa faible intensité, l'étude soutient que la production biologique provenant des monts sous-marins assure la même fonction écologique que les systèmes insulaires riches en biodiversité. Ceci est soutenu par : (1) la grande étendue spatiale des efflorescences phytoplanctoniques détectées dans les cartes de couleur de l'eau (des milliers de kilomètres de large) et (2) leur similitude avec les efflorescences des îles de l'océan Austral en termes de communautés phytoplanctoniques dominantes, estimées à partir d'analyses spectrales par satellite, qui sont plus susceptibles de soutenir des vastes réseaux trophiques se développant jusqu'aux grands prédateurs [Cushing, 1989; Moline et al., 2004; Pakhomov et al., 2019].

Davantage de recherches sont nécessaires pour élucider les mécanismes dynamiques qui contrôlent les processus bottom-up reliant l'océan profond à la couche de surface. Néanmoins, les résultats contenus dans cette thèse renforcent d'ores et déjà la nécessité de considérer la continuité de la zone du Courant Circumpolaire Antarctique et de ses processus biophysiques, tant sur le plan scientifique que sur celui de la conservation. Or, les politiques de conservation dans la zone du Courant Circumpolaire Antarctique, i.e. l'océan Austral loin des glaces, sont aujourd'hui dominées par les programmes nationaux, et présentent par conséquent des discontinuités importantes dues aux cadres juridiques (par exemple aux zones économiques exclusives). Par conséquent, la Partie III de cette thèse vise à répondre à la question suivante : *Comment l'étude des forçages profonds sur les écosystèmes pélagiques peut-elle contribuer aux politiques de conservation dans la zone d'étude ?*

La conservation des ressources marines vivantes dans l'océan Austral est sous la responsabilité de plusieurs États ayant des territoires d'outre-mer dans ces eaux (les îles sous la juridiction nationale du Royaume-Uni, de la Norvège, de l'Afrique du Sud, de la France ou de l'Australie) et un organisme international, la Convention pour la Conservation de la Flore et la Faune Marine Antarctiques (CCAMLR). Dans les différents systèmes, la conservation et la gestion des ressources vivantes ont lieu sur la base d'avis scientifiques. Cependant, les politiques de conservation peuvent adopter différentes formes, tout comme

les contributions scientifiques qui leur sont apportées. La deuxième partie de la thèse étudie ainsi les similitudes et différences de l'approche de conservation et plus en particulier, de la contribution scientifique à de telles politiques, adoptées dans le cadre de la CCAMLR et dans les cadres des Terres Australes Françaises (i.e. dans les eaux d'outre mer Françaises de l'océan Austral).

Les analyses contenues dans la Partie II de cette thèse mettent en évidence la présence d'habitats importants pour les écosystèmes pélagiques dans la région du Courant Circumpolaire Antarctique et apportent une nouvelle compréhension des forçages biophysiques à la base de ces écosystèmes. Ces hotspots biologiques se situent loin des îles et de leurs espaces maritimes nationaux, les seuls actuellement couverts par des Aires Marines Protégées dans cette région océanique. Par conséquent, le Chapitre 1 de la Partie III explore la contribution de la compréhension de ces processus biophysiques aux efforts de conservation au sein de la CCAMLR. Plus précisément, ce chapitre est constitué d'une part, d'une présentation de la CCAMLR et de la stratégie de protection de l'environnement adoptée par celle-ci, et d'autre part, de deux rapports scientifiques soumis à la CCAMLR auxquelles j'ai apporté ma contribution. La première étude, [o'Toole et al. \[2018\]](#), revisite la distribution des hotspots trophiques des prédateurs supérieurs subantarctiques dans une large base de données et évalue leur couverture par le réseau de zones protégées existant dans cette région. La deuxième étude, [Sergi et al. \[2019\]](#), évalue la prise en compte des processus bottom-up considérés dans la Partie II de cette thèse par la stratégie de conservation établie par la CCAMLR. Ensemble, ces travaux démontrent la nécessité d'inclure des zones de haute mer dans le système d'Aires Marines Protégées voulu par la CCAMLR et indiquent comment ces zones peuvent être identifiées en tenant compte de la connectivité liée à la circulation marine et des processus biophysiques associés à cette dernière.

Dans le Chapitre 2 de la Partie III, la région d'étude est étendue vers des latitudes plus basses, tout en considérant un acteur important pour les politiques de conservation dans l'océan Austral : les Terres Australes Françaises. Ce chapitre analyse la contribution scientifique au projet actuel d'expansion de la Réserve Nationale Naturelle des Terres Australes Françaises dans le sud de l'océan Indien, autour des îles Saint-Paul et Amsterdam (38 °S 77,5 °E), en mettant l'accent sur la contribution que j'ai pu y apporter pendant ma thèse. Comme dans les projets passés d'extension de la Réserve Naturelle autour des archipels de Crozet et de Kerguelen, pour cette zone subtropicale la Réserve a adopté la

même démarche : la mise en place d'une consultation avec la communauté scientifique dans le but de spatialiser et prioriser les enjeux de conservation dans la zone de Saint-Paul et Amsterdam. Cependant, d'un point de vue scientifique, les régions de l'océan Austral (Kerguelen et Crozet) et du sud de l'océan Indien (Saint-Paul et Amsterdam) sont bien distinctes. Alors que les zones océaniques de Kerguelen et de Crozet font l'objet de recherches intenses depuis plusieurs décennies [Koubbi et al., 2016b,a], les connaissances scientifiques autour des îles Saint-Paul sont beaucoup plus rares. Afin de combler ce manque de connaissances pélagiques, le Chapitre 2 de la Partie III évalue les modes de variabilité de la biomasse phytoplanctonique dans cette zone d'étude et leurs possibles forçages.

Les travaux effectués identifient deux biorégions, différenciées par la phénologie et la biomasse phytoplanctonique ainsi que par la profondeur de la couche de mélange hivernal : une zone subantarctique, au sud des îles, et une zone subtropicale, au nord de celles-ci. À cette variabilité nord-sud s'ajoute l'augmentation saisonnière de la biomasse phytoplanctonique autour des îles Saint-Paul et Amsterdam qui, malgré sa faible étendue spatiale, domine la saisonnalité de la biomasse phytoplanctonique à grande échelle (centaines de kilomètres). Celle-ci est probablement liée à l'augmentation du mélange diapycnal induit par le déferlement des ondes internes de marée (la turbulence générée est comprise entre  $10^{-9}$  et  $10^{-8}$  W/kg sur toute la colonne d'eau, une caractéristique unique à cette zone sur une échelle spatiale de 1500 km). Des différences significatives entre les régions nord et sud sont observées au sein de différents compartiments de la chaîne trophique (zooplancton, téléostéens et oiseaux de mer) et émerge ainsi comme particulièrement significative dans le cadre des travaux de régionalisation pour la Réserve Nationale Naturelle. Par conséquent, les données environnementales ont été utilisées pour reproduire la variabilité temporelle de la zone de transition entre les environnements subantarctique et subtropical et tenir compte de l'évolution future de l'environnement sous l'effet du changement climatique. Ce chapitre développe ainsi davantage le concept d'écologie marine "end-to-end" et constitue un cas d'étude dans lequel l'analyse des processus biophysiques à la base du réseau trophique pélagique est intégrée dans le processus officiel d'extension d'une Aire Marine Protégée.

En conclusion, les travaux contenus dans cette thèse mettent en évidence des forçages bottom-up liés aux apports profonds en fer façonnant le paysage marin à grande échelle

( $O(10^3 \text{ km})$ ) dans l'océan Austral hauturier. En identifiant des hotspots biologiques en aval de monts sous marins et des vents hydrothermaux, les résultats obtenus remettent en question le paradigme passé de la région du Courant Circumpolaire Antarctique, souvent vue comme un désert océanique ponctué d'oasis autour des îles. Ces travaux ouvrent ainsi des perspectives importantes à la fois en termes de biogéochimie et d'écologie. La compréhension des forçages physiques sur les écosystèmes, y compris des forçages liés à ces nouveaux apports en fer, constituera donc une étape importante pour la future prise en compte de leurs vulnérabilités face aux changements climatiques. D'autre part, du point de vue des systèmes de gestion des ressources marines, des enjeux majeurs concernent le développement d'instruments et de pratiques permettant d'intégrer l'information sur les changements climatiques dans toutes les étapes des actions de conservation. La confirmation des engagements politiques déclarés dans les objectifs internationaux de conservation (e.g., Coalition de la Haute Ambition pour la Nature et les Peuples) demeure également essentielle pour le développement des mesures de conservation.

## *Acknowledgements*

Pendant ces années de thèse j'ai reçu énormément d'aide et soutien de beaucoup, beaucoup, beaucoup, de personnes, que vous soyez sur cette liste ou non : merci !

Merci tout d'abord à Francesco, sans qui ces années de thèse n'auraient pas eu lieu. Francesco, je te remercie pour ces années passées ensemble, pour ta confiance, même avant que l'aventure ne commence. Merci pour ta passion, tes intérêts ouverts et variés et ton encadrement essentiel tout le long de la thèse, qui ont fait de cette expérience une période extrêmement stimulante. Outre ton soutien et ton aide scientifique, je souhaite te remercier encore une fois pour ton côté humain, ta bienveillance et ton attention à ceux qui t'entourent.

Grazie a te Alberto, che mi hai accompagnata nei primi passi nel mondo della ricerca. Grazie per le discussioni stimolanti, per i tuoi insegnamenti e consigli che mi sono tenuta stretta fino in fondo (e grazie per aver sopportato la mia euforia, forse esagerata!). Je remercie dans ce contexte aussi mes autres collègues, étudiants, post-doctorants et chercheurs, avec qui j'ai eu la chance de travailler pendant ces années : merci Cédric, Malcolm, Mathieu, Guilhem, Sayane, Boris, Clara, et Clara encore, Florian, Casey, Damien et Yan.

Merci Philippe, merci Marc, pour votre accompagnement lors des travaux de la CCAMLR. Les expériences auxquelles vous m'avez fait participer ont été parmi les plus formatrices et enrichissantes de ma thèse et je suis extrêmement reconnaissante de la chance que j'ai eue d'y participer.

Merci à l'ensemble des collègues des TAAF, en particulier à Cédric et Anne-Gaelle qui m'ont accueillie dès mon stage et qui m'ont permis de participer à des projets si intéressants. Merci aussi à Capucine et à l'ensemble des collègues avec qui j'ai travaillé pendant ces années.

Merci également à l'équipe de la RNMR pour m'avoir accueillie, avec toute sa bienveillance, et m'avoir fait découvrir son merveilleux monde fait de récifs, pêcheurs bavards et tortues.

Merci Hélène et Andrea pour votre relecture attentive et vos précieux commentaires, qui m'ont beaucoup aidée à rattraper mes bêtises et améliorer ce manuscrit. Mon manuscrit doit également beaucoup à toi Camille, merci pour ton interminable patience et ta relecture

attentionnée. Merci à vous tous, membres de mon Jury de thèse, pour les discussions extrêmement enrichissantes. Merci à vous ainsi qu'à tous ceux qui m'ont accompagnée en cette journée : vous avez fait de ce moment une journée magnifique dont je garderai un très beau souvenir.

Merci à tous mes compagnons et amis de thèse : Gina, Georges, Yona, Gaston, Katia, Nestor, Titou, Sarah, Clément, Inès, Pierre et Pierre encore, Keerthi, Cinthia, Sri, Lulu, et vous autres passagers de couloirs, compagnons de table. Merci de m'avoir accompagnée dans ce long périple et, surtout, de m'avoir montré vos magnifiques personnes. Merci à toi Carla, parcourir cette fin de thèse avec toi a été la meilleure chose qui pouvait m'arriver et m'a énormément aidée à la vivre avec plus de légèreté, voire même du divertissement (ce qui n'est pas peu dire...!).

Merci aux collègues du LOCEAN, pour les échanges, le soutien, la bienveillance et la présence pendant ces nombreuses années.

Merci aux amis de SWINGS, aux navigateurs et aux scientifiques ! Un merci particulier à Hélène et Catherine sans qui cette expérience incroyable n'aurait pas pu avoir lieu, vous êtes des super cheffes. Et merci à Julie, merci pour ton aide dans cette aventure, tu es une super présence pour les doctorants du LOCEAN. Grazie di nuovo a te Francesco, che non hai mai smesso di propormi di prendere il largo. Un merci spécial aussi à tous les collègues du LOCEAN avec qui j'ai partagé ces deux mois de navigation : Coco et Coco, Damien, Jonathan, Léa, Claire, Guillaume, Cédric, Fréd et Claude.

Mes amis, ma famille, et toutes les belles personnes que j'ai croisées pendant mon chemin, je fais le choix de ne pas lister vos noms ici, mais j'adresse mes pensées d'amour à chacun d'entre vous. Je ne peux pas trouver les justes mots pour décrire tout ce que vous m'avez apporté. Je vous remercie donc par mes émotions, mes sourires et mes larmes, le tout se combinant pour former un bagage d'affection et de gratitude sincères pour vous tous !





# Contents

<b>Abstract</b>	<b>v</b>
<b>Résumé détaillé en français</b>	<b>viii</b>
<b>Acknowledgements</b>	<b>xvi</b>
<b>List of Figures</b>	<b>xxiii</b>
<b>List of Tables</b>	<b>xxv</b>
<b>Acronyms</b>	<b>xxvii</b>
<b>I Introduction</b>	<b>1</b>
<b>1 Research context and challenges</b>	<b>3</b>
1.1 The pelagic seascape . . . . .	3
1.2 The case of the Southern Ocean . . . . .	6
1.2.1 Critical role of iron . . . . .	6
1.2.2 Going with the flow: prominent structuring effect of advection . . . . .	8
1.2.3 From biological contrasts to conservation policies . . . . .	10
1.3 Potential important role of <i>deep</i> nutrient sources . . . . .	12
1.4 Objectives and structure of this thesis . . . . .	14
<b>2 Tools and approach</b>	<b>17</b>
2.1 Observation of the pelagic food web . . . . .	17
2.2 Environmental context . . . . .	20
2.2.1 Multi-satellite data and reanalysis . . . . .	20
2.2.2 Lagrangian analysis of horizontal stirring . . . . .	22

<b>II</b>	<b>Unravelling pathways for deep bottom-up forces in the open Southern Ocean</b>	<b>29</b>
<b>1</b>	<b>Emergent nutrient sources: ecological role of hydrothermal vents</b>	<b>31</b>
1.1	Ardyna et al., 2019: Hydrothermal vents trigger massive phytoplankton blooms in the Southern Ocean; Nature Communications . . . . .	32
1.2	Schine et al., 2021: Massive Southern Ocean phytoplankton bloom fed by iron of possible hydrothermal origin; Nature Communications . . . . .	33
1.3	Synthesis and perspectives . . . . .	53
1.3.1	Summary of key results . . . . .	53
1.3.2	Further insights from horizontal transport analysis . . . . .	54
1.3.3	Ecological impact of hydrothermal activity in the Southern Ocean . . . . .	58
<b>2</b>	<b>Unexplained pelagic hotspots: ecological role of seamounts</b>	<b>61</b>
2.1	Sergi et al., 2020: Interaction of the Antarctic Circumpolar Current With Seamounts Fuels Moderate Blooms but Vast Foraging Grounds for Multiple Marine Predators; Frontiers in Marine Sciences . . . . .	62
2.2	Synthesis . . . . .	82
2.2.1	Summary of key results . . . . .	82
2.2.2	Conclusions . . . . .	84
<b>III</b>	<b>From the identification of biophysical forcing pathways to the management of marine environment</b>	<b>87</b>
<b>1</b>	<b>Conservation of the high seas: the case of the Antarctic Circumpolar Current region</b>	<b>91</b>
1.1	Context . . . . .	92
1.1.1	CCAMLR’s structure, functioning and mechanisms for scientific research contribution . . . . .	92
1.1.2	Origin and ingredients of CCAMLR’s conservation strategy . . . . .	93
1.2	CCAMLR conservation effort in the ACC region . . . . .	96
1.2.1	Predator trophic hotspots in the Indian sector of the subantarctic Southern Ocean: how do they overlap with marine protected areas? CCAMLR-WS-SM-18-07 . . . . .	98
1.2.2	Unfolding the connectivity patterns along the Antarctic Circumpolar Current in the Sub-Antarctic region. CCAMLR-WG-EMM-19-71 . . . . .	102
1.2.3	Future issues for achieving conservation targets in the ACC region . . . . .	106
<b>2</b>	<b>“End-to-end” marine ecology: the case of the Saint Paul and Amsterdam Islands Marine Protected Area</b>	<b>111</b>
2.1	Context . . . . .	111

2.1.1	National Natural Reserves of the French Southern Lands . . . . .	111
2.1.2	Conservation process at the Saint Paul and Amsterdam region . . . . .	115
2.2	Analysis of bottom-up controls at the basis of the pelagic food-web . . . . .	116
2.2.1	Spatial and seasonal variability modes of phytoplankton biomass in the SPA region . . . . .	118
2.2.2	Modulation of the phytoplankton biomass by physical drivers . . . . .	121
2.2.3	Identification of pelagic bioregions . . . . .	124
2.3	Integration of the pelagic analysis in the consultation process with the sci- entific community and the RNN . . . . .	127
2.3.1	Characterisation of the transition zone . . . . .	128
2.3.2	Long term variability under climate change . . . . .	130
<b>IV</b>	<b>Conclusions and perspectives</b>	<b>133</b>
<b>1</b>	<b>Summary of main findings</b>	<b>135</b>
<b>2</b>	<b>Perspectives</b>	<b>143</b>
2.1	Nutrients pathways from the deep to the upper ocean: limits of this work and way forward . . . . .	143
2.2	Towards a comprehensive analysis of the Antarctic Circumpolar Current trophic web: including the meso-pelagic community and gelatinous organisms	148
2.3	Implications for future conservation policies . . . . .	151
<b>Appendix</b>		<b>157</b>
A.1	o'Toole et al 2018: Predator trophic hotspots in the Indian sector of the subantarctic Southern Ocean: how do they overlap with marine protected areas?; CCAMLR-WS-SM-18-07 . . . . .	157
A.2	Sergi et al 2020: Unfolding the connectivity patterns along the Antarctic Circumpolar Current in the Sub-Antarctic region; CCAMLR-WG-EMM- 19-71 . . . . .	180
A.3	Godet et al 2020: Matching zooplankton abundance and environment in the South Indian Ocean and Southern Ocean; Deep Sea Research Part I . . .	199
<b>Bibliography</b>		<b>211</b>



# List of Figures

1.1	Stommel diagram of spatial and time scales for typical biophysical phenomenon and observational capacity in marine environment . . . . .	4
1.2	Phytoplankton contrasts and iron delivery from horizontal transport in the Southern Ocean . . . . .	9
1.3	Marine Protected Areas in the Southern Ocean . . . . .	11
1.4	Upwelling hotspots in the Southern Ocean . . . . .	13
2.1	Schematic representation of the pelagic trophic chain considered in this thesis and observational tools used . . . . .	19
2.2	Schematics steps to the Lagrangian analysis of fluid dynamics used in this thesis . . . . .	22
2.3	Computation of a Lagrangian plume from a theoretical nutrient source: detailed steps . . . . .	27
1.1	Position of the bloom relative to the position of the Lagrangian plume generated by releasing particles at the surface above the vents . . . . .	55
1.2	Schematic representation of the Southern Ocean reservoir of hydrothermal $^3\text{He}$ . . . . .	56
1.3	Preliminary analysis of the transport control on the interannual variability of Net Primary Production plumes sustained by hydrothermal iron: comparison to the Lagrangian plumes standing from the hydrothermal vents . . . . .	58
1.1	Contribution of scientific research in CCAMLR conservation activities . . . . .	94
1.2	Distribution of predator track from the Crozet, Kerguelen and Heard Islands' colonies. . . . .	99
1.3	Proportion of the foraging hotspots' coverage included in each area of competence (different national EEZ, CCAMLR and SIOFA) . . . . .	101
1.4	Schematic representation of the spatial and temporal lags structuring the trophic chain along the Antarctic Circumpolar Current . . . . .	104
1.5	Horizontal connectivity between Exclusives Economic Zones in the Southern Ocean. . . . .	106

---

1.6	Timeline of spatial planning effort in the Antarctic Circumpolar Current region and contextualisation of the scientific contribution considered in this thesis. . . . .	109
2.1	National Natural Reserves under the French Southern and Antarctic Lands	113
2.2	Schematic representation of steps leading to the establishment of a Marine Protected Area in the French Southern Lands: contribution of the scientific community . . . . .	114
2.3	Phytoplankton and nutrient distribution in the South Indian Ocean . . . .	117
2.4	Variability modes of the seasonal phytoplankton biomass in the Saint-Paul and Amsterdam region. . . . .	120
2.5	Spatial distribution of physical drivers of deep nutrients into the Saint-Paul and Amsterdam euphotic layer: winter mixing and turbulent mixing induced by internal waves . . . . .	123
2.6	Pelagic bioregionalisation of the Saint-Paul and Amsterdam oceanic environment under physical drivers of phytoplankton biomass. . . . .	125
2.7	Transition zone between the Subantarctic and Subtropical environments in the Saint-Paul and Amsterdam region during the period 1997-2017. . . . .	129
2.8	Surface warming trends estimated from sea surface temperature between 1985 and 2017 in the South Indian Ocean . . . . .	130
1.1	Fertilizing from below: schematic representation of iron sources and delivery mechanisms to the euphotic layer driving major phytoplankton contrasts in the Southern Ocean. . . . .	137
2.1	Distribution of shallow seamounts ( $\leq 1000$ m deep) and active hydrothermal vents in the Southern Ocean. . . . .	147
2.2	Distribution of predator hotspots and climatology of physical drivers in the Indian sector of the Southern Ocean. . . . .	149
2.3	Distribution of Important Marine Mammals Areas in the Southern Ocean and bottom-up processes analysed in this thesis. . . . .	152

# List of Tables

1.1	Main modes of Southern Ocean iron supply at local and basin scale . . . . .	7
-----	---	---





# Acronyms

<b>AAR</b>	<b>A</b> ntarctic- <b>A</b> ustralian <b>R</b> idge
<b>ACC</b>	<b>A</b> ntarctic <b>C</b> ircumpolar <b>C</b> urrent
<b>BGC</b>	<b>B</b> io <b>G</b> eo <b>C</b> hemical
<b>CCAMLR</b>	<b>C</b> onvention for the <b>C</b> onservation of <b>A</b> ntarctic <b>M</b> arine <b>L</b> iving <b>R</b> esources
<b>CMEMS</b>	<b>C</b> opernicus <b>M</b> arine <b>E</b> nvironment <b>M</b> onitoring <b>S</b> ervice
<b>EEZ</b>	<b>E</b> xclusive <b>E</b> conomical <b>Z</b> one
<b>EKE</b>	<b>E</b> ddy <b>K</b> inetic <b>E</b> nergy
<b>EOF</b>	<b>E</b> mpirical <b>O</b> rthogonal <b>F</b> unction
<b>GPS</b>	<b>G</b> lobal <b>P</b> ositioning <b>S</b> ystem
<b>HNLC</b>	<b>H</b> igh <b>N</b> utrient <b>L</b> ow <b>C</b> hlorophyll
<b>IUCN</b>	<b>I</b> nternational <b>U</b> nion for <b>C</b> onservation of <b>N</b> ature and <b>N</b> atural <b>R</b> esources
<b>MLD</b>	<b>M</b> ixed <b>L</b> ayer <b>D</b> epth
<b>MPA</b>	<b>M</b> arine <b>P</b> rotected <b>A</b> rea
<b>NPP</b>	<b>N</b> et <b>P</b> rimary <b>P</b> roduction
<b>RFMO</b>	<b>R</b> egional <b>F</b> isheries <b>M</b> anagement <b>O</b> rganization
<b>RK</b>	<b>R</b> unge- <b>K</b> utta
<b>RNN</b>	<b>R</b> eserve <b>N</b> aturelle <b>N</b> ationale (National Natural Reserve in English)
<b>SCAR</b>	<b>S</b> cientific <b>C</b> ommittee on <b>A</b> Antarctic <b>R</b> esearch
<b>SEAFO</b>	<b>S</b> outh <b>E</b> ast <b>A</b> tlantic <b>F</b> ishery <b>O</b> rganization
<b>SIOFA</b>	<b>S</b> outhern <b>I</b> ndian <b>O</b> cean <b>F</b> ishery <b>A</b> greement

---

<b>SRS</b>	<b>S</b> hona <b>R</b> idge <b>S</b> ystem
<b>SSH</b>	<b>S</b> ea <b>S</b> urface <b>H</b> eight
<b>SPA</b>	<b>S</b> aint- <b>P</b> aul and <b>A</b> msterdam
<b>SWIR</b>	<b>S</b> outh- <b>W</b> est <b>I</b> ndian <b>R</b> idge
<b>TAAF</b>	<b>T</b> erres <b>A</b> ustrales et <b>A</b> ntarctiques <b>F</b> rancaises (French Southern and Antarctic Lands in English)
<b>UNCLOS</b>	<b>U</b> nited Nations <b>C</b> onvention on the <b>L</b> aw of the <b>S</b> ea

# Part I

## Introduction



# Chapter 1

## Research context and challenges

### 1.1 The pelagic seascape

Spatial organization of terrestrial living resources in the landscape has been largely studied since the 19<sup>th</sup> century and has progressively informed ecosystem management practices [Turner et al., 2003; Turner, 2005; Kavanaugh et al., 2016]. More recently, the concept of landscape has been extended to the marine environment [Pittman, 2018]. Similarly to terrestrial environments, marine seascapes appear as a mosaic of spatially heterogeneous biomes: geochemical and dynamical environmental complexity, resources patchiness and stressors' repartition shape the distribution of marine organisms and biodiversity across a large spectrum of temporal and spatial scales [e.g., Pittman et al., 2011; d'Ovidio et al., 2010; Lehahn et al., 2018; cotté et al., 2011; Della Penna et al., 2015]. The characterisation of spatio-temporal patterns of marine communities is at the basis of environmental policies [Caldow et al., 2015; Lewison et al., 2015; Maxwell et al., 2015].

Unlike landscape, “*pelagic seascapes are embedded in a turbulent, advective ocean*”<sup>1</sup>. Ocean physical dynamics drive, shape and continuously modify marine life, affecting it at both spatial and temporal scales (some examples are provided in Figure 1.1). Dynamical oceanic

---

<sup>1</sup>Citation from Kavanaugh et al. [2016]

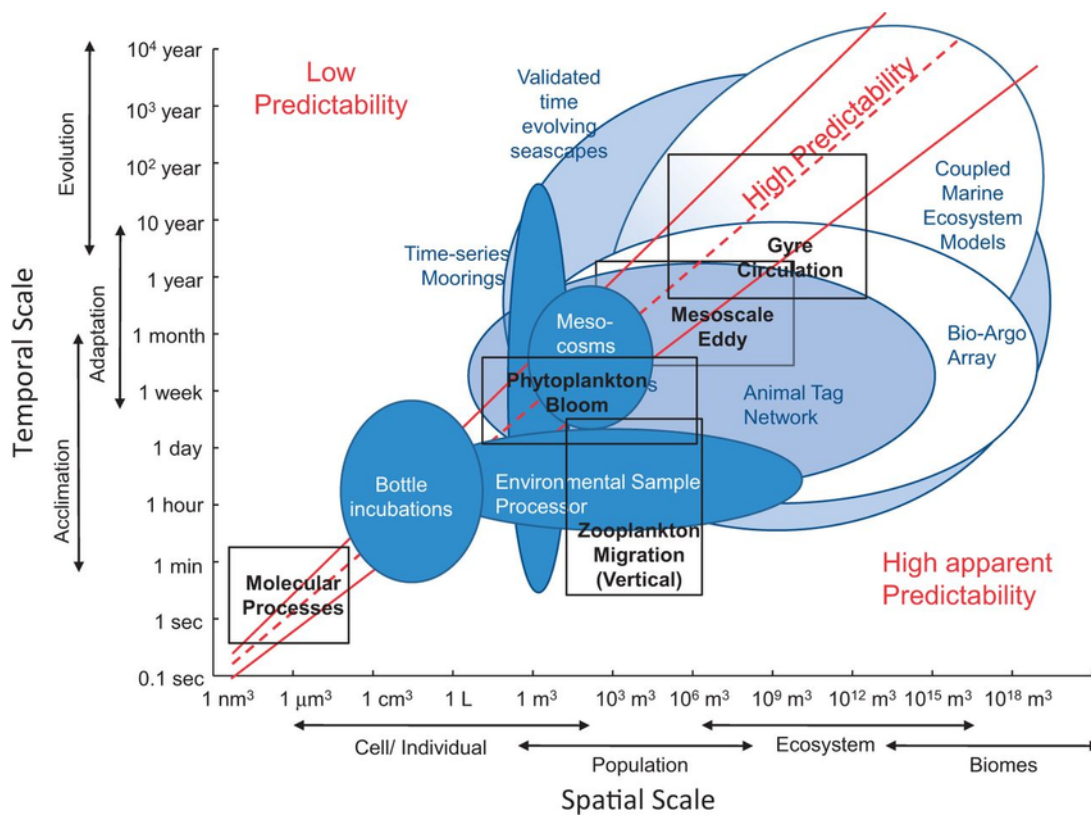


FIGURE 1.1: **Stommel diagram showing time and space scales for typical biogeochemical and physical phenomenon (squares) and our current observational capacity (ovals).** Shading denotes level of ecological complexity that the measurements provide: from basic ecological information (lightest) to the explicit community structure (darkest). From [Kavanaugh et al. \[2016\]](#).

processes, ranging from molecular processes to internal waves, fine scales activities or larger climatic patterns largely affect marine organisms [e.g. [Lévy et al., 2018](#); [Lehahn et al., 2018](#)]. The interplay of biogeochemical and physical processes acting at different scales creates complex spatial patterns. For instance, in Eastern Boundary Upwelling Systems fine-scale dynamics inhibit phytoplankton abundance [[Lathuiliere et al., 2011](#)] or nutrient input in the euphotic layer [[Gruber et al., 2011](#)], differently to what is observed in most other oceanic regions. Similarly, same physical processes can have different biological responses depending on the scale that they are considered at [[Lévy et al., 2012](#)]. Despite the complexity and the interplay of biochemical and physical interactions, biodiversity

hotspots can emerge at different spatial scales under the effect of mechanistic processes [Hazen et al., 2013; Kavanaugh et al., 2016]. This thesis considers mechanistic processes overlapping biological and dynamical organization at broad scales, considered here at thousands of kilometres with multi-year observations of environment and biology, allowing us to represent ecosystem processes (Figure 1.1).

Bottom-up forces control a large fraction of marine ecosystem variability [Wollrab et al., 2012; Di Lorenzo et al., 2013; Lynam et al., 2017; Hazen et al., 2013] and have been largely studied under multiple perspectives. For example, modelling ecological studies analyse energy pathways in the food-web and evaluate the equilibrium response of food-webs to changes, such as modifications in resource supply and/or in mortality of a top consumer [Wollrab et al., 2012; McCormack et al., 2020], or, using a physical perspective, by investigating the dynamical mechanisms controlling resources availability for an ecosystem. This last point has been the target of this thesis. Upwelling in eastern boundary current systems are probably the most well known example of persistent trophic hotspot driven by bottom-up processes [Bakun, 1996; Hazen et al., 2013; Croll et al., 2005; Santora et al., 2017]. In these regions, seasonal upwelling of nutrient-rich water supports high primary production and associated higher trophic levels [Hutchings et al., 1995; Ohman et al., 2013]. In addition to the predominant control of vertical dynamics, horizontal mixing and stirring also exerts multiple ecological controls on these systems. For instance, alongshore and cross-shelf transport of nutrients and organisms are important drivers of ecological contrasts in the largely studied California Current Ecosystem [Ohman et al., 2013; Di Lorenzo et al., 2013]. The effect of horizontal advection in ecosystem functions (productivity, community composition, spatial connectivity) largely exceed upwelling systems and is then referred to as “*a new bottom-up forcing paradigm*” shaping pelagic seascapes worldwide [see for instance the study cases summarised in Di Lorenzo et al., 2013].

This thesis studies dynamical pathways for bottom-up forces in the Southern Ocean and their role in informing environmental policies. The interest of this region is due to the strong effect of bottom-up processes in shaping biological contrasts and a particularly



profitable conservation framework for incorporating scientific knowledge into management plans. In the following section we develop these two arguments by showing current knowledge of dynamical pathways for bottom-up effects in the Southern Ocean, their effects in shaping biological hotspots and management policies, and the issues that arise from this.

## 1.2 The case of the Southern Ocean

### 1.2.1 Critical role of iron

In the Southern Ocean, the largest High Nutrient Low Chlorophyll (HNLC) region of the global ocean, productivity is critically limited by iron availability [Martin, 1990; de Baar, 2005; Sohrin et al., 2000; Martínez-García et al., 2014]. This essential element for phytoplankton growth, controlling photosynthesis, nitrate assimilation and acquisition of dissolved organic phosphorus, has been found to limit primary production rates, biomass accumulation, and ecosystem structure [e.g., Mark Moore et al., 2009; Browning et al., 2017; Moore et al., 2013; Henley et al., 2020]. However, due to its chemical properties, iron is absorbed over particulate material, both organic and inorganic, and removed from the euphotic layer [Boyd et al., 2015, 2017].

Magnitude, distribution and variability of iron supply mechanisms have been largely studied in the last decades. The concept of iron availability for biota is largely debated in the biogeochemistry community and depends on a multitude of parameters (iron forms, organic speciation, ligands availability, desorption and dissolution mechanisms etc.) [e.g., Norman et al., 2014; Raiswell et al., 2016; Mahowald et al., 2018; Abadie et al., 2017; Duce and Tindale, 1991]. Table 1.1 summarise main supply mechanisms of dissolved iron in the Southern Ocean following the recent review by Henley et al. [2020]. Entrainment due to winter mixing is the main source of iron to the euphotic layer at the basin scale, i.e. the whole Southern Ocean [Tagliabue et al., 2014, and Table 1.1]. However, as the main contributors of a shallow ferricline, at the regional scale, ice and coastal margins emerge

TABLE 1.1: **Main modes of Southern Ocean dissolved iron (dFe) supply at local and basin scale.** Adapted from [Henley et al. \[2020\]](#).

<b>Mode</b>	<b>Spatial scale</b>	<b>dFe supply</b> ( $\mu\text{molFe}$ $\text{m}^{-2}\cdot\text{y}^{-1}$ )	<b>Total dFe supply</b> ( $\mu\text{molFe}\cdot\text{y}^{-1}$ )	<b>Percentage of total dFe supply (%)</b>
<b>Deep winter mixing</b>	Basin	100	42000	45.88
<b>Continental Shelves</b>	Regional	296	27205	29.72
<b>Ice melt</b>	Regional	483	15630	17.07
<b>Biological Internal recycling</b>	Basin	10	4000	4.37
<b>Diffusion</b>	Basin	3	1260	1.38
<b>Atmospheric deposition</b>	Regional	19	1159	1.27
<b>Topography-induced upwelling (bottom pressure torque)</b>	Local	55	275	0.30
<b>Hydrothermal</b>	Local	3	15	0.02

from the background with highest iron fluxes and driving important contrasts in the iron availability in the Southern Ocean’s productive layer [see [Henley et al. \[2020\]](#), references therein and Table 1.1]. Iron fluxes at ice margins are mostly driven by sea ice melting and, to a lesser extent, by iceberg melting [[Henley et al., 2020](#), and references therein]. Fluxes linked to coastal margins include resuspension of sediments at shallow depths and increased vertical diffusion [[Blain et al., 2007](#); [Henley et al., 2020](#)]. These high iron fluxes in turn sustain intense phytoplankton blooms (see Figure 1.2A) with major geochemical and ecological impacts [[Sullivan et al., 1993](#); [Boyd et al., 2000](#); [Blain et al., 2007](#); [Thomalla et al., 2011](#); [Ardyna et al., 2017](#)]. For instance, despite their important patchiness, blooms at the margins of the ice zone can contribute to 25-67 % of the Southern Ocean planktonic production [[Petrou et al., 2016](#)] representing a key process for the biological carbon pump. From an ecological view point, the phytoplankton biomass generated at these

regions sustains multiple organisms, from zooplankton to marine top predators, driving intense pelagic contrasts in the Southern Ocean seascape [De Broyer et al., 2014; Bestley et al., 2020]. Positive relationships between annual primary production in Antarctic polynyas and pup production by ice-dependent Weddell seals [Paterson et al., 2015] reflect the intensity of the bottom-up effects in this oceanic region.

### 1.2.2 Going with the flow: prominent structuring effect of advection

The Southern Ocean circulation is dominated by the eastward geostrophic Antarctic Circumpolar Current driven by westerly winds and buoyancy forcings [Rintoul and Naveira Garabato, 2013]. Horizontal advection has multiple structuring effects on the pelagic seascape of the Southern Ocean. Transport of iron is one of the most prominent effects. In the case of ice-derived iron fluxes, horizontal transport is the major driver of iceberg drift and sub-sequential iron delivery from iceberg melting [Wadley et al., 2014]. Similarly, horizontal advection induces off-shelf export of sediment-derived iron from Antarctica into the Weddell sea [de Jong et al., 2012; Henley et al., 2020]. Within the intense Antarctic Circumpolar Current (ACC; mean annual flow 135 Sv, with  $1 \text{ Sv} = 10^6 \text{ m}^3/\text{s}$ , [Klinck and Nowlin, 2001]) the prominent effect of the velocity field over geochemical tracers is even more evident. Horizontal advection is the primary driver of iron fluxes downstream of coastal margins shaping the extension of phytoplankton blooms over hundreds and thousands of kilometres [e.g. Blain et al., 2007; Bakker et al., 2007; Sullivan et al., 1993; Lancelot et al., 2009; Mongin et al., 2009; Borrione et al., 2014; d'Ovidio et al., 2015; Sokolov and Rintoul, 2007]. The horizontal transport of water masses of the upper ocean having been in contact with topographies drives iron delivery and the following distribution of phytoplankton biomasses downstream of topographies in the Southern Ocean (Figure 1.2 A and B).

The ecological effect of the ACC also extends to higher levels of the pelagic trophic chain. At the sea ice margins, fish, seabirds and marine mammals largely depends on the advection of zooplankton [Hunt et al., 2016]. Similarly, in the open ocean, numerous

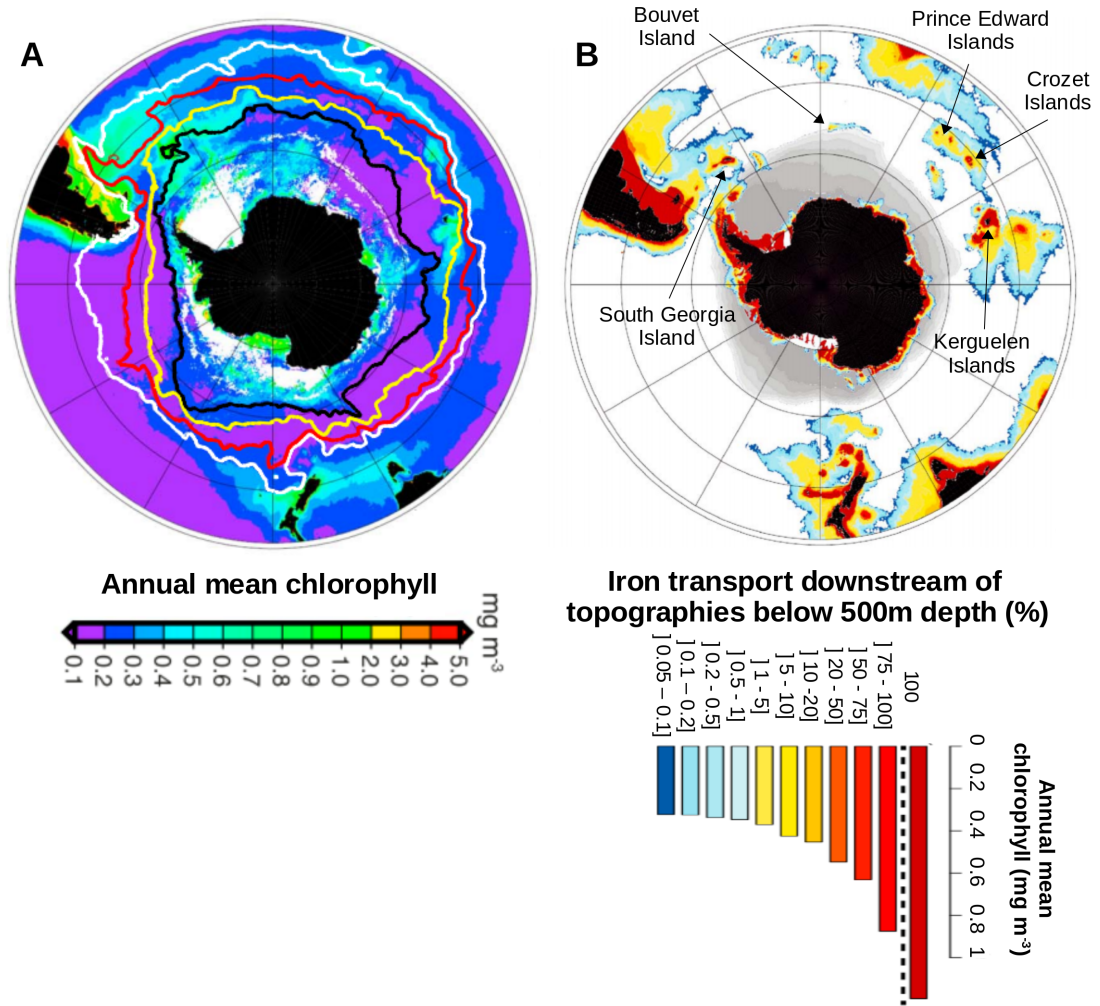


**FIGURE 1.2: Phytoplankton contrasts and iron delivery from horizontal transport in the Southern Ocean.** (A) Annual mean chlorophyll a concentration in the Southern Ocean (1998-2014). (B) Estimation of iron delivery from horizontal transport downstream of topographies shallower than 500 m (%; percent of iron remaining in a water parcel after estimated scavenging in respect to its initial concentration acquired in shallow areas; red to blue; further details on the methods adopted are provided in [Ardyna et al. \[2017\]](#)). Mean annual chlorophyll a concentration is shown in function of the horizontal iron delivery. Lines in panel A locates the main fronts of the Southern Ocean: the Subtropical Front (white), the Subantarctic Front (red), the Polar Front (yellow), and the South Antarctic Circumpolar Current Front (black). Red and grey areas in panel B respectively show regions shallower of 500 m and regions characterized by the seasonal sea ice cover. Islands of interest are indicated in panel B. Figure adapted from [Ardyna et al. \[2017\]](#).

land-breeding seabirds and pinnipeds forage on the summertime phytoplankton blooms advected downstream of islands, reflecting a profitable aggregation of mid-trophic preys in these water masses [De Broyer et al., 2014; O’Toole et al., 2017; Lea et al., 2006; Cotté et al., 2015; Guinet et al., 2001; Rogers et al., 2015]. After the phytoplankton bloom period, pelagic seascapes continue to drift along the ACC. For instance, coherent spatial ranges have been observed for the advection of biologically enriched waters masses and Southern elephant seals trips downstream of Kerguelen Island all along the post-bloom season [Cotté et al., 2015].

### 1.2.3 From biological contrasts to conservation policies

Spatial measurements are widely used for managing multiple activities in the marine space and promoting a ecosystem-based management of natural resources [Douve, 2008]. Among them, Marine Protected Areas (MPAs) are a primary management tool for mitigating threats to marine ecosystems and increasing their resilience to climate change effects [Edgar et al., 2014; Lester et al., 2009; O’Leary et al., 2016; Roberts et al., 2017; Davies et al., 2017, e.g.]. In the Southern Ocean, multiple institutional frameworks are responsible for the management and conservation of marine living resources there. Several archipelagos are under national jurisdiction, these are, from east to the west: the English South Georgia and Sandwich Islands, the Norwegian Bouvet Islands, the South Africans Prince Edward Islands, the French Crozet’s and Kerguelen’s archipelagos and the Australians Heard and McDonald Islands. In the high seas, the Commission for the Conservation of Marine Living Resources (CCAMLR) is responsible for the management and conservation of the marine ecosystems there included (competence boundaries of CCAMLR are shown in white in Figure 1.3).

The remoteness of this region from inhabited lands and from maritime traffic routes reduces the direct sources of pressures to its ecosystems [e.g. Lebouvier, 2007] and the few activities present there (mainly scientific research and few fisheries) facilitate the management of this space. Since its establishment almost 40 years ago, CCAMLR became a pioneer

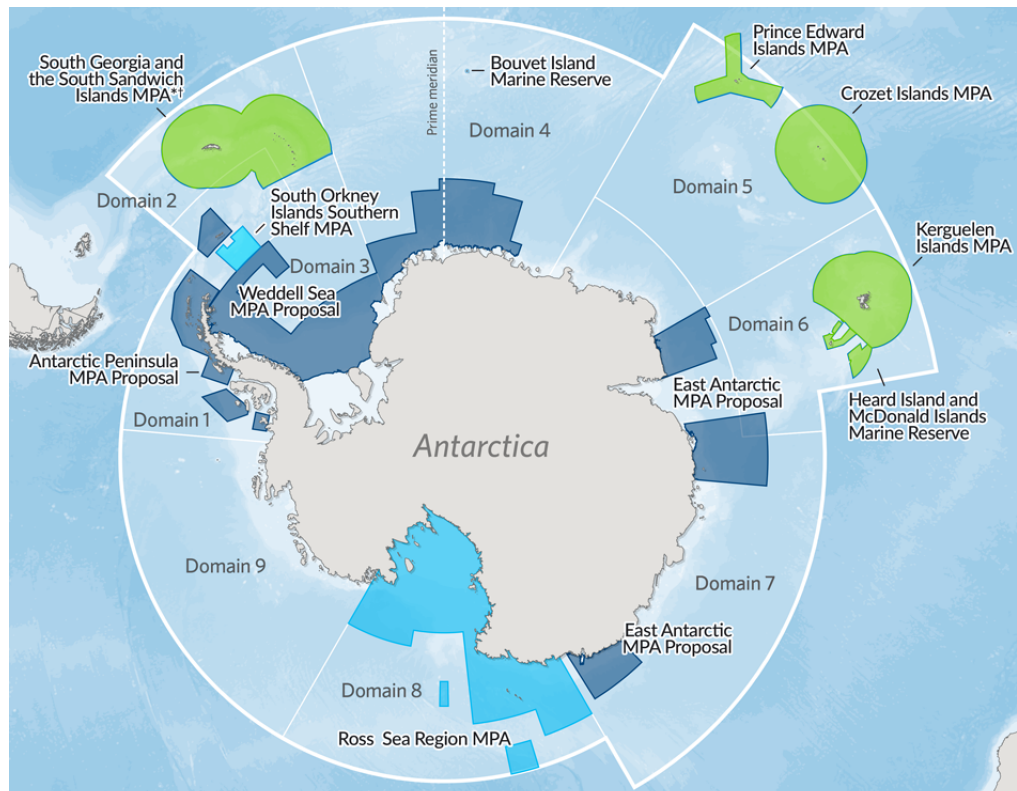


FIGURE 1.3: **Marine Protected Areas in the Southern Ocean.** Marine environments around islands are covered by multiple MPAs: national reserves (green) and CCAMLR's South Orkney Islands MPA (light blue). Marine environments around the Antarctic continent are covered by the CCAMLR's Ross Sea MPA (light blue) and several CCAMLR MPAs proposals (dark blue). White lines shows CCAMLR planning domains. Adapted from the Pew Charitable Trust.

and a leader in high seas marine resource management [Cullis-Suzuki and Pauly, 2010; Osterblom and Folke, 2013; Molenaar, 2001; Kock et al., 2007; Pinto, 2012; Ruckelshaus et al., 2008] and is pursuing the objective to develop a representative system of MPAs across its Convention Area<sup>2</sup>. Today, the ecological hotspots downstream of islands and at sea-ice margins are covered or considered by multiple national MPAs, CCAMLR MPAs or CCAMLR MPAs' proposals (Figure 1.3).

<sup>2</sup>CCAMLR-XXVII (2008), par. 7.2

### 1.3 Potential important role of *deep* nutrient sources

The bottom-up processes driving pelagic hotspots near and downstream of ice and coastal margins, under the main iron control, are largely documented by robust scientific knowledge and part of conservation planning efforts. However, in addition to these sources, visible from the sea surface, other features in the ocean interior may draw our attention.

A remarkable example of this are hydrothermal vents. These are fissures on the seafloor, from which water geothermally enriched in many chemical elements, including dissolved iron, discharges, and are known to be associated to unique local ecosystems [Desbruyeres et al., 2006]. However, for a long time, iron input from hydrothermal vents into the deep ocean was assumed to be negligible. This was due to the abundant generation of polymetallic particulate phases and the following precipitation of introduced iron [Feely et al., 1987; Mottl and McConachy, 1990; German et al., 1991]. During the last decades, new discoveries regarding the distribution, number, type and activity of hydrothermal vent systems are forcing us to revisit this paradigm and the impact of hydrothermal iron on ocean biogeochemistry [Bennett et al., 2008; Tagliabue et al., 2010; Wu et al., 2011; Yücel et al., 2011; Resing et al., 2015; Fitzsimmons et al., 2017; Tagliabue and Resing, 2016]. Hydrothermal signals from submarine volcanic calderas, generally occurring at depth inferior to 1500 m, have already been observed to penetrate into the productive layer in other oceanic basins [Hawkes et al., 2014; Guieu et al., 2018].

Similarly to hydrothermal vents, seamounts, which are defined as geomorphological features having a vertical elevation of more than 1000 m from the seafloor, are also known to be associated to particular local ecosystems. These submerged features have been identified as unique environments, hotspots of biodiversity and endemism for both benthic and pelagic ecosystems [Tsukamoto, 2006; Pitcher et al., 2007; Morato et al., 2008, 2010; Rowden et al., 2010]. However, most of these observations are restrained to few sites and require further investigations in order to assess their representativeness at the global scale [Wessel et al., 2010; Rowden et al., 2010]. From a geochemical point of view, dynam-



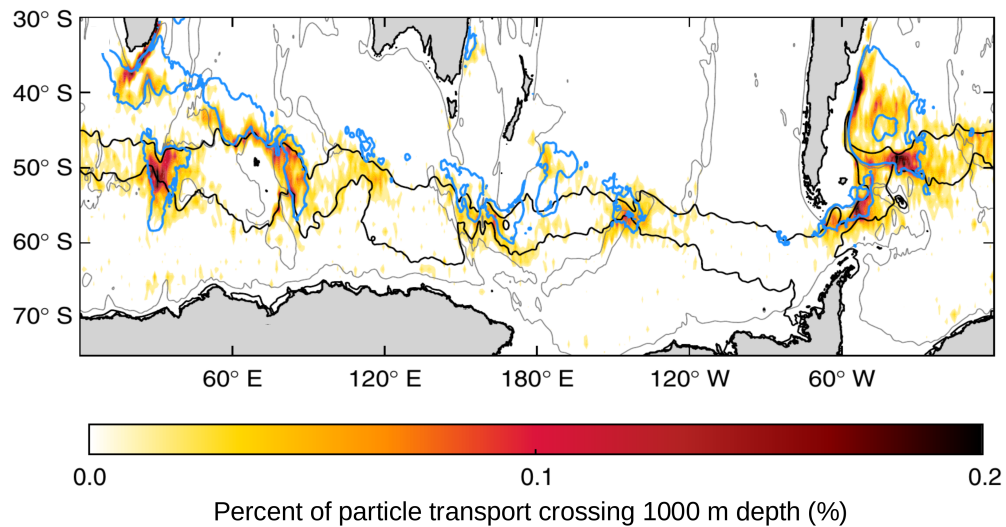


FIGURE 1.4: **Upwelling hotspots in the Southern Ocean.** Percent of total upwelling particle transport crossing the 1000 m depth horizon, which is representative of upwelling in the interior and lies above major topographic features (%), white to red). Blue contours indicate regions high mean Eddy Kinetic Energy at 1000 m ( $> 75 \text{ cm}^2 \text{ s}^{-2}$ ). Thick black lines represent the main path of the Antarctic Circumpolar Current. The analysis has been performed with the Geophysical Fluid Dynamics Laboratory’s Climate Model version 2.6. The figure has been adapted from [Tamsitt et al. \[2017\]](#).

ics at seamounts are known to generate increased vertical nutrient fluxes and promote productivity [[Pitcher et al., 2007](#)].

On another hand, topographic interactions are now recognized as primary driver of nutrients, and notably iron, into the Southern Ocean mixed layer [[Sokolov and Rintoul, 2007](#); [Tamsitt et al., 2017](#)]. These upwelling hotspots are now well documented (Figure 1.4) and could induce important spatial contrasts in the deep iron supplies, notably from hydrothermal iron, to the surface Southern Ocean. However, possible ecological impacts of deep bottom-up processes in this iron-depleted region, both in terms of primary production and subsequent impact on higher trophic levels, are still unexplored. In the following, the term “deep” will be employed to characterise bottom-up processes driven by features which are not visible from the surface: submerged features distant from ice and continental margins.



## 1.4 Objectives and structure of this thesis

The aim of this thesis is to investigate the role of deep bottom-up processes in shaping open ocean trophic hotspots. In this aim, it addresses the following questions:

1. What is the ecological role of deep nutrient sources and how do they influence the pelagic seascape in the Southern Ocean?
2. How can the analysis of deep bottom-up forcings on pelagic ecosystems be used to inform marine conservation policies?

The first question is addressed in Chapters 1 and 2 of Part II. In Chapter 1, we reconsider the iron sources driving phytoplankton biomass contrasts in the Southern Ocean. In particular, two regional studies analyse intense phytoplankton blooms located downstream of active hydrothermal vents and unexplained by “classical” iron sources. By combining *in-situ* and remote observations of phytoplankton biomass, measurements of geochemical elements like iron concentrations and  $\delta^3\text{He}$ , with analysis of ocean dynamics, these studies evaluate the role of hydrothermal iron in sustaining intense phytoplankton blooms in the Southern Ocean. Chapter 2 explores dynamical pathways of bottom-up forces sustaining an upper predator hotspot identified in the literature and unexplained by known biogeochemical and biophysical mechanisms. More precisely, it combines multiple observations of phytoplankton blooms with analyses of water masses trajectories derived from altimetry, in order to investigate the ecological role of seamounts in this region. All together, the processes considered in this thesis emphasize the important connecting role of the ACC and provide examples of bottom-up controls driven by deep nutrient sources shaping the pelagic seascape at large scales ( $O(10^3 \text{ km})$ ).

As introduced previously, understanding how mechanistic processes shape the pelagic seascape provides valuable information for marine environmental management. The interconnections between the definition of deep bottom-up forcing on the pelagic ecosystems and marine conservation policies are investigated in Chapters 1 and 2 of Part III, where

this issue is addressed within different management frameworks. Firstly, Chapter 1 analyses the development of conservation measures in the high seas within the CCAMLR framework. More specifically, it addresses the inclusion of bottom-up processes studied in Part II in the CCAMLR framework and within its conservation strategy. Then, Chapter 2 further develops the concept of “end-to-end” marine ecology providing a study case which extends from the identification of bottom-up forces to the establishment of a Marine Protected Area. The results presented in this Chapter are an official contribution to the scientific basis supporting the project of extension of the Natural Marine Reserve of Saint-Paul and Amsterdam islands within the French Southern Territories framework.



## Chapter 2

# Tools and approach

In order to explore ecosystem processes, in this thesis I use observational tools covering a wide range of large spatial and temporal scales (as schematized in Figure 1.1). This chapter aims to briefly introduce these tools and the main approach used in this thesis. Detailed description of products (technical characteristics, spatial and temporal resolutions and coverages) and specific analyses performed on these are provided in the material and methods sections of each chapter.

### 2.1 Observation of the pelagic food web

Figure 2.1 provides a schematic representation of the pelagic food web of the Southern Ocean and the tools considered in this thesis for observing some compartments of it. The food web's representation is adapted from Trebilco et al. [2020], but excludes compartments associated to the benthic realm, including demersal species (toothfish). As introduced previously, this thesis considers the pelagic food web with a bottom-up view, i.e. considering the effect resources' limitations on living organisms. In this aim, I used observations of phytoplankton organisms, which are at the basis of the pelagic trophic chain. Measurements of chlorophyll *a* concentration, a proxy for phytoplankton biomass,

are evaluated in this thesis within two complementary datasets:

- **Global Ocean Color maps:** Estimation of chlorophyll *a* concentration in the surface ocean from remote sensing reflectance: the ratio of upwelling radiance to the downwelling irradiance at the ocean’s surface. Satellite Ocean Color maps provide a continuous and global time series since the launch of SeaWiFS in August 1997 with quasi-synoptical measurements. Ocean Color products used in this thesis merge multiple sensors (SeaWiFS, MODIS, MERIS, VIIRS, OLCI-S3A&S3B) and are accessed through the open access European Copernicus Marine Environment Service (CMEMS).
- **Biogeochemical Argo floats** (thereafter BGC-Argo): *In-situ* subsurface estimation of chlorophyll *a* concentrations through the measurement of fluorescence. This profiling observing system has progressively emerged since the 2010s. Compared to satellite images, BGC-Argo arrays have three major benefits. They provide (1) *in-situ* measurements which are (2) vertically distributed in the productive layer and (3) unconstrained by cloud coverages [Claustre, 2010]. Vertical profiles of BGC-Argo floats are accessed through the open access CORIOLIS Global Data Assembly Center.

Within higher trophic levels, different grazers organisms may result in different food webs. In particular, gelatinous zooplankton, as salps, are usually considered a “dead end” in the pelagic food web. Due to their low nutritional value, these organisms are a minor food item for large vertebrates and belong to an alternative food web: the microbial food chain [Verity and Smetacek, 1996; Sommer et al., 2002; Pakhomov et al., 2019]. As schematised in Figure 2.1, while large phytoplankton (diatoms) are mostly consumed by krill [González et al., 2016; Perissinotto, 1992] and copepods [Frederiksen et al., 2006], salps mostly feed on small phytoplankton (flagellates). In this context, remote sensing analyses allowing to distinguish between phytoplankton communities (large and small phytoplankton) are

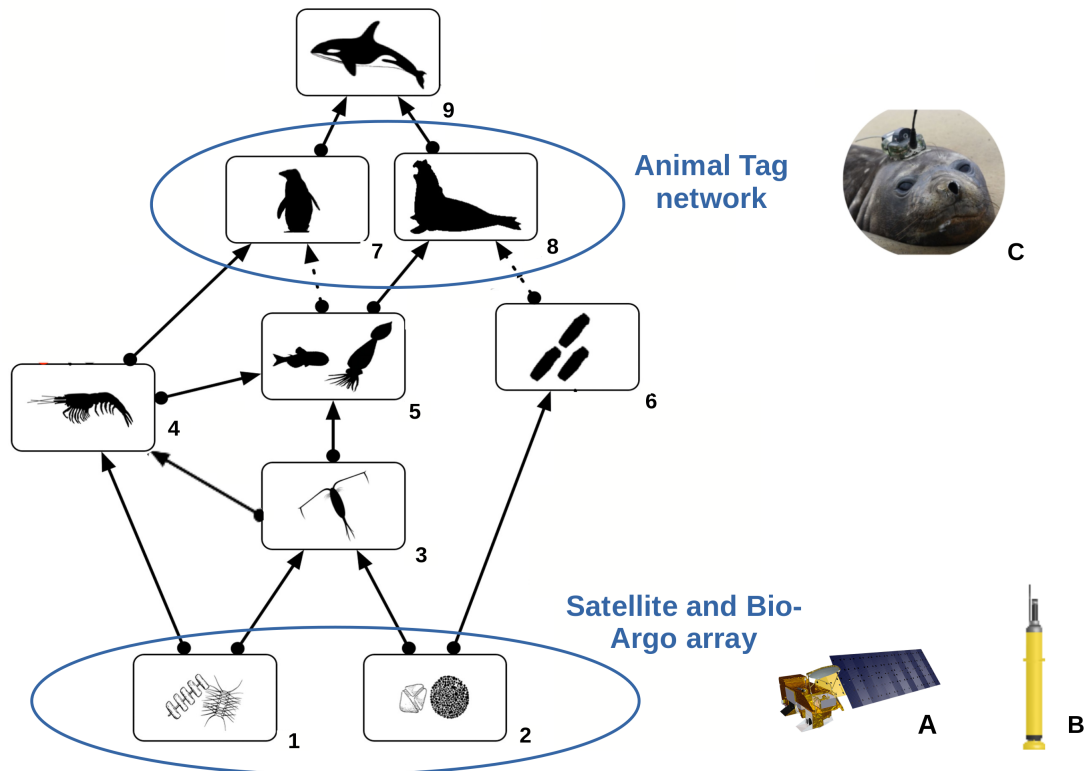


FIGURE 2.1: **Schematic representation of the Southern Ocean pelagic food web and observational tools used in this thesis.** <sup>1</sup>Large phytoplankton ( $> 10\mu\text{m}$ ; mainly diatoms and large dinoflagellates), <sup>2</sup>Small phytoplankton ( $\leq 10\mu\text{m}$ ; mainly picophytoplankton, coccolithophores, *Phaeocystis sp.*, and small autotrophic flagellates), <sup>3</sup>Mesozooplankton (copepods etc.), <sup>4</sup>Krill, <sup>5</sup>Mesopelagic fishes and squids, <sup>6</sup>Salps, <sup>7</sup>Low-trophic level foragers, <sup>8</sup>Mesopelagic foragers, <sup>9</sup>Apex predators. Sea-ice dependent organisms are not considered in this thesis, consequently the krill compartment is only represented by subantarctic krill species, which can be important prey for penguins [Green et al., 1998; Deagle et al., 5 05]. The schematic illustration of the food web has been adapted from Trebilco et al., 2020. Observations tools used for considered compartments (ovals) are schematised in the right part of the figure: <sup>A</sup>Satellite observations, <sup>B</sup>Bio-Argo array, <sup>C</sup>Animal tag networks. Source of the images: <sup>A</sup>*Aqua* spacecraft from NASA, <sup>B</sup>Argo Program UCSD, <sup>C</sup>C. Guinet (CEBC).

also used for obtaining information on the pelagic ecosystem. These are evaluated with PHYSAT analysis [Alvain et al., 2005, 2008]].

Finally, this thesis considers land-breeding predators, particularly seals and seabirds, for locating biological hotspots:

- **Animal telemetry data:** Localisations of land-breeding, recorded through the Argo satellite system since the 1970s and through the Global Positioning Systems since the early 2000s, are increasingly used for identifying important ecological areas and informing management policies [Hays et al., 2019; Hindell et al., 2020; Dias et al., 2017]. Time-spent metric, known as first-passage time, can be applied on animal tracking data in order to identify searching locations, an indicator of foraging grounds [Fauchald and Tveraa, 2003].

The significance of considering land-breeding high predators distributions in this thesis is twofold. Firstly, because the numerous national and international animal telemetry programs provide us a large observational abilities (circumpolar spatial scales and multi-decadal time series) [e.g. Ropert-Coudert et al., 2020]. Secondly, because marine top predators are widely used as indicators by ecologists and conservationists [e.g., Camphuysen, 2006; Bossart, 2011; Delord et al., 2013; Thiers et al., 2017]. This thesis mainly considers high predators hotspots already identified in the literature by telemetry data, as a consequence, the description of this kind of data is concise.

## 2.2 Environmental context

### 2.2.1 Multi-satellite data and reanalysis

Biological observations previously described are contextualized with multi-satellite observations and derived 3D ocean distribution of physical properties. Main properties analysed in this thesis are briefly described here:

- **Sea Surface Temperature:** Measurements of temperature of the surface ocean by passive remote sensing with satellite infrared or microwave radiometers. Thanks to the early development of this technology, since 1985, these data provide the longest continuous daily time series of ocean observations at the global scale. In this thesis

I use the Operational Sea Surface Temperature and Ice Analysis (OSTIA) system run by the UK's Met Office [Good et al., 2020]. This level-4 satellite product merges satellite measurements from both infrared and microwave radiometers with *in-situ* measures from ships, drifting and moored buoys.

- **Vertical distribution of temperature:** Two reprocessing methods allow to obtain from irregular observations regular grid distributions of sea properties, from the surface to the bottom. A first method is ocean reanalysis. This method deploys ocean circulation models which assimilate different sources of observations (often with a Kalman filter). In this thesis I use the Ocean GLORYS-12v1 (Global Ocean ReanalYsis and Simulations product) model. This product is performed by Mercator using the NEMO model and assimilating satellite products (altimetry, sea surface temperature and Sea Ice Concentration) and *in situ* temperature and salinity vertical profiles. A second method used for obtaining regular grid of vertical ocean properties consists in applying statistical analyses to observations. This method is applied with two principal steps. Firstly, satellite data are projected onto the vertical via multiple linear regression methods and covariances deduced from historical observations. Secondly, optimal interpolation methods combine these synthetic fields with T/S *in situ* profiles. In this thesis I use the Armor3D product processed by the CLS [Guinehut et al., 2012; Mulet et al., 2012]. Both Glorys and Armor3D products are available since 1993 thanks to the development of satellite altimeters. However, due to limited coverage of *in situ* observations of the remote Southern Ocean, in this thesis I only uses these datasets after 2005, in order to benefit of Conductivity-Temperature-Depth measures obtained from Argo programs and instrumented pinnipeds [Meyssignac et al., 2019].
- **Mixed Layer Depth (MLD):** The thickness of the mixed layer is obtained either directly from Glorys or Armor3D products previously described, either by calculating it from Argo density profiles whether these are employed. Glorys and Armor3D products define the MLD as the depth where the temperature decrease of 0.2 °C



compared to the temperature at 10 m. However for a better calculation of the mixed layer thickness, when individual T/S profiles are used, the MLD is defined as a density difference of  $0.03 \text{ kg m}^{-3}$  from a reference value at 10 m [Montégut et al., 2004].

Similarly to Ocean Color maps, these data are accessed through the CMEMS service. In addition, this thesis considers the important structuring role of the horizontal transport on the pelagic seascape by analysing the altimetry-derived velocity fields in the Lagrangian framework. Key assumptions made and the basis of the approach used for analysing kinematic properties in this thesis are described in the following section.

### 2.2.2 Lagrangian analysis of horizontal stirring

The analysis of the ocean dynamics adopted in this thesis can be summarised in three steps schematized in Figure 2.2. These steps are detailed below.

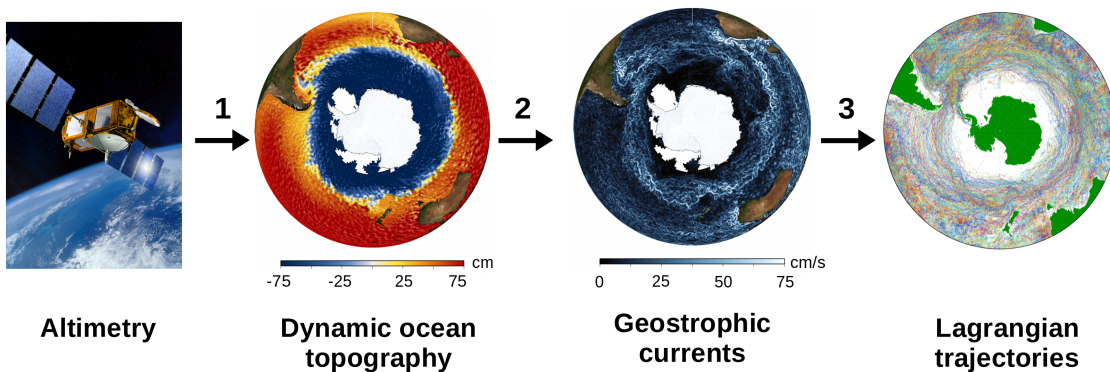


FIGURE 2.2: **Basic steps to the Lagrangian analyses of fluid dynamics used in this thesis.** (1) Estimation of dynamic ocean topography from satellite altimetry. (2) Computation of geostrophic currents. (3) Estimation of Lagrangian trajectories from the velocity field. Sources: all the images are provided by Aviso CNES/CLS, with the exception of the trajectory map from van Sebille et al. [2018]

**Step 1: Dynamic ocean topography.** Altimetry is the measurement of surface height via the emission of radar waves from satellites (active remote sensing). These radar al-

timeters calculate the satellite-to-surface distance. Surface height, named sea surface height for the ocean, is then evaluated by subtracting satellite-to-surface distance from the satellite altitude: satellite's distance with respect to the reference ellipsoid, a rough approximation of the Earth's surface (computed by GPS or other methods). Finally, ocean dynamic topography, which represents the sea level driven by ocean thermodynamic processes, is evaluated by subtracting the geoid height from the sea surface height. Altimetry missions has started in 1975 and regular time series of sea surface height with good mesoscale resolving capabilities ( $O(10^2)$  km) are available since the early 1990s. Indeed, since 1992 satellite altimetry measurements have always been covered by at least two satellite missions flying together.

**Step 2: Altimetry-derived geostrophic velocities.** Geostrophic currents are estimated from satellite altimetry, by solving the equation for geostrophic equilibrium, the balance between the horizontal pressure gradient force and the Coriolis force, as following:  $u = -\frac{g}{fR_T} \frac{\partial h_{ssh}}{\partial \varphi}$ ,  $v = -\frac{g}{fR_T \cos(\varphi)} \frac{\partial h_{ssh}}{\partial \lambda}$ , where  $g$  is the gravity,  $f$  the Coriolis parameter,  $R_T$  the Earth radius,  $h_{ssh}$  the sea surface height,  $\varphi$  the latitude and  $\lambda$  the longitude.

Two assumptions are made in this aim: a low Rossby number constrained by large scale circulation ( $> 10^3$  km) and the hydrostatic approximation allowing to neglect the baroclinic and atmospheric contributions to the pressure gradient. The low vertical stratification of the Southern Ocean induces a quasi-barotropic structure of the ACC: strong vertical coherence of the velocity field [see Phillips and Bindoff, 2014, and references therein]. Consequently, the altimetry-derived geostrophic field appears as a good estimator for horizontal transport in the ACC region over a large part of the water column (hundreds of meters). This thesis directly uses altimetry-derived geostrophic velocities computed by DUACS and distributed by CMEMS (product id: SEALEVEL\_GLO\_PHY\_L4\_REP\_OBSERVATIONS\_008.047).

**Step 3: Defining water parcel trajectories.** The velocity field derived from altimetry is here analysed with a Lagrangian approach. This consists in centring the coordinate

system on individual water parcels and following them during their flow. A key benefit of the Lagrangian approach is to produce a synthetic view of water masses' *histories* during a time period. The first step in this aim consists in computing numerical trajectories from the velocity field. A trajectory is defined as the integration of the position of the water parcels during a time laps, since its given initial position  $X_0$  at the initial time  $t_0$ . Mathematically, the variation of the position of the water parcel in function of time, noted  $dX/dt$ , equals to the velocity field  $V$  at the position  $X$  defined at the coordinates  $(x, y)$  and at the time  $t$ . Indeed the velocity field  $U$  is defined in the position  $X$  and at the time  $t$ . This results in resolving the following ordinary differential equation:

$$\begin{cases} \frac{dX(x,y)}{dt} = U(X_t(x,y), t) \\ X_{t_0}(x,y) = 0 \end{cases} \quad (1)$$

This differential equation can be resolved by discretizing the variable  $t$  and applying a numerical scheme. We thus define a step-size  $h$ , as following:  $h = t_{n+1} - t_n$ . By integrating the differential equation between  $t_n$  and  $t_{n+1}$  we obtain:

$$X_{t_{n+1}}(x,y) - X_{t_n}(x,y) = \int_{t_n}^{t_{n+1}} U(X_t(x,y), t) dt \quad (2)$$

A 4<sup>th</sup> order Runge Kutta (RK4) with  $h = 6$  hours, meaning 8 time steps by day, is applied for resolving this equation. RK4 approximates the integral in equation (2) with the Simpson method. This consists in replacing the function  $U(X_t(x,y), t)$  with a parabola intersecting the points  $X_n$  and  $X_{n+1}$  and the midpoint. Applied to the integral in equation (2) we obtain:

$$\int_{t_n}^{t_{n+1}} U(X_t(x,y), t) dt \simeq \frac{h}{6} [U(X_{t_n}(x,y), t_n) + 4U(X_{t_{n+\frac{1}{2}}}(x,y), t_{n+\frac{1}{2}}) + U(X_{t_{n+1}}(x,y), t_{n+1}))] \quad (3)$$

Therefore:

$$\begin{aligned}
 X_{t_{n+1}}(x, y) &= X_{t_n}(x, y) + \\
 &+ \frac{h}{6} \left[ U(X_{t_n}(x, y), t_n) + 4U(X_{t_{n+\frac{1}{2}}}(x, y), t_{n+\frac{1}{2}}) + U(X_{t_{n+1}}(x, y), t_{n+1}) \right] + \\
 &+ O(h^5)
 \end{aligned} \tag{4}$$

Where  $O(h^5)$  represents the local truncation error. By contrast, the total accumulated error is on the order of  $O(h^4)$ .

This equation is resolved with the following algorithm:

$$X_{n+1} = X_n + h \left[ \frac{1}{6}k_1 + \frac{1}{3}k_2 + \frac{1}{3}k_3 + \frac{1}{6}k_4 \right] \tag{5}$$

With  $k_1 = f(X_n, t_n)$ ;  $k_2 = f(X_n + \frac{1}{2}hk_1, t_n + \frac{1}{2}h)$ ;  $k_3 = f(X_n + \frac{1}{2}hk_2, t_n + \frac{1}{2}h)$ ;  $k_4 = f(X_n + hk_3, t_n + h)$ .

The function  $f(X_n, t_n)$  in equation (5) has to be resolved in both the  $u$  and  $v$  directions of the  $U$  velocity field. This Lagrangian computation code has been developed by F. d'Ovidio [d'Ovidio et al., 2004] and has been used in multiple applications, ranging from the analysis of bio-physical processes to more applied studies such as the support of conservation actions or the definition of monitoring networks [e.g., d'Ovidio et al., 2010, 2015; Sanial et al., 2015; Lehahn et al., 2018; cotté et al., 2011; Della Penna et al., 2015, 2017; Baudena et al., 2019]. In this thesis I apply this method and perform analyses of the Lagrangian trajectories in order to extract relevant information from them.

**Synthetic view of trajectories: Lagrangian plumes.** The ensemble of numerical trajectories contain a wide range of informations on oceanic dynamics. Lagrangian diagnostics are usually performed in order to extract synthetic and relevant information from “spaghetti-like” snapshots (as Figure 2.3A). A property which provides valuable information on the ocean circulation from Lagrangian trajectories is the “age” of water masses:

the transit time of particles between defined regions [d'Ovidio et al., 2015; Ardyna et al., 2017; van Sebille et al., 2018]. This type of analysis has been largely applied to study the delivery of sedimentary nutrients [d'Ovidio et al., 2015; Sanial et al., 2015; Ardyna et al., 2017; Della Penna et al., 2017]. In these cases the analysis consist in computing the distance in time of water masses to the continental shelves defined by a certain bathymetric level. In this thesis I apply a similar approach in order to reproduce the Lagrangian plumes stemming from any region suspected to introduce nutrients into the productive layer (this source region can be represented by an upwelling region, hydrothermal vents or seamounts). A Lagrangian plume is here considered as the ensemble of the water masses that have been in contact with a prescribed region within a time period. Figure 2.3 illustrates basic steps for the computation of the Lagrangian plume. Firstly, all the water masses of the study area are advected backward in time since a time period  $t_0$  for a time period  $\delta_t$  (in Fig 2.3  $\delta_t = 90$  days). Secondly, the trajectories that crossed within the time period  $\delta_t$  the target region (defined by the black circle in Fig 2.3) are selected (Figure 2.3B). Finally, we assign to each water parcel which was in contact to the interesting region in the period  $\delta_t$  before  $t_0$  the time stamp of its contact. Usually  $t_0$  is defined as the phytoplankton bloom period, in this case the method aims to compare the Lagrangian plume stemming from a prescribed region to the phytoplankton plumes observed in satellite maps. Therefore this Lagrangian analysis validates or not the hypothesis that water masses displaying high phytoplankton biomasses in satellite maps were in contact with a specific nutrient source in the previous few months.

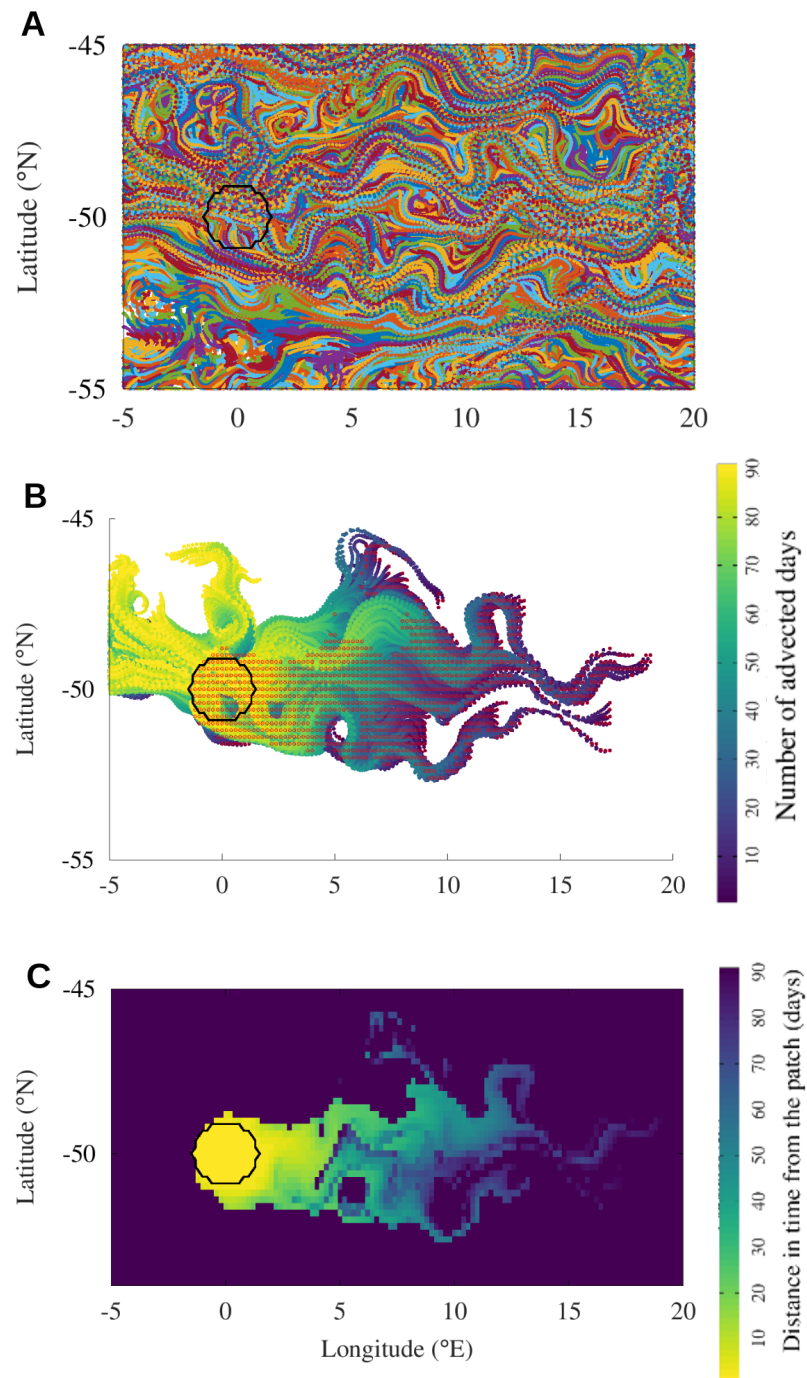


FIGURE 2.3: **Steps for the computation of a Lagrangian plume from a nutrient source (defined here by the black circle).** (A) All the water masses of the study region are advected backward since the 1<sup>st</sup> January 2015 ( $t_0$ ) for  $\delta_t = 90$  days. (B) We select the water masses that crossed the nutrient source in the  $\delta_t = 90$  days before  $t_0$ . Trajectories are displayed in function of the number of advected days since  $t_0$  and the red circles show the initial position of selected trajectories (i.e. at time  $t_0$ ). (C) Lagrangian plume: we assign to each water parcel previously selected its distance in time to the nutrient source.



## Part II

# Unravelling pathways for deep bottom-up forces in the open Southern Ocean





## Chapter 1

# Emergent nutrient sources: ecological role of hydrothermal vents

Our understanding of hydrothermal impact on ocean iron budget has dramatically changed during the last decade due to multiple key findings. Firstly, a modelling study has demonstrated that observations of dissolved iron in the Southern Ocean can only be replicated in simulations by including hydrothermal sources [Tagliabue et al., 2010]. Secondly, evidences of the stabilization of hydrothermal iron plumes over huge distances (thousands of kilometres) have been observed in several oceanic basins [Bennett et al., 2008; Wu et al., 2011; Resing et al., 2015; Fitzsimmons et al., 2017; Tagliabue and Resing, 2016]. These findings are substantiated by recent advances in ocean biogeochemistry: contrary to past paradigms, hydrothermal iron does not completely precipitate at the proximity of the vent. Indeed, iron's complexation with ligand keeps it in a stable form and makes it more bioavailable [Sander and Koschinsky, 2011; Bennett et al., 2008]. In addition, about 10% of dissolved iron (<200  $\mu\text{m}$ ) input from the hydrothermal vents to the deep ocean is in the form of nano-particulate pyrite which has been suggested to be more resistant

to oxidation than dissolved Fe(II) and FeS [Yücel et al., 2011]. Consequently, the role of hydrothermal iron in enhancing biological activity is suspected to be largely underestimated, especially in the iron-limited Southern Ocean [Tagliabue et al., 2010]. However, observational evidences supporting these conclusions are missing.

The two studies presented in this chapter are the first observational evidences of massive phytoplankton blooms stimulated by hydrothermal iron in the Southern Ocean. The [first study](#) considers an hydrothermal vent field located over the South-West Indian Ridge, while the [second one](#) investigates two hydrothermal vent fields situated over the Australian-Antarctic Ridge. My specific contribution to these studies was to reconstruct the horizontal connectivity pathways linking the intense phytoplankton blooms either to upwelled hydrothermally-influenced deep waters (Figure 4 E, F in section 1.2), either directly to the hydrothermal vent's locations (Supplementary Figure 3 in section 1.2). In both studies, I adopted a Lagrangian approach in order to test whether the phytoplankton biomasses observed could be reproduced by Lagrangian plumes stemming from the hydrothermal vents, as described in the introduction (subsection 2.2.2). In section 1.3, I summarise key findings of these studies, focusing on the role of horizontal connectivity pathways.

## 1.1 Ardyna et al., 2019: Hydrothermal vents trigger massive phytoplankton blooms in the Southern Ocean; Nature Communications

Here below is inserted the original manuscript by [Ardyna et al. \[2019\]](#).

## **1.2 Schine et al., 2021: Massive Southern Ocean phytoplankton bloom fed by iron of possible hydrothermal origin; Nature Communications**



Here below is inserted the original manuscript by [Schine et al. \[2021\]](#).

ARTICLE

<https://doi.org/10.1038/s41467-019-09973-6>

OPEN

# Hydrothermal vents trigger massive phytoplankton blooms in the Southern Ocean

Mathieu Ardyna<sup>1,2</sup>, Léo Lacour<sup>1,3</sup>, Sara Sergi<sup>4</sup>, Francesco d'Ovidio<sup>4</sup>, Jean-Baptiste Sallée <sup>4</sup>,  
Mathieu Rembauville<sup>1</sup>, Stéphane Blain<sup>5</sup>, Alessandro Tagliabue<sup>6</sup>, Reiner Schlitzer <sup>7</sup>, Catherine Jeandel<sup>8</sup>,  
Kevin Robert Arrigo<sup>2</sup> & Hervé Claustre<sup>1</sup>

Hydrothermal activity is significant in regulating the dynamics of trace elements in the ocean. Biogeochemical models suggest that hydrothermal iron might play an important role in the iron-depleted Southern Ocean by enhancing the biological pump. However, the ability of this mechanism to affect large-scale biogeochemistry and the pathways by which hydrothermal iron reach the surface layer have not been observationally constrained. Here we present the first observational evidence of upwelled hydrothermally influenced deep waters stimulating massive phytoplankton blooms in the Southern Ocean. Captured by profiling floats, two blooms were observed in the vicinity of the Antarctic Circumpolar Current, downstream of active hydrothermal vents along the Southwest Indian Ridge. These hotspots of biological activity are supported by mixing of hydrothermally sourced iron stimulated by flow-topography interactions. Such findings reveal the important role of hydrothermal vents on surface biogeochemistry, potentially fueling local hotspot sinks for atmospheric CO<sub>2</sub> by enhancing the biological pump.

<sup>1</sup>Sorbonne Université & CNRS, Laboratoire d'Océanographie de Villefranche (LOV), 181 Chemin du Lazaret, F-06230 Villefranche-sur-mer, France.

<sup>2</sup>Department of Earth System Science, Stanford University, Stanford, CA 94305, USA. <sup>3</sup>Takuvik Joint International Laboratory, Laval University (Canada) - CNRS (France), Département de biologie et Québec-Océan, Université Laval, Québec, Québec G1V 0A6, Canada. <sup>4</sup>Sorbonne Université, CNRS, IRD, MNHN, Laboratoire d'Océanographie et du Climat: Expérimentations et Approches Numériques (LOCEAN-IPSL), F-75005 Paris, France. <sup>5</sup>Sorbonne Université & CNRS, Laboratoire d'Océanographie Microbienne (LOMIC), Observatoire Océanologique, F-66650 Banyuls/mer, France. <sup>6</sup>Department of Earth, Ocean and Ecological Sciences, School of Environmental Sciences, University of Liverpool, Liverpool, UK. <sup>7</sup>Alfred Wegener Institute, Helmholtz-Center for Polar- and Marine Research, Am Alten Hafen 26, 27568 Bremerhaven, Germany. <sup>8</sup>LEGOS (Université de Toulouse, CNRS, CNES, IRD, UPS), 14 avenue Edouard Belin, 31400 Toulouse, France. Correspondence and requests for materials should be addressed to M.A. (email: [ardyna@stanford.edu](mailto:ardyna@stanford.edu))

Iron is an important resource limiting the efficiency of the biological pump over large areas of the global ocean<sup>1–3</sup>. Until recently, the role of hydrothermal activity in governing the ocean iron inventory and its effect on global biogeochemical cycles has been largely underestimated<sup>4</sup>. New discoveries regarding the distribution, number, type and activity of hydrothermal vent systems are forcing us to revisit existing paradigms related to hydrothermal vents and their impact on ocean biogeochemistry<sup>2,4,5</sup>. For example, a large plume of hydrothermal dissolved iron was recently observed extending several thousand kilometers westward from the southern East Pacific Rise across the South Pacific Ocean<sup>6</sup>. Based on these observations, estimates of the global hydrothermal dissolved iron input to the ocean interior has been increased to three to four gigamoles per year, which is more than fourfold higher than previous estimates<sup>6</sup>.

Because the Southern Ocean (SO) is the largest iron-limited region of the global ocean, local phytoplankton are particularly sensitive to iron inputs<sup>7,8</sup>. The current paradigm holds that iron supplied from continental margins and sea ice drive hot spots of biological activity in the SO<sup>8,9</sup>. However, global model simulations indicate that the biological pump can be directly impacted by hydrothermal iron released along ridges within and outside the SO<sup>10</sup>. Winter mixing and/or upwelling brings these deep iron-enriched waters to the surface in the SO where, when coupled with intense lateral stirring, they may play an important role in fueling planktonic blooms over wide areas<sup>11,12</sup>. However, there is no observational evidence supporting the conclusion by models that hydrothermal iron is an important source enhancing biological activity. Here, we combine data from new autonomous platforms and satellite-derived observations to show that the upwelled hydrothermally influenced deep waters can indeed stimulate massive phytoplankton blooms in the Southern Ocean.

## Results

**Two unexpectedly large open ocean blooms.** By analyzing a circumpolar compilation of phytoplankton blooms captured by BGC-Argo floats (117 phytoplankton blooms, Fig. 1a), we observed two unexpectedly massive phytoplankton blooms in typically High Nutrient Low Chlorophyll (HNLC) waters of the SO (Fig. 1, red dots; see also the Supplementary Note for similar patterns based on particle backscattering). These phytoplankton blooms (in 2014 and 2015; Fig. 2) were observed in the Indian Sector of the SO (30–38°E, 48–55°S) using two phytoplankton biomass proxies: chlorophyll *a* (Chl *a*) and particle backscattering (Fig. 2b, c). The magnitude of these blooms (maximum depth-integrated biomass of 83.0 and 96.5 mg Chl *a* m<sup>-2</sup>, respectively) is similar to those observed in highly iron-enriched waters downstream of the Crozet and Kerguelen Plateaus (mean 98.1 mg Chl *a* m<sup>-2</sup>; Fig. 1, green dots) and in proximity to the sea-ice edge (mean 70.0 mg Chl *a* m<sup>-2</sup>, purple dots), and more than twice that of HNLC waters of the SO (mean 42.0 mg Chl *a* m<sup>-2</sup>, blue dots).

Such levels of phytoplankton biomass can only be achieved by significant iron enrichment. However, the location of these blooms is far from typical iron sources such as shallow continental shelves, melting sea-ice (Fig. 1a), and atmospheric dust deposition<sup>13</sup>. Therefore, the most plausible iron source for these blooms is upwelling from deep waters. Interestingly, these two massive blooms are in the vicinity of the eastward-flowing Antarctic Circumpolar Current (ACC), directly downstream of an arc of known active hydrothermal vents<sup>14,15</sup> (from 3517 to 4170 m deep; Fig. 2a, b), which should elevate deep ocean iron concentrations, and also directly downstream of the Southwest Indian Ridge (SWIR), which could promote vertical mixing and thus deliver these iron-enriched waters to the surface. This is supported by a suite of evidence indicating that deep-waters in

the region have a strong hydrothermal vent signature and are therefore likely to be iron-enriched (Fig. 3); flow-topography interactions in the region enhance turbulence and vertical advection, so that deep-waters are efficiently transported to the surface (Fig. 4); and once waters reach the surface, they are efficiently transported downstream into two branches feeding the regions where we observed massive phytoplankton blooms (Fig. 4).

## Hydrothermally influenced waters downstream of the SWIR.

Hydrothermal vents along spreading ocean ridges release large amounts of primordial He originating from the Earth's mantle, which is associated with high  $\delta^3\text{He}$  isotopic signature.  $\delta^3\text{He}$  is a conservative tracer and is commonly used to detect the presence of hydrothermal vent fluids in oceanic waters<sup>6,16</sup>. It has also been shown that hydrothermal vents are associated with elevated concentrations of iron, resulting in a tight covariance with He<sup>6,16,17</sup>. In the only pseudo-Lagrangian study of dispersal of iron from a hydrothermal plume, a constant relationship between dissolved iron concentration and  $\delta^3\text{He}$  was observed<sup>6</sup>.

Two vertical sections of  $\delta^3\text{He}$  in the vicinity of the sampled blooms demonstrate a strong signature of hydrothermal vent activity in the waters of the SWIR region, which would imply iron-rich deep waters (Fig. 3). Along a meridional section at 30°E that crosses the SWIR, the high level of  $\delta^3\text{He}$  in waters above ~2000 m (10–12%) clearly indicates a hydrothermal signal between ~2000 m and the permanent thermocline (Fig. 3c). Note that  $\delta^3\text{He}$  drops above the permanent thermocline due to atmospheric exchange. Furthermore, a second section along ~55°S highlights the zonal variability in  $\delta^3\text{He}$ , whereby the elevated  $\delta^3\text{He}$  signature in deep water is only present downstream (east) of the SWIR (~25°E; Fig. 3b). These  $\delta^3\text{He}$  data clearly indicate that the arc of hydrothermal vents along the SWIR have a widespread influence on downstream iron release into waters between 2000 m and the permanent thermocline.

**Mixing by flow-topography interactions.** Furthermore, the dynamics associated with flow-topography interactions at the SWIR suggest that these hydrothermally-enriched deep waters are transported efficiently to the surface. Downstream of the SWIR, the flow is steered by topography into two branches associated with elevated eddy kinetic energy (EKE; one eastward branch around 50°S, and one southward branch around 35°E; Figs 3, 4a, b). Note that the trajectories of the two BGC-Argo floats (that drift at 1000 m) that recorded the two large blooms followed these two high EKE branches. This topographic flow increases EKE throughout the water column directly downstream, which likely enhances cross-stream buoyancy flux, whose vertical divergence is related to the upward transport of along-stream momentum<sup>12,18</sup>. In other words, deep waters are upwelled along the ACC branches downstream of the SWIR in the region of elevated EKE.

High-resolution numerical simulations of the dynamics of flow-topography interactions in the region<sup>12,18</sup> also strongly suggest that the ACC interacts with the SWIR. These numerical solutions<sup>12,18</sup> indeed highlight two signatures of these dynamics and the associated deep-water upwelling, including a deep enhancement of EKE and an along-stream shallowing of isopycnals at depth. Consistent with these simulations, we find that the study region is associated both with elevated EKE at depth (derived from Argo trajectory-based velocities, Fig. 4b; see the Methods for more details) and a large along-stream vertical displacement of isopycnals (shallowing; up to an increase of 0.2 kg m<sup>-3</sup> at 750 m in the region between 28 and 38°E; Fig. 4c, d; see the Methods for more details). Such observational evidence

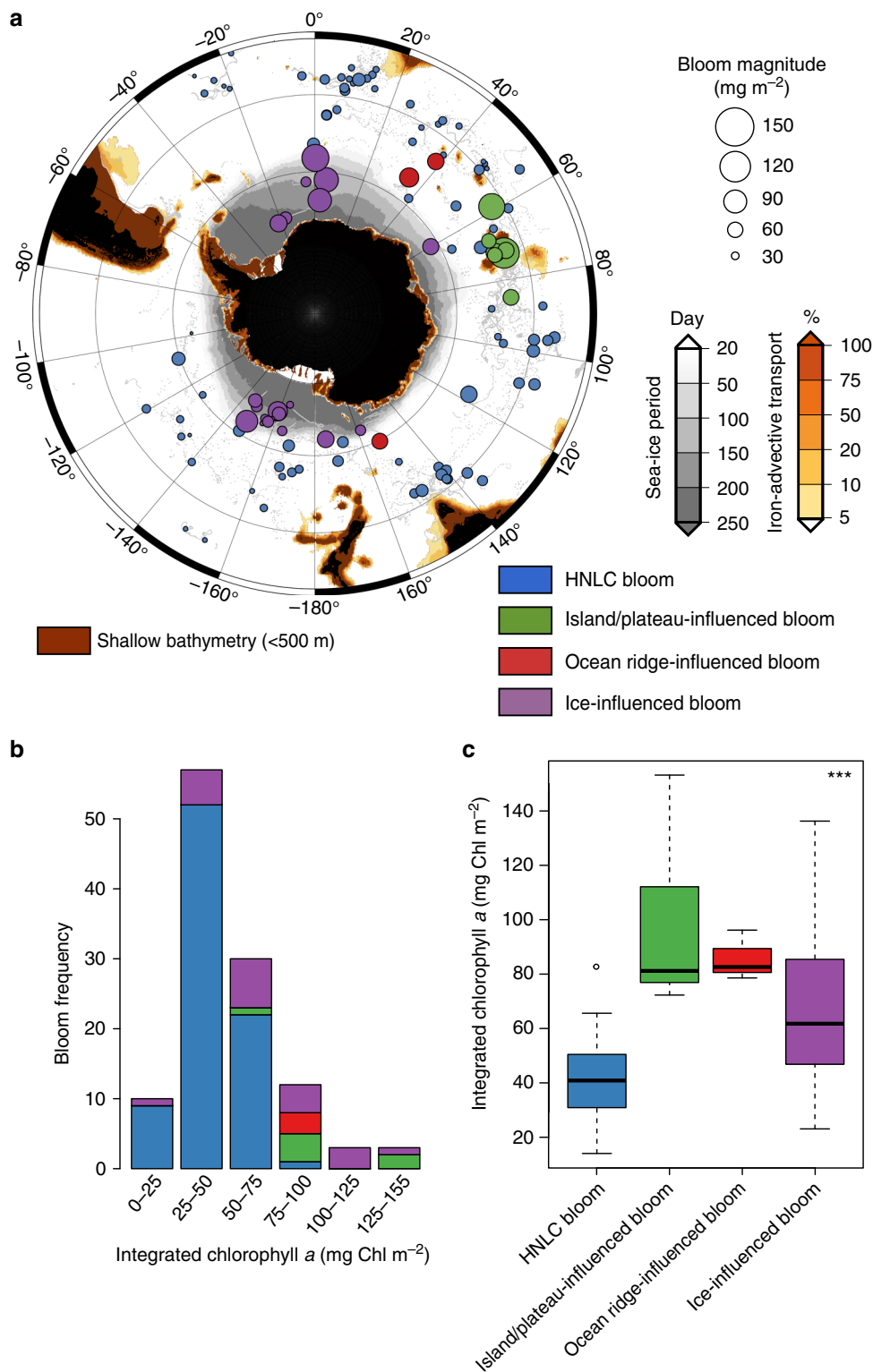


**Fig. 1** Phytoplankton bloom distribution, type and biomass in the Southern Ocean. Map **(a)** of the different bloom types (i.e., blue circles: HNLC; green circle: island/plateau-influenced; red circle: ocean ridge-influenced; purple circle: ice-influenced) sampled. The magnitude of the bloom (i.e., the maximum depth-integrated biomass) is related to the size of the colored circles. The gray dots indicate the individual float profiles. The red, orange, and gray zones are, respectively, shallow areas (>500 m), areas with downstream iron delivery (%; percent of iron remaining in a water parcel after scavenging relative to its initial concentration in shallow areas based on the Lagrangian modeling of horizontal iron delivery), and areas characterized by a seasonal sea ice cover. Histograms **(b)** of the frequency of and boxplot **(c)** according to the bloom type are displayed in relation to the bloom magnitude. In **c**, the top and bottom limits of each box are the 25th and 75th percentiles, respectively. The lines extending above and below each box, i.e., whiskers, represent the full range of non-outlier observations for each variable beyond the quartile range. The results of the Kruskal-Wallis H test are shown in panel **c** and depict regions with statistically significant differences between the magnitudes of the bloom at the 95 % level ( $p < 0.05$ ). Asterisks (\*\*\*) denote highly significant results ( $p < 0.0001$ )



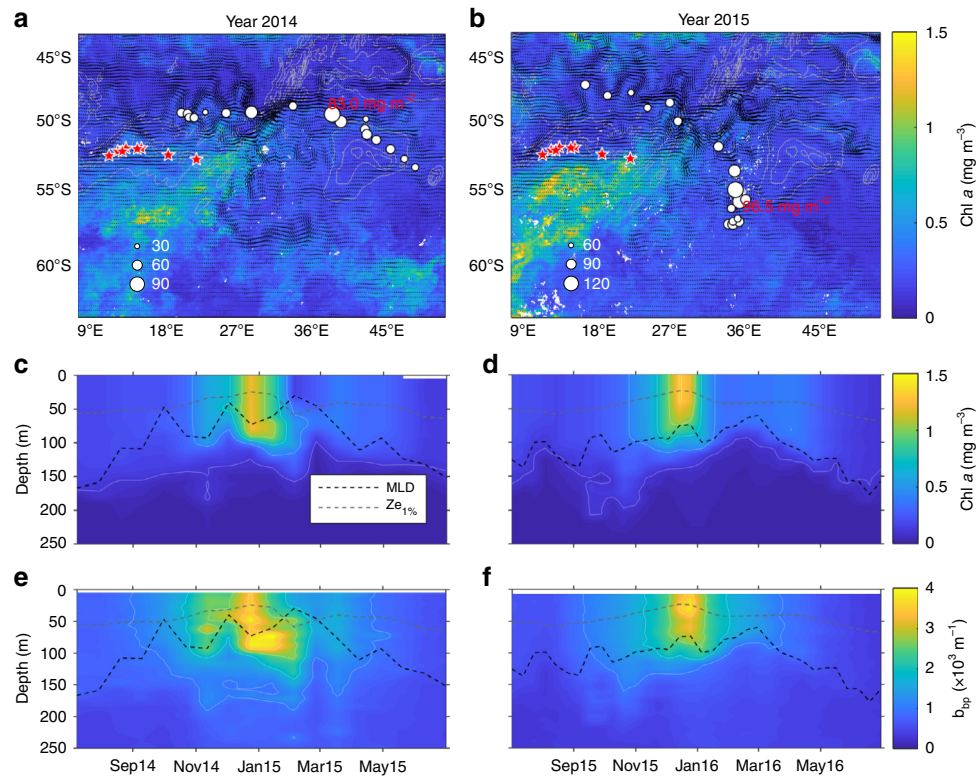


**Fig. 2** Massive phytoplankton blooms stimulated by upwelled hydrothermally influenced deep waters along the Southwest Indian Ridge (SWIR). Maps (**a** and **b**) of the SWIR in the Indian sector of the Southern Ocean and float trajectories. The maximum depth-integrated biomass (mg Chl  $m^{-2}$ ) is depicted according to the size of the circles. Satellite-derived surface chlorophyll *a* climatologies (8-days GLOBcolour composite products) were retrieved from November to January **a** 2014–2015 and **b** 2015–2016. Black arrows correspond to altimetry-derived geostrophic velocities (AVISO MADT daily product) averaged over the same period. Gray lines represent the 2000, 3000 and 4000 m isobaths. Time series of the 0–250 m vertical distribution of chlorophyll *a* (**c** and **d**) and backscattering (**e** and **f**) for the two BGC-Argo floats (WMO 6901585 and 2902130). The black and gray dashed lines are, respectively, representing the mixed layer depth (determined by a density-derived method with a density threshold of  $0.03 \text{ kg m}^{-3}$ ) and the euphotic zone depth (defined as the depth of 1% of surface irradiance according Morel et al.<sup>35</sup>; Eq. 10). The red stars indicate the position of hydrothermal vents from Tao et al.<sup>14</sup>

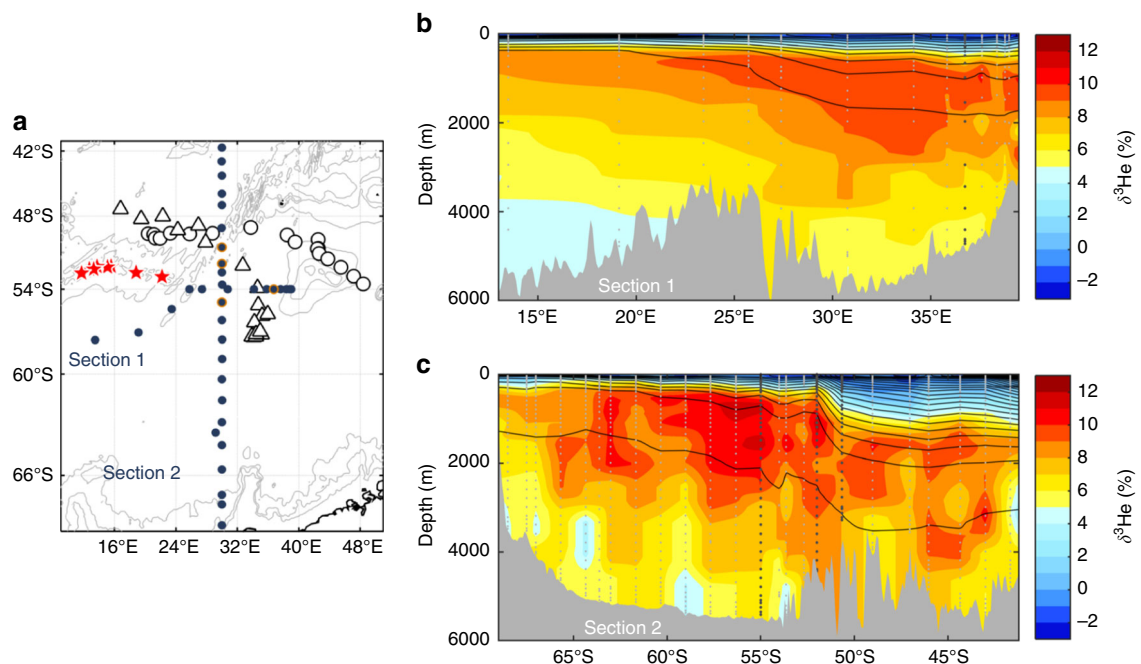


**Fig. 3** Hydrothermally influenced deep waters along the SWIR. Map (**a**) showing the locations of the bathymetry of the SWIR (contour levels: 2000, 3000, and 4000 m), the hydrothermal vents (red stars), the two BGC-Argo floats (black triangle dots: float WMO 6901585 and black circle dots: float WMO 2902130), and of the two sections (filled blue circle dots; **b** and **c**) of interpolated  $\delta^3\text{He}$ . Note that all the vertical  $\delta^3\text{He}$  profiles, where the surface eddy kinetic energy is high (EKE;  $>150 \text{ cm}^2 \text{ s}^{-2}$ ), have been highlighted by additional orange circle dots in **a** and by darker gray in **b** and **c**



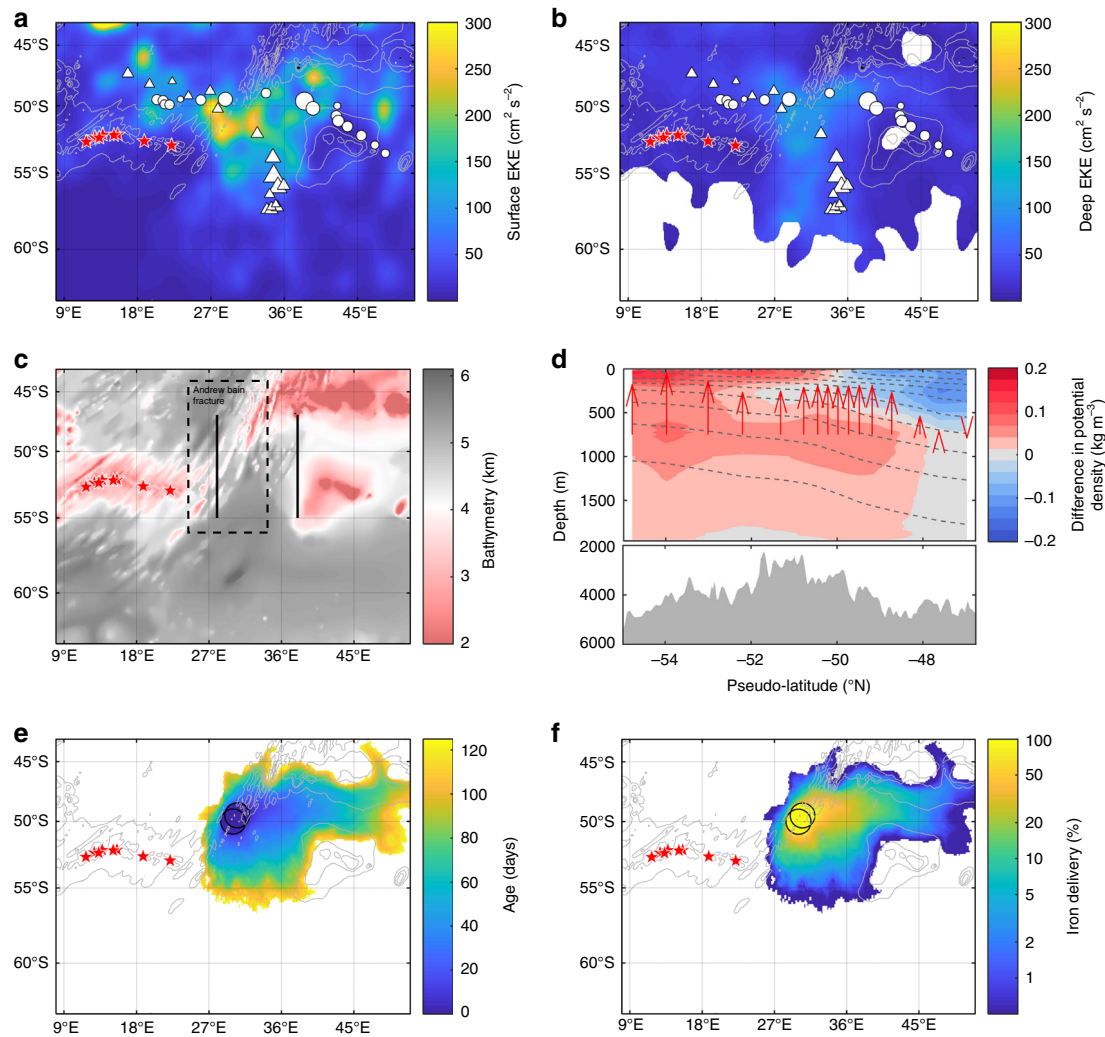


**Fig. 4** Topographically upwelled waters in the vicinity of the Antarctic Circumpolar Current along the SWIR. Maps of the eddy kinetic energy (EKE) at the surface (**a**) and at depth (**b**, approximately 1000 meters). The surface EKE was derived from altimetry-derived velocities (AVISO MADT daily product) over the 2003–2017 period. The deep EKE was calculated from the Argo-derived velocities during their parking depth and available in the ANDRO dataset (2000–2016). The maximum depth-integrated biomass ( $\text{mg Chl } a \text{ m}^{-2}$ ) is also depicted according the size of the dots (triangle: float WMO 6901585 and circle: float WMO 2902130). **c** Maps of bathymetry of the SWIR, the Andrew Bain fracture zone (as indicated by the dashed box; <http://www.marineregions.org/gazetteer.php?p=details&id=7253>) and the two meridional sections at 28°E and 38°E (between latitude 47°–55°S; plain black lines) where the difference in potential density  $\Delta\sigma$  shown in panel **d** was determined. **d** Climatological difference of potential density,  $\Delta\sigma$ , between the two meridional sections at 38°E and 28°E in the upper 2000 m (between latitude 47°–55°S). Gray shading represents the mean bottom topography between 28 and 38°E, and the red arrows are provided to show the sense of downstream isopycnal adjustment at 750-m depth. The difference in  $\Delta\sigma$  is an alongstream difference across the two sections, which is converted back to latitude for ease of reading (therefore referred to as pseudo-latitude). See the Methods for more details. **e–f** Satellite altimetry-derived Lagrangian modeling of the iron pathways from the departure of the SWIR as shown in **e** age (days since having left the SWIR) and in **f** iron delivery. Black circles in **e–f** indicate the origin of the iron pathways in the surface layer. The red stars in **a–c**, **e** and **f** are related to the position of hydrothermal vents from Tao et al.<sup>14</sup>. The continuous and dashed gray lines indicate, respectively, the bathymetry (**a**, **b**, **e** and **f**) of the SWIR (contour levels: 2000, 3000, and 4000 m) and the isopycnals (**d**)

suggests that deep, iron rich waters are upwelled directly downstream of the SWIR in the ACC path.

**Horizontal stirring of hydrothermally influenced waters.** To evaluate the advection of upwelled hydrothermally influenced (and likely iron-enriched) waters through horizontal stirring at the surface, we used a Lagrangian satellite altimetry-based method<sup>19</sup>. Briefly, this approach is based on a simple exponential model for iron scavenging over trajectories derived from altimetry and has been extensively validated at similar latitudes in the Kerguelen region<sup>19–21</sup>. As expected, the particles follow the two branches of the ACC and reach the region where we observed

massive bloom 1–2 months later, delivering 10–30% of the surface iron (assuming some particle scavenging<sup>8,19</sup>) contained in waters where the particles originated (Fig. 4e, f). Together, this observationally-based evidence supports a scenario whereby deep-waters are upwelled directly downstream of the SWIR in the ACC path and are then horizontally transported to the area where we observed the large-scale, intense phytoplankton blooms.

**Discussion**

Over the last decade, the conceptual view of the impact of hydrothermal activity on the iron cycle has drastically changed (mostly due to the findings of GEOTRACES expeditions). Model

simulations now suggest that ocean ventilation pathways are potential vectors of spreading hydrothermal trace-elements (including iron) in the SO, hence potentially enhancing the efficiency of the biological pump<sup>10</sup>. Documenting the dynamics of these pathways is particularly challenging because of the remoteness and the extreme conditions of the SO, and the need to be in the right place at the right time. The network of BGC-Argo floats offers the first observational evidence to confirm inferences from models about how hydrothermally stimulated biology is correlated to where <sup>3</sup>He is being upwelled<sup>10</sup>, and more importantly, the direct effect of hydrothermal vents on surface biological activity.

Such mechanisms are likely to be more common than we suspected in the SO (as well as in the global ocean), due to the high number of hydrothermal vents (i.e., those identified with many more still undiscovered) and topographically upwelling-favorable features. Here, we captured two massive blooms primarily supported by iron hydrothermal origin. Note that a fraction of hydrothermal iron reported here could also be transported from other basins and remote hydrothermal vents, given evidence suggesting that hydrothermal iron is largely stabilized and so may have a long residence time<sup>4,10</sup>. These results possibly suggest that the other blooms thought to be linked to other iron sources may in fact be due to hydrothermal activity. For example, we suspect that an additional large bloom (maximum depth-integrated biomass of 79.0 mg Chl *a* m<sup>-2</sup>) in proximity to the sea-ice and an active hydrothermal vent in the northwest Ross Sea (AAR KR2<sup>15</sup>), may be influenced by hydrothermal iron (Fig. 1, red dot).

The implications of such hot spots of biological activity supported by hydrothermal iron are highly significant, by potentially supporting marine ecosystems and sequestering carbon in the SO under the appropriate physical regimes. Traditionally, we assumed that SO phytoplankton blooms were being supported either from continental margin or sea-ice derived iron, but here we demonstrate that hydrothermalism is one additional important forcing for phytoplankton blooms, when associated with the right physics. In summary, a circumpolar analysis is clearly needed to evaluate the overall impact of hydrothermal activity on the carbon cycle in the SO, which appears to trigger local hotspots of enhanced biological pump activity and increase its potential as a sink for atmospheric CO<sub>2</sub>.

## Methods

**Satellite-derived products.** A satellite-derived Level-3 data set of Chl *a* concentration (mg m<sup>-3</sup>) was obtained from the European Space Agency's GlobColour project (<http://www.globcolour.info>). The 8-day composite Chl *a* concentrations using standard Case 1 water algorithms were used (i.e., OC4Me for Medium-Resolution Imaging Spectrometer, and OC3v5 for Moderate Resolution Imaging Spectroradiometer/Visible Infrared Imaging Radiometer Suite sensors). The altimetry-derived geostrophic velocities (AVISO MADT daily product) were produced by CLS/AVISO (Collecte Localisation Satellites/Archiving, Validation, and Interpretation of Satellite Oceanographic data), with the support from the CNES (Centre National d'Etudes Spatiales; <http://www.aviso.altimetry.fr/duacs/>).

**BGC-Argo network.** The BGC-Argo dataset used in the present study is publicly available at <ftp://ftp.ifremer.fr/ifremer/argo/dac/coriolis/>, an Argo Global Data Assembly Center. This dataset represents an international initiative by compiling 132 BGC-Argo floats (a total of 14,415 stations) from AOML-NOAA, BODC, CORIOLIS, CSIRO, and INCOIS. It covers the time period from July 2010 to June 2017 and involves a variety of float platforms (NKE's PROVOR, Webb's APEX, and SeaBird's NAVIS) performing different missions (in dive depths, frequency of profiling, and data acquisition) and equipped with different sensors for measuring Chl *a* and backscattering at 700 nm (Seabird MCOMS, WETLabs Eco-Triplet, and Eco-FLBB).

A quality control procedure was achieved on the CTD<sup>22</sup>, Chl *a*<sup>23</sup> and backscattering<sup>24</sup> data. Fluorescence data were corrected for non-photochemical quenching on daytime profiles following the method of Xing et al.<sup>25</sup> as follows: the maximum Chl *a* value above the mixed layer depth (MLD), defined as a density difference of 0.03 kg m<sup>-3</sup> from a reference value at 10 m, is extrapolated toward the surface. Fluorescence data are then converted to Chl *a* concentration (mg m<sup>-3</sup>) by

first applying the calibration (dark value and slope) and then multiplying by a SO-specific correction factor.

To decide which calibration factor to apply, we carried out a robust analysis by applying the radiometric method of Xing et al.<sup>6</sup> to retrieve F<sub>490</sub> (a refined calibration factor with respect to factory calibration) based on all available BGC-floats equipped with a downward irradiance sensor at 490 nm (OC4 radiometer, Satlantic). We allocated the various BGC-Argo profiles according to SO provinces to detect any potential intra-regional variability in F<sub>490</sub>. The average F<sub>490</sub> within provinces ranges between 0.26 and 0.33 (Supplementary Fig. 1, analysis of 3321 profiles), which translates into an overestimation factor of 3 to 4 with respect to the factory calibration. This value is actually lower than overestimates derived from HPLC Chl *a*<sup>26,27</sup>. We note here that these HPLC-based estimates (1) are relevant to a spatio-temporal domain restricted to the float deployment (the estimated correction factor might change as environment and community composition change during the float journey) and (2) present a large (yet unexplained) variability. Here, we use a conservative value of 0.3 for F<sub>490</sub> (corresponding to a factory calibration overestimation of 3.3). This value has the advantage of integrating a broad spatio-temporal domain (e.g., winter conditions) and a large dataset for the estimation of this correction (more than 3300 profiles).

**ANDRO dataset.** The ANDRO atlas ASCII file (available at <http://www.coriolis.eu.org/>) contains the float parking pressure (actually a representative parking pressure which is generally an average of the measured pressures during float drift at depth) and temperature, deep and surface displacements, and associated times, deep and surface associated velocities with their estimated errors (see Ollitrault and Rannou<sup>28</sup>). ANDRO data originate from AOML, Coriolis, JMA, CSIRO, BODC, MEDS, INCOIS, KORDI, KMA, and CSIO and represent a total of 6271 floats contributing to 612,462 displacements.

Each float cycle (deep displacement between two profiles) provides an estimate of the zonal and meridional current velocities at their drifting depth (mostly around 1000 m). From 2002 to 2016, around 21,300 cycles were available close to the SWIR (Supplementary Fig. 2). These velocities were binned into 1° by 1° boxes and then averaged in space and time. Only the box containing more than 5 data points were kept. Standard deviation of the zonal (*u*) and meridional (*v*) velocity components in each box were used to calculate the mean deep eddy kinetic energy (EKE) as follows:

$$\overline{\text{EKE}} = \frac{1}{2} (u^2 + v^2) \quad (1)$$

where the overbar denotes the time average over the whole period (2002–2016). EKE was then interpolated on a finer grid by a Gaussian correlation function, weighted by the local number of data, with a decorrelation radius of 100 km.

**Helium dataset.** The helium data were extracted from the GLObal Ocean Data Analysis Project (GLODAP) Version 2, a cooperative effort to coordinate global synthesis projects funded through NOAA/DOE and NSF as part of the Joint Global Ocean Flux Study–Synthesis and Modeling Project (JGOFS-SMP)<sup>29</sup>. The GLODAP Version 2 data product (available at <https://www.glodap.info>) is composed of data from 724 scientific cruises covering the global ocean. Here, two different expeditions (06AQ19960317; March 23–31, 1996 on the *Polarstern*) and (35MF19960220; February 28–March 25, 1996 on the *Marion Dufresne*) were used to generate the two sections of δ<sup>3</sup>He.

**Isopycnals between meridional section.** A combination of hydrographic profiles from different sources are used to construct a 3-D climatology of potential density in the region 0–55°E and 55–45°S, with a half degree horizontal resolution, and a 25 m vertical resolution.

We use three distinct sources of observations to maximize the number of profiles. The first set of observations is conductivity-temperature-depth (CTD) data from ship-recorded observations during the period 1906–2016 from the NOAA World Ocean Database (<https://www.nodc.noaa.gov/OC5/SELECT/dbsearch/dbsearch.html>). We only use profiles that have a quality control flag of 1, containing information on their position, date, temperature, and salinity. The second set of observations we use is float observations from the Argo international program. The Argo float profiles of pressure, salinity, and temperature used in this study were gathered in the period 2002–2016. They provide temperature and salinity between 0 and 2000 m. We only use profiles that have a quality control flag of 1, and contain information on their position, date, temperature, and salinity. As a final data set, we use profiles derived from the animal-borne sensor program MEOP (<http://www.meop.net/>; Treasure et al.<sup>30</sup>). Similar to the other datasets, we only use profiles with control flag of 1, and that contains position, date, temperature, and salinity. Altogether, we gathered 33096 profiles in the region 0–55°E–55–45°S.

From this dataset, we computed potential density for each 25 m vertical interval between the sea surface and 2000 m. Then, for each interval, we produced maps of climatological fields of potential density using an Optimal Interpolation procedure. The Optimal Interpolation and gridding method are described in detail in Schmidtko et al.<sup>31</sup>. As a brief summary, we interpolate onto a 0.5° grid in the region 0–55°E–55–45°S. We used a 550 km isotropic decorrelation scale, incorporating an anisotropic isobath-following component using a “Fast Marching” algorithm, as

well as front-sharpening components. In addition, recent data are emphasized in the mapping, which produces a climatology typical of the years 2000–2010 (see Schmidtko et al.<sup>31</sup> for more details on the mapping).

Two vertical sections of density are extracted at 28°E and 38°E from the produced climatology:  $\sigma_{28^\circ}(\text{P, lat})$  and  $\sigma_{38^\circ}(\text{P, lat})$ . Because the ACC is not entirely zonal, comparing the density structure of these two sections as a zonal difference would compare density structure from south and north of given ACC fronts. Instead, we determined how the density structure differed between 28°E to 38°E but alongstream, i.e., following the ACC structures. For that, we use the dynamical height (dh) provided by AVISO for the period 1993–2012 (<http://www.aviso.altimetry.fr/>) at these two sections to convert  $\sigma_{28^\circ}(\text{P, lat})$  and  $\sigma_{38^\circ}(\text{P, lat})$  into  $\sigma_{28^\circ}(\text{P, dh})$  and  $\sigma_{38^\circ}(\text{P, dh})$ . Because fronts and jets tend to follow individual contours of dynamical height (e.g., Sokolov and Rintoul<sup>32</sup>; Sallée et al.<sup>33</sup>), comparing these two sections in dynamic height coordinate ensures an alongstream comparison, i.e., dynamically consistent with regards to the ACC. We therefore produce a difference section:  $\Delta\sigma(\text{P, dh})$ , and using the mean dynamic height in the sector 28–38°E, we produce a mean relationship between dynamic height and latitude:  $\text{lat} = f(\text{dh})$ , where lat is referred to as pseudo-latitude, which we use to produce  $\Delta\sigma(\text{P, lat})$ .

**Lagrangian modeling of horizontal iron delivery.** An advection scheme based on altimetry was used here to estimate iron delivery due to horizontal stirring from (1) shallow bathymetry (<500 m; as shown in Fig. 1 and in Ardyna et al.<sup>8</sup>) and from (2) the initial location of the iron pathways in the surface layer along the SWIR (Fig. 4e, f). According to the analysis on vertical divergence (Fig. 4d), the origin of the iron pathways in the surface layer is located in the area of vertical displacement of isopycnals, suggesting the upwelling on the SWIR corresponds to the Andrew Bain fracture zone (see Fig. 4c). This feature is located between (24.5°E–56°S) and (34.2°E–44°S) (<http://www.ngdc.noaa.gov/gazetteer/>). Thus, the enrichment of the two BGC-Argo floats was identified in the region where the floats crossed this geological structure with a high isopycnal adjustment (Fig. 4d). This area has been represented by two overlapping disks centered in (30°E–50°S and 30.5°E–49.5°S), and with a 1° radius, as shown in Fig. 4e, f. We note that another possible upwelling region may occur north or south to this area, according to the analysis of vertical displacement of isopycnals (Fig. 4d).

The advection scheme seeds each location of the study region with a spatial resolution of 1/4° (Fig. 1) and 1/8° (Fig. 4e–f). Trajectories are derived from surface velocities by applying a Runge–Kutta fourth-order scheme with a time step of 6 h, in which velocity fields have been linearly interpolated in both space and time. The advection scheme then finds the particle's most recent contact with an iron source (shallow bathymetry and upwelled input along the SWIR) and provides the time at which the contact took place. The iron content of each particle that was in contact with a potential source of iron was estimated with an exponential scavenging relation. This relation reproduces the decreasing concentration of bioavailable iron along the trajectory after the contact with the iron source. This approach was initially developed for predicting the development of the Kerguelen phytoplanktonic plume<sup>19</sup> and thereafter extended to the entire Southern Ocean<sup>8</sup>. The model has been calibrated and validated in the Crozet and Kerguelen regions by combining satellite data (altimetry and ocean color), lithogenic isotopes, iron measurements, and drifters<sup>19–21</sup> (see d'Ovidio et al.<sup>19</sup> for further details). Here the advection scheme is applied to the period 2010–2015 and for the planktonic bloom season, November to March, in order to obtain a mean climatological signal.

**Bloom characterization.** To determine the bloom magnitude, each float time series was divided into individual annual cycles, starting on 1 July. Cycles that do not cover the theoretical bloom period (from early November to late February the next year) with at least eight float profiles were discarded. For each remaining cycle, float profiles were binned into a 20-day period corresponding to the decorrelation scale of float Chl *a* records<sup>34</sup>. The magnitude of the bloom was then computed as the maximum in integrated Chl *a* biomass from the surface down to either the MLD or the euphotic depth, whichever was deeper. The euphotic depth is the depth at which light is 1% of its surface value, based on the surface Chl *a* according to Morel et al.<sup>35</sup>.

## Data availability

All the data used in this research are freely available and may be downloaded through the links detailed in the Methods section.

Received: 29 June 2018 Accepted: 8 April 2019

Published online: 05 June 2019

## References

- Moore, J. K., Doney, S. C., Glover, D. M. & Fung, I. Y. Iron cycling and nutrient-limitation patterns in surface waters of the World Ocean. *Deep Sea Res. Pt. 2* **49**, 463–507 (2001).

- Tagliabue, A. et al. The integral role of iron in ocean biogeochemistry. *Nature* **543**, 51–59 (2017).
- Boyd, P. W. & Ellwood, M. J. The biogeochemical cycle of iron in the ocean. *Nat. Geosci.* **3**, 675 (2010).
- Tagliabue, A. et al. Hydrothermal contribution to the oceanic dissolved iron inventory. *Nat. Geosci.* **3**, 252–256 (2010).
- Tagliabue, A., Aumont, O. & Bopp, L. The impact of different external sources of iron on the global carbon cycle. *Geophys. Res. Lett.* **41**, 920–926 (2014).
- Resing, J. A. et al. Basin-scale transport of hydrothermal dissolved metals across the South Pacific Ocean. *Nature* **523**, 200–203 (2015).
- Boyd, P. W., Arrigo, K. R., Strzpek, R. & van Dijken, G. L. Mapping phytoplankton iron utilization: insights into Southern Ocean supply mechanisms. *J. Geophys. Res.* **117**, C06009 (2012).
- Ardyna, M. et al. Delineating environmental control of phytoplankton biomass and phenology in the Southern Ocean. *Geophys. Res. Lett.* **44**, 5016–5024 (2017).
- Arrigo, K. R., van Dijken, G. L. & Bushinsky, S. Primary production in the Southern Ocean, 1997–2006. *J. Geophys. Res.* **113**, C08004 (2008).
- Tagliabue, A. & Resing, J. Impact of hydrothermalism on the ocean iron cycle. *Phil. Trans. R. Soc. A* **374**, 20150291 (2016).
- Tagliabue, A. et al. Surface-water iron supplies in the Southern Ocean sustained by deep winter mixing. *Nat. Geosci.* **7**, 314–320 (2014).
- Tamsitt, V. et al. Spiraling pathways of global deep waters to the surface of the Southern Ocean. *Nat. Commun.* **8**, 172 (2017).
- Jickells, T. D. & Moore, C. M. The importance of atmospheric deposition for ocean productivity. *Annu. Rev. Ecol. Evol. Syst.* **46**, 481–501 (2015).
- Tao, C. et al. First active hydrothermal vents on an ultraslow-spreading center: Southwest Indian Ridge. *Geology* **40**, 47–50 (2012).
- Beaulieu, S. E. InterRidge Global Database of Active Submarine Hydrothermal Vent Fields: prepared for InterRidge, Version 3.4. (World Wide Web electronic publication, 2015).
- Saito, M. A. et al. Slow-spreading submarine ridges in the South Atlantic as a significant oceanic iron source. *Nat. Geosci.* **6**, 775 (2013).
- Boyle, E. A., Bergquist, B. A., Kayser, R. A. & Mahowald, N. Iron, manganese, and lead at Hawaii Ocean Time-series station ALOHA: Temporal variability and an intermediate water hydrothermal plume. *Geochim. Cosmochim. Acta* **69**, 933–952 (2005).
- Thompson, A. F. & Naveira Garabato, A. C. Equilibration of the Antarctic Circumpolar Current by Standing Meanders. *J. Phys. Oceanogr.* **44**, 1811–1828 (2014).
- d'Ovidio, F. et al. The biogeochemical structuring role of horizontal stirring: Lagrangian perspectives on iron delivery downstream of the Kerguelen Plateau. *Biogeosciences* **12**, 5567–5581 (2015).
- Sanial, V. et al. Use of Ra isotopes to deduce rapid transfer of sediment-derived inputs off Kerguelen. *Biogeosciences* **12**, 1415–1430 (2015).
- Sanial, V. et al. Study of the phytoplankton plume dynamics off the Crozet Islands (Southern Ocean): a geochemical-physical coupled approach. *J. Geophys. Res. Oceans* **119**, 2227–2237 (2014).
- Wong, A., Keeley, R., Carval, T. Argo Quality Control Manual For CTD and Trajectory Data. Argo <https://doi.org/10.13155/33951> (Argo data management, 2015).
- Schmechtig, C., Claustre, H., Poteau, A. & D'Ortenzio, F. Bio-Argo quality control manual for the Chlorophyll-A concentration. 1–16 <https://doi.org/10.13155/35385> (2014).
- Schmechtig, C. et al. Processing Bio-Argo particle backscattering at the DAC level. 1–15 <https://doi.org/10.13155/39459> (Argo data management, 2016).
- Xing, X. et al. Combined processing and mutual interpretation of radiometry and fluorimetry from autonomous profiling Bio-Argo floats: Chlorophyll a retrieval. *J. Geophys. Res.* **116**, C06020 (2011).
- Roesler, C. et al. Recommendations for obtaining unbiased chlorophyll estimates from in situ chlorophyll fluorometers: a global analysis of WET Labs ECO sensors. *Limnol. Oceanogr. Methods* **15**, 572–585 (2017).
- Haëntjens, N., Boss, E. & Talley, L. D. Revisiting Ocean Color algorithms for chlorophyll a and particulate organic carbon in the Southern Ocean using biogeochemical floats. *J. Geophys. Res.* **122**, 6583–6593 (2017).
- Ollitrault, M. & Rannou, J.-P. ANDRO Dataset contents and format. (2013).
- Olsen, A. et al. The Global Ocean Data Analysis Project version 2 (GLODAPv2)—an internally consistent data product for the world ocean. *Earth Syst. Sci. Data* **8**, 297–323 (2016).
- Treasure, A. M. et al. Marine mammals exploring the oceans pole to pole: a review of the MEOP Consortium. *Oceanography* **30**, 132–138 (2017).
- Schmidtko, S., Johnson, G. C. & Lyman, J. M. MIMOC: A global monthly isopycnal upper-ocean climatology with mixed layers. *J. Geophys. Res.* **118**, 1658–1672 (2013).
- Sokolov, S. & Rintoul, S. R. Multiple Jets of the Antarctic Circumpolar Current South of Australia. *J. Phys. Oceanogr.* **37**, 1394–1412 (2007).
- Sallée, J. B., Speer, K. & Morrow, R. Response of the Antarctic Circumpolar Current to Atmospheric Variability. *J. Clim.* **21**, 3020–3039 (2008).

34. Boss, E. & Behrenfeld, M. In situ evaluation of the initiation of the North Atlantic phytoplankton bloom. *Geophys. Res. Lett.* **37**, L18603 (2010).
35. Morel, A. et al. Examining the consistency of products derived from various ocean color sensors in open ocean (Case 1) waters in the perspective of a multi-sensor approach. *Remote Sens. Environ.* **111**, 69–88 (2007).

### Acknowledgements

M.A. was supported by a CNES (Centre National d'Etudes Spatiales) Postdoctoral Fellowship and by a European Union's Horizon 2020 Marie Skłodowska-Curie grant (no. 746748). This work represents a contribution to the remOcean project (REMotely sensed biogeochemical cycles in the OCEAN, GA 246777) funded by the European Research Council and to the project SOCLIM (Southern Ocean and climate) supported by the French research program LEFE-CYBER of INSU-CNRS, the Climate Initiative of the foundation BNP Paribas, the French polar institute (IPEV), the CNES Tosca/OSTST (project LAECOS) and Sorbonne Université. J.-B.S. was funded by the European Research Council (ERC) under the European Union's Horizon 2020 research and innovation program (grant agreement 637770). A.T. was funded by the European Research Council (ERC) under the European Union's Horizon 2020 research and innovation program (grant agreement 724289). We would like to thank the international agencies and programs, including the U.S. National Science Foundation's Southern Ocean Carbon and Climate Observations and Modeling (SOCCOM) for freely providing access to their float data.

### Author contributions

M.A., L.L., S.S., F.d'O., J.-B.S., M.R., A.T. conducted the data analysis. M.A., J.-B.S., A.T., F.d'O., K.R.A. wrote the manuscript. All authors contributed to the ideas and commented on the manuscript.

### Additional information

**Supplementary Information** accompanies this paper at <https://doi.org/10.1038/s41467-019-09973-6>.

**Competing interests:** The authors declare no competing interests.

**Reprints and permission** information is available online at <http://npg.nature.com/reprintsandpermissions/>

**Journal peer review information:** *Nature Communications* thanks Veronica Tamsitt for their contribution to the peer review of this work. Peer reviewer reports are available.

**Publisher's note:** Springer Nature remains neutral with regard to jurisdictional claims in published maps and institutional affiliations.







**Open Access** This article is licensed under a Creative Commons Attribution 4.0 International License, which permits use, sharing, adaptation, distribution and reproduction in any medium or format, as long as you give appropriate credit to the original author(s) and the source, provide a link to the Creative Commons license, and indicate if changes were made. The images or other third party material in this article are included in the article's Creative Commons license, unless indicated otherwise in a credit line to the material. If material is not included in the article's Creative Commons license and your intended use is not permitted by statutory regulation or exceeds the permitted use, you will need to obtain permission directly from the copyright holder. To view a copy of this license, visit <http://creativecommons.org/licenses/by/4.0/>.

© The Author(s) 2019



# Massive Southern Ocean phytoplankton bloom fed by iron of possible hydrothermal origin

Casey M. S. Schine <sup>1✉</sup>, Anne-Carlijn Alderkamp<sup>2</sup>, Gert van Dijken <sup>1</sup>, Loes J. A. Gerringa<sup>3</sup>, Sara Sergi<sup>4</sup>, Patrick Laan<sup>3</sup>, Hans van Haren<sup>3</sup>, Willem H. van de Poll <sup>5</sup> & Kevin R. Arrigo <sup>1</sup>

Primary production in the Southern Ocean (SO) is limited by iron availability. Hydrothermal vents have been identified as a potentially important source of iron to SO surface waters. Here we identify a recurring phytoplankton bloom in the high-nutrient, low-chlorophyll waters of the Antarctic Circumpolar Current in the Pacific sector of the SO, that we argue is fed by iron of hydrothermal origin. In January 2014 the bloom covered an area of ~266,000 km<sup>2</sup> with depth-integrated chlorophyll *a* > 300 mg m<sup>-2</sup>, primary production rates >1 g C m<sup>-2</sup> d<sup>-1</sup>, and a mean CO<sub>2</sub> flux of -0.38 g C m<sup>-2</sup> d<sup>-1</sup>. The elevated iron supporting this bloom is likely of hydrothermal origin based on the recurrent position of the bloom relative to two active hydrothermal vent fields along the Australian Antarctic Ridge and the association of the elevated iron with a distinct water mass characteristic of a nonbuoyant hydrothermal vent plume.

<sup>1</sup>Department of Earth System Science, Stanford University, Stanford, CA 94305, USA. <sup>2</sup>Biology Department, Foothill College, Los Altos Hills, CA 94022, USA. <sup>3</sup>Royal Netherlands Institute for Sea Research (NIOZ), PO Box 59, 1790 AB Den Burg, the Netherlands. <sup>4</sup>Sorbonne Université, CNRS, IRD, MNHN, Laboratoire d'Océanographie et du Climat: Expérimentations et Approches Numériques (LOCEAN-IPSL), F-75005 Paris, France. <sup>5</sup>Department of Ocean Ecosystems, Energy, and Sustainability Research Institute Gronigen, Faculty of Science and Engineering, University of Groningen, Nijenborgh 7, 9747 AG Groningen, the Netherlands. ✉email: [cmsmith9@stanford.edu](mailto:cmsmith9@stanford.edu)

Primary productivity in the Southern Ocean (SO) is critical in governing atmospheric CO<sub>2</sub> levels<sup>1</sup>. Because net primary productivity (NPP) in the SO is limited by the availability of iron (Fe)<sup>2–4</sup>, understanding the distribution of Fe availability in the SO and its relationship to spatial patterns in NPP is essential to quantify the capacity of the SO to act as a carbon sink.

In 2010, Tagliabue et al.<sup>5</sup> proposed that Fe of hydrothermal origin is an essential part of the SO Fe budget and that the observed Fe distribution in the SO cannot be replicated without the inclusion of hydrothermal sources of Fe. Tagliabue et al.<sup>5</sup> further proposed that the utilization of hydrothermal Fe by phytoplankton fuels increased NPP in the SO that results in 5–30% more carbon export. The first report of hydrothermal vent emissions fueling a large phytoplankton bloom was from the Indian sector of the SO around 40°E near the Southwest Indian Ridge (SWIR). Ardyna et al.<sup>6</sup> used historical measurements of elevated δ<sup>3</sup>He to suggest that deep water concentrations of Fe in the vicinity of the bloom (observed by BGC-Argo floats) were elevated and of hydrothermal origin. They further demonstrated that enhanced eddy kinetic energy (EKE) resulting from the interaction of currents with bottom topography brought the hydrothermal vent emissions to the surface, stimulating phytoplankton growth.

Two active hydrothermal vent fields were recently found along the Australian Antarctic Ridge (AAR; Fig. 1), a series of ridge segments and transform faults in the Pacific Sector of the SO<sup>7</sup>. KR1, the southerly of the two vent systems (KR2 is further to the northwest), coincides with the positions of the southern boundary of the Antarctic Circumpolar Current (sbACC) and the southern ACC front (sACCf), which run very close together in this part of the ACC (Fig. 1a). The position of KR1 is also coincident with a large area of perennially elevated chlorophyll *a* (Chl *a*) and NPP (Fig. 1b) visible in satellite-based climatologies extending back to 1978<sup>8–12</sup>. This indicates that a phytoplankton bloom develops in the same location near KR1 almost every year.

Here we describe observations from a SO research cruise that, for the first time, sampled surface waters above the AAR in the region of perennially elevated NPP near KR1. During that cruise, we measured the hydrographic conditions, seawater chemistry, and biological responses associated with a massive phytoplankton bloom in the otherwise high-nutrient, low-chlorophyll (HNLC) waters of the ACC. By combining field data and satellite imagery, we were able to shed light on the likely cause for such an intense phytoplankton bloom in a region of generally low NPP.

## Results

**Characteristics of the AAR bloom.** Satellite imagery showed that the position of the bloom, adjacent to the AAR and the sbACC (Fig. 1c), to the northwest of the Ross Sea (Fig. 1d) (hereafter referred to as the AAR bloom), remained relatively stationary from December 2013 through February 2014 and did not track the receding ice edge (Supplementary Fig. 1). From ocean color data, we calculated that the area of the AAR bloom where the mean Chl *a* concentration from November through February exceeded 0.25 mg m<sup>-3</sup> was ~266,000 km<sup>2</sup>.

Our in situ measurements confirmed that the AAR bloom observed in satellite imagery was characterized by elevated phytoplankton biomass and NPP. Our underway data showed an increase in fluorescence (Supplementary Fig. 1) associated with the AAR bloom identified in satellite images. Chl *a* concentration within the top 40 m of the water column (Fig. 2a) ranged from 5.00–7.09 mg m<sup>-3</sup> inside the bloom (stations 130/151, 131, and 150) and only 0.33–0.97 mg m<sup>-3</sup> outside the bloom (stations 119 and 140/149). The depth-integrated Chl *a* ranged from 56.7 mg m<sup>-2</sup> at station 119 and 60.0 mg m<sup>-2</sup> at station 140 outside of the

bloom to 114.8 mg m<sup>-2</sup> at station 135 on the edge of the bloom to 319.0 mg m<sup>-2</sup> at station 130 and 255.0 mg m<sup>-2</sup> at station 131, in the interior of the bloom. Five stations (130/151, 131, and 150 inside the bloom as well as 120 and 133 on the edge of the bloom) had depth-integrated Chl *a* exceeding 140 mg m<sup>-2</sup>. Particulate organic carbon (POC) concentrations inside the bloom ranged from 705.4 to 833.9 mg m<sup>-3</sup>, with values of only 101.2–189.9 mg m<sup>-3</sup> outside the bloom (Fig. 2b).

Depth-integrated NPP inside the AAR bloom was around three times higher than outside of the bloom. At stations 130 and 150 where Chl *a* and POC concentrations were high, NPP reached 1.14 and 1.10 g C m<sup>-2</sup> d<sup>-1</sup>, respectively. In contrast, at stations with low Chl *a* and POC (stations 119 and 140) depth-integrated NPP was only 0.40 and 0.35 g C m<sup>-2</sup> d<sup>-1</sup>, respectively.

The AAR bloom was also associated with significant CO<sub>2</sub> and nutrient drawdown by phytoplankton. Surface *p*CO<sub>2</sub> outside the bloom ranged from 394 to 410 μatm while *p*CO<sub>2</sub> inside the bloom was reduced to 196–228 μatm (Fig. 1d). Similarly, nitrate concentrations inside the bloom ranged from 13.52 to 18.86 μM in the top 30 m, much lower than near-surface concentrations outside of the bloom of 27.03–29.62 μM and subsurface concentrations below 40 m of 30.45–32.73 μM at stations both inside and outside of the bloom (Fig. 2c). The depth of the mixed layer (MLD) showed a wide range across all sampling stations and we found no relationship between MLD and Chl *a* or POC concentration in the upper mixed layer. MLD at stations inside the bloom (stations 130/151, 131, and 150) ranged from 23 to 30 m, outside the bloom (stations 119 and 140/149) from 16 to 35 m, and on the margin of the bloom (stations 120, 133, 135, and 136) from 17 to 41 m.

CHEMTAX analysis of HPLC pigments (confirmed by microscopy) showed that the AAR bloom was dominated by the haptophyte *Phaeocystis antarctica*, which accounted for 90–100% (*n* = 9) of the phytoplankton Chl *a* inside the bloom. Outside the bloom, diatoms were dominant, comprising 61.6–90.4% (*n* = 11) of phytoplankton Chl *a*. The dominance of *P. antarctica* inside the bloom was also strongly indicated by the lack of silicate drawdown, despite high nitrate drawdown, with silicate concentrations inside the bloom (65.10–67.89 μM) roughly equivalent to those outside the bloom (60.15–71.88 μM).

Dissolved Fe (DFe) was substantially depleted in surface waters both inside and outside the AAR bloom, with concentrations falling to 0.04–0.05 nM (Fig. 2d). The substantial depletion of DFe in surface waters at bloom stations combined with the incomplete drawdown of nitrate indicates that DFe was limiting the productivity of the bloom at the time of our sampling. However, mean subsurface DFe (Fig. 3a) concentrations measured just below the ferricline (from 90 to 250 m) at bloom stations (0.29–0.35 nM at 150 m) were significantly higher (*p* < 0.0001) than DFe concentrations measured below the ferricline at stations outside the bloom (0.13–0.16 nM at 150 m). Deep (>250 m) DFe concentrations inside the bloom were also significantly elevated relative to those outside the bloom down to our deepest sampling depth of 2000 m (*p* < 0.0001). Vertical diffusivity (log-transformed to comply with normality assumptions) was significantly higher (*p* = 0.0002) in subsurface (90–250 m) waters beneath the bloom (mean = 2.8 × 10<sup>-3</sup> m<sup>-2</sup> s<sup>-1</sup>) than outside the bloom (mean = 0.5 × 10<sup>-3</sup> m<sup>-2</sup> s<sup>-1</sup>; Fig. 3b).

Additionally, profiles of DFe (Fig. 3d), potential temperature (Fig. 3e), salinity (Fig. 3f), and oxygen (Fig. 3g) plotted against density reveal that elevated subsurface DFe concentrations are associated with an anomalous water mass located within the potential density anomaly range of 27.6–27.8 kg m<sup>-3</sup>. At bloom stations, waters with a potential density anomaly between 27.6 and 27.8 kg m<sup>-3</sup> were colder, fresher, and more oxygenated than at non-bloom stations.

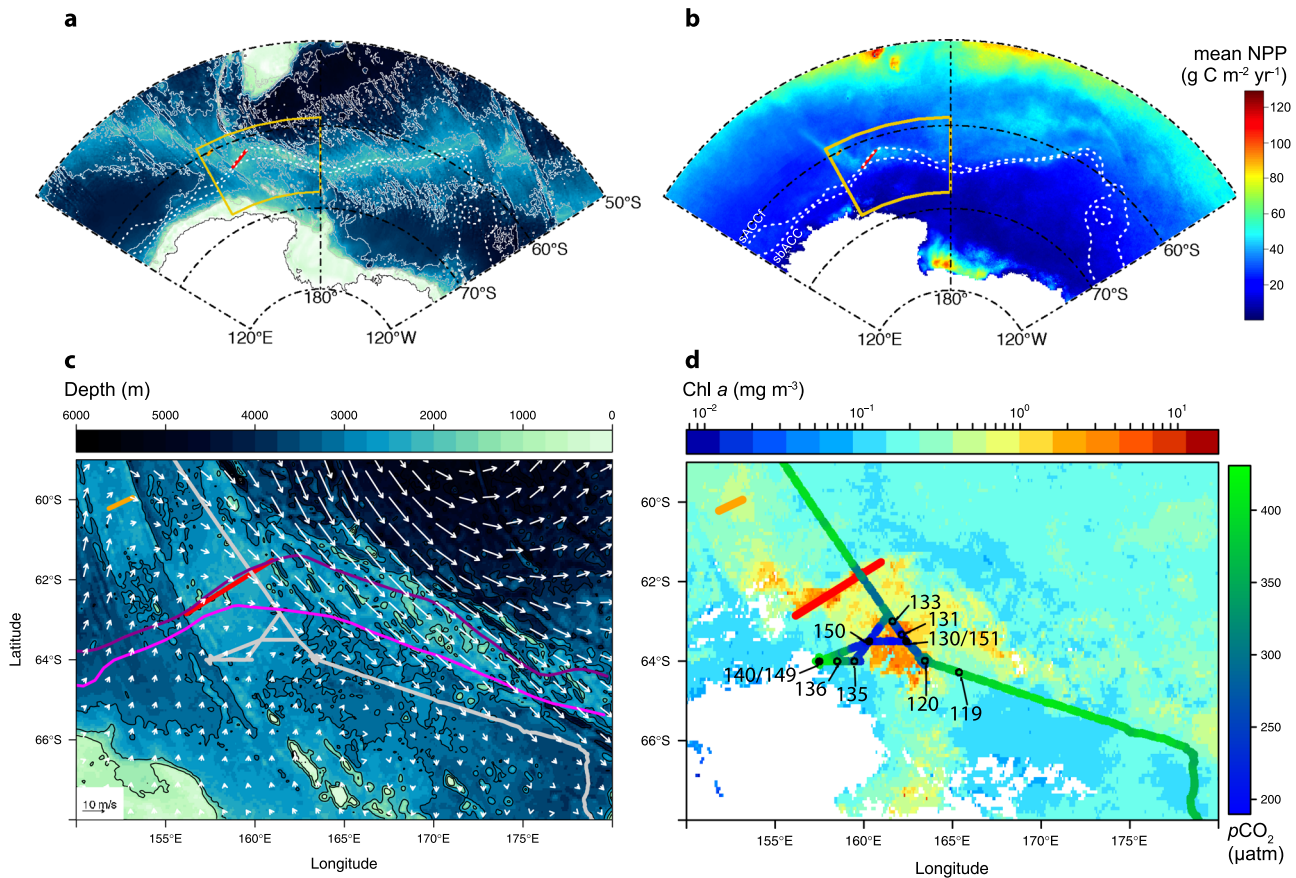


**Fig. 1 Bathymetry and phytoplankton distribution in the Pacific sector of the Southern Ocean.** On all figures, red and orange lines indicate the positions of the ridges KR1 and KR2, respectively<sup>7</sup>. The positions of southern Antarctic Circumpolar Current (ACC) front (sACCf) and the more southerly positioned southern boundary of the ACC (sbACC)<sup>35</sup>, are shown by the white dashed lines in **a** and **b** and by the pink lines in **c**. **a** Map of Pacific sector bathymetry, with yellow inset box that corresponds to the areas shown in **c** and **d**. **b** Map of Pacific sector climatological net primary production (NPP; 1997–2019), indicating the return of the bloom to the same location most years. **c** Map of bathymetry and January 2014 geostrophic currents from Dotto et al.<sup>14</sup>. Cruise track is shown as solid gray line. **d** Map of mean satellite chlorophyll *a* (Chl *a*) from November 2013–February 2014 with underway *p*CO<sub>2</sub> overlaid along the cruise track. Stations are indicated by black circles and labeled with a station number. Closed circles indicate stations where a cast to 2000 m was conducted to sample dissolved Fe (DFe). The distance from the center of KR1 to station 150 is 168 km. Bathymetry data are from <https://www.ngdc.noaa.gov/mgg/global/>. White areas indicate land in **a** and **b** and an absence of valid Chl *a* data in **d** which is either land, sea-ice, or persistent cloud cover. Note that the satellite Chl *a* image that covers the bloom period **d** is a composite of multiple months and the location of the bloom in this image may not exactly match our in situ measurements. The convergence zone visible to the south of our study area **c** falls within the boundaries of the western side of the Ross Gyre. However, the location of this zone shifts substantially on a monthly timescale and is unlikely to impact the bloom.

**DFe supply.** To determine if the observed drawdown of DFe in surface waters of the AAR bloom was sufficient to support the accumulated phytoplankton biomass, we calculated the ratio of DFe removed from surface waters (assuming the depletion in DFe concentration between the surface and 150–200 m depth was due to phytoplankton uptake) to POC accumulated (the average POC concentration above 40 m). At stations within the bloom, the ratio of DFe removed to POC accumulated ranged from 4.0 to 5.2  $\mu\text{mol mol}^{-1}$ , which falls within the range of cellular Fe:C ratios reported for *P. antarctica* (2.3–8.6  $\mu\text{mol mol}^{-1}$ )<sup>13</sup>, the dominant phytoplankton inside the bloom. At stations outside of the bloom, the ratio of DFe removed to POC accumulated ranged from 13.0 to 21.2  $\mu\text{mol mol}^{-1}$ , which is consistent with the range of cellular Fe:C ratios for diatoms (10–20  $\mu\text{mol mol}^{-1}$ )<sup>13</sup>, the dominant phytoplankton group in these waters. These findings demonstrate that the amount of DFe removed from surface waters was sufficient to support the observed phytoplankton biomass accumulation both inside and outside of the bloom.

In order to assess whether the rate of CO<sub>2</sub> fixation (i.e., NPP) by phytoplankton measured in situ could be supported by the

delivery of DFe across the ferricline, we compared the calculated vertical DFe flux to depth-integrated NPP for stations 130 and 150 inside the bloom and stations 119 and 140 outside of the bloom. The ratio of DFe delivered to CO<sub>2</sub> fixed inside the bloom was 4.37–4.70  $\mu\text{mol:mol}$ , consistent with the cellular Fe:POC range for *P. antarctica*<sup>13</sup>. Outside the bloom, the DFe delivery to CO<sub>2</sub> fixation ratio was 2.82–3.14  $\mu\text{mol:mol}$ , which is much lower than the cellular Fe:POC range for diatoms<sup>13</sup>, suggesting that the community of diatoms growing outside of the bloom would be extremely Fe-stressed. Presumably, *P. antarctica* was the dominant phytoplankton in the AAR bloom due to its favorable Fe requirements.

We also examined the relationship between depth-integrated Chl *a* and vertical DFe flux using linear regression analysis. Depth-integrated Chl *a* was significantly correlated with vertical DFe flux such that higher DFe flux was associated with higher depth-integrated Chl *a* (Fig. 3c;  $p = 0.04$ ,  $r^2 = 0.45$ ). Depth-integrated Chl *a* was not significantly correlated with either vertical diffusivity ( $p = 0.18$ ) or the DFe concentration gradient across the ferricline ( $p = 0.14$ ).

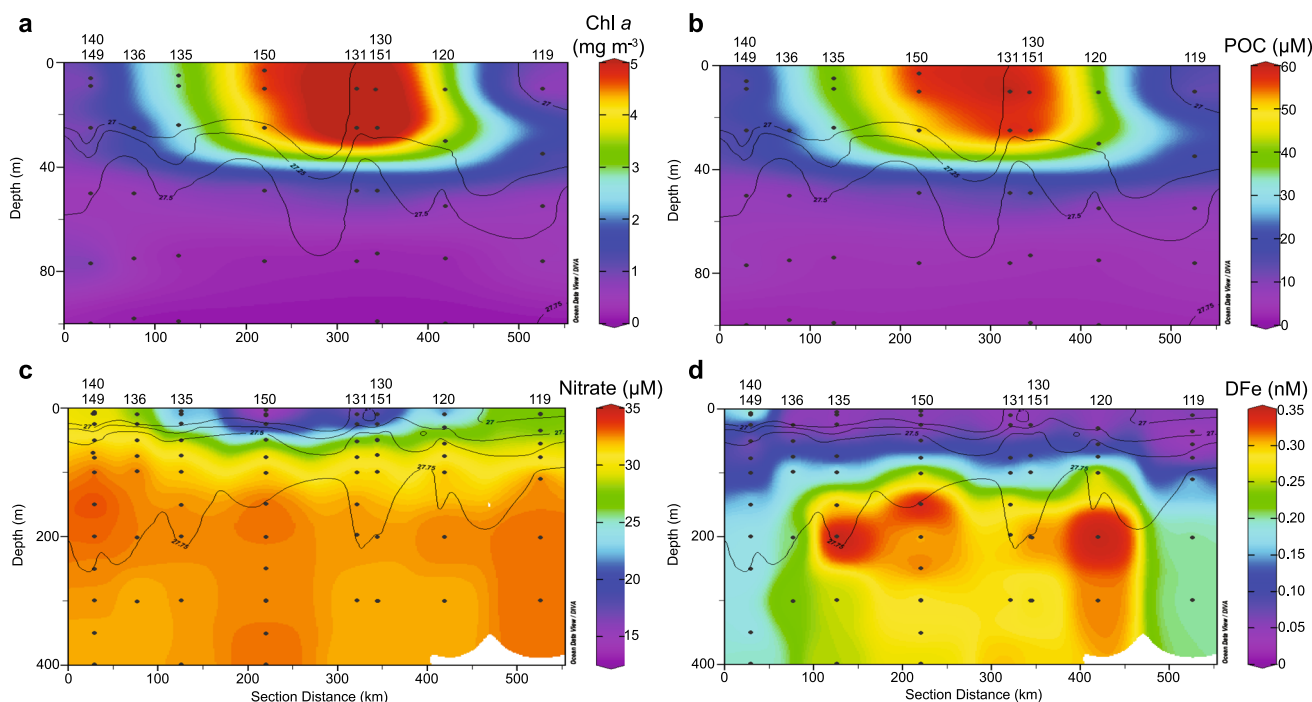


**Fig. 2 Biomass and nutrients in the water column in and around the bloom.** Vertical sections of **a** chlorophyll *a* (Chl *a*), **b** particulate organic carbon (POC), **c** nitrate, and **d** dissolved Fe (DFe) from in situ measurements. Note that the depth in panels **a** and **b** extends only to 100 m, while the depth in panels **c** and **d** extends to 400 m. Station numbers are listed above each section, block dots indicate sampling depths, and black lines show isopycnals. A map of the portion of the cruise shown in these sections and the stations that correspond with the stations here is shown in Fig. 1d. Station 133 is on the map but not included in the section.

**Hydrologic context.** To better understand the hydrologic conditions influencing the AAR bloom, we examined the NPP, deep EKE, isopycnal depth, and bathymetry of the waters in and around the bloom (Supplementary Fig. 2), looking specifically at the way these variables change along the sACCF between 100°E and 180°E (Fig. 4). Along the sACCF, the shallower bathymetry of KR1 begins around 156°E, although isopycnals reach their minimum depth upstream (~150°E) of this shift in bathymetry. Deep EKE (at ~1000 m) in the region of the AAR is low, falling below  $10 \text{ cm}^2 \text{ s}^{-2}$  between 150°E and 160°E. NPP along the sACCF climbs steadily starting around 153°E, reaching a maximum near 160°E downstream of where the sACCF passes over KR1.

A Lagrangian particle tracking climatology (1997–2019; Supplementary Fig. 3) shows that particles released directly above KR1 follow prevailing surface currents to the west and that particles released above KR2 move both to the southeast and the northwest, consistent with the climatological shape of the bloom observed in our satellite NPP analysis (Fig. 1b). The currents in this region tend to be slow (Fig. 1c) and thus the residence time of water that has moved through the region above the vents is long (Supplementary Fig. 3). Geostrophic surface currents (calculated from satellite altimetry data<sup>14</sup>) were directed southeasterly during the month of January 2014 in the vicinity of the AAR bloom, decreasing in intensity from the northeast to the southwest across the bloom (Fig. 1c). The geostrophic surface currents in January 2014 are consistent with the results from the Lagrangian particle tracking climatology.

## Discussion

The AAR bloom that we sampled in the Pacific Sector of the SO was large, long-lived, and contained a substantial amount of phytoplankton biomass. Both climatological NPP (Fig. 1b) and

annual satellite Chl *a* imagery (Supplementary Fig. 4) show that the bloom has developed in the vicinity of KR1, KR2, or both vent ridges in 20 out of the last 22 years. During our cruise in January of 2014, the standing stock of Chl *a* in the AAR bloom ( $140\text{--}300 \text{ mg Chl } a \text{ m}^{-2}$ ) exceeded the depth-integrated Chl *a* of the most intense ACC bloom thus far measured by BGC-Argo floats ( $98.1 \text{ mg Chl } a \text{ m}^{-2}$ )<sup>6</sup>. It also eclipsed the large Fe-enriched blooms located downstream of the relatively shallow Kerguelen (south of the Polar Front, which excludes the portion of the bloom directly downstream of the island) and Crozet plateaus, which have a mean phytoplankton biomass of  $\sim 120 \text{ mg Chl } a \text{ m}^{-2}$ <sup>15,16</sup> and  $180\text{--}229 \text{ mg Chl } a \text{ m}^{-2}$ <sup>17</sup>, respectively. The maximum depth-integrated Chl *a* measured in our bloom is more than three times higher than that measured in the hydrothermally-driven SWIR blooms<sup>6</sup>.

The productivity rates in the AAR bloom were also very high compared with other blooms in the ACC. Our daily NPP measurements in the bloom ( $1.10\text{--}1.14 \text{ g C m}^{-2} \text{ d}^{-1}$ ) are 2.7–3.8 times higher than the satellite-based daily NPP estimates at the peak of the spring bloom in open SO waters ( $0.30\text{--}0.40 \text{ g C m}^{-2} \text{ d}^{-1}$ )<sup>11</sup>. NPP in the AAR bloom was within the range of that measured over the Crozet Plateau ( $0.52\text{--}3.00 \text{ g C m}^{-2} \text{ d}^{-1}$ ) at stations where depth-integrated Chl *a* exceeded  $50 \text{ mg m}^{-2}$ <sup>17</sup>. The areal extent of the AAR bloom ( $266,000 \text{ km}^2$ ) is also within the range for the Crozet Plateau bloom ( $70,500\text{--}355,000 \text{ km}^2$  from 1998 to 2007), although it was substantially smaller than the Kerguelen Plateau bloom ( $340,000\text{--}1,600,000 \text{ km}^2$  from 1998 to 2007)<sup>18</sup>. The Kerguelen bloom typically persists from November through January and the Crozet bloom from October through December<sup>18</sup>, which is approximately equivalent to the length of the AAR bloom (December through February).

The high biomass and longevity of the AAR bloom is likely explained by the combination of elevated DFe concentrations in surface waters at the onset of the growing season as well as high



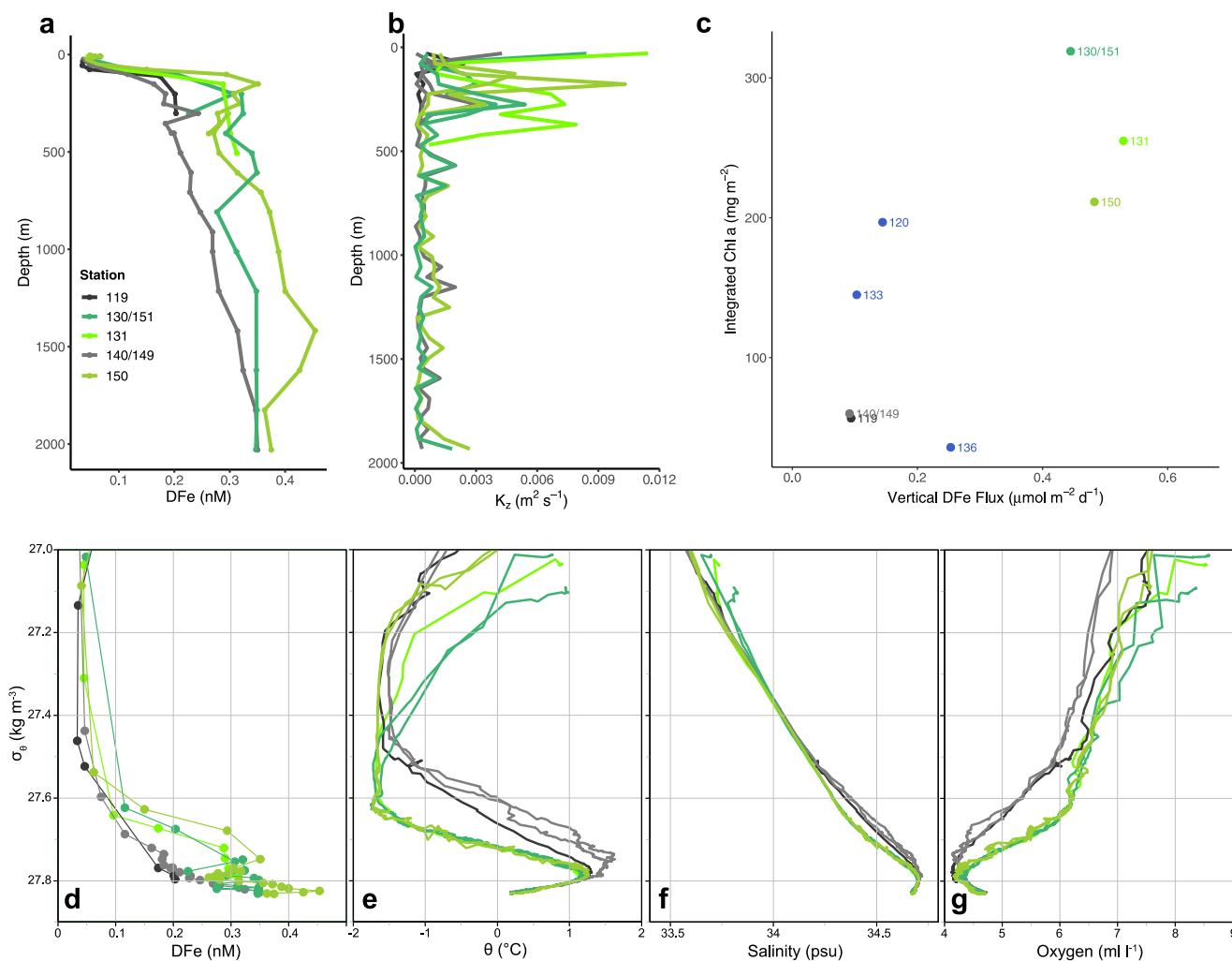


**Fig. 3** Water mass characteristics in the bloom versus outside of the bloom. Depth profiles of **a** dissolved Fe (DFe) and **b** vertical diffusivity ( $K_z$ ) for stations inside the bloom (green lines) and stations outside the bloom (gray lines). **c** Depth-integrated chlorophyll *a* (Chl *a*) versus DFe flux. Density profiles of **d** DFe, **e** potential temperature, **f** salinity, and **g** oxygen concentration. We do not include error bars for our DFe measurements or our depth-integrated Chl *a* measurements in either the depth or density profiles because the standard deviation for all DFe measurements was below 0.012 nM, and the error associated with all depth-integrated Chl *a* measurements was below 0.12%. Stations shown in blue **c** fall on the edge of the bloom and are not included in the other plots.

rates of DFe delivery to the upper mixed layer through the austral summer, consistent with the bloom phenology proposed by Tagliabue et al.<sup>19</sup>. Higher rates of DFe delivery to surface waters inside the AAR bloom are driven by substantially greater DFe concentrations below the ferricline (0.31–0.35 nM) compared to that of non-bloom stations (0.12–0.17 nM) combined with a higher vertical gradient of DFe measured at our bloom stations is only slightly higher than that reported for the Kerguelen Plateau<sup>20</sup>, the vertical DFe fluxes we calculated ( $0.44\text{--}0.53\ \mu\text{mol m}^{-2}\ \text{d}^{-1}$  at stations 130, 131, and 150; Fig. 3c) are substantially higher. Blain et al.<sup>20</sup> reported a vertical DFe flux at a high biomass station near the Southern Kerguelen Plateau of  $0.03\ \mu\text{mol m}^{-2}\ \text{d}^{-1}$  and Tagliabue et al.<sup>19</sup> estimated a vertical diffusive DFe flux range of  $0.0016\text{--}0.0157\ \mu\text{mol m}^{-2}\ \text{d}^{-1}$  for the SO. Our vertical DFe fluxes are an order of magnitude higher than these values.

The difference between our vertical DFe flux estimates and those reported previously<sup>19,20</sup> originates from the fact that our calculated vertical diffusivity ( $K_z$ ) across the ferricline ( $0.9\text{--}4.4 \times 10^{-3}\ \text{m}^2\ \text{s}^{-1}$ ) is an order of magnitude higher than the mean value generally reported for the SO of  $10^{-4}$  to  $10^{-5}\ \text{m}^2\ \text{s}^{-1}$ <sup>19–22</sup>.

Although our  $K_z$  values are relatively high, they still fall within the range of values reported previously in the SO.  $K_z$  values as high as  $10^{-1}$  have been reported in the upper mixed layer of the SO during times of strong winds<sup>23,24</sup>, and values of  $10^{-3}$  to  $10^{-4}$  are typical of the seasonal pycnocline<sup>23</sup>. We observed that buoyancy frequency was slightly higher at bloom stations (though not significantly) at the same depths where elevated  $K_z$  was observed (Supplementary Fig. 5) and that these elevated buoyancy frequency values extended deeper into the water column at bloom stations. Therefore, it is possible that the stronger stratification measured at bloom stations could have led to the breaking of surface-generated near-inertial waves, thereby generating the elevated vertical diffusivities we observed<sup>25</sup>.

The potential sources of new Fe in the SO that could fuel the AAR bloom are aeolian dust deposition<sup>26,27</sup>, iceberg<sup>13,28</sup> and sea ice melt<sup>13,29,30</sup>, sediments (continental shelf advection)<sup>31</sup>, upwelling of deep water<sup>19,32</sup>, and hydrothermal vent emissions that recently have been shown to be a significant source of Fe to deep waters in the SO<sup>5,32,33</sup>. We can rule out aeolian dust flux and iceberg melt, as estimates of dust deposition south of 60°S are vanishingly small ( $0.001\text{--}0.003\ \text{mmol Fe m}^{-2}\ \text{yr}^{-1}$ )<sup>26,27</sup> and the

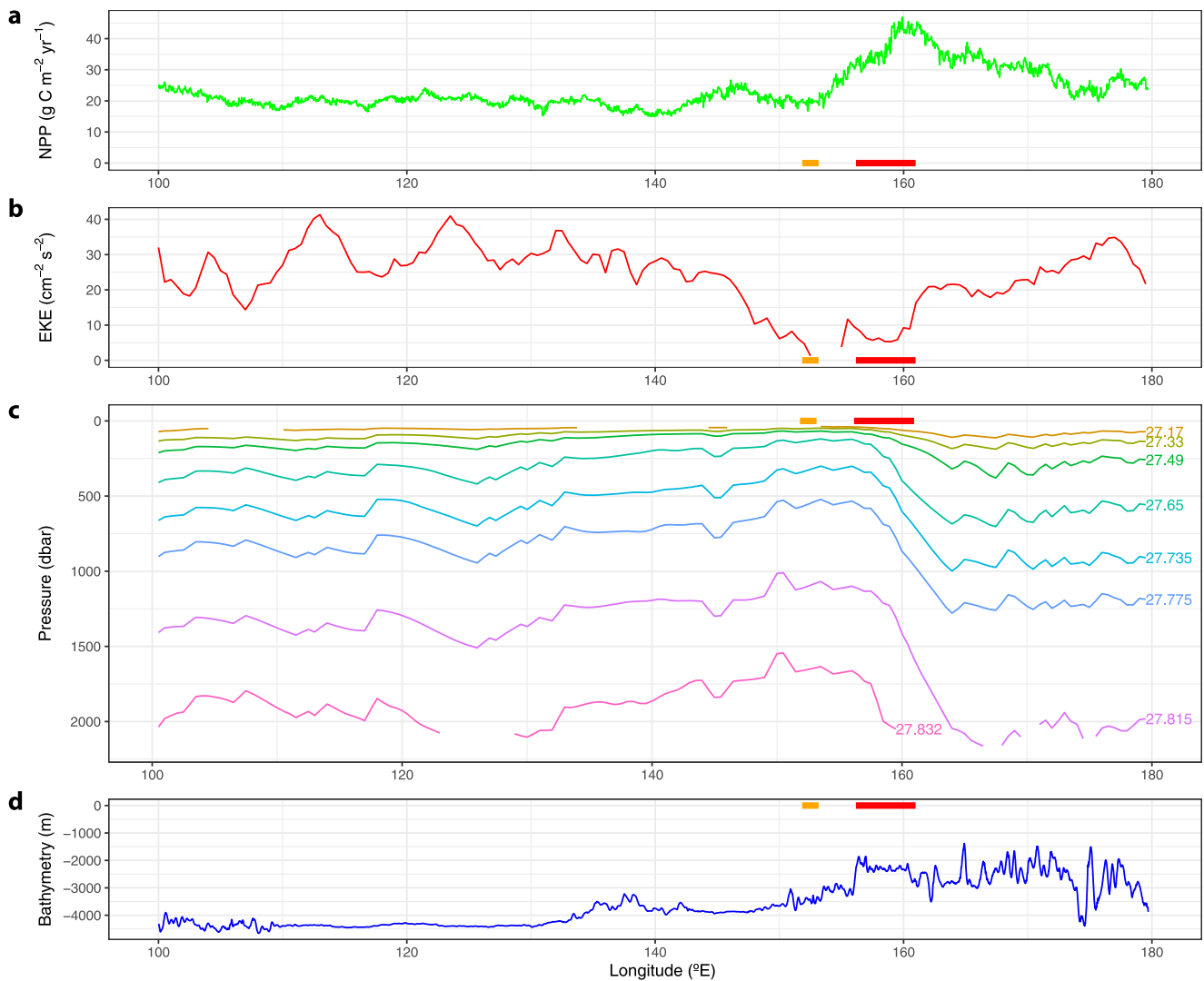


**Fig. 4** Position of the bloom relative to factors that promote upwelling along the southern Antarctic Circumpolar (ACC) front (sACCf). **a** Net primary production (NPP), **b** eddy kinetic energy (EKE), **c** isopycnal pressure, and **d** bathymetry along the sACCf according to the front positions of Orsi et al.<sup>35</sup>. Supplementary Fig. 2 shows maps of the data used in this figure with the position of the sACCf. The longitudinal position of KR1 and KR2 are shown by the red line and orange line, respectively, on each panel. Bathymetry data are from <https://www.ngdc.noaa.gov/mgg/global/>.

path of icebergs in the Pacific sector of the SO lies too far south to impact the AAR bloom<sup>28</sup>. While sea ice may account for some DFe input<sup>30</sup>, we can rule it out as the primary source of DFe since the bloom does not track the sea ice edge (Supplementary Fig. 1). Furthermore, the input of DFe from dust deposition, iceberg melt, and sea ice cannot account for the elevated DFe concentrations observed down to 2000 m. Advection from continental shelves is also not a strong candidate. While weak currents appear to move from the region of the shelf in the south into our study area, results from a Lagrangian model of horizontal DFe delivery shows almost no advected DFe from continental shelves making it to the vicinity of the AAR bloom<sup>6,31</sup>. Most notably, none of these potential Fe sources can explain why the bloom recurs in the same location every year. The remaining potential sources of DFe are upwelling of Upper Circumpolar Deep Water (UCDW) and hydrothermal vent emissions.

Upwelling is undoubtedly playing a major role in waters around the AAR bloom. The co-location of an upwelling front with a bathymetric feature such as a ridge, both of which are present at the AAR bloom site, has been shown to result in persistent blooms associated with upwelling fronts<sup>10</sup>. The position of the AAR bloom is adjacent to the sbACC and sACCf,

which flow very close together in this region. This means that the AAR bloom is positioned close to the steeply tilted and outcropping isopycnals associated with these fronts. In addition to the meridional shallowing of isopycnals southward across the sACCf and sbACC, there is also a zonal shallowing of isopycnals along the sACCf as the ACC flows over the AAR (Fig. 4c). Isopycnals along the sACCf reach their minimum depth (Fig. 4c) slightly upstream (~150°E) of the bathymetric shift near the AAR (Fig. 4d). Furthermore, convective mixing as a result of the high temperature and low salinity of fluids expelled from hydrothermal vents can enhance local vertical diffusivity and increase vertical advection, resulting in upwelling rates an order of magnitude higher than background rates within 300 m of the seafloor<sup>34</sup>. The AAR bloom is in a unique location where all of these upwelling mechanisms are potentially at work.

UCDW comes close enough to the surface between the sACCf and sbACC to be entrained in surface waters through deep winter mixing<sup>35,36</sup>. While nitrate concentrations in UCDW are uniform, DFe concentrations are highly variable. In a GEOTRACES transect to the west of our study area (along ~140°E), nitrate concentrations in the density range associated with UCDW (27.35–27.75 kg m<sup>-3</sup>)<sup>35,36</sup> was 31.1–36.6 μM, while DFe

concentrations varied over a full order of magnitude from 0.07 to 0.70 nM (Supplementary Fig. 6)<sup>37</sup>. The variability in the DFe data shows that UCDW does not have a uniform DFe signature and indicates that point sources of Fe, such as hydrothermal vents, may influence the DFe inventory of upwelling deep water between the sACCf and sbACC.

While deep mixing during winter and upwelling throughout the spring and summer are key components facilitating the development of the AAR bloom, we contend that it is the increased Fe inventory in the upwelled water resulting from hydrothermal vent emissions that stimulates and sustains the AAR bloom each year. The Fe inventory of upwelled water determines the amount of biomass that can be supported, and we have shown that the elevated DFe inventory in surface waters at the beginning of the growing season and the entrainment of DFe-rich deep water from beneath bloom stations throughout the summer can support 2–3-fold more *P. antarctica* biomass than at stations outside of the bloom.

While the shoaling of isopycnals along the sACCf in the region of the AAR is indicative of upwelling, these isopycnals reach their minimum depth at ~150°E (Fig. 4c), far upstream of any change in NPP along the sACCf (Fig. 4a). It is only downstream of KR2 that NPP starts to increase and downstream of KR1 (the vent system much closer to the sACCf) where there is a truly substantial increase in NPP, presumably because the hydrothermal vents provide a source of Fe<sup>7,38</sup>. If upwelling alone, as indicated by the shoaling of isopycnals, were enough to produce a bloom, there would be increased NPP in waters where the isopycnals shoal upstream as well as downstream of the vents.

The consistent shape and position of the AAR bloom each year, visible in the NPP climatology (Fig. 1b) and annual Chl *a* images (Supplementary Fig. 4), suggest a stationary source of elevated DFe to surface waters, such as the hydrothermal vent fields KR1 and KR2. This conclusion is further supported by the climatological particle distribution from our Lagrangian satellite altimetry-based simulation. When particles are released directly above either KR1 or KR2, they closely approximate the climatological shape of the bloom. Thus, the geostrophic currents in the region indicate that the waters with elevated NPP must have passed above either KR1 or KR2, providing further evidence that these vent fields act as the source of Fe for the AAR bloom.

Depth and density profiles of DFe are also consistent with our having sampled through the nonbuoyant plume downstream of a hydrothermal vent. A plume emanating from a hydrothermal vent has two parts, the buoyant plume and the nonbuoyant plume<sup>39,40</sup>. The buoyant plume rises from a hydrothermal vent due to the higher buoyancy of the high-temperature hydrothermal fluids injected into the water column<sup>39,40</sup>. As the plume rises, the turbulence resulting from the shear stress between the rising plume and the surrounding waters, entrains the ambient water into the rising plume until the plume is diluted and reaches neutral buoyancy with surrounding waters<sup>39,40</sup>. After reaching neutral buoyancy, it becomes a nonbuoyant plume, which is then advected by the prevailing currents at the depth of neutral buoyancy<sup>39,40</sup>. We sampled the nonbuoyant plume downstream of KR1, as evidenced by the elevated subsurface (75–300 m) DFe concentrations at bloom stations (Fig. 3a). At depths below 300 m, the difference in the concentration of DFe between bloom and non-bloom stations was much less pronounced, indicating that those depths were below the nonbuoyant plume.

We submit that further evidence of the nonbuoyant plume is visible in profiles of DFe, potential temperature, salinity, and dissolved oxygen plotted against density (Fig. 3d–g). Elevated DFe concentrations at bloom stations are associated with an anomalous water mass, between the 27.6 and 27.8 kg m<sup>-3</sup> isopycnals, that is colder, fresher, and more oxygenated than waters of the

same density range at non-bloom stations. These observations are consistent with the turbulent entrainment of deep waters by a buoyant hydrothermal vent plume, which will be most strongly influenced by the water mass properties of the deep waters at the depth of the vent emissions<sup>41</sup> (~1800–2000 m in the case of KR1), and will bear the signature of the water mass properties (temperature, salinity and oxygen in this case) at that depth<sup>41</sup>. The water mass properties in our depth profiles between 1800 and 2000 m, which we use as a proxy for the water mass at the same depth immediately adjacent to the vent, are colder and more oxygenated than the overlying UCDW (Supplementary Fig. 7). Therefore, a water mass generated by emissions from these vents will bear this colder and more oxygenated signal<sup>41</sup>, which is consistent with the properties of the anomalous water mass between the 27.6 and 27.8 kg m<sup>-3</sup> isopycnals seen at bloom stations.

Salinity profiles are less straightforward to explain. While the salinity decreases below ~300 m (Supplementary Fig. 7b), the shift is slight, and the mixing of this water would not create a large enough change in salinity to explain the deviation observed in our density and depth profiles at blooms stations between the 27.6 and 27.8 kg m<sup>-3</sup> isopycnals (Fig. 3f). However, there is a clear deviation from the linear mixing line in salinity, when plotted against density, at bloom stations (Fig. 3f) between the 27.6 and 27.8 kg m<sup>-3</sup> isopycnals, indicative of the influence of a lower salinity water mass. In addition to carrying elevated DFe into the region of the bloom, the nonbuoyant plume may also be responsible for the stratification of the water column, creating local stratification maxima, which may be linked to the elevated vertical diffusivity<sup>25</sup> and therefore enhanced Fe delivery at bloom stations. While storms moving through the region would generate the same downward-propagating near-inertial waves, the vertical distribution of turbulence in the water column could be focused in the nonbuoyant plume.

Thus far, there has been only one study that observed a direct connection between hydrothermal vent activity and phytoplankton blooms<sup>6</sup>. The AAR bloom is different from the blooms attributed to hydrothermal vent activity downstream of the SWIR<sup>6</sup> in two key respects. The AAR bloom begins directly above the hydrothermal vent system as opposed to ~1200 km downstream, and the AAR bloom recurs so consistently in the same shape and location that it is visible in climatologies of Chl *a*<sup>8–12</sup> and NPP (Fig. 1b). We attribute these differences to multiple factors that could affect hydrothermal plume rise height, namely the vertical position of the hydrothermal vents in the water column, the position of the vents in relation to major upwelling fronts, and their arrangement relative to each other. The vents of KR1 and KR2 are substantially shallower (~1800–2000 m deep) than those associated with the SWIR blooms (3517–4170 m deep). This means that the plume does not have to rise nearly as far to reach a depth where it could be entrained into surface waters through winter mixing. The position of the AAR vents, and KR1 in particular, near the region of strong upwelling south of the sACCf means that the hydrothermal plume from this vent is being injected into a field of steeply sloping isopycnals. This suggests that the plume rise height will be greater as it travels vertically along isopycnals. It is likely that because the plume from KR1 and KR2 rises to depths so much closer to the surface, the location of the bloom is more interannually consistent. This contrasts to the blooms downstream of the SWIR where Fe is drawn to the surface by high EKE over 1000 km downstream of the vents, allowing for more deviation in the position where this Fe surfaces.

We propose that the AAR bloom is a new type of natural Fe fertilization system that receives its DFe subsidy in a way that is much different from previously described systems on the Kerguelen and Crozet Plateaus. Instead of being supported by DFe

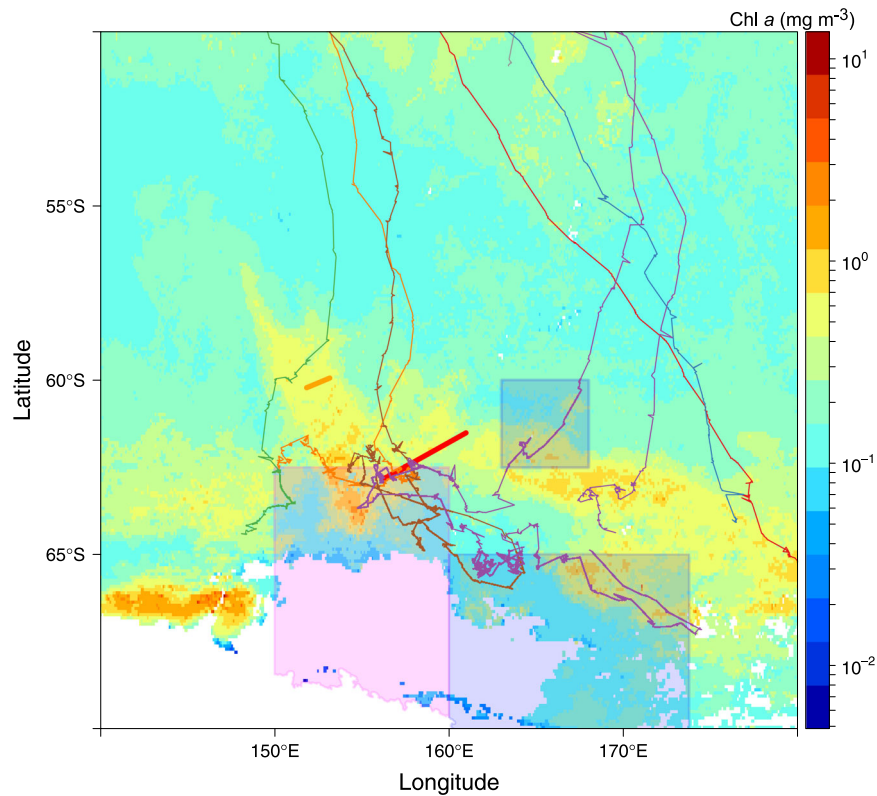


**Fig. 5 Position of Humpback whales relative to the bloom.** Map of mean chlorophyll *a* (Chl *a*) (MODIS/Aqua) from November 2008 through February 2009 overlaid with the position of Humpback whales tagged off the coast of Eden in Southeastern Australia. Humpback whale position data are from Andrews-Goff et al.<sup>45</sup>. The General Protection Zone and Krill Protection Zone of the Ross Sea Marine Protected Area are indicated by the blue boxes and pink box, respectively. The white areas indicate no data due to land or persistent sea-ice and/or cloud cover, and the red and orange lines indicate the positions of the ridges KR1 and KR2, respectively<sup>7</sup>.

from the advection of a shelf source, the AAR bloom is most likely supported by DFe from hydrothermal vent emissions. Systems receiving persistent natural Fe fertilization are marked by higher export efficiencies<sup>20</sup> and act as strong CO<sub>2</sub> sinks, as does the AAR bloom. Based on pCO<sub>2</sub> and wind speed measurements made during our cruise, we calculate a mean air-sea CO<sub>2</sub> flux for the AAR bloom of  $-32 \text{ mmol m}^{-2} \text{ d}^{-1}$  ( $0.38 \text{ g C m}^{-2} \text{ d}^{-1}$ ) and a maximum CO<sub>2</sub> flux of  $-131 \text{ mmol m}^{-2} \text{ d}^{-1}$  ( $-1.57 \text{ g C m}^{-2} \text{ d}^{-1}$ ). These values are much higher than the mean CO<sub>2</sub> flux measured at the peak of the Kerguelen bloom in November ( $-17.9 \text{ mmol m}^{-2} \text{ d}^{-1}$ )<sup>42</sup> and the mean CO<sub>2</sub> flux in the Ross Sea in January ( $-12.5 \text{ mmol m}^{-2} \text{ d}^{-1}$ )<sup>43</sup>.

The consistent location and productivity of the AAR bloom has apparently made it a hotspot for upper trophic level activity. Tynan<sup>44</sup> found high concentrations of both krill and cephalopods around the sbACC, including the area encompassing the AAR bloom, and suggested that the physical processes along the sbACC provide predictably productive foraging opportunities. Humpback whales tagged near Eden, off the southeast coast of Australia, in October of 2008<sup>45</sup>, fed primarily downstream of KR1 and KR2 in the region of elevated Chl *a* associated with the AAR bloom (Fig. 5). Whales tagged in subsequent years along the Sunshine Coast in Australia and in Antarctica also visited the region of the AAR bloom, suggesting well-established migratory pathways and persistent use of this feeding ground<sup>45</sup>. The AAR bloom has implications for conservation efforts in the region. The Ross Sea Marine Protected Area covers a few small portions of the AAR bloom region (Fig. 5), however, the majority of this important foraging area remains unprotected.

The AAR bloom is the first recurring bloom that is likely to be stimulated by hydrothermal Fe to be identified in the SO. The

importance of the AAR bloom to upper trophic levels and its potential role as a CO<sub>2</sub> sink makes it essential to develop a more comprehensive understanding of this system. The SO is changing rapidly as the result of climate change, and the Pacific sector of the SO, including the region of the AAR bloom, has seen a significant decrease in NPP since 1997<sup>12</sup>. Interannual variability in NPP across most of the Pacific sector is linked with either changes in the number of open water days or sea surface temperature or both, but NPP in the region of the AAR bloom shows no significant relationship with either<sup>12</sup>. NPP in the region of the AAR bloom has decreased in response to an increasingly positive phase of the Southern Annular Mode (SAM)<sup>12</sup> over the last several decades<sup>46</sup>. However, our understanding of the changes in ocean circulation that result from a positive SAM suggest that NPP in the AAR bloom should increase due to increased upwelling of nutrient-rich deep water<sup>47</sup> instead of the decrease observed. Perhaps the decrease in NPP in the AAR bloom is due to light limitation of phytoplankton growth resulting from an increase in MLD<sup>48</sup>. Regardless, without understanding the mechanisms controlling production in the AAR bloom, we cannot predict how it will be impacted by future changes anticipated for the SO, and how those will affect the role of the AAR bloom as a CO<sub>2</sub> sink and upper trophic level hotspot.

## Methods

**Phantastic I cruise (NBP1310).** During the NBP1310 cruise aboard the RVIB Nathaniel B. Palmer, we sampled an area of the Pacific sector of the SO to the northwest of the Ross Sea, just south of the sACCf and adjacent to the sbACC from 7–15 January 2014 (Fig. 1c, d), where remotely sensed Chl *a* concentrations were unusually high. We sampled a total of nine stations, six of which extended to a depth of 400 m and three to 2000 m. Bottom depth at our sampling stations ranged from 2762 m at station 135 to 3126 m at station 140/149 (Fig. 1c, d).



Underway measurements of temperature (Seabird SBE-38), salinity (Seabird SBE-45), oxygen (Oxygen Optode 3835), fluorescence (WET Lab AFL), and  $p\text{CO}_2$  (using the Lamont Doherty Earth Observatory system<sup>49</sup>) were collected from the flow-through seawater system. Wind speed was measured using a Gill 1390-PK-062/R anemometer. At each station, vertical profiles of conductivity, temperature, and depth (CTD) were measured (24 Hz sampling rate) using a Sea Bird 911 plus CTD package and fluorescence was measured using a WET Labs ECO-HFL/FL fluorometer. The depth of the upper mixed layer (MLD) was defined as depth of the maximum buoyancy frequency<sup>50</sup>.

Discrete water samples were collected during each cast using both a trace-metal clean CTD-rosette package (TMC-CTD)<sup>33</sup>, and a conventional CTD-rosette package. For biological sampling, water was collected at depths of 10, 25, 50, 75, and 100 m, and an additional six to seven depths between 100 and 400 m. Water samples were collected for dissolved Fe (DFe), macronutrients (nitrate, nitrite, phosphate, and silicate), Chl *a*, particulate organic carbon (POC), phytoplankton pigments, and simulated in situ primary production (SIS). Additionally, for the three casts conducted down to 2000 m, we collected water every 200 m below 400 m with the TMC-CTD-rosette for DFe analysis.

DFe samples were collected and filtered (Sartorius®, 0.2 µm; Satorbran 300) in a trace metal clean van. Handling of DFe samples prior to analysis was conducted on a laminar flow bench inside a positive pressure, TMC, plastic bubble. DFe samples were analyzed onboard using the automated flow injection analysis method<sup>32,51</sup>.

Samples for macronutrients were filtered through 0.2 µm Acrodisk filters. Separate samples were taken for silicate, which were stored at 4 °C, and for nitrate and nitrite, which were stored frozen. After the cruise, nutrient samples were analyzed colorimetrically on a Bran and Luebbe trAACS 800 Autoanalyzer<sup>52</sup>. Measurements were made for silicate, nitrate and nitrite together, and nitrite separately. All measurements were calibrated with standards diluted in low nutrient seawater, which was also used as rinse water between the samples.

Samples for POC analysis were filtered onto precombusted (450 °C for 4 h) 25 mm Whatman GF/F filters. Filters were dried at 60 °C for analysis on a Costech Elemental Analyzer using acetonilide as a calibration standard<sup>53</sup>.

Samples for Chl *a* were collected and analyzed on board with a Turner Model 10 AU fluorometer using the acidification method<sup>54</sup>. Depth-integrated Chl *a* was calculated down to 100 m at all stations by linearly interpolating between discrete Chl *a* samples. An integration depth of 100 m was chosen to ensure that all phytoplankton biomass was accounted for and to enable direct comparison with depth-integrated Chl *a* values reported elsewhere in the SO. Below 50 m, Chl *a* concentrations were very low and contributed a negligible amount to depth-integrated values.

Samples for HPLC analysis of phytoplankton pigments were filtered onto 25 mm Whatman GF/F filters, flash-frozen in liquid nitrogen, and stored at -80 °C until analysis within six months of collection. Filters for pigment analysis were extracted in 90% acetone (48 h at 4 °C) and then separated by HPLC (Waters 2695, with a Zorbax Eclipse XDB-C8 column, 3.5 µm particle size)<sup>53</sup>. Detection was based on retention time and diode array spectroscopy (Waters 996) at 436 nm<sup>53</sup>. The CHEMTAX analysis package (version 1.95)<sup>55,56</sup> was used to assess phytoplankton class abundance<sup>57</sup>.

Depth-integrated daily NPP was assessed at four different stations (119, 130, 140, and 150) using <sup>14</sup>C-based SIS production on-deck incubations<sup>58</sup>. Depth-integrated NPP was calculated to the depth of the 1% light level. The depth of light levels used for the integration (85%, 65%, 25%, 10%, 5%, 1%) were calculated using Beer's Law and a diffuse attenuation coefficient that was a function of the mean Chl *a* concentration in the mixed layer at each station<sup>59</sup>. The depth of the 1% light level at stations 119 (87 m) and 140 (107 m) outside of the bloom was much deeper than at bloom stations 130 (30 m) and 150 (35 m).

The vertical flux of DFe across the ferricline for each station was calculated by multiplying the DFe concentration gradient by the mean vertical diffusivity. Vertical diffusivity ( $K_z$ ) was calculated from vertical density profiles using Thorpe-scale analysis<sup>33,60</sup> (additional details provided in the Supplementary Material). The DFe concentration gradient for each station was calculated as the slope of the ferricline (defined as the difference between the minimum DFe concentration between 15 and 56 m and the maximum DFe concentration between 150 and 205 m) divided by the thickness of the ferricline (defined as the vertical interval between the minimum and maximum DFe concentrations). Mean vertical diffusivity was calculated as the mean  $K_z$  in the ferricline. Station 135 was excluded from this analysis because it had an anomalously high vertical diffusivity coefficient that was more than two standard deviations above the mean.

Air-sea  $\text{CO}_2$  flux inside the bloom was calculated for each  $p\text{CO}_2$  measurement where underway Chl *a* fluorescence exceeded  $5 \text{ mg m}^{-3}$ , using the corresponding shipboard measurements of wind speed and underway temperature, salinity, and the partial pressure of  $\text{CO}_2$  in water ( $p\text{CO}_{2w}$ ) and the atmosphere ( $p\text{CO}_{2a} = 400 \text{ µatm}$ )<sup>61</sup>. Air-sea  $\text{CO}_2$  flux (negative values denote flux into the ocean) was calculated as<sup>62</sup>:

$$F = kK_0(p\text{CO}_{2w} - p\text{CO}_{2a}) \quad (1)$$

where  $k$  is the gas transfer velocity and  $K_0$  is the solubility of  $\text{CO}_2$  in seawater<sup>63</sup>.

**Satellite imagery.** MODIS/Aqua Chl *a* images were obtained daily during the cruise and were used to target areas of high Chl *a*. To obtain bloom information

after the cruise, we used monthly Chl *a* concentrations from level 3 MODIS/Aqua data (4 km resolution; Supplementary Fig. 1). Additionally, monthly Chl *a* (Oct–Mar) from SeaWiFS (1997–2002) and MODIS/Aqua (2002–2019) were used to calculate images of mean seasonal Chl *a* (Supplementary Fig. 4). Monthly SSMIS (Special Sensor Microwave Imager/Sounder) sea ice concentration data, taken from the NOAA/NSIDC Climate Data Record of Passive Microwave Sea Ice Concentration, Version 3<sup>64</sup>, were used to track the receding sea ice edge, defined as the 50% sea ice concentration contour (25 km resolution). Satellite-based NPP was calculated using the algorithm of Arrigo et al.<sup>11</sup> (details in Arrigo et al.<sup>29</sup>) using IDL (Interactive Data Language, L3Harris Geospatial) and SeaDAS version 7.5.3 (NASA). Geostrophic currents derived from satellite altimetry were produced by Ssalto/Duacs and distributed by the European Copernicus Marine Environment Monitoring Services. This multi-satellite global product provides daily velocities with a  $1/4^\circ$  spatial resolution.

**Lagrangian plume modeling.** A lateral advection scheme based on geostrophic currents from satellite altimetry was used to model the Lagrangian plume downstream from the hydrothermal vents. The plume was estimated by reproducing the dispersion pathways (using satellite-based geostrophic currents) during the high NPP period (Nov–Apr)<sup>65</sup>. Lagrangian trajectories were derived by applying a Runge–Kutta fourth-order scheme with a time step of six hours to the velocity fields, which are linearly interpolated in both space and time. For each advection period, the model identified the most recent contact of each water parcel to the area at the surface directly above the hydrothermal vents. As in Sergi et al.<sup>65</sup>, hydrothermal vents were identified with disks of 50 km radii centered in the hydrothermal vents' locations. For each phytoplankton growing season from 1997–2019, a map was produced every 15 days between 1 November and 30 April. The climatological signal (Supplementary Fig. 3) was created by taking an average of each annual map.

**Argo-derived data products.** The Argo New Displacements Rannou and Ollitrault (ANDRO) dataset uses the displacement of Argo floats at their parking depth to map global ocean circulation<sup>66</sup>. We used the  $3^\circ \times 3^\circ$  resolution gridded climatology data to look at eddy kinetic energy (EKE; calculated as one half of the sum of the standard deviation of the meridional velocity and the zonal velocity) in our region of interest.

The Monthly Isopycnal/Mixed-layer Ocean Climatology (MIMOC) provides global monthly ocean property maps at  $0.5^\circ$  resolution<sup>67</sup>. The maps are based primarily on Argo CTD data, supplemented by shipboard and ice-tethered profiler CTD data. The optimal interpolated (0–1950 dbar) sigma-gridded data for January were used to plot the zonal change in the pressure associated with different isopycnals.

**Statistical analysis.** A two-sample *t*-test was used to compare DFe and  $K_z$  values at stations inside the bloom to those outside the bloom for different depth bins. A Shapiro–Wilk normality test was used to evaluate the normality of the variable distributions. Linear regression analysis was used to evaluate the relationship between vertical DFe flux, vertical DFe gradient, and vertical diffusivity and depth-integrated Chl *a*. Statistical analyses were considered significant for *p* values < 0.05. Statistical analysis was done using R version 3.6.2 (R Project for Statistical Computing).

**Reporting summary.** Further information on research design is available in the Nature Research Reporting Summary linked to this article.

## Data availability

The satellite data that support these findings are freely available and may be downloaded from the links provided here: MODIS/Aqua Chl *a* images are available from <https://oceancolor.gsfc.nasa.gov/>, SSMIS sea ice concentration data are available from <https://www.nsidc.org/data/g02202>, SSALTO/DUACS global gridded sea surface height (product id SEALEVEL\_GLO\_PHY\_L4\_REP\_OBSERVATIONS\_008\_047) is available from <https://marine.copernicus.eu>, the ANDRO dataset is available from <http://www.coriolis.eu.org/Data-Products/Products/ANDRO>, and the MIMOC dataset is available from <https://www.pmel.noaa.gov/mimoc/>. The cruise data that support these findings are available at the Stanford Digital Depository (permanent URL: <https://purl.stanford.edu/sn954dk6470>).

Received: 26 March 2020; Accepted: 22 January 2021;

Published online: 22 February 2021

## References

- Marinov, I., Gnanadesikan, A., Toggweiler, J. R. & Sarmiento, J. L. The Southern Ocean biogeochemical divide. *Nature* **441**, 964–967 (2006).
- Boyd, P. W. et al. Mesoscale iron enrichment experiments 1993–2005: Synthesis and future directions. *Science* **315**, 612–617 (2007).

3. de Baar, H. J. W. et al. On iron limitation of the Southern Ocean: experimental observations in the Weddell and Scotia Seas. *Mar. Ecol. Prog. Ser.* **65**, 105–122 (1990).
4. Martin, J. H., Gordon, R. M. & Fitzwater, S. E. Iron in Antarctic waters. *Nature* **345**, 156–158 (1990).
5. Tagliabue, A. et al. Hydrothermal contribution to the oceanic dissolved iron inventory. *Nat. Geosci.* **3**, 252–256 (2010).
6. Ardyna, M. et al. Hydrothermal vents trigger massive phytoplankton blooms in the Southern Ocean. *Nat. Commun.* **10**, 2451 (2019).
7. Hahm, D. et al. First hydrothermal discoveries on the Australian–Antarctic Ridge: discharge sites, plume chemistry, and vent organisms. *Geochem. Geophys. Geosystems* **16**, 3061–3075 (2015).
8. Sullivan, C. W., Arrigo, K. R., McClain, C. R., Comiso, J. C. & Firestone, J. Distributions of phytoplankton blooms in the southern ocean. *Science* **262**, 1832–1837 (1993).
9. Moore, J. K. & Abbott, M. R. Phytoplankton chlorophyll distributions an primary production in the Southern Ocean. *J. Geophys. Res.* **105**, 28709–28722 (2000).
10. Sokolov, S. & Rintoul, S. R. On the relationship between fronts of the Antarctic Circumpolar Current and surface chlorophyll concentrations in the Southern Ocean. *J. Geophys. Res. Oceans* **112**, 17 (2007).
11. Arrigo, K. R., van Dijken, G. L. & Bushinsky, S. Primary production in the Southern Ocean, 1997–2006. *J. Geophys. Res.* **113**, C08004 (2008).
12. Schine, C. M. S., van Dijken, G. & Arrigo, K. R. Spatial analysis of trends in primary production and relationship with large-scale climate variability in the Ross Sea, Antarctica (1997–2013). *J. Geophys. Res.-Oceans* **121**, 368–386 (2016).
13. Boyd, P. W., Arrigo, K. R., Strzepek, R. & van Dijken, G. L. Mapping phytoplankton iron utilization: Insights into Southern Ocean supply mechanisms. *J. Geophys. Res. Oceans* **117**, 18 (2012).
14. Dotto, T. S. et al. Variability of the Ross Gyre, Southern Ocean: drivers and responses revealed by satellite altimetry. *Geophys. Res. Lett.* **45**, 6195–6204 (2018).
15. Lasbleiz, M. et al. Composition of diatom communities and their contribution to plankton biomass in the naturally iron-fertilized region of Kerguelen in the Southern Ocean. *FEMS Microbiol. Ecol.* **92**, 16 (2016).
16. Schallenberg, C. et al. Sustained upwelling of subsurface iron supplies seasonally persistent phytoplankton blooms around the Southern Kerguelen Plateau, Southern Ocean. *J. Geophys. Res. Oceans* **123**, 5986–6003 (2018).
17. Poulton, A. J. et al. Phytoplankton community composition around the Crozet Plateau, with emphasis on diatoms and Phaeocystis. *Deep Sea Res. II* **54**, 2085–2105 (2007).
18. Robinson, J., Popova, E. E., Srokosz, M. A. & Yool, A. A tale of three islands: downstream natural iron fertilization in the Southern Ocean. *J. Geophys. Res. Oceans* **121**, 3350–3371 (2016).
19. Tagliabue, A. et al. Surface-water iron supplies in the Southern Ocean sustained by deep winter mixing. *Nat. Geosci.* **7**, 314–320 (2014).
20. Blain, S. et al. Effect of natural iron fertilization on carbon sequestration in the Southern Ocean. *Nature* **446**, 1070–U1071 (2007).
21. Law, C. S., Abraham, E. R., Watson, A. J. & Liddicoat, M. I. Vertical eddy diffusion and nutrient supply to the surface mixed layer of the Antarctic Circumpolar Current. *J. Geophys. Res. Oceans* **108**, 14 (2003).
22. Law, C. S., Watson, A. J., Liddicoat, M. I. & Stanton, T. Sulphur hexafluoride as a tracer of biogeochemical and physical processes in an open-ocean iron fertilisation experiment. *Deep Sea Res. II* **45**, 977–994 (1998).
23. Cisewski, B., Strass, V. H. & Prandke, H. Upper-ocean vertical mixing in the Antarctic Polar Front Zone. *Deep Sea Res. II* **52**, 1087–1108 (2005).
24. Nicholson, S. A., Levy, M., Llort, J., Swart, S. & Monteiro, P. M. S. Investigation into the impact of storms on sustaining summer primary productivity in the Sub-Antarctic Ocean. *Geophys. Res. Lett.* **43**, 9192–9199 (2016).
25. Alford, M. H. & Gregg, M. C. Near-inertial mixing: modulation of shear, strain and microstructure at low latitude. *J. Geophys. Res. Oceans* **106**, 16947–16968 (2001).
26. Mahowald, N. M. et al. Change in atmospheric mineral aerosols in response to climate: Last glacial period, preindustrial, modern, and doubled carbon dioxide climates. *J. Geophys. Res. Atmospheres* **111**, 22 (2006).
27. Moore, J. K. & Braucher, O. Sedimentary and mineral dust sources of dissolved iron to the world ocean. *Biogeosciences* **5**, 631–656 (2008).
28. Lancelot, C. et al. Spatial distribution of the iron supply to phytoplankton in the Southern Ocean: a model study. *Biogeosciences* **6**, 2861–2878 (2009).
29. Arrigo, K. R., van Dijken, G. L. & Strong, A. L. Environmental controls of marine productivity hot spots around Antarctica. *J. Geophys. Res. Oceans* **120**, 5545–5565 (2015).
30. Lannuzel, D., Schoemann, V., de Jong, J., Tison, J. L. & Chou, L. Distribution and biogeochemical behaviour of iron in the East Antarctic sea ice. *Mar. Chem.* **106**, 18–32 (2007).
31. Ardyna, M. et al. Delineating environmental control of phytoplankton biomass and phenology in the Southern Ocean. *Geophys. Res. Lett.* **44**, 5016–5024 (2017).
32. Klunder, M. B., Laan, P., Middag, R., De Baar, H. J. W. & van Ooijen, J. C. Dissolved iron in the Southern Ocean (Atlantic sector). *Deep Sea Res. II* **58**, 2678–2694 (2011).
33. Gerringa, L. J. A. et al. Sources of iron in the Ross Sea Polynya in early summer. *Mar. Chem.* **177**, 447–459 (2015).
34. Downes, S. M., Sloyan, B. M., Rintoul, S. R. & Lupton, J. E. Hydrothermal heat enhances abyssal mixing in the Antarctic Circumpolar Current. *Geophys. Res. Lett.* **46**, 812–821 (2019).
35. Orsi, A. H., Whitworth, T. & Nowlin, W. D. On the meridional extent and fronts of the Antarctic Circumpolar Current. *Deep Sea Res. I* **42**, 641–673 (1995).
36. Hiscock, M. R. et al. Primary productivity and its regulation in the Pacific Sector of the Southern Ocean. *Deep Sea Res. II* **50**, 533–558 (2003).
37. Schlitzer, R. et al. The GEOTRACES intermediate data product 2017. *Chem. Geol.* **493**, 210–223 (2018).
38. Resing, J. A. et al. Basin-scale transport of hydrothermal dissolved metals across the South Pacific Ocean. *Nature* **523**, 200–U140 (2015).
39. Morton, B., Taylor, G. I. & Turner, J. S. Turbulent gravitational convection from maintained and instantaneous sources. *Proc. R. Soc. Lond. Ser. A. Math. Phys. Sci.* **234**, 1–23 (1956).
40. Turner, J. *Buoyancy effects in fluids*, (Cambridge University Press Cambridge, 1973).
41. Speer, K. G. & Rona, P. A. A model of an Atlantic and Pacific hydrothermal plume. *J. Geophys. Res. Oceans* **94**, 6213–6220 (1989).
42. Monaco, C. L., Metzl, N., d'Ovidio, F., Llort, J. & Ridame, C. Rapid establishment of the CO<sub>2</sub> sink associated with Kerguelen's bloom observed during the KEOPS2/OISO20 cruise. *Biogeosci. Discuss.* 17543–17578, <https://doi.org/10.5194/bgd-11-17543-2014> (2014).
43. DeJong, H. B. & Dunbar, R. B. Air-Sea CO<sub>2</sub> exchange in the Ross Sea, Antarctica. *J. Geophys. Res. Oceans* **122**, 8167–8181 (2017).
44. Tynan, C. T. Ecological importance of the Southern Boundary of the Antarctic Circumpolar Current. *Nature* **392**, 708–710 (1998).
45. Andrews-Goff, V. et al. Humpback whale migrations to Antarctic summer foraging grounds through the southwest Pacific Ocean. *Sci. Rep.* **8**, 14 (2018).
46. Marshall, G. J. Trends in the Southern Annular Mode from observations and reanalyses. *J. Clim.* **16**, 4134–4143 (2003).
47. Lovenduski, N. S. & Gruber, N. Impact of the Southern Annular Mode on Southern Ocean circulation and biology. *Geophys. Res. Lett.* **32**, <https://doi.org/10.1029/2005GL022727> (2005).
48. Panassa, E., Volker, C., Wolf-Gladrow, D. & Hauck, J. Drivers of interannual variability of summer mixed layer depth in the Southern Ocean Between 2002 and 2011. *J. Geophys. Res. Oceans* **123**, 5077–5090 (2018).
49. Bates, N. R., Takahashi, T., Chipman, D. W. & Knap, A. H. Variability of pCO<sub>2</sub> (2) on diel to seasonal timescales in the Sargasso Sea near Bermuda. *J. Geophys. Res. Oceans* **103**, 15567–15585 (1998).
50. IOC, SCOR & IAPSO. *The international thermodynamic equation of seawater - 2010: Calculation and use of thermodynamic properties.*, Vol. 56 (UNESCO, 2010).
51. Gerringa, L. J. A. et al. Iron from melting glaciers fuels the phytoplankton blooms in Amundsen Sea (Southern Ocean): Iron biogeochemistry. *Deep Sea Res. II* **71-76**, 16–31 (2012).
52. Grasshoff, K., Kremling, K. & Ehrhardt, M. *Methods of seawater analysis.* (John Wiley & Sons, 2009).
53. Alderkamp, A. C. et al. Effects of iron and light availability on phytoplankton photosynthetic properties in the Ross Sea. *Mar. Ecol. Prog. Ser.* **621**, 33–50 (2019).
54. Holm-Hansen, O., Lorenzen, C. J., Holmes, R. W. & Strickland, J. D. H. Fluorometric determination of chlorophyll. *J. Cons. Perm. int. Explor. Mer.* **30**, 3–15 (1965).
55. Mackey, M. D., Mackey, D. J., Higgins, H. W. & Wright, S. W. CHEMTAX - a program for estimating class abundances from chemical markers: application to HPLC measurements of phytoplankton. *Mar. Ecol. Prog. Ser.* **144**, 265–283 (1996).
56. Wright, S. W. et al. Analysis of phytoplankton of the Australian sector of the Southern Ocean: comparisons of microscopy and size frequency data with interpretations of pigment HPLC data using the 'CHEMTAX' matrix factorisation program. *Mar. Ecol. Prog. Ser.* **144**, 285–298 (1996).
57. Alderkamp, A. C. et al. Fe availability drives phytoplankton photosynthesis rates during spring bloom in the Amundsen Sea Polynya, Antarctica. *Elem. Sci. Anthr.* **3**, 26 (2015).
58. Joy-Warren, H. L. et al. Light is the primary driver of early season phytoplankton production along the Western Antarctic Peninsula. *J. Geophys. Res. Oceans* **124**, 7375–7399 (2019).
59. Morel, A. Optical modeling of the upper ocean in relation to its biogenous matter content (case I waters). *J. Geophys. Res. Oceans* **93**, 10749–10768 (1988).

60. Thorpe, S. A. Turbulence and mixing in a Scottish loch. *Philos. Trans. R. Soc. A Math. Phys. Eng. Sci.* **286**, 125–181 (1977).
61. Wanninkhof, R. Relationship between wind speed and gas exchange over the ocean revisited. *Limnol. Oceanogr. Meth.* **12**, 351–362 (2014).
62. Wanninkhof, R. Relationship between wind speed and gas exchange over the ocean. *J. Geophys. Res. Oceans* **97**, 7373–7382 (1992).
63. Weiss, R. F. Carbon dioxide in water and seawater: the solubility of a non-ideal gas. *Mar. Chem.* **2**, 203–215 (1974).
64. Peng, G., Meier, W. N., Scott, D. J. & Savoie, M. H. A long-term and reproducible passive microwave sea ice concentration data record for climate studies and monitoring. *Earth Syst. Sci. Data* **5**, 311–318 (2013).
65. Sergi, S. et al. Interaction of the Antarctic Circumpolar Current With seamounts fuels moderate blooms but vast foraging grounds for multiple marine predators. *Front. Marine Sci.* **7**, <https://doi.org/10.3389/fmars.2020.00416> (2020).
66. Ollitrault, M. & Rannou, J.-P. ANDRO: an argo-based deep displacement dataset. *J. Atmos. Ocean. Technol.* **30**, 759–788 (2013).
67. Schmidtko, S., Johnson, G. C. & Lyman, J. M. MIMOC: a global monthly isopycnal upper-ocean climatology with mixed layers. *J. Geophys. Res. Oceans* **118**, 1658–1672 (2013).

### Acknowledgements

We thank the captain and crew of the RVIB Nathaniel B. Palmer for their assistance during the cruise. We also thank all the members of the Phantastic I research team, whose tireless work contributed greatly to this research. This work was supported by the National Science Foundation, Office of Polar Programs (ANT-1063592).

### Author contributions

C.M.S.S., A.-C.A. and G.v.D. conducted the data analysis. C.M.S.S. wrote the paper. K.R. A. wrote the original grant proposal. L.J.A.G. and P.L. collected and analyzed trace metal samples. H.v.H. calculated vertical diffusivity. W.H.v.d.P. analyzed pigment samples. S.S. provided the Lagrangian particle tracking results. All authors contributed to the ideas and commented on the manuscript.

### Competing interests

The authors declare no competing interests.

### Additional information

**Supplementary information** The online version contains supplementary material available at <https://doi.org/10.1038/s41467-021-21339-5>.

**Correspondence** and requests for materials should be addressed to C.M.S.S.

**Peer review information** *Nature Communications* thanks Michael Ellwood, Joseph Resing and other, anonymous, reviewers for their contributions to the peer review of this work. Peer review reports are available.

**Reprints and permission information** is available at <http://www.nature.com/reprints>

**Publisher's note** Springer Nature remains neutral with regard to jurisdictional claims in published maps and institutional affiliations.



**Open Access** This article is licensed under a Creative Commons Attribution 4.0 International License, which permits use, sharing, adaptation, distribution and reproduction in any medium or format, as long as you give appropriate credit to the original author(s) and the source, provide a link to the Creative Commons license, and indicate if changes were made. The images or other third party material in this article are included in the article's Creative Commons license, unless indicated otherwise in a credit line to the material. If material is not included in the article's Creative Commons license and your intended use is not permitted by statutory regulation or exceeds the permitted use, you will need to obtain permission directly from the copyright holder. To view a copy of this license, visit <http://creativecommons.org/licenses/by/4.0/>.

© The Author(s) 2021

## 1.3 Synthesis and perspectives

### 1.3.1 Summary of key results

BGC-Argo floats provide important insights on the circumpolar distribution of phytoplankton blooms. In section 1.2, three intense blooms (maximum depth-integrated biomass superior to  $80 \text{ mg Chla m}^{-2}$ ) are detected in an otherwise low productive region: these are located surrounding or downstream of active hydrothermal vents at the South West Indian Ridge (SWIR) or the Australian-Antarctic Ridge (AAR) (red dots in Figure 1 A of section 1.2). None of these blooms can be explained by known iron inputs (sea ice, continental shelves or atmospheric deposition). Sections 1.2 and 1.2 use multiple observations in order to shed light on the origin of such important phytoplankton biomasses downstream of the SWIR and the AAR, respectively.

In section 1.2, vertical distributions of  $\delta^3\text{He}$ , a conservative tracer of hydrothermal iron, demonstrate its presence in the water column. In section 1.2, the likely presence of hydrothermal iron is corroborated by important dissolved iron concentrations in the bloom region (from the subsurface down to 2000 m; significantly higher than outside the bloom). These iron-laden water masses are characteristic of a non-buoyant hydrothermal vent plume (colder, fresher and more oxygenated) different from the overlying deep Upper Circumpolar Deep Water.

The ability of hydrothermal input to reach the productive layer from shallow ( $<500 \text{ m}$ ) hydrothermal vent fields has already been demonstrated in the Pacific Ocean [Guieu et al., 2018; Hawkes et al., 2014]. Contrary to the shallow volcanic systems of the Pacific Ocean, hydrothermal vents in the Southern Ocean are significantly deeper ( $\sim 2000 \text{ m}$  deep for the ones considered in Schine et al. [2021] and  $>3500 \text{ m}$  deep for those in Ardyna et al. [2019]). Consequently, important vertical connections are needed for introducing the hydrothermal signal into the productive layer. Two mechanisms are considered for driving up the hydrothermal iron. Firstly, the buoyant plume rises from the hydrothermal vent due to



density difference and it is advected once it reaches the neutral buoyancy [Morton et al., 1956; Turner, 1979]. Secondly, an upwelling motion is needed for rising the non-buoyant plume until the euphotic layer. The intense ACC is known to be able to generate intense upward movements, particularly when it interacts with topography [Sokolov and Rintoul, 2007; Tamsitt et al., 2017].

In our studies, several *in situ* observations corroborate these upward movements. Firstly, an along-stream shallowing of isopycnal is observed both at the SWIR and AAR regions. Secondly, intense deep ( $\sim 1000$  m) Eddy Kinetic Energy values are observed in the SWIR region ( $> 200 \text{ cm}^{-2} \text{ s}^{-2}$ , Ardyna et al. [2019]); while intense vertical diffusivities are measured across the ferricline in the AAR region ( $0.9 - 4.4 \cdot 10^{-3} \text{ m}^{-2} \text{ s}^{-1}$ , Schine et al. [2021]). The Lagrangian analyses of geostrophic velocities are the final pieces of the puzzles. In section 1.2, the analysis reproduces the horizontal delivery of deep upwelled water masses down to the large-scale intense phytoplankton blooms observed by the BGC-Argo floats. In section 1.2, the extension and shape of the high net primary production (NPP) plume estimated by satellites between 1997 and 2019 is successfully reproduced by the analysis of geostrophic currents: almost all the regions of the AAR displaying climatological high NPP values (up to  $45 \text{ gC m}^{-2} \text{ y}^{-1}$ ) were in the four months before the bloom period (November to April) above the hydrothermal vents (Figure 1.1).

### 1.3.2 Further insights from horizontal transport analysis

Iron residence time is a key concept in biogeochemistry with profound implications [Bergquist et al., 2007; Boyd and Ellwood, 2010; Shaked and Lis, 2012]. A recent global study combining  $^{234}\text{Th}$ - and sediment-trap data from several GEOTRACES transects has estimated a residence time of iron ranging between 10 and 100 days in the surface ocean (0-250 m) [Black et al., 2020]. By contrast, in the ocean interior, considered deeper than 1500 m depth, this lifetime increases up to 100 years [Bruland et al., 1994; Bergquist and Boyle, 2006; Weber, 2020]. Residence time of hydrothermal iron in the ocean interior is even more difficult to evaluate, due the lack of observations. Modelling studies have estimated

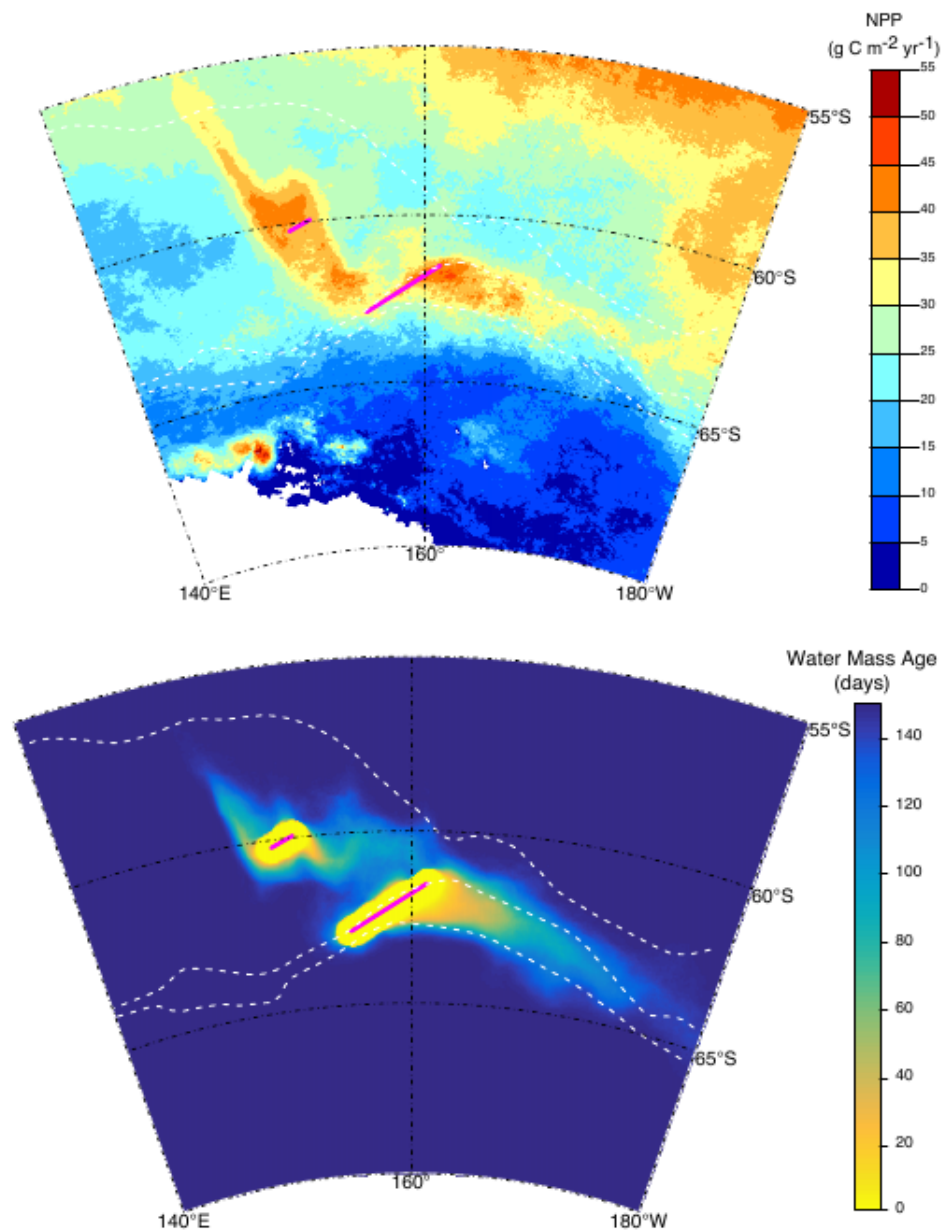


FIGURE 1.1: **Position of the bloom relative to the position of the Lagrangian plume generated by releasing particles at the surface above the vents.** Maps of (a) Net Primary Production (NPP) climatology (1997-2019) and the (b) climatology of the Lagrangian plume stemming from the surface directly above the position of the hydrothermal vents. The Lagrangian plume shows the distance in time of water masses to the vents. Vent positions are indicated by the pink lines. The positions of the polar front, the southern ACC front (sACCf), and the southern boundary of the ACC (sbACC) from north to south, respectively, are shown by the white dashed lines. Supplementary Figure 3 from Schine et al. [2021].

the lifetime of iron-binding ligands from hydrothermal vents between 1 and 1000 years, depending on the ligand concentration [Tagliabue and Resing, 2016]. Even if the accurate estimation of the residence time of hydrothermal iron in the ocean interior cannot be defined yet, the observed distal iron signals associated with hydrothermal systems observed in many oceanic basins and the quasi-conservative behaviour of dissolved iron observed within hydrothermal plumes, confirm the stabilisation of this element in the ocean interior during a period of orders of tens of years [Resing et al., 2015; Tagliabue and Resing, 2016].

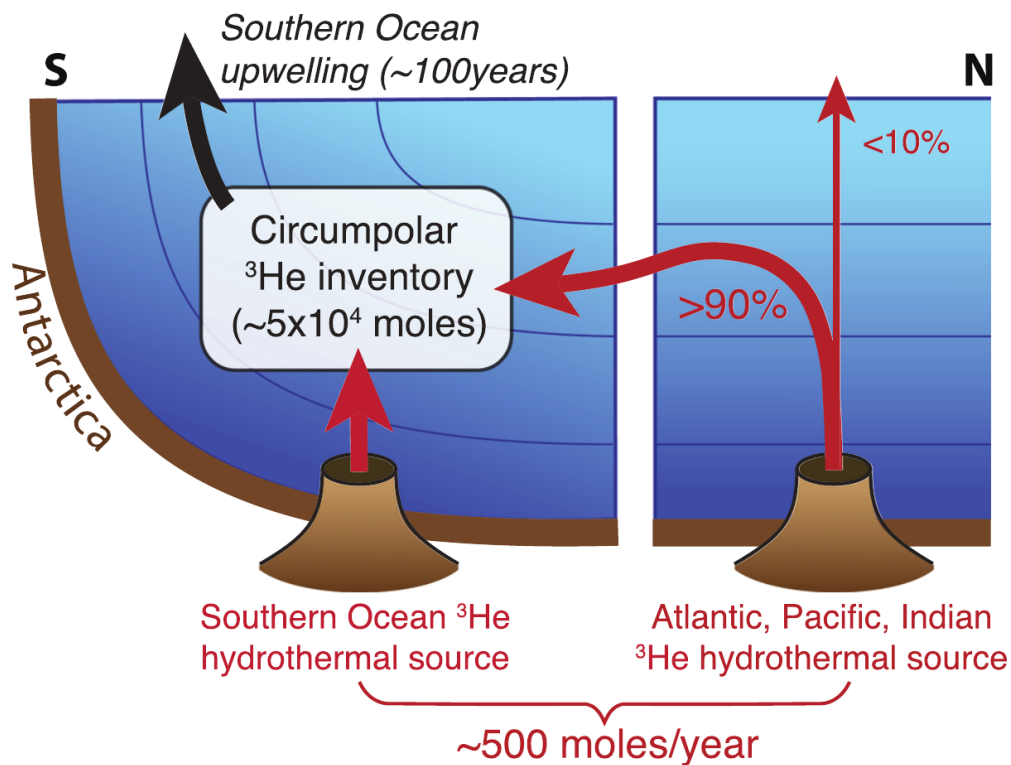


FIGURE 1.2: **Schematic representation of the Southern Ocean reservoir of hydrothermal  $^3\text{He}$ .** The reservoir of  $^3\text{He}$  housed in Circumpolar Deep Water is sourced from both circumpolar hydrothermal vents (local) or from hydrothermal vents within other oceanic basins (remote). From Weber [2020]

Therefore, due to important stabilisation of hydrothermal iron and to the global overturning circulation, the circumpolar reservoir of hydrothermal iron is thought to be maintained

by both local and remote hydrothermalism [Tagliabue and Resing, 2016; Weber, 2020]. Figure 1.2 provides a schematic representation of the hydrothermal  $^3\text{He}$  reservoir in the Southern Ocean, enhancing the substantial part of global hydrothermal  $^3\text{He}$  which is ventilated in the Southern Ocean from other basins. The relative impact of local (circumpolar) compared to remote (other basins) ridge systems in fuelling the Southern Ocean hydrothermal reservoir has been evaluated [Tagliabue and Resing, 2016; Jenkins, 2020]. The observations considered in our studies do not allow us to differentiate the part of hydrothermal iron tied to local versus remote vent systems cannot. In this context, the evaluation of horizontal dispersion pathways is a key information. Indeed, in section 1.2, the Lagrangian analyses allow us to connect the interannual consistent position of the high NPP plume directly to the hydrothermal vents, suggesting a close effect of local hydrothermal iron over primary production. By comparison, in section 1.2 the phytoplankton blooms are connected to an upwelling region, where both local and remote hydrothermal iron can be injected to the surface layer.

Due to the recurrent position of phytoplankton blooms in the AAR region (Supplementary Figs. 3 and 4 in Schine et al. [2021]), the possible direct effect of hydrothermal iron sources on local primary production can be further investigated by looking at interannual variability of the stirring pathways. In the preliminary analyses shown in Figure 1.3, the extension of the high NPP plume is compared to the spatial extension of the Lagrangian plume during two contrasted years. During the year 2004/2005 the high NPP plume has a limited extension, contrary to the year 2008/2009. The Lagrangian analysis reveals that during the year 2008/2009 the water masses that were in contact with the vents travelled about 300 km further downstream than the ones during the year 2004/2005. Following this preliminary result, it could be interesting to analyse whether the interannual variability in the extension of the NPP plume above the hydrothermal fields can be explained by the interannual variability of horizontal advection. Similarly, the spatial extension of island mass effects of Kerguelen, Crozet and South Georgia Islands and the horizontal advection in these regions have been investigated over interannual time scales in order to understand their possible relationships [Robinson et al., 2016].

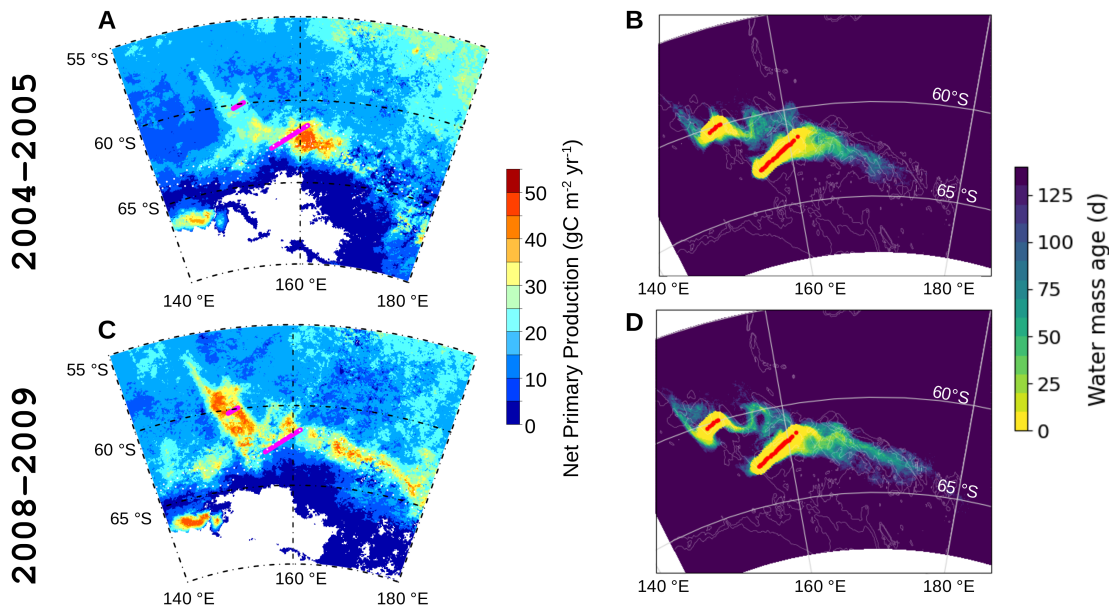


FIGURE 1.3: **Preliminary analysis of contrasted extensions of the high Net Primary Production (NPP) plume and the Lagrangian plume standing from hydrothermal vents.** During the year 2004/2005 the high NPP and the Lagrangian plumes have both limited extension (A, B), contrary to the year 2008/2009 (C, D). The Lagrangian plumes were computed during the high NPP period. For each phytoplankton growing season (years 2004/2005 and 2008/2009) it averages the Lagrangian plumes computed every 15 days between the 31 of December and the 30 of April. Hydrothermal vents are identified with disks of 50 km radii centered in hydrothermal vents' locations as in Schine et al. [2021]. Hydrothermal vents' locations are represented in pink (A, C) or in red (B, D). Satellite-based NPP maps are from the Supplementary Information of Schine et al. [2021].

### 1.3.3 Ecological impact of hydrothermal activity in the Southern Ocean

As introduced previously, hydrothermal signal has already been observed to penetrate into the surface layer in the tropical Pacific ocean. This was observed close to patches of high chlorophyll *a* concentrations linked to the occurrence of  $N_2$ -fixing organisms which need high iron supply. However, no direct connections between the high phytoplankton patches and the hydrothermal signal has been established yet [Guieu et al., 2018]<sup>1</sup>. To

<sup>1</sup>This could be challenged soon. The TONGA oceanographic cruise (PIs: S. Bonnet and C. Guieu) sampled the same region in 2019 in order to investigate the possible hydrothermal origin of a phytoplankton oasis located in the same region.

our knowledge, the studies presented in this Chapter are the first observations of direct connections between hydrothermal iron and surface primary production. The intense phytoplankton responses observed here (e.g., maximum depth-integrated biomass measured by profiling floats superior to  $80 \text{ mg Chla m}^{-2}$ ) are likely due to the strong iron limitation of primary production in the Southern Ocean [Martin, 1990; de Baar, 2005; Sohrin et al., 2000; Martínez-García et al., 2014]. The hydrothermal iron fuelling these phytoplankton biomasses is susceptible to have potential important implications for both carbon biological pump and pelagic ecosystems. As for instance, in January 2014, the AAR bloom sampled by the Phantastic I cruise was associated to a mean air-sea  $\text{CO}_2$  flux of  $-32 \text{ mmol m}^{-2} \text{ d}^{-1}$  (section 1.2). This is three times higher than maximum air-sea  $\text{CO}_2$  flux measured in the Kerguelen bloom [Merlivat et al., 2015]. In addition, co-authors of section 1.2 showed that humpback whales migrating between Australia and Antarctica frequently fed in the AAR bloom, indicating a potential trophic hotspot (Figure 5 of section 1.2 and Andrews-Goff et al. [2018]). On the other hand, the upwelling region considered for the SWIR bloom (section 1.2) has already been suggested as a foraging hotspot for the populations of seabirds and seals breeding at the Prince Edward Islands [Nel et al., 2001]. In this case, the hydrothermal iron observed in section 1.2 would have significant ecological implications in this region. The ecological impact of alternative iron delivery pathways in the Southern Ocean is further explored in the following Chapter.



## Chapter 2

# Unexplained pelagic hotspots: ecological role of seamounts

The two studies presented in the previous Chapter looked at intense phytoplankton blooms unexplained by known iron inputs in the Southern Ocean and investigated their origins. This Chapter adopts a complementary approach: it uses upper trophic levels hotspots for selecting the study region. As evoked in [the Introduction](#), marine top predators are widely used by ecologists and conservationists as biological indicators in the open ocean. Indeed, regions preferred by multiple predators species may be indicative of the high level presence of lower trophic biomass and biodiversity [[Thiers et al., 2017](#); [Lascelles et al., 2012](#); [Hindell et al., 2020](#)]. The [following study](#) identifies an open ocean region consistently targetted by multiple upper predators (seals and penguins) breeding at the South African Prince Edward Islands. This region, distant from known high iron supplies, lies downstream of numerous seamounts. The interaction of current with topographies has already been demonstrated to frequently enhance the phytoplankton biomass [[Sokolov and Rintoul, 2007](#)], however past studies did not detect phytoplankton enhancements over the submerged topographies present in this region [[Mongin et al., 2009](#); [Ardyna et al., 2017](#)]. More generally, the inter-islands waters in the ACC region are often considered to play



a negligible role in the Southern Ocean productivity [Mongin et al., 2009; Ardyna et al., 2017]. The study contained in this Chapter reevaluates the apparent oligotrophic nature of the study region revealed by climatological Ocean Color maps and the role of seamount in sustaining its productivity. The novelty of our approach relies on two main aspects: (1) it uses a recent high resolution seamount database, (2) it assumes an ecological perspective differently to the biogeochemical perspective adopted in Mongin et al. [2009] and Ardyna et al. [2017]. This ecological perspective is required to study smaller and shorter spatial and time scales compared to past circumpolar and climatological studies.

## **2.1 Sergi et al., 2020: Interaction of the Antarctic Circumpolar Current With Seamounts Fuels Moderate Blooms but Vast Foraging Grounds for Multiple Marine Predators; *Frontiers in Marine Sciences***

Here below is inserted the original manuscript by Sergi et al. [2020].



# Interaction of the Antarctic Circumpolar Current With Seamounts Fuels Moderate Blooms but Vast Foraging Grounds for Multiple Marine Predators

Sara Sergi<sup>1\*</sup>, Alberto Baudena<sup>1,2</sup>, Cédric Cotté<sup>1</sup>, Mathieu Ardyna<sup>2,3</sup>, Stéphane Blain<sup>4</sup> and Francesco d'Ovidio<sup>1</sup>

<sup>1</sup> Sorbonne Université, CNRS, IRD, MNHN, Laboratoire d'Océanographie et du Climat: Expérimentations et Approches Numériques (LOCEAN-IPSL), Paris, France, <sup>2</sup> Laboratoire d'Océanographie de Villefranche (LOV), Sorbonne Université, CNRS, Villefranche-sur-Mer, France, <sup>3</sup> Department of Earth System Science, Stanford University, Stanford, CA, United States, <sup>4</sup> Laboratoire d'Océanographie Microbienne (LOMIC), Sorbonne Université, CNRS, Banyuls-sur-Mer, France

## OPEN ACCESS

### Edited by:

Andrew John Constable,  
Australian Antarctic Division, Australia

### Reviewed by:

Peter Strutton,  
University of Tasmania, Australia  
Vladimir Laptikhovskiy,  
Centre for Environment, Fisheries  
and Aquaculture Science (Cefas),  
United Kingdom

### \*Correspondence:

Sara Sergi  
sara.sergi@locean-ipsl.upmc.fr

### Specialty section:

This article was submitted to  
Global Change and the Future Ocean,  
a section of the journal  
Frontiers in Marine Science

**Received:** 22 January 2020

**Accepted:** 12 May 2020

**Published:** 09 June 2020

### Citation:

Sergi S, Baudena A, Cotté C,  
Ardyna M, Blain S and d'Ovidio F  
(2020) Interaction of the Antarctic  
Circumpolar Current With Seamounts  
Fuels Moderate Blooms but Vast  
Foraging Grounds for Multiple Marine  
Predators. *Front. Mar. Sci.* 7:416.  
doi: 10.3389/fmars.2020.00416

In the Antarctic Circumpolar Current region of the Southern Ocean, the massive phytoplankton blooms stemming from islands support large trophic chains. Contrary to islands, open ocean seamounts appear to sustain blooms of lesser intensity and, consequently, are expected to play a negligible role in the productivity of this area. Here we revisit this assumption by focusing on a region of the Antarctic Circumpolar Current zone which is massively targeted by marine predators, even if no island fertilizes this area. By combining high resolution bathymetric data, Lagrangian analyses of altimetry-derived velocities and chlorophyll *a* observations derived from BGC-Argo floats and ocean color images, we reveal that the oligotrophic nature of the study region considered in low chlorophyll *a* climatological maps hides in reality a much more complex environment. Significant (chlorophyll *a* in excess of 0.6 mg/m<sup>3</sup>) phytoplankton blooms spread over thousands of kilometers and have bio-optical signatures similar to the ones stemming from island systems. By adopting a Lagrangian approach, we demonstrate that these moderate blooms (i) originate at specific sites where the Antarctic Circumpolar Current interacts with seamounts, and (ii) coincide with foraging areas of five megafauna species. These findings underline the ecological importance of the open ocean subantarctic waters and advocate for a connected vision of future conservation actions along the Antarctic Circumpolar Current.

**Keywords:** open ocean seamounts, phytoplankton blooms, Antarctic Circumpolar Current, Lagrangian approach, pelagic hotspots

## INTRODUCTION

Marine phytoplankton production drives ecosystem trophic structures (Iverson, 1990; Frederiksen et al., 2006; Boersma et al., 2009; Block et al., 2011) and ecosystem services, ranging from carbon export (Michaels and Silver, 1988; Legendre and Rassoulzadegan, 1995; Heinze et al., 2015) to fisheries production (Chassot et al., 2010). Consequently, understanding the factors underpinning phytoplankton productivity has major implications for process studies. These

include the parameterization of nutrient input adopted in biogeochemical models (Aumont and Bopp, 2006; Lancelot et al., 2009; Tagliabue et al., 2014) and the identification of biological hotspots for the management and conservation of marine living resources (Gove et al., 2016; Santora et al., 2017).

In the Atlantic and Indian sectors of the Antarctic Circumpolar Current (ACC) region (**Figure 1A**), iron limitation generates intense contrasts in the biological productivity (e.g., Martin, 1990; Sullivan et al., 1993; De Baar et al., 1995; Boyd et al., 2000) affecting the distribution of pelagic ecosystems, from primary producers to upper predators (De Broyer et al., 2014). The major source of iron for the shallow ocean is provided by the interaction of the eastward ACC flow with the shallow bathymetry around islands (Sullivan et al., 1993; Thomalla et al., 2011; Ardyna et al., 2017). The island mass effect stimulates dramatic phytoplankton blooms, such as the ones occurring downstream of South Georgia, Crozet, and the Kerguelen Plateau (Sohrin et al., 2000; Blain et al., 2001, 2007; Moore and Abbott, 2002; Lancelot et al., 2009; Pollard et al., 2009; Borriane et al., 2014; d'Ovidio et al., 2015; see also **Figure 1A**). This large phytoplankton biomass is at the basis of the pelagic food web which sustains numerous colonies of predators breeding in the subantarctic islands (De Broyer et al., 2014). Pinnipeds and seabirds intensively forage in the phytoplankton plumes extending in the Antarctic Polar Front (PF) region downstream of South Georgia (Barlow and Croxall, 2002; Staniland et al., 2004; Scheffer et al., 2010; Rogers et al., 2015) and the Kerguelen Plateau (Guinet et al., 2001; Lea et al., 2006; Cotté et al., 2015; O'Toole et al., 2017).

Away from the islands, the interaction of the ACC with large and deep (>2500 m) topographic features, as mid-ocean ridges, is recognized to generate intense upward movements (Sokolov and Rintoul, 2007; Rintoul, 2018). These vertical motions regularly sustain some phytoplankton productivity through the injection of iron into the euphotic layer (Sokolov and Rintoul, 2007). However, with the notable exception of isolated contributions from hydrothermal vents (Ardyna et al., 2019), these vast open ocean regions show a yearly averaged phytoplankton biomass much lower than the island systems. Thereby, their contribution to the primary production of the ACC region is considered comparatively negligible (Graham et al., 2015; Ardyna et al., 2017). Furthermore, these regionally contrasted quantitative assessments of primary production are accompanied by differences in phytoplankton community composition. Islands blooms are dominated by diatoms, while the open ocean low productive (low phytoplankton) regions are generally described by other lower size (nano-, pico-plankton) phytoplankton communities, like for instance *Phaeocystis* (Detmer and Bathmann, 1997; Gervais et al., 2002; Smetacek et al., 2004; Queguiner, 2013). These High Nutrient Low Chlorophyll (HNLC) communities are less likely to support pelagic ecosystems that include large predators as marine

mammals or seabirds (Cushing, 1989; Moline et al., 2004; Pakhomov et al., 2019).

It is becoming therefore tempting to see the ACC as an (iron limited) HNLC phytoplankton-desert, punctuated by oases in the wake of islands or hydrothermal vents. However, this view is not consistent with megafauna observations. One of the supposedly low productive regions has been recently associated to intense foraging activity of five species of swimming predators breeding at the Prince Edward Islands: Antarctic Fur Seals (*Arctocephalus gazella*), Southern Elephants Seals (*Mirounga leonina*), King Penguins (*Aptenodytes patagonicus*), Macaroni Penguins (*Eudyptes chrysolophus*), and Southern Rockhopper Penguins (*Eudyptes chrysocome chrysocome*) (Arthur et al., 2017; Pistorius et al., 2017; Reisinger et al., 2018). Differently from the colonies of the South Georgia and Kerguelen Islands, penguins and seals, after moving to the PF region, travel upstream and explore an apparently oligotrophic area (**Figure 1A**). Although some of the animals focus on an area associated to intense phytoplankton blooms sustained by upwelled water masses enriched by hydrothermal iron (downstream of 30°E; Ardyna et al., 2019), some others travel and forage further upstream, in the supposedly HNLC biologically-desert area. These long trips are recurrent and energy-consuming and require to be balanced by profitable prey captures. But what is the origin of the phytoplankton production sustaining this prey field?

This paper addresses this question, reassessing from an ecological viewpoint the productivity and nutrient delivery of vast open ocean regions in the ACC area. In particular, our work proposes to extend the biogeochemical island mass effect to the numerous seamounts located upstream of the foraging grounds of marine high-level predators (**Figure 1C**). In respect to previous studies which assessed the seamounts effect as negligible compared with the island one (e.g., Graham et al., 2015; Ardyna et al., 2017), we propose to investigate it further through two new main datasets. First of all, we use the high resolution seamount inventory provided by Yesson et al. (2011) (an illustrative example is depicted in the bottom panels of **Figure 1**). Previous studies analyzed coarser bathymetric dataset, thus not allowing to identify most of the seamounts. Secondly, we assume a regional ecological perspective, while previous works had a large-scale biogeochemical focus (Graham et al., 2015; Ardyna et al., 2017). In this aim, we investigate the seamount effect over seasonal time scales and we complement the satellite images with profiling floats' observations, which allow us to infer the total phytoplankton biomass contained in the water column. Indeed, from a circumpolar biogeochemical viewpoint, moderate phytoplankton biomass may appear almost invisible on annual mean climatology when compared to the dramatic production occurring in the wake of the subantarctic islands. However, from an ecological perspective, seasonal secondary blooms may represent a critical input of biomass for local trophic chains. This is especially true when considering the possible effect of these blooms in sustaining foraging grounds of predators who are tied to a specific region for energetic or physiological purposes.

We stress that understanding the factors behind the foraging activity of land-breeding predators is of urgent concern, given the

**Abbreviations:** ACC, Antarctic Circumpolar Current; BGC-Argo, Biogeochemical Argo; CCAMLR, Commission for the Conservation of Antarctic Marine Living Resources; chl *a*, chlorophyll *a*; PF, Antarctic Polar Front; SRS, Shona Ridge System; SWIR, South-West Indian R.

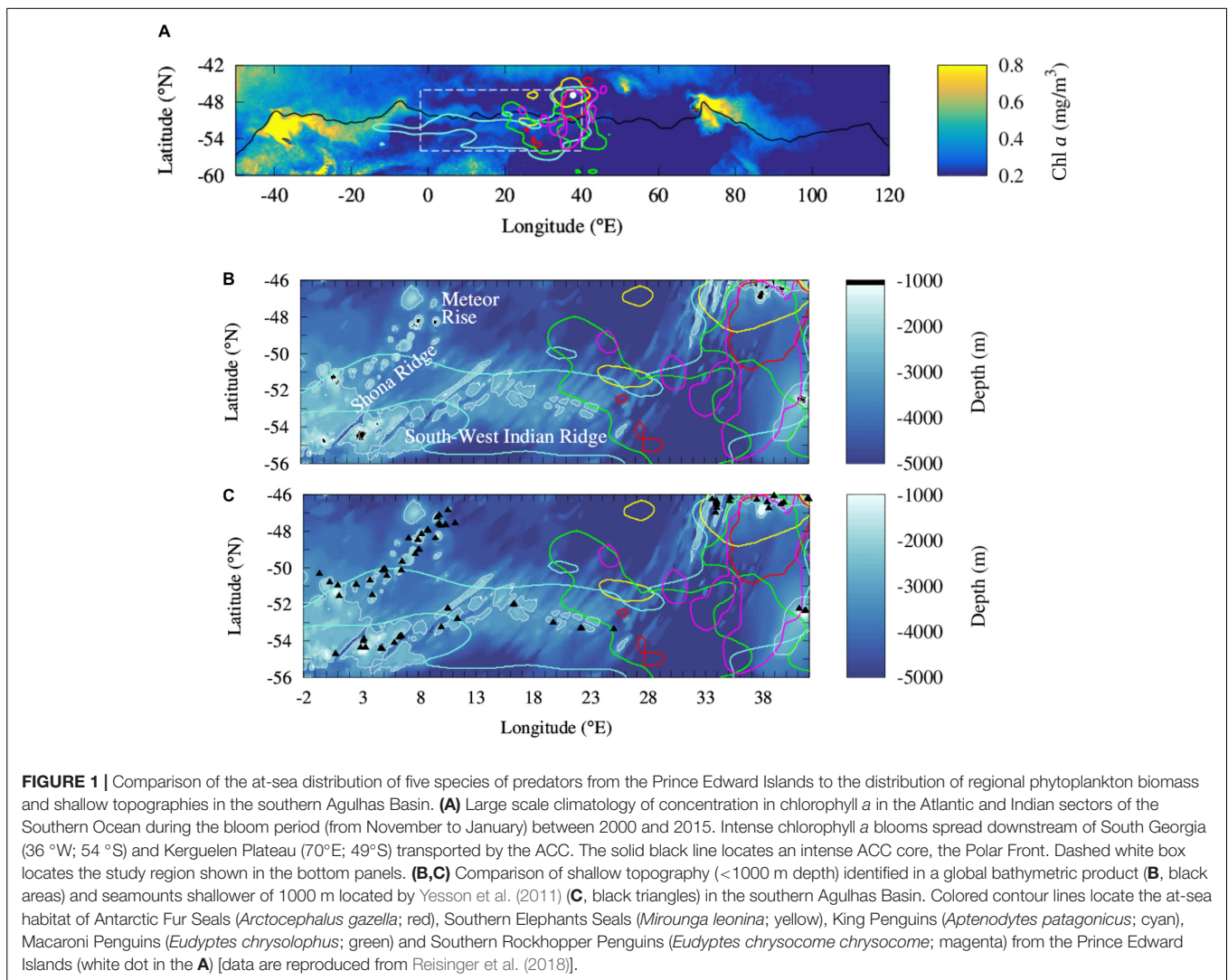


**FIGURE 1** | Comparison of the at-sea distribution of five species of predators from the Prince Edward Islands to the distribution of regional phytoplankton biomass and shallow topographies in the southern Agulhas Basin. **(A)** Large scale climatology of concentration in chlorophyll a in the Atlantic and Indian sectors of the Southern Ocean during the bloom period (from November to January) between 2000 and 2015. Intense chlorophyll a blooms spread downstream of South Georgia (36°W; 54°S) and Kerguelen Plateau (70°E; 49°S) transported by the ACC. The solid black line locates an intense ACC core, the Polar Front. Dashed white box locates the study region shown in the bottom panels. **(B,C)** Comparison of shallow topography (<1000 m depth) identified in a global bathymetric product **(B)**, black areas) and seamounts shallower of 1000 m located by Yesson et al. (2011) **(C)**, black triangles) in the southern Agulhas Basin. Colored contour lines locate the at-sea habitat of Antarctic Fur Seals (*Arctocephalus gazella*; red), Southern Elephant Seals (*Mirounga leonina*; yellow), King Penguins (*Aptenodytes patagonicus*; cyan), Macaroni Penguins (*Eudyptes chrysolophus*; green) and Southern Rockhopper Penguins (*Eudyptes chrysocome chrysocome*; magenta) from the Prince Edward Islands (white dot in the **A**) [data are reproduced from Reisinger et al. (2018)].

increasing attention that the subantarctic open ocean is receiving within the Commission for the Conservation of Antarctic Marine Living Resources (e.g., Sc-Camlr-XXXVII (2018), Annex 7, para. 3.74; Ccamlr-XXXVII (2018), para. 6.60). A key step to that end is to improve our comprehension of the biophysical processes which sustain biological productivity up to megafauna species. Using a Lagrangian approach (Lehahn et al., 2018), we propose here to test how seamounts complement the island mass effect in fueling pelagic ecosystems within the ACC domain and how they affect the biological production inferred from land-based top predators.

## MATERIALS AND METHODS

### Predators Distribution

Predators distribution is estimated from tracking data of seabirds and seals from the Prince Edward Islands between 2003 and 2014 and collected from research programs supported by the National Research Foundation and the South African

Department of Environmental Affairs (Reisinger et al., 2017)<sup>1</sup>. The animals' trajectories we use in this work have been analyzed in detail in Reisinger et al. (2018): here we report only the information relevant for our study, which is the large-scale geographical extension of their habitat utilization, i.e., the whole smoothed spatial range of predators. In this study we consider only the tracking data of seals and penguins, because they display a more selective habitat than flying seabirds (Reisinger et al., 2018). The Subantarctic Fur Seals (*Arctocephalus tropicalis*) are not considered because the at-sea distribution of this colony is mostly located north of the Subantarctic Front which bound our study region [see **Figure 2** in Reisinger et al. (2018)]. Kernel densities of Antarctic Fur Seals (*Arctocephalus gazella*), Southern Elephant Seals (*Mirounga leonina*), King Penguins (*Aptenodytes patagonicus*), Macaroni Penguins (*Eudyptes chrysolophus*) and Southern Rockhopper Penguins (*Eudyptes chrysocome chrysocome*) from the Prince Edward Islands were calculated using the “kde2d” function from

<sup>1</sup>[https://figshare.com/articles/\\_/5613016](https://figshare.com/articles/_/5613016)



the R-package “MASS” on the observed tracks (Venables and Ripley, 2002). The habitat utilization for each colony is identified with a threshold of 95% of each predator density (complete kernel utilization distributions are available for each species in Reisinger et al., 2018; **Figure 2**). This allows us to identify the whole spatial range used by multiple subantarctic predators including different phases and behavior of their trajectories (usually traveling and foraging).

## Seamounts

Seamounts are defined as geomorphological features having a vertical elevation of more than 1000 m from the seafloor with limited extent across the top summit region (Menard, 1964; Staudigel et al., 2010). The seamounts' summit location is extracted from Yesson et al. (2011). We retain here only the shallower structures having a maximal water depth of 1000 m, in order to compare them with the ocean upper layer horizontal velocity fields derived from altimetry. In the following, a seamount is defined by a disk centered in the seamount summit and with a 70 km radius. In the same way, the region under the influence of Bouvet Island is defined by a disk centered in the island (3.36°E; 54.42°S) with a 70 km radius.

## Satellite Observations and Reanalysis Data

Geostrophic velocities, surface chlorophyll *a* (Chl *a*) and temperature reanalysis are evaluated between 2000 and 2015 from different products distributed by the European Copernicus Marine Environment Monitoring Service<sup>2</sup>.

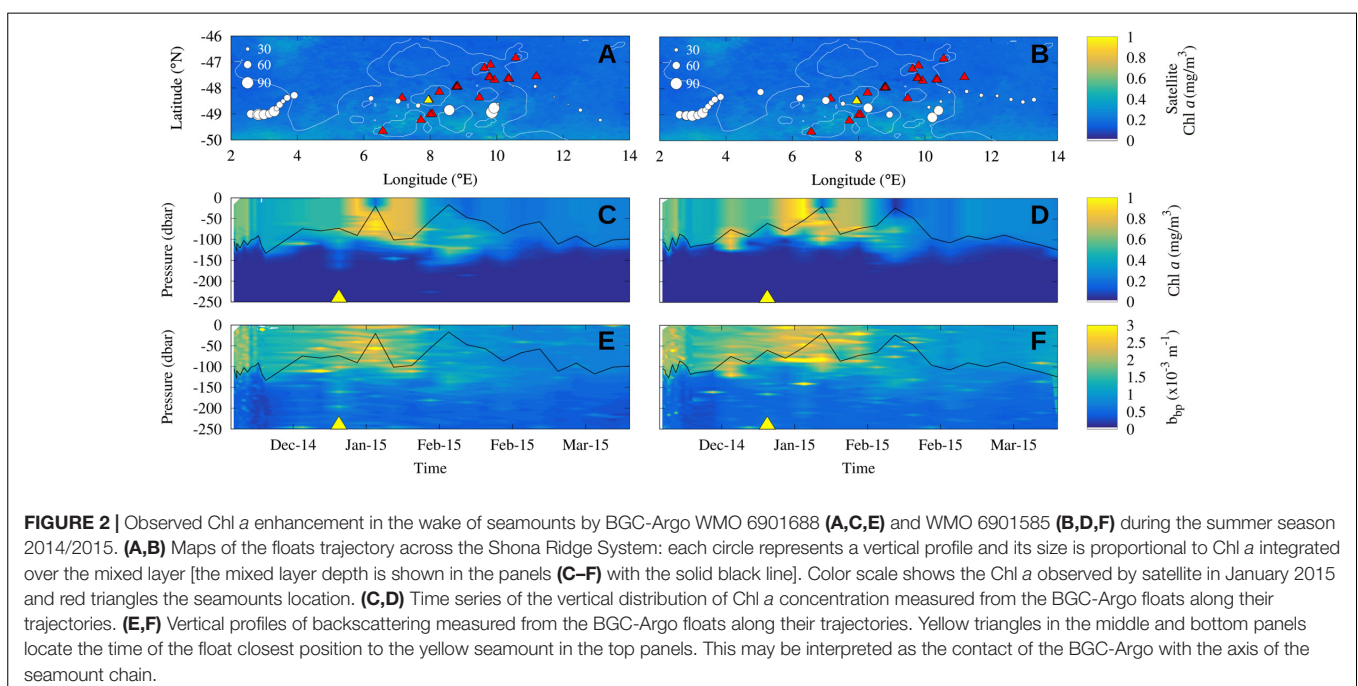
Geostrophic currents are quantified through an altimetry multi-satellite global product (product id: SEALEVEL\_GLO\_

PHY\_L4\_REP\_OBSERVATIONS\_008\_047) produced by SSALTO/DUACS. This product processes data from all altimeter missions (Jason-3, Sentinel-3A, HY-2A, Saral/AltiKa, CryoSat-2, Jason-2, Jason-1, T/P, ENVISAT, GFO, ERS1/2) and has temporal and spatial resolutions of, respectively, 1 day and 1/4°. Trajectories are derived by applying a Runge–Kutta fourth order scheme with a time step of 6 h. Velocity fields are linearly interpolated in both space and time.

Satellite surface Chl *a* concentration is analyzed with the Global Ocean Color product (product id: OCEANCOLOUR\_GLO\_CHL\_L4\_REP\_OBSERVATIONS\_009\_082) produced by ACRI-ST. The product evaluated has a 1/24° spatial resolution. Here, we consider monthly-mean composites in order to reduce the cloud coverage and at the same time preserve the mesoscale variability of the Chl *a* blooms. Similarly to previous studies, the term “bloom” refers to regions of relative elevated Chl *a* compared to the background concentration (Sokolov and Rintoul, 2007). The statistical significance of the Chl *a* enhancement is evaluated with the bootstrap method (a detailed description of the method used for the identification of Chl *a* blooms is provided in the section “Seamount Mass Effect: Detection of the Lagrangian Plume Stemming From the Seamounts”). Chl *a* values are investigated in spring and summer (from October to February) ahead of the maximum feeding activities of higher trophic levels (Laws, 1985; Moline et al., 2004; De Broyer et al., 2014).

Phytoplankton dominance is evaluated from the PHYSAT observations (Alvain et al., 2005, 2008) between 2000 and 2011 from the month of December and January, when we expect a larger diatoms dominance (Smetacek et al., 1990; Alvain et al., 2008). The PHYSAT method has already been validated at the global and regional scale in the Southern Ocean (Alvain et al., 2005, 2008, 2013; see in particular

<sup>2</sup><http://marine.copernicus.eu/>



d'Ovidio et al., 2010 **Supplementary Material** for a validation at the latitudes used here). The method identifies probable specific dominant phytoplankton groups based on the analysis of spectral measurements computed by ocean-color sensors. These are nano-eukaryotes, *Prochlorococcus*, *Synechococcus*, diatoms, *Phaeocystis*-like and coccolithophores. Note that a phytoplankton group is defined as dominant when it is a major contributor to the total pigment (Alvain et al., 2005). As demonstrated in Della Penna et al. (2018), a large number of pixels of PHYSAT daily maps are flagged as not classified in this oceanic region, so that composite maps must span very large periods in order to provide meaningful spatial patterns. For this reason, and because we study large scale features, in our analysis we have used multi-year PHYSAT composites, without resolving interannual variability.

Vertical distribution of temperatures is evaluated with the global ocean reanalysis GLORYS2V4 produced by Mercator Ocean for the Global Ocean and Sea Ice Physics (product id: GLOBAL\_REANALYSIS\_PHY\_001\_025). This product is performed with NEMOv3.1 ocean model in configuration ORCA025\_LIM and has horizontal spatial resolution of 1/4° with 75 vertical levels. For the analyses we used the product version averaged by month. The water masses associated to the position of the Antarctic Polar Front (PF) are identified as the northern extent of the presence of the 2°C isotherm minimum in the subsurface (0–500 m depth) (Botnikov, 1963).

### Biogeochemical Argo Floats

The vertical profiles of Chl *a* concentration and backscattering measured from the Biogeochemical Argo (thereafter BGC-Argo) floats have been extracted from the CORIOLIS Global Data Assembly Center<sup>3</sup>. Quality control tests have been achieved on the Chl *a* and backscattering data (Schmechtig et al., 2014, 2018). Non-photochemical quenching on daytime profiles are also corrected on the Chl *a* data following (Xing et al., 2012). In this aim, the maximal Chl *a* value above the mixed layer depth is extrapolated until the surface and corrected with a specific correction factor. In order to adapt the correction procedure to the study region, the non-photochemical quenching is corrected with the calibration factor of 3.3 used by Ardyna et al. (2019) in the same region. The mixed layer depth is evaluated in each profile as the depth of a density difference of 0.03 kg/m<sup>3</sup> in respect to the density at 10 m depth. The density is computed based on International Thermodynamic Equation of Seawater (Sérazin, 2011).

### Seamount Mass Effect: Detection of the Lagrangian Plume Stemming From the Seamounts

In order to identify the effects of seamounts on phytoplanktonic blooms we analyze whether possible water parcels displaying enhanced Chl *a* have, or have not, been in contact with the seamounts. To achieve this, we compute a backward-in-time, altimetry-based Lagrangian calculation from the bloom periods. This calculation allows us to identify the water parcels that transited over a seamounts area, defined here as a disk of

70 km radius. This value is chosen considering that altimetry data are expected to resolve features on the order of 70 km or larger (Pascual et al., 2006). The aim is to compare the water dispersion pathways computed downstream of the seamounts, in the following referred to as the Lagrangian water plume, to the Chl *a* plume. This approach has already been validated for the island mass effect, to reproduce the Kerguelen bloom (d'Ovidio et al., 2015; Sanial et al., 2015) and the Crozet bloom (Sanial et al., 2014) at mesoscale precision.

For each studied period the analysis is conducted in two steps:

(1) Identification of the seamounts that are located within deep iron-enriched hydrographic regions. For each seamount we verify if, in the 4 months before the bloom, it was located within the PF. This current core of the ACC is associated to enhanced dissolved iron concentrations (De Baar et al., 1995; Löscher et al., 1997; Measures and Vink, 2001; Mengelt et al., 2001; Viljoen et al., 2018) presumably upwelled from the deep layer (Sokolov and Rintoul, 2007). The PF is identified for the whole period in the vertical temperature reanalysis as described in section “Satellite Observations and Reanalysis Data.” We applied the same approach to the water parcels that have been in contact with Bouvet Island, which is also a potential source of iron to the environment (Perissinotto et al., 1992; Croot et al., 2004). The latter contact is estimated by detecting the water masses which transited over the island in the 4 months before the bloom.

(2) Identification of the Lagrangian water plume from the selected seamounts. Each water parcel of the study region is advected backward-in-time from the blooming period for 4 months. The parcels which are found to come from an area where a seamount is present are then given a timestamp with the time, in days, since they left that topographic features. The 4-month time window chosen for the integration assumes that the extension springtime bloom is pre-conditioned by the winter-time advection of iron rich waters (Mongin et al., 2009).

The enhancement of the Chl *a* concentration within the 100-day Lagrangian water plume is evaluated with the bootstrap method in order to obtain its statistical significance. The bootstrap is conducted on sub-sampled Chl *a* maps, selecting one pixel each five both in longitude and latitude directions. This is done to remove spatial correlations of the order of the typical size of a mesoscale eddy of this region (about 100 km). For the region under the influence of Bouvet, the Lagrangian water plume spreading downstream of the island is removed from the Lagrangian water plume reconstructed with the seamounts. This allows us to distinguish the plume from the seamounts in respect to the one induced by the island.

## RESULTS

### Chlorophyll *a* Enhancement Observed From BGC-Argo Downstream of Seamounts

Two BGC-Argo floats (WMO 6901585 and 6901688) sampled the Shona Ridge region. They crossed the seamount chain around 49°S between the end of December 2014 and January 2015 with a time lag of a few days (**Figure 2**). A local increase of the

<sup>3</sup>ftp://ftp.ifremer.fr/ifremer/argo/dac/coriolis/

depth-integrated biomass over the mixed layer downstream of seamounts (8–10°E) is recorded by the profiling floats: the Chl *a* content doubled in the float WMO 6901585 (**Figure 2A**) and increased by approximately one third in the float WMO 6801688 (**Figure 2B**). These observations contrast with the homogeneous low Chl *a* concentration (about 0.3 mg/m<sup>3</sup>) observed by satellite in January 2015 in the near surface (background images in **Figures 2A,B**). When looking at the Chl *a* content in the water column, neglecting the variability of the mixed layer depth which is deeper than 100 m upstream of the seamounts and shallower than 40 m over them, the intensification of the Chl *a* signature downstream of the seamounts is evident in both floats (**Figures 2C,D**). The vertical profiles depict an increase in Chl *a* and backscattering values in the first 100 m depth downstream of the seamounts (respectively, about 1 mg/m<sup>3</sup> and  $3.0 \times 10^{-3} \text{ m}^{-1}$ ) compared to the water masses upstream (respectively, about 0.6 mg/m<sup>3</sup> and  $2.0 \times 10^{-3} \text{ m}^{-1}$ ). Note that the yellow triangles in **Figures 2C,E** (respectively, **Figures 2D,F**) locate the time of the closest position of the BGC Argos trajectories with the yellow seamount in **Figure 2A** (respectively, **Figure 2B**). They symbolize the crossing of the seamount chain. The phytoplankton enhancement downstream of seamounts is further investigated with satellite observations which have larger spatial and temporal covers.

## Altimetry-Based Lagrangian Reconstruction of the Seamount Mass Effect

We assume here the hypothesis of a *seamount mass effect* on phytoplankton biomass, in analogy to the well known island mass effect. This hypothesis implies the formation of phytoplanktonic blooms induced by natural iron fertilization spreading downstream of the seamounts. We discuss the possible mechanisms of iron upwelling in section “Discussion”.

Two seamount chains are susceptible to lift iron-laden deep waters to the surface layer and consequently enhance the phytoplankton biomass in the studied region: the Shona Ridge System (SRS), which is composed by the Shona Ridge and the Meteor Rise, and the South-West Indian Ridge (SWIR) (see **Figures 1B,C** for their localization). Yesson et al. (2011) identified 36 seamounts shallower than 1000 meters depth associated with the SRS, with one third of them shallower than 100 m depth, and 26 seamounts shallower than 1000 m associated to the SWIR in the study region (between 0 and 30°E). When looking at Chl *a* images not yearly averaged, but over time periods of 1 month during spring or summer, Chl *a* signatures significantly above the background (around 2-fold) do appear downstream of both the seamount chains (as illustrated in **Figures 3A,B, 4A**).

In order to further sustain the hypothesis of a seamount mass effect, we study the morphology of the satellite-observed Chl *a* plumes detected in the vicinity of seamounts. In particular, we analyze whether the shape of these plumes is consistent with a dispersal pattern stemming from a seamount. In order to achieve this, we reproduce the Lagrangian plumes associated with the seamounts during the blooms event using altimetry-derived currents. The analysis consists in detecting the water parcels

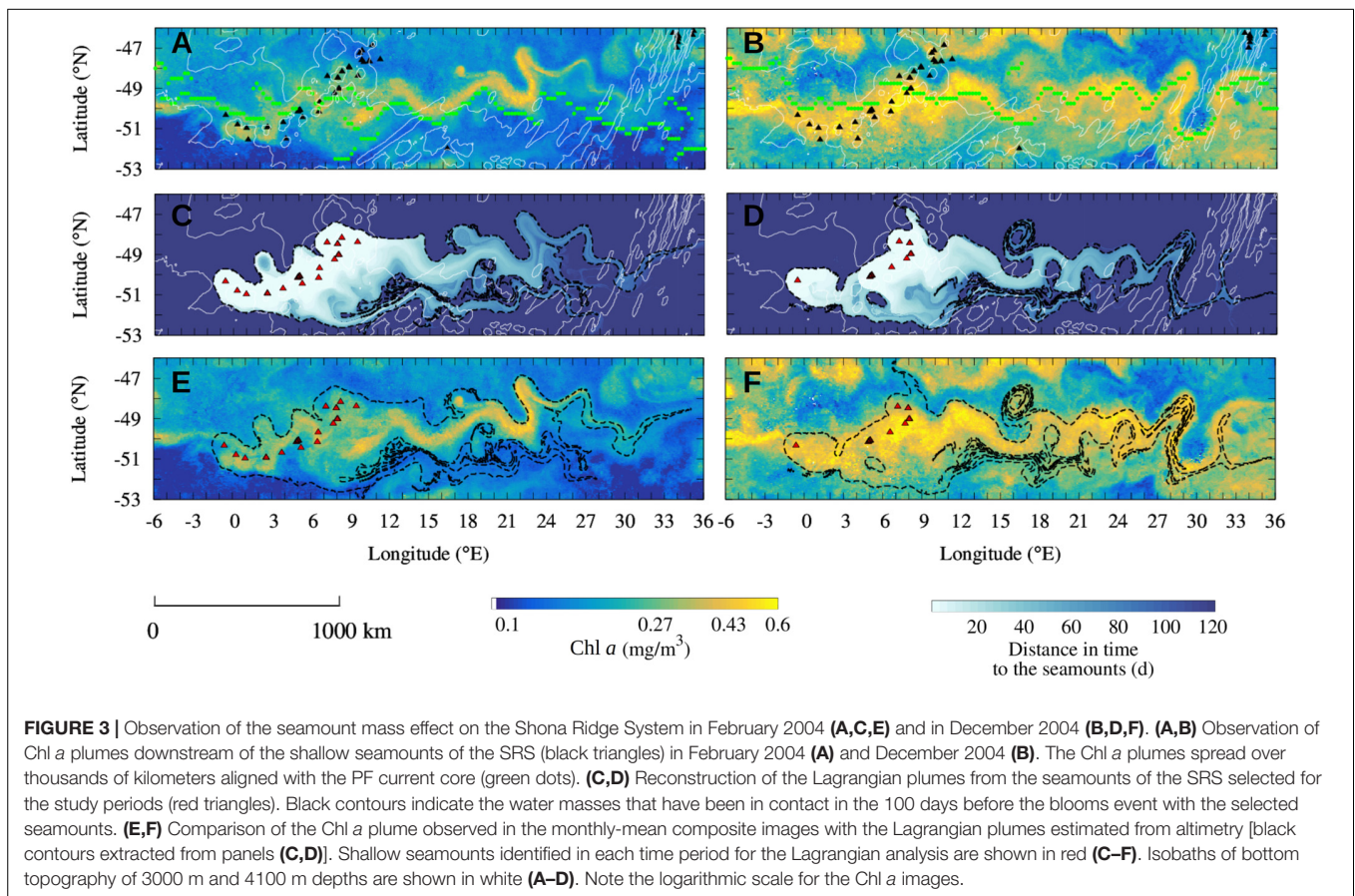
which transited above the seamounts in a certain time period with a Lagrangian approach. As explained in section (Seamount Mass Effect: Detection of the Lagrangian Plume Stemming From the Seamounts), for each bloom period the Lagrangian plumes are derived only from the subset of seamounts which were in contact with potentially deep iron-enriched hydrographic provinces. Here we consider two regions that have been identified in the literature for displaying higher iron concentration, the water masses downstream of Bouvet Island (Perissinotto et al., 1992; Croot et al., 2004) and the water masses located in the ACC along the jet associated with the PF (De Baar et al., 1995; Löscher et al., 1997; Measures and Vink, 2001; Mengelt et al., 2001; Viljoen et al., 2018). This hypothesis will be discussed in section “Drivers of the Seamount Mass Effect.” We illustrate the analysis region by region.

### Shona Ridge System

The ACC crosses longitudinally the SRS between 0 and 10°E. In both February and December 2004, a distinct Chl *a* plume topping at 0.6 mg/m<sup>3</sup> spreads downstream of the SRS aligned with the PF current core (**Figures 3A,B**). The monthly-mean composite images of Chl *a* are compared to the altimetry-derived Lagrangian reconstruction of the water plumes emanating from the seamounts of the SRS which have been in contact with iron-enriched water masses (**Figures 3C,D**). These plumes represent the water transported by the ACC which has transited over shallow seamounts in the 4 months before the blooms. The color of **Figures 3C,D** represents the number of days since last contact, i.e., a pixel color coded with “30 days” was on the top of a seamount 30 days before the date of the image. The 100-day Lagrangian water plumes (black contours in **Figures 3C,D**) are overlapped to the Chl *a* plumes (**Figures 3E,F**). The Lagrangian analysis reveals that, in both studied periods, the Chl *a* plume extending downstream of the seamounts matches up to fine details the reconstructed water masses that transited over the seamounts few months previous the bloom.

The good prediction of the extension and shape of Chl *a* gives us confidence about the role of the selected seamounts. Remarkable examples of the match between ocean-color and altimetry-derived features are the correspondence of meanders and mesoscale features between the two signatures, such as the distinct Chl *a* patch trapped by a mesoscale eddy around 17°E 48.5°S in February 2004 (**Figure 3A**). Note that even if the Chl *a* plume is aligned with the PF current core, particularly in December 2004 (**Figure 3D**), the complexity of the Chl *a* plume is captured just with the advection of water masses that surrounded the seamounts. This is the case for instance for the latitudinal extension of the plume close to the SRS, between 3 and 9°E, in December 2004 (**Figures 3D,F**) or the extension of the plume between 15 and 30°E in February 2004 (**Figures 3A,C**). We remark also that the selected seamounts are different in February and December 2004 and that similarly, the same seamounts may be located in different productivity regimes at the two periods. For instance, in December 2004 the shallow seamounts at 48 °S were not in contact with the current core of the ACC (they are not identified in **Figure 3D**) and seems to not display enhanced phytoplankton biomass (**Figure 3F**). Conversely, the





same seamounts are associated by the Lagrangian analysis to the Chl *a* plume in February 2004 (**Figures 3C,E**). This different behavior suggests a temporal variability of the biological response associated to submerged topography features.

During the study periods, February 2004 and December 2004, the mean Chl *a* concentration in the water masses that transited in the last 100 days over seamounts in contact with the current core is, respectively, 49 and 40% higher than elsewhere in the region depicted in **Figure 3**. In order to test whether the observed differences in the Chl *a* content inside and outside of the Lagrangian plumes are significant, a bootstrap sampling is carried out for each studied period over the whole image size. The null hypothesis states that the observed difference in Chl *a* content inside and outside the Lagrangian plume is not significant. Standard deviation of the bootstrap distributions inside and outside the plumes are, respectively,  $1.2 \times 10^{-3}$  and  $5.0 \times 10^{-4}$  mg/m<sup>3</sup> for the year 2003/2004 and  $2.1 \times 10^{-3}$  and  $7.1 \times 10^{-4}$  mg/m<sup>3</sup> for the year 2004/2005. In all the study cases the null hypothesis is rejected with >99% confidence. These analyses provide observational evidence of a seamount mass effect associated to the SRS.

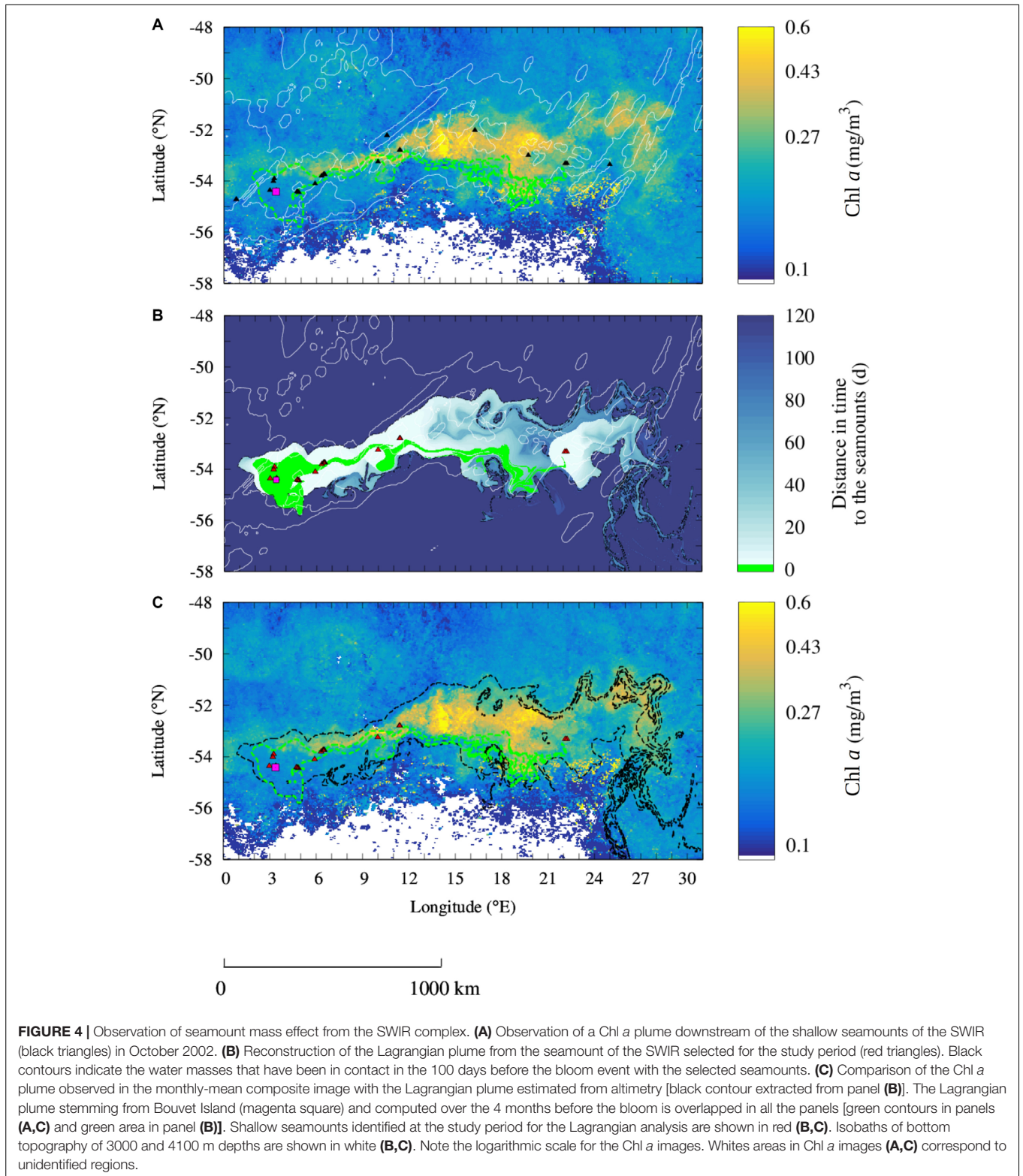
### South-West Indian Ridge

Bouvet Island (3.36°E and 54.42°S, indicated by a square in **Figure 4**) lies on a volcanic system about 50 km west to the SWIR (Georgen et al., 2001) and represents a known iron input

in the south-west of the study region (Croot et al., 2004). The island has been associated with enhanced Chl *a* concentrations and primary production compared to the surrounding areas. However, its effect seems to be locally restricted (e.g., Perissinotto et al., 1992; Croot et al., 2004, refers also to **Figure 1A**). Differently to what was found in previous studies, in October 2002 a Chl *a* plume spreads over almost 2000 km downstream of Bouvet Island (**Figure 4A**). However, the altimetry-derived Lagrangian plume stemming from Bouvet Island (green area in **Figure 4A**) overlaps only partially the Chl *a* plume observed from the satellite in this period. Indeed, the Chl *a* plume extended over a much larger area nearby 26 seamounts shallower than 1000 m (**Figure 4A**).

Similarly, to the analysis of the SRS, here we consider whether the seamounts of the SWIR may explain the Chl *a* enhancement which is not explained by the island alone. Specifically, we reproduce the altimetry-derived Lagrangian plume from the seamounts that have been in contact with the water masses enriched in iron at Bouvet Island in the few months before the bloom. Indeed, the few seamounts in the north edge of the SWIR that were not in contact with the iron-enriched water masses stemming from the island did not display enhanced Chl *a* concentrations. The Lagrangian water plume emanating from the selected seamounts allows us to reproduce the Chl *a* plume integrally (black contour in **Figure 4C**), differently to the island Lagrangian plume (green contour). As for the SRS, the Chl *a* plume and the Lagrangian plume stemming from





the seamounts are qualitatively very similar. In addition, the mean Chl *a* concentration inside the Lagrangian plume is two thirds higher than the mean concentration outside (respectively,  $0.26 \pm 0.098 \text{ mg/m}^3$  inside and  $0.16 \pm 0.071 \text{ mg/m}^3$  outside).

Therefore, we infer that the region with highest Chl *a* values corresponds to water masses that transited, in the 100 days before the bloom, over the seamounts (black contours in **Figures 4B,C**). A bootstrap sampling carried out on the part of the SWIR

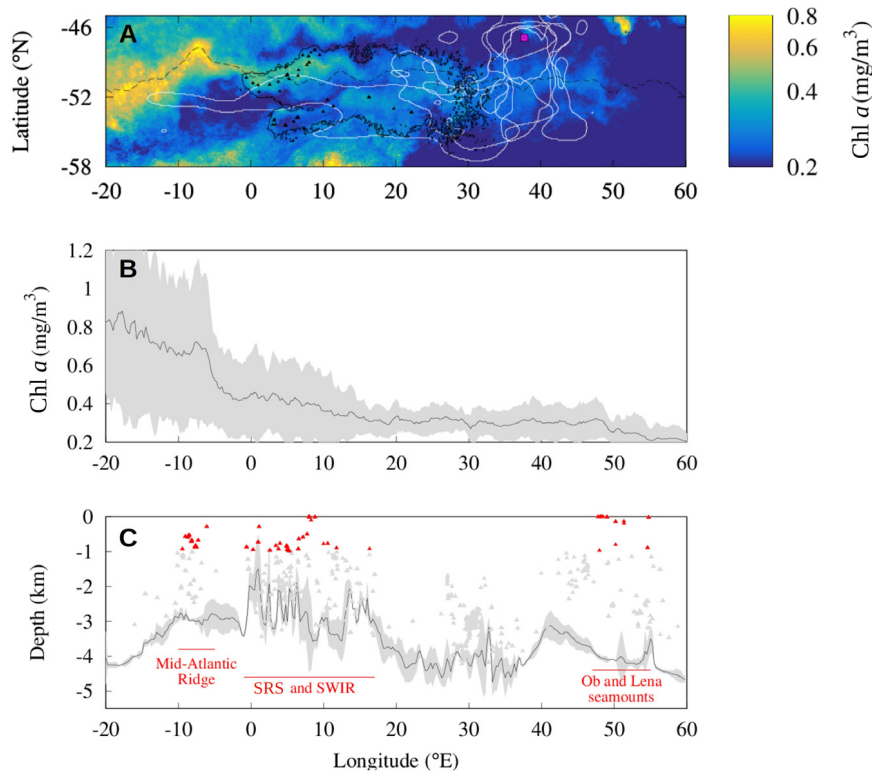


**FIGURE 5 |** Distribution of predators, Chl *a* concentration and seamount mass effect during December between 2000 and 2015 around the PF current core. **(A)** The distribution of top predators (white lines) from the Prince Edward Islands (magenta square) is compared to the distribution of the Lagrangian plumes (black solid line) constructed from the seamounts (black triangles) for every December between 2000 and 2015. Data are displayed with the Chl *a* climatology and the PF position (black dashed line) during December between 2000 and 2015. **(B,C)** Mean Chl *a* concentration **(B)** and mean shallowest depth **(C)** in a latitudinal band of 1° north and 1° south of the current core for every December from 2000 until 2015. Shaded areas show standard deviation associated with these lines. Gray and red triangles indicate the depth of the seamounts (respectively, deeper and shallower of 1000 m) identified by Yesson et al. (2011) in the same region **(C)**.

plume which is not superposed with the island's plume rejects the null hypothesis with >99% confidence. Standard deviation of the bootstrap distributions inside and outside the plumes are, respectively,  $2.4 \times 10^{-3}$  and  $4.8 \times 10^{-4}$  mg/m<sup>3</sup>.

### Comparison of Predators' Distribution, Phytoplankton Biomass and Seamounts Locations in the Southern Agulhas Basin

A 15-year climatology of the December Chl *a* concentration in the southern Agulhas Basin is shown in **Figure 5**, which corresponds to the time of Chl *a* peak in the region (Sokolov and Rintoul, 2007). A 15-year climatology of the Lagrangian water plume issued from the seamounts from the SHS and the SWIR (black triangles), computed as in section "Altimetry-Based Lagrangian Reconstruction of the Seamount Mass Effect," is overlapped to the Chl *a* map (black contour). The region covered by the Lagrangian water plume is upstream of the pinnipeds and penguins ranges (white contours). This indicates that the water masses targeted by the predators' colonies have been under the influence of the seamounts in the previous months (the Lagrangian water plume is represented with a 100-day threshold,

as in the analyses of section "Altimetry-Based Lagrangian Reconstruction of the Seamount Mass Effect"). The similarity between the climatological Chl *a* and Lagrangian plumes is less evident compared to the monthly analyses previously considered. This is primarily due to the smoothed signal in the Chl *a* climatology. However, where the mean pigment distribution is more contrasted, as in the northern edge of the Lagrangian plume, the two signals appear to have qualitatively similar patterns.

In order to investigate the signal of the seamounts in the climatological phytoplankton biomass we compute the mean Chl *a* concentration in a 2° latitude narrow band centered on the current core of the ACC which we identify by the PF, between 2000 and 2015 (**Figure 5B**). **Figure 5B** shows that the highest values (mean Chl *a* about 0.7 mg/m<sup>3</sup>) are observed upstream of the study region, between 20 and 5°W and decrease eastward. Intense Chl *a* concentrations extend downstream of South Georgia (36°W, 54°S) over wide distances due to the intense transport (e.g., Korb et al., 2004; Sokolov and Rintoul, 2007; De Jong et al., 2012; Borriione et al., 2014; Graham et al., 2015) and to the regular iron inputs linked to flow-topography interactions (Sokolov and Rintoul, 2007). The averaged Chl *a* level do not significantly increase

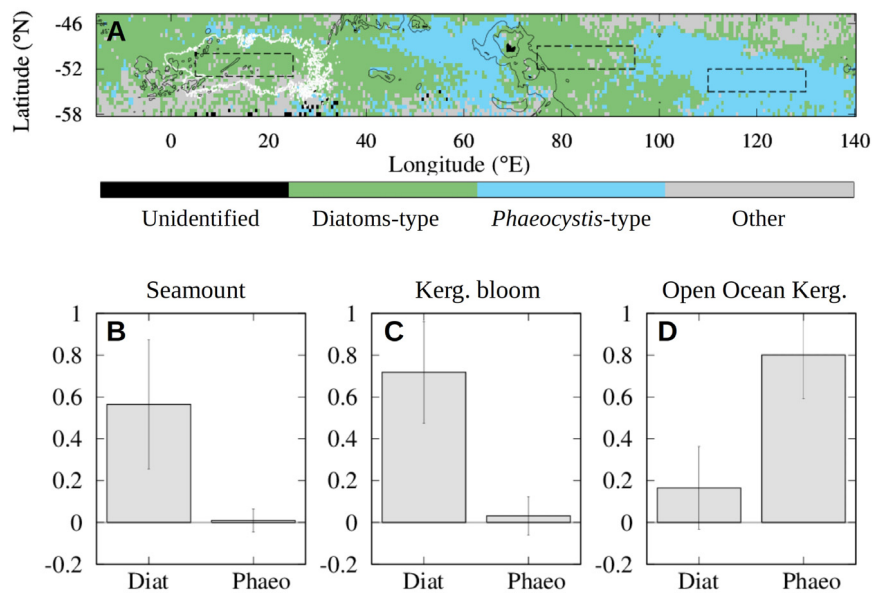


**FIGURE 6** | Climatology maps (2000–2011) of dominant phytoplankton groups in December and January estimated using PHYSAT. **(A)** Most abundant phytoplankton type estimated from PHYSAT over the 2000–2011 time period. The distribution of the Lagrangian plumes from the seamounts (white solid line) is shown as in **Figure 5**. **(B–D)** Mean percentage of time that the seamount region **(B)**, Kerguelen (abbreviated Kerg. in the image) bloom region bloom region **(C)** and open ocean region downstream of it **(D)** are dominated by diatoms or *phaeocystis* types (respectively abbreviated Diat and Phaeo in the image) during December and January between 2000 and 2011. The three regions are located in the dashed black contours in the top panel. From left to the right these are: seamount region **(B)**, Kerguelen bloom region **(C)** and open ocean region downstream of it **(D)**. Error bars indicate the standard deviation over each region.

in correspondence of the interaction between the ACC and the shallow seamounts of the SRS (**Figure 5B**). However, we note the high standard deviation of the signal between 0 and 15°E compared to the downstream signal (respectively,  $\sigma \approx 0.2 \text{ mg/m}^3$  and  $\sigma \approx 0.1 \text{ mg/m}^3$ ) indicating an important interannual variability. Compared to the SHS, the Ob and Lena seamounts close to 50°E display a lower mean Chl *a* concentration ( $\Delta\mu \approx 0.1 \text{ mg/m}^3$ ) and a lower standard deviation ( $\Delta\sigma \approx 0.1 \text{ mg/m}^3$ ), indicating a lower phytoplankton biomass and a low temporal variability.

### Phytoplankton Composition: Comparison of the Seamount Region, Kerguelen Bloom and Open Ocean Region

The possibility for primary production of sustaining the large trophic chain up to megafauna, is known to largely depend not only on its abundance but also on the phytoplankton composition (e.g., Moline et al., 2004). We thus analyze our study region with maps produced with the PHYSAT algorithm (Alvain et al., 2005, 2008). The latter cluster together the ocean color spectral signal into classes associated to typical phytoplanktonic types which are statistically dominant for those bio-optical anomalies.

PHYSAT patterns downstream of the SRS and SWIR seamounts (0–30°E, 50–53°S in **Figure 6**) mainly contain the same classes found in island-induced blooms (70–100°E, 50–53°S in **Figure 6**) and differ from the type classes found in the Australian-Antarctic Basin (i.e., downstream of the Kerguelen

bloom about 100–130°E) (**Figure 6A**). According to the PHYSAT observations, during December and January between 2000 and 2011, the seamount region is dominated more than 55% of the time by diatoms ( $\sigma = 30\%$ ) and less than 1% of the time by *Phaeocystis* ( $\sigma = 5\%$ ). By comparison, the Kerguelen bloom (and respectively, the offshore region downstream of this bloom) is dominated 70% (respectively 16%) of the time by diatoms and 3% (respectively 80%) of the time by the small *Phaeocystis* (**Figures 6B–D**).

## DISCUSSION

Enhanced primary production has been episodically reported in the past over some deep (>2000 m depth) submerged topographic features of the Southern Ocean, such as the Northwest Georgia Rise (Meredith et al., 2003) and the Maud Rise in the Weddell Gyre (Van Bennekom et al., 1988). At a circumpolar scale, Sokolov and Rintoul (2007) observed that blooms are initiated where the ACC crosses most of the deep bathymetric features and they persist for long distances. However, the biogeochemical focus of subsequent works has led to the conclusion that Chl *a* enhancements downstream of submerged features are negligible because on average they are much less intense than the ones in the wake of the subantarctic islands (e.g., Graham et al., 2015; Ardyna et al., 2017). These ideas have reinforced the view of the region in between the subantarctic islands as a HNLC phytoplankton-desert area. Here we revisit this apparently low chlorophyll region investigating its ecological



implications, in particular for land breeding marine predators for which the possibility of accessing a large islands' bloom far away from their colony may be associated to excessive energetic locomotion costs. This is the case for instance with several species of penguins and pinnipeds breeding at the Prince Edward Islands. A very limited island mass effect is observed around and downstream Prince Edward Islands because of its very narrow plateau (Perissinotto et al., 2000). Competition for food is thus expected to be high in this small productive area. Animals colonizing this island appear indeed to prefer the lower productive but extended inter-island waters than other targets, such as the small productive area around Prince Edward Islands (where competition may be high) or the larger blooms further away, costly to reach.

Our study targets two topographic systems of the southern Agulhas Basin: the Shona Ridge System and part of the South-West Indian Ridge, between 0° and 30°E. By focusing on shorter time scales and on higher bathymetric resolution than former studies, our results identify new phytoplankton blooms associated to the water masses that transited over these shallow topographic highs and provide a detailed description of them. Firstly, an increase in phytoplankton biomass is observed by BGC-Argo floats in the wake of the seamounts during the summer period, between the middle of January and the middle of February. This late Chl *a* enhancement suggests a possible positive biological effect linked to the presence of the topographic highs which is not simply linked to the seasonal bloom phenology (Sallée et al., 2015; Ardyna et al., 2017). Due to the important limitation of the primary production by iron in this region (e.g., Martin, 1990; Sullivan et al., 1993; De Baar et al., 1995), a relative enhancement of the Chl *a* values should be related to iron inputs in the surface waters. Secondly, the seamount effect is further investigated with satellite observations which have larger spatial and temporal covers. By identifying isolated Chl *a* plumes on monthly-mean maps and comparing them to the Lagrangian water plumes stemming from the topographic features we demonstrate the widespread influence of seamounts on the surface seasonal phytoplankton distribution. Therefore, the advection of water parcels from shallow topography can be considered as a powerful tool for identifying the effect of isolated submerged topography, similarly, to the analyses computed on islands (e.g., Mongin et al., 2009; Sanial et al., 2014, 2015; d'Ovidio et al., 2015; Ardyna et al., 2017). By comparison, Graham et al. (2015) investigated the spatial variability of the annual mean Chl *a* at the regional scale in the study area and concluded that, at this time scale, the phytoplankton biomass is not visibly enhanced over or downstream of the seamounts. However, we note that most of seamounts identified in our high resolution bathymetric data were not identified in this previous analysis (see for instance their **Figure 5A**), which could also influence their conclusions. Similarly, the Lagrangian pathways computed at the circumpolar scale using a bathymetric threshold also do not identify Chl *a* plumes in the southern Agulhas Basin, because no shallow topography was detected there with these data (Ardyna et al., 2017). These different outcomes highlight

the need to consider both high resolution bathymetric data and short time scales for investigating a potential biological effect of seamounts.

In the following we firstly discuss the possible mechanisms at the origin of the seamount mass effect observed in the present study, the limits of the methods employed, and their applicability to other study cases. Secondly, we explore the ecological role of seamounts in the southern Agulhas Basin, from primary production to predators' distribution, as well as some implications of these new insights for conservation activities.

## Drivers of the Seamount Mass Effect

What is the origin of the blooms observed in the wake of seamounts in the southern Agulhas Basin? In most of the previous studies, the Chl *a* anomalies observed over the seamounts and in the surrounding waters were linked to the shallow seamount depths. However, the spatial and temporal variability of biological effects were rarely understood due to the complex nature of the physical processes involved there (e.g., Venrick, 1991; Pitcher et al., 2007; Pauly et al., 2017). The process presented here is framed by the limiting effect of iron on primary production (Martin, 1990) and the preponderant structuring effect of the horizontal transport on biochemical properties and ecosystems in the ACC region. The two necessary conditions identified for the fertilization of water masses in the open ocean southern Agulhas Basin are thus: (i) the presence of hydrographic regions associated, according to the literature, to potential enhanced dissolved iron content at intermediate depth; and (ii) upwelling dynamics due to the interaction of seamounts shallower than 1000 m depth with an energetic branch of the ACC.

In terms of iron content, two possibly enriched regions are identified in the southern Agulhas Basin. The first one is composed by the water masses that have transited over Bouvet Island, which is a known iron source (Perissinotto et al., 1992; Croot et al., 2004). The second one, is composed by the water masses located in the ACC, along the jet associated with the PF. Numerous *in situ* observations have recorded enhanced iron concentrations in the surface waters close to this ACC front, both in the Atlantic sector (De Baar et al., 1995; Löscher et al., 1997; Viljoen et al., 2018) and elsewhere (Measures and Vink, 2001; Mengelt et al., 2001). In the deeper ocean, iron measurements are less frequent (e.g., Tagliabue et al., 2012). Nevertheless, enhanced iron concentrations appear to occur in the Circumpolar Deep Water close to the PF region in correspondence of the Mid-Atlantic Ridge (Löscher et al., 1997). Furthermore, the analysis of the global GEOTRACES database indicates a sharp ferricline in the Atlantic ACC region reflecting the signature of subsurface lateral transfer of dissolved iron from the subantarctic islands (Tagliabue et al., 2014). Indeed numerous studies have concluded that the intense velocities of the PF current core result in a strong transport of nutrients downstream of South Georgia (Korb et al., 2004; Venables and Meredith, 2009; Venables et al., 2012; Borrione et al., 2014) and in a regular iron supply to the surface water due to the ACC-bathymetry interactions (Sokolov and Rintoul, 2007).

In terms of upward dynamics, the interaction of the ACC with sharp topographic features is well known to generate upwelling hotspots carrying deep waters to the surface (Viglione and Thompson, 2016; Tamsitt et al., 2017) and enhancing surface Chl *a* concentrations (Sokolov and Rintoul, 2007). Three different mechanisms have been identified in the past for explaining upwelling in the presence of seamounts. The first mechanism is eddy fluxes which are intensified when the ACC encounters a rough topography due to an increase in baroclinicity. The eddy activity enhanced in this way at seamounts can vigorously drive upward northern-sourced deep water along steeply sloping isopycnals in the PF region (Tamsitt et al., 2017; Rintoul, 2018). The enhanced eddy activity at seamounts is also associated to intense flow shear, which in turn preconditions an ageostrophic submesoscale circulation characterized by deep reaching vertical motion (Lévy et al., 2018; Siegelman et al., 2019). A second possible mechanism for upwelling is the bottom pressure torque created when the ACC impinges over bathymetric obstacles. This process induces upwelling upstream of a seamount and downwelling downstream of it (Hughes, 2005; Sokolov and Rintoul, 2007; Thompson and Naveira Garabato, 2014; Rintoul, 2018). This situation has been described in the Atlantic sector of the ACC region, at the South and North Scotia Ridges, the South Orkney Islands and the South-West Indian Ridge (Sokolov and Rintoul, 2007). Finally, a third mechanism which is able to connect deep water to the surface layer is the generation of internal lee waves at seamounts. These waves propagate upward and break, enhancing diapycnal mixing (Watson et al., 2013) and fluorescence signature over the seamounts (Brink, 1995; Kunze and Sanford, 1997; Eriksen, 1998). This has been observed for instance at the seamounts of the SWIR, at the northeast of the southern Agulhas Basin (Read and Pollard, 2017).

The interaction of a strong current with a topographic sharp relief is also known to produce Taylor columns, that is, semi-permanent anticyclones on the top of the topographic obstacle which can trap water for periods of months or longer (Taylor, 1923; Meredith et al., 2015). These features can have a special ecological interest because they may retain over the seamounts aging trophic webs, thus providing predictable preying hotspots (e.g., Pitcher et al., 2007; Morato et al., 2010; Cascão et al., 2017). Such circulations, more intense at high latitudes due to the enhanced Coriolis force (Owens and Hogg, 1980; Chapman and Haidvogel, 1992), have been observed in the Southern Ocean at the Maud Rise (Van Bennekom et al., 1988) and conditions conducive to their formation have been found at the Georgia Rise, South Scotia Ridge and at the Prince Edward plateau (Perissinotto and Rae, 1990; Meredith et al., 2003, 2015).

All together, the mechanisms here proposed for the Atlantic ACC region are schematized in **Figure 7**. The iron content increases in the surface layer at the South Georgia Island and sinks to the subsurface along the flow direction, with regular upward movements due to the interactions between the ACC and the topography. The Chl *a* blooms identified in the study cases (**Figures 3, 4**) and the important temporal variability of the climatological surface Chl *a* content close to the seamounts (**Figure 5**) are the surface expression of this topography-ACC

interactions, usually hidden in the mean climatological Chl *a* signal when compared with subantarctic island-blooms (e.g., Graham et al., 2015; Ardyna et al., 2017). By highlighting the role of iron content of the upstream water masses, the mechanism here suggested could explain why seamounts seem to display re-enhanced phytoplankton biomass when they are close to rich systems, such as coastal margins (Van Bennekom et al., 1988; Perissinotto and Rae, 1990; Meredith et al., 2003; Graham et al., 2015; Oliveira et al., 2016; Lemos et al., 2018), or whether they are located in productive frontal zones (Djurhuus et al., 2017). On the other hand (and following Sokolov and Rintoul, 2007) our results identify processes extending at much larger spatial scales compared with the local phytoplankton enhancements described in previous studies which have focused on seamounts in other regions (e.g., Oliveira et al., 2016; Lemos et al., 2018). This larger extent is due to intense advection by the ACC, in analogy to the spread of non-consumed iron from the subantarctic islands in wintertime which preconditions the size of the islands' blooming area (Mongin et al., 2009; d'Ovidio et al., 2015; Graham et al., 2015).

Our approach does not explain all the patterns of primary production in the ACC region. The ACC core also interacts with a group of shallow seamounts (<1000 m depth) between 10°W and 6°E (**Figure 5C**) which corresponds to climatological Chl *a* concentrations topping at 0.7 mg/m<sup>3</sup> (**Figure 5B**). Differently from the analysis of the SHS and SWIR (black contour in **Figure 5A**) the Lagrangian plume spreading from the seamounts close to 10°W only partially explain the Chl *a* plume in this region (result not shown). Most of Chl *a* seems to be aggregated close to the current core, which, constrained by the Mid-Atlantic Ridge, shifts northward close to 10°W (Boehme et al., 2008). The specific regional circulation catalyzed by the topography may explain the Chl *a* distribution. On the other hand, our analysis leaves open the question concerning why seamounts of other regions do not seem to be associated to intense Chl *a* plumes, such as the shallow Ob and Lena seamounts (~50°E in **Figure 5**). This could be explained by the mechanism schematized in **Figure 7**. The deep iron, primarily upwelled to the intermediate layer at the South Georgia Island (Korb et al., 2004; Borriero et al., 2014), is assumed to slowly decay along the flow direction from west to east. Following this hypothesis, it seems plausible that the seamount effect may be less intense for topography features located further downstream of the South Georgia Island (~35°W), as the Ob and Lena seamounts (~50°E), compared to the closer ones (as the SRS and SWIR). We note that the mechanism here proposed consider primarily external iron inputs, i.e., the upstream iron transport. However, some local processes have also been identified as sources of surface nutrient supply at seamounts. For instance, the interaction of the porewater with sandy sediment releases reduced metal species to the water column (Huettel et al., 1998) and leads to an enhanced erosion of the sediments due to the physical and chemical actions of potential benthic communities (Rhoads and Boyer, 1982). For all these reasons, more detailed studies should be done in order to unambiguously identify the mechanisms at the origin of the Chl *a* enhancements observed in this study.

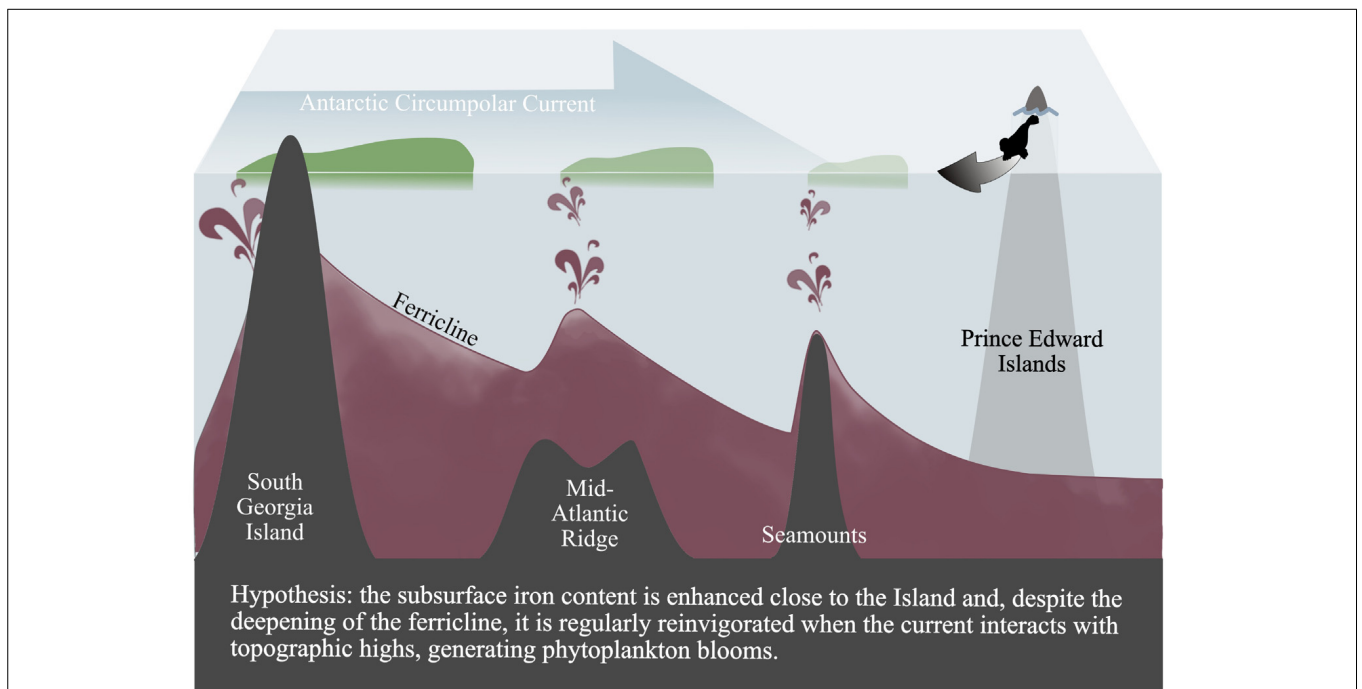


**FIGURE 7 |** Schematic summarizing of phytoplankton productivity in the Atlantic ACC region. The interaction of the ACC with topographic highs generates upward movements and facilitates the injection of iron in the euphotic layer (symbolized by the burgundy-colored jets). Lightening of the phytoplankton blooms (green) is an indication of the decreasing of the Chl *a* concentration. Subantarctic pinnipeds and penguins from Prince Edward Islands (symbolized by the gray arrow) are foraging on this complex biological system.

## Ecological Significance of the Seamount Mass Effect in the Southern Agulhas Basin and Implications for Conservation

The surface Chl *a* concentrations observed in satellite images downstream of seamounts are minor compared to the ones occurring downstream of islands. For instance, in the Crozet bloom Chl *a* concentrations exceed  $2 \text{ mg/m}^3$  (Bakker et al., 2007), four times the ones observed in our analysis. However, we stress that, to assess the total phytoplankton biomass of a given region, one must integrate Chl *a* concentration over the mixed layer (ML) (e.g., Ardyna et al., 2019). The ML in the seamount region is at least between 10 and 30% deeper of the ML in the Kerguelen bloom region during January and February and between 30 and 50% deeper during December (**Supplementary Figure S1**). When compared to the Crozet and the South Georgia blooming regions the seamount ML increases up to 60–100% (**Supplementary Figure S1**). Therefore, the phytoplankton biomass integrated over the ML may present less intense contrasts between the seamount open ocean and the island bloom regions than the surface signals. Furthermore, we note that a deeper ML may also induce a lower Chl *a* signal in the satellite images, intensifying the observed surface differences between the two regions.

The analysis of the phytoplankton composition of the seamount plumes provides further insights about the relevance of this biological production from an ecological perspective. The phytoplankton community identified in the Atlantic ACC

shows a bio-optical signature similar to the ones found in diatom-dominated island blooms, such as the region downstream of Kerguelen, and different from the nearby oligotrophic waters, characterized by *Phaeocystis*-types (**Figure 6**). This nanophytoplankton is known to be rapidly consumed by the microbial food web (Detmer and Bathmann, 1997; Pakhomov et al., 2019) and therefore its occurrence is not associated with profitable foraging grounds for top predators (Cushing, 1989; Moline et al., 2004; Pakhomov et al., 2019). Conversely, diatom-dominated blooms are more likely to support large trophic webs which lead to fish and crustaceans and higher predators (Cushing, 1989; Moline et al., 2004; Pakhomov et al., 2019). Presence of a large and rich (in terms of diversity) megafauna in our study region is confirmed by biologging data (Arthur et al., 2017; Pistorius et al., 2017; Reisinger et al., 2018). The similarity between the seamounts region to the island blooms is supported also by *in situ* measurements showing diatom enhanced concentrations at the Atlantic PF region in the vicinity of the Islas Orcadas Rises and Mid-Atlantic Ridge (Laubscher et al., 1993; Froneman et al., 1995; Bathmann et al., 1997; Detmer and Bathmann, 1997; Smetacek et al., 1997). On the other hand, the contrasted phytoplankton community between the seamount region and the classic HNLC areas (as the one between  $110$  and  $130^\circ\text{E}$  in **Figure 6**) would emphasize the interest of regions downstream of topographic highs. However, the lack of *in situ* phytoplankton observations in this low chlorophyll region prevent us to conclude on the potential zonal differences in the circumpolar phytoplankton communities of

the PF region. Observation of mid trophic levels would also be valuable for linking the primary producers to the higher predators and verifying these hypotheses. Flynn and Williams (2012) showed that the topography-flow interaction over the Macquarie Ridge (160°E) seems to induce an increased biomass of the lanternfishes, a key prey for pinnipeds and seals (e.g., De Broyer et al., 2014). Further analyses of intermediate trophic levels should be done for explaining the biological productivity inferred from land-based top predators and assessing how each colony specifically relies on seamounts production. For instance, the distribution of surface and low trophic level foragers, such as Southern Rockhopper Penguin and Macaroni Penguin (Brown and Klages, 1987; Adams and Brown, 1989; Wilson et al., 1997; Crawford et al., 2003; Whitehead et al., 2016), might be more closely related to the surface productivity than the distribution of mesopelagic foragers.

Our analyses advocate for a connected vision of the biological productivity of the ACC region. Following the ACC, the high Chl *a* concentration decreases from west to east downstream of the South Georgia Island around the ACC core, but it is re-enhanced after the ACC interacts with submerged topographic features, in particular the SRS (as schematized in **Figure 7**). A more comprehensive view may have consequences especially in conservation policies. Currently, conservation planning in the ACC region is dominated by national programs and consequently displays important discontinuities constrained by the jurisdictional framework (e.g., exclusive economic zones). National Marine Protected Areas have been established around Heard and McDonald Islands, Kerguelen Islands, Crozet Islands, and Prince Edward Islands in order to conserve the rich and diverse ecosystems hosted in these oceanic waters. By comparison, the high seas of the southern Agulhas Basin, which are already managed for the fishing activities (**Supplementary Figure S2**), are currently not considered in conservation plans. However, our observations, along with the numerous foraging hotspots of numerous predators occurring in this latitudinal band, both from Bouvet Island and other subantarctic colonies (Biuw et al., 2010; Hindell et al., 2016; Arthur et al., 2017), highlight the need to consider the subantarctic range as a continuum. Current attempts made under the Commission for the Conservation of Antarctic Marine Living Resources (CCAMLR) aim at characterizing the ecosystems structure and function in the subantarctic region and eventually identifying priority areas for conservation. Therefore, efforts shall address the continuity of this oceanic region and the biophysical processes across the high seas and the multiple economic exclusive zones.

## SUMMARY AND CONCLUSION

In the Antarctic Circumpolar Current (ACC) region, island blooms stretch for hundreds of kilometers along the current. Island related production plays a primary role in the biogeochemical cycles of the Southern Ocean and sustains large trophic chains up to megafauna species. Conversely, submerged topography is also known to stimulate primary

production in its interaction with the ACC, but this productivity is comparatively much less intense (e.g., Sokolov and Rintoul, 2007; Graham et al., 2015; Ardyna et al., 2017). As a consequence, its contribution has been considered negligible at the basin scale, and the ACC waters are often described as a high nutrient low phytoplankton desert, punctuated by massive blooms in the wake of the islands. Conservation efforts are in line with this description, with subantarctic marine protected areas only occurring in the economic exclusive zones around the islands.

Here we revisited the role of seamounts in this framework, focusing on a region of the Indo-Atlantic ACC zone. This area is massively targeted by marine predators, even if no islands fertilize it. By combining high resolution bathymetric data, multi-satellite data, and BGC-Argo observations, we found that the oligotrophic nature of the study region apparent in Chl *a* climatological maps hides a much more complex situation. Important production (in excess of 0.6 mg/m<sup>3</sup>, **Figures 2, 3**) occurs there and spreads over huge distances, comparable to the extension of the islands' blooms.

By applying a Lagrangian analysis to these lesser blooms we connected unambiguously these blooms to specific seamount systems. Our Lagrangian scheme was then depicted to track at mesoscale precision the thousands of kilometers long water plume influenced by each individual seamount system (**Figures 3, 4**).

In order to estimate the type of phytoplankton present in these blooms, we used the PHYSAT product, which provides maps of putative planktonic functional types. The PHYSAT algorithm revealed that the signatures of seamounts' bloom are similar to the ones found in the islands' wake, and not nearby less productive waters (**Figure 6**). This is consistent with the presence in both systems of foraging grounds for megafauna species.

The ecological role of seamounts in sustaining large trophic chains was finally confirmed by comparing climatologies of Chl *a* to the predators' distributions (**Figure 5**). Our results allow us to conclude that, although temporally intermittent, less predictable, and less effective than the ones associated with the island mass effect, the blooms downstream of seamounts cannot be neglected. Our findings advocate for a connected vision of the ecosystems along the ACC and may support future conservation actions by providing the tools to track the areas under the seamount effect.

## DATA AVAILABILITY STATEMENT

All the data used in this research are freely available and may be downloaded through the links detailed in the section "Materials and Methods."

## ETHICS STATEMENT

Ethical review and approval was not required for the animal study because this study analyzed observations of vertebrate animals previously published by another study reviewed and approved by an animal ethics committee (doi: 10.1111/ddi.12702).



## AUTHOR CONTRIBUTIONS

SS conducted the data analysis. SS and Fd'O wrote the manuscript. All authors contributed to the ideas and to the revision of the manuscript.

## FUNDING

SS was supported by a Sorbonne University doctoral contract (ED129 Doctoral School of Environmental Sciences). Part of this study was supported by CNES.

## ACKNOWLEDGMENTS

This work was a contribution to the French ANR-11-IDEX-0004-17-EURE-0006. The authors acknowledge the International Argo Program, the Global Ocean Observing System of which it is a part, and the national programs that contributed to it (<http://www.argo.ucsd.edu>, <http://argo.jcommops.org>). The authors

are grateful to the National Research Foundation and the South African Department of Environmental Affairs for the collection of predators tracking data, and the numerous fields' biologists who contributed to this database, including the authors of Reisinger et al. (2018). The authors also acknowledged Aviso, ACRI-ST and the European Copernicus Marine Environment Monitoring Service for the production and the delivery of environmental data. Fd'O acknowledged the support from the Cnes OSTST Tosca project LAECOS. The authors thank Ryan Reisinger for useful discussions and Severine Alvain and Anne-Hélène Reve-Lamarche for their help in accessing the PHYSAT data (Inter Deposit Digital Number IDDN.FR.001.330003.000.S.P.2012.000.30300).

## SUPPLEMENTARY MATERIAL

The Supplementary Material for this article can be found online at: <https://www.frontiersin.org/articles/10.3389/fmars.2020.00416/full#supplementary-material>

## REFERENCES

- Adams, N. J., and Brown, C. R. (1989). Dietary differentiation and trophic relationships in the sub-antarctic penguin community at Marion Island. *Mar. Ecol. Prog. Ser. Oldendorf* 57, 249–258. doi: 10.3354/meps057249
- Alvain, S., Le Quéré, C., Bopp, L., Racault, M. F., Beaugrand, G., Dessailly, D., et al. (2013). Rapid climatic driven shifts of diatoms at high latitudes. *Remote Sens. Environ.* 132, 195–201. doi: 10.1016/j.rse.2013.01.014
- Alvain, S., Moulin, C., Dandonneau, Y., and Bréon, F. M. (2005). Remote sensing of phytoplankton groups in case 1 waters from global SeaWiFS imagery. *Deep Sea Res. Part I Oceanogr. Res. Pap.* 52, 1989–2004. doi: 10.1016/j.dsr.2005.06.015
- Alvain, S., Moulin, C., Dandonneau, Y., and Loisel, H. (2008). Seasonal distribution and succession of dominant phytoplankton groups in the global ocean: a satellite view. *Global Biogeochem. Cycles* 22:GB3001.
- Ardyna, M., Claustre, H., Sallée, J. B., d'Ovidio, F., Gentili, B., Van Dijken, G., et al. (2017). Delineating environmental control of phytoplankton biomass and phenology in the Southern Ocean. *Geophys. Res. Lett.* 44, 5016–5024. doi: 10.1002/2016gl072428
- Ardyna, M., Lacour, L., Sergi, S., d'Ovidio, F., Sallée, J. B., Rembauville, M., et al. (2019). Hydrothermal vents trigger massive phytoplankton blooms in the Southern Ocean. *Nat. Commun.* 10:2451.
- Arthur, B., Hindell, M., Bester, M., De Bruyn, P. N., Trathan, P., Goebel, M., et al. (2017). Winter habitat predictions of a key Southern Ocean predator, the Antarctic fur seal (*Arctocephalus gazella*). *Deep Sea Res. Part II Top. Stud. Oceanogr.* 140, 171–181. doi: 10.1016/j.dsr2.2016.10.009
- Aumont, O., and Bopp, L. (2006). Globalizing results from ocean in situ iron fertilization studies. *Global Biogeochem. Cycles* 20:GB2017. doi: 10.1029/2005GB002591
- Bakker, D. C., Nielsdóttir, M. C., Morris, P. J., Venables, H. J., and Watson, A. J. (2007). The island mass effect and biological carbon uptake for the subantarctic Crozet Archipelago. *Deep Sea Res. Part II Top. Stud. Oceanogr.* 54, 2174–2190. doi: 10.1016/j.dsr2.2007.06.009
- Barlow, K. E., and Croxall, J. P. (2002). Seasonal and interannual variation in foraging range and habitat of macaroni penguins *Eudyptes chrysolophus* at South Georgia. *Mar. Ecol. Prog. Ser.* 232, 291–304. doi: 10.3354/meps232291
- Bathmann, U. V., Scharek, R., Klaas, C., Dubischar, C. D., and Smetacek, V. (1997). Spring development of phytoplankton biomass and composition in major water masses of the Atlantic sector of the Southern Ocean. *Deep Sea Res. Part II Top. Stud. Oceanogr.* 44, 51–67. doi: 10.1016/s0967-0645(96)00063-x
- Biuw, M., Nøst, O. A., Stien, A., Zhou, Q., Lydersen, C., and Kovacs, K. M. (2010). Effects of hydrographic variability on the spatial, seasonal and diel diving patterns of southern elephant seals in the eastern Weddell Sea. *PLoS One* 5:e13816. doi: 10.1371/journal.pone.0013816
- Blain, S., Quéguiner, B., Armand, L., Belviso, S., Bombled, B., Bopp, L., et al. (2007). Effect of natural iron fertilization on carbon sequestration in the Southern Ocean. *Nature* 446:1070.
- Blain, S., Tréguer, P., Belviso, S., Bucciarelli, E., Denis, M., Desabre, S., et al. (2001). A biogeochemical study of the island mass effect in the context of the iron hypothesis: kerguelen Islands. Southern Ocean. *Deep Sea Res. Part I Oceanogr. Res. Pap.* 48, 163–187. doi: 10.1016/s0967-0637(00)00047-9
- Block, B. A., Jonsen, I. D., Jorgensen, S. J., Winship, A. J., Shaffer, S. A., Bograd, S. J., et al. (2011). Tracking apex marine predator movements in a dynamic ocean. *Nature* 475, 86–90. doi: 10.1038/nature10082
- Boehme, L., Meredith, M. P., Thorpe, S. E., Biuw, M., and Fedak, M. (2008). Antarctic Circumpolar current frontal system in the south atlantic: monitoring using merged argo and animal-borne sensor data. *J. Geophys. Res. Oceans* 113:C09012. doi: 10.1029/2007JC00464
- Boersma, P. D., Rebstock, G. A., Frere, E., and Moore, S. E. (2009). Following the fish: penguins and productivity in the South Atlantic. *Ecol. Monogr.* 79, 59–76. doi: 10.1890/06-0419.1
- Borrione, I., Aumont, O., Nielsdóttir, M. C., and Schlitzer, R. (2014). Sedimentary and atmospheric sources of iron around South Georgia, Southern Ocean: a modelling perspective. *Biogeosciences* 11, 1981–2001. doi: 10.5194/bg-11-1981-2014
- Botnikov, V. N. (1963). Geographical position of the Antarctic Convergence Zone in the Antarctic Ocean. *Soviet Antarctic Exped. Inform. Bull.* 41, 324–327.
- Boyd, P. W., Watson, A. J., Law, C. S., Abraham, E. R., Trull, T., Murdoch, R., et al. (2000). A mesoscale phytoplankton bloom in the polar Southern Ocean stimulated by iron fertilization. *Nature* 407, 695–702. doi: 10.1038/35037500
- Brink, K. (1995). Tidal and lower frequency currents above Fieberling Guyot. *J. Geophys. Res.* 100, 10817–10832.
- Brown, C. R., and Klages, N. T. (1987). Seasonal and annual variation in diets of Macaroni (*Eudyptes chrysolophus chrysolophus*) and Southern rockhopper (*E. chrysocome chrysocome*) penguins at sub-Antarctic Marion Island. *J. Zool.* 212, 7–28. doi: 10.1111/j.1469-7998.1987.tb05111.x
- Cascão, I., Domokos, R., Lammers, M. O., Marques, V., Domínguez, R., Santos, R. S., et al. (2017). Persistent enhancement of micronekton backscatter at the summits of seamounts in the azores. *Front. Mar. Sci.* 4:25. doi: 10.3389/fmars.2017.00025
- Camlr-XXXVII (2018). *Report of the Thirty-Seven Meeting of the Commission.* Hobart: Commission for the Conservation of Antarctic Marine Living Resources, 54.



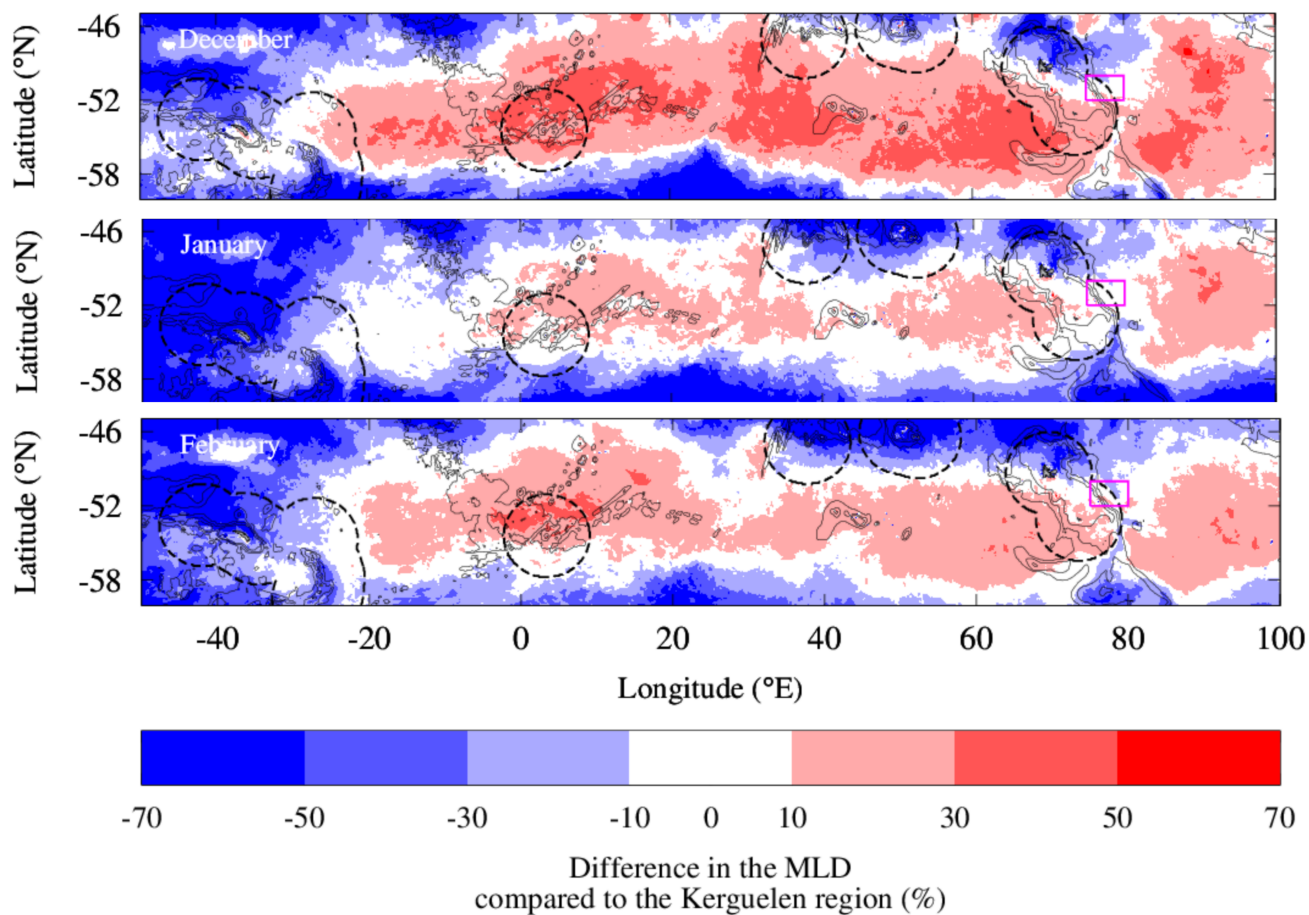
- Chapman, D. C., and Haidvogel, D. B. (1992). Formation of Taylor caps over a tall isolated seamount in a stratified ocean. *Geophys. Astrophys. Fluid Dyn.* 64, 31–65. doi: 10.1080/03091929208228084
- Chassot, E., Bonhommeau, S., Dulvy, N. K., Mélin, F., Watson, R., Gascuel, D., et al. (2010). Global marine primary production constrains fisheries catches. *Ecol. Lett.* 13, 495–505. doi: 10.1111/j.1461-0248.2010.01443.x
- Cotté, C., d'Ovidio, F., Dragon, A. C., Guinet, C., and Lévy, M. (2015). Flexible preference of southern elephant seals for distinct mesoscale features within the antarctic circumpolar current. *Prog. Oceanogr.* 131, 46–58. doi: 10.1016/j.pocean.2014.11.011
- Crawford, R. J. M., Cooper, J., and Dyer, B. M. (2003). Population of the macaroni penguin *Eudyptes chrysolophus* at Marion Island, 1994/95–2002/03, with information on breeding and diet. *Afr. J. Mar. Sci.* 25, 475–486. doi: 10.2989/18142320309504036
- Croot, P. L., Andersson, K., Öztürk, M., and Turner, D. R. (2004). The distribution and speciation of iron along 6 E in the Southern Ocean. *Deep Sea Res. Part II Top. Stud. Oceanogr.* 51, 2857–2879. doi: 10.1016/j.dsr2.2003.10.012
- Cushing, D. H. (1989). A difference in structure between ecosystems in strongly stratified waters and in those that are only weakly stratified. *J. Plankton Res.* 11, 1–13. doi: 10.1093/plankt/11.1.1
- De Baar, H. J., De Jong, J. T., Bakker, D. C., Löscher, B. M., Veth, C., Bathmann, U., et al. (1995). Importance of iron for plankton blooms and carbon dioxide drawdown in the Southern Ocean. *Nature* 373, 412–415. doi: 10.1038/373412a0
- De Broyer, C., Koubbi, P., Griffiths, H. J., Raymond, B., Udekem, D. A. C. D., Van de Putte, A. P., et al. (eds) (2014). *Biogeographic Atlas of the Southern Ocean*. Cambridge: Scientific Committee on Antarctic Research, 498.
- De Jong, J., Schoemann, V., Lannuzel, D., Croot, P., de Baar, H., and Tison, J. L. (2012). Natural iron fertilization of the Atlantic sector of the Southern Ocean by continental shelf sources of the antarctic peninsula. *J. Geophys. Res. Biogeosci.* 117:G01029.
- Della Penna, A., Trull, T. W., Wotherspoon, S., De Monte, S., Johnson, C. R., and d'Ovidio, F. (2018). Mesoscale variability of conditions favoring an iron-induced diatom bloom downstream of the kerguelen plateau. *J. Geophys. Res. Oceans* 123, 3355–3367. doi: 10.1029/2018jc013884
- Detmer, A. E., and Bathmann, U. V. (1997). Distribution patterns of autotrophic pico- and nanoplankton and their relative contribution to algal biomass during spring in the Atlantic sector of the Southern Ocean. *Deep Sea Res. Part II Top. Stud. Oceanogr.* 44, 299–320. doi: 10.1016/s0967-0645(96)00068-9
- Djurhuus, A., Read, J. F., and Rogers, A. D. (2017). The spatial distribution of particulate organic carbon and microorganisms on seamounts of the South West Indian Ridge. *Deep Sea Res. Part II Top. Stud. Oceanogr.* 136, 73–84. doi: 10.1016/j.dsr2.2015.11.015
- d'Ovidio, F., De Monte, S., Alvain, S., Dandonneau, Y., and Lévy, M. (2010). Fluid dynamical niches of phytoplankton types. *Proc. Natl. Acad. Sci. U.S.A.* 107, 18366–18370. doi: 10.1073/pnas.1004620107
- d'Ovidio, F., Della Penna, A., Trull, T. W., Nencioli, F., Pujol, M. I., Rio, M. H., et al. (2015). The biogeochemical structuring role of horizontal stirring: lagrangian perspectives on iron delivery downstream of the Kerguelen plateau. *Biogeosciences* 12, 5567–5581. doi: 10.5194/bg-12-5567-2015
- Eriksen, C. C. (1998). Internal wave reflection and mixing at Fieberling Guyot. *J. Geophys. Res.* 103, 2977–2994. doi: 10.1029/97jc03205
- Flynn, A. J., and Williams, A. (2012). Lanternfish (Pisces: *Myctophidae*) biomass distribution and oceanographic-topographic associations at Macquarie Island, Southern Ocean. *Mar. Freshw. Res.* 63, 251–263.
- Frederiksen, M., Edwards, M., Richardson, A. J., Halliday, N. C., and Wanless, S. (2006). From plankton to top predators: bottom-up control of a marine food web across four trophic levels. *J. Anim. Ecol.* 75, 1259–1268. doi: 10.1111/j.1365-2656.2006.01148.x
- Froneman, P. W., Perissinotto, R., McQuaid, C. D., and Laubscher, R. K. (1995). Summer distribution of net phytoplankton in the Atlantic sector of the Southern Ocean. *Polar Biol.* 15, 77–84.
- Georgen, J. E., Lin, J., and Dick, H. J. (2001). Evidence from gravity anomalies for interactions of the Marion and Bouvet hotspots with the Southwest Indian Ridge: effects of transform offsets. *Earth Planet. Sci. Lett.* 187, 283–300. doi: 10.1016/s0012-821x(01)00293-x
- Gervais, F., Riebesell, U., and Gorbunov, M. Y. (2002). Changes in primary productivity and chlorophyll a in response to iron fertilization in the Southern Polar Frontal Zone. *Limnol. Oceanogr.* 47, 1324–1335. doi: 10.4319/lo.2002.47.5.1324
- Gove, J. M., McManus, M. A., Neuheimer, A. B., Polovina, J. J., Drazen, J. C., Smith, C. R., et al. (2016). Near-island biological hotspots in barren ocean basins. *Nat. Commun.* 7:10581. doi: 10.1038/ncomms10581
- Graham, R. M., De Boer, A. M., van Sebille, E., Kohfeld, K. E., and Schlosser, C. (2015). Inferring source regions and supply mechanisms of iron in the Southern Ocean from satellite chlorophyll data. *Deep Sea Res. Part I Oceanogr. Res. Pap.* 104, 9–25. doi: 10.1016/j.dsr.2015.05.007
- Guinet, C., Dubroca, L., Lea, M. A., Goldsworthy, S., Cherel, Y., Duhamel, G., et al. (2001). Spatial distribution of foraging in female Antarctic fur seals *Arctocephalus gazella* in relation to oceanographic variables: a scale-dependent approach using geographic information systems. *Mar. Ecol. Prog. Ser.* 219, 251–264. doi: 10.3354/meps219251
- Heinze, C., Meyer, S., Goris, N., Anderson, L., Steinfeldt, R., Chang, N., et al. (2015). The ocean carbon sink—impacts, vulnerabilities and challenges. *Earth Syst. Dyn.* 6, 327–358. doi: 10.5194/esd-6-327-2015
- Hindell, M. A., McMahon, C. R., Bester, M. N., Boehme, L., Costa, D., Fedak, M. A., et al. (2016). Circumpolar habitat use in the southern elephant seal: implications for foraging success and population trajectories. *Ecosphere* 7:e01213.
- Huettel, M., Ziebig, W., Forster, S., and Luther, G. W. III. (1998). Advective transport affecting metal and nutrient distributions and interfacial fluxes in permeable sediments. *Geochim. Cosmochim. Acta* 62, 613–631. doi: 10.1016/s0016-7037(97)00371-2
- Hughes, C. W. (2005). Nonlinear vorticity balance of the antarctic circumpolar current. *J. Geophys. Res. Oceans* 110:C11008. doi: 10.1029/2004JC002753
- Iverson, R. L. (1990). Control of marine fish production. *Limnol. Oceanogr.* 35, 1593–1604. doi: 10.4319/lo.1990.35.7.1593
- Korb, R. E., Whitehouse, M. J., and Ward, P. (2004). SeaWiFS in the southern ocean: spatial and temporal variability in phytoplankton biomass around South Georgia. *Deep Sea Res. Part II Top. Stud. Oceanogr.* 51, 99–116. doi: 10.1016/j.dsr2.2003.04.002
- Kunze, E., and Sanford, T. B. (1997). Tidally driven vorticity, diurnal shear and turbulence atop Fieberling Seamount. *J. Phys. Oceanogr.* 27, 2663–2693. doi: 10.1175/1520-0485(1997)027<2663:tdvdsa>2.0.co;2
- Lancelot, C., Montety, A. D., Goosse, H., Becquevort, S., Schoemann, V., Pasquer, B., et al. (2009). Spatial distribution of the iron supply to phytoplankton in the Southern Ocean: a model study. *Biogeosciences* 6, 2861–2878. doi: 10.5194/bg-6-2861-2009
- Laubscher, R. K., Perissinotto, R., and McQuaid, C. D. (1993). Phytoplankton production and biomass at frontal zones in the Atlantic sector of the Southern Ocean. *Polar Biol.* 13, 471–481.
- Laws, R. M. (1985). The ecology of the Southern Ocean. *Am. Sci.* 73, 26–40.
- Lea, M. A., Guinet, C., Cherel, Y., Duhamel, G., Dubroca, L., Pruvost, P., et al. (2006). Impacts of climatic anomalies on provisioning strategies of a Southern Ocean predator. *Mar. Ecol. Prog. Ser.* 310, 77–94. doi: 10.3354/meps310077
- Legendre, L., and Rassoulzadegan, F. (1995). Plankton and nutrient dynamics in marine waters. *Ophelia* 41, 153–172. doi: 10.1080/00785236.1995.10422042
- Lehahn, Y., d'Ovidio, F., and Koren, I. (2018). A satellite-based Lagrangian view on phytoplankton dynamics. *Annu. Rev. Mar. Sci.* 10, 99–119. doi: 10.1146/annurev-marine-121916-063204
- Lemos, A. T., Ghisolfi, R. D. R., and Mazzini, P. L. F. (2018). Annual phytoplankton blooming using satellite-derived chlorophyll-a data around the Vitória-Trindade Chain, Southeastern Brazil. *Deep Sea Res. Part I Oceanogr. Res. Pap.* 136, 62–71. doi: 10.1016/j.dsr.2018.04.005
- Lévy, M., Franks, P. J. S., and Smith, K. S. (2018). The role of submesoscale currents in structuring marine ecosystems. *Nat. Commun.* 9:4758. doi: 10.1038/s41467-018-07059-3
- Löscher, B. M., De Baar, H. J., De Jong, J. T. M., Veth, C., and Dehairens, F. (1997). The distribution of Fe in the Antarctic circumpolar current. *Deep Sea Res. Part II Top. Stud. Oceanogr.* 44, 143–187.
- Martin, J. H. (1990). Glacial-interglacial CO<sub>2</sub> change: the iron hypothesis. *Paleoceanography* 5, 1–13. doi: 10.1029/pa005i001p00001
- Measures, C. L., and Vink, S. (2001). Dissolved Fe in the upper waters of the Pacific sector of the Southern Ocean. *Deep Sea Res. Part II Top. Stud. Oceanogr.* 48, 3913–3941. doi: 10.1016/s0967-0645(01)00074-1

- Menard, H. W. (1964). *Marine Geology of the Pacific*. New York: McGraw-Hill, xiv + 271. Available online at: <https://www.worldcat.org/title/marine-geology-of-the-pacific/oclc/545637>
- Mengelt, C., Abbott, M. R., Barth, J. A., Letelier, R. M., Measures, C. I., and Vink, S. (2001). Phytoplankton pigment distribution in relation to silicic acid, iron and the physical structure across the Antarctic Polar Front, 170° W, during austral summer. *Deep Sea Res. Part II Top. Stud. Oceanogr.* 48, 4081–4100. doi: 10.1016/s0967-0645(01)00081-9
- Meredith, M. P., Meijers, A. S., Naveira Garabato, A. C., Brown, P. J., Venables, H. J., Abrahamson, E. P., et al. (2015). Circulation, retention, and mixing of waters within the Weddell-Scotia Confluence, Southern Ocean: the role of stratified Taylor columns. *J. Geophys. Res. Oceans* 120, 547–562. doi: 10.1002/2014jc010462
- Meredith, M. P., Watkins, J. L., Murphy, E. J., Cunningham, N. J., Wood, A. G., Korb, R., et al. (2003). An anticyclonic circulation above the northwest Georgia rise, Southern Ocean. *Geophys. Res. Lett.* 30:2061. doi: 10.1029/2003GL018039
- Michaels, A. F., and Silver, M. W. (1988). Primary production, sinking fluxes and the microbial food web. *Deep Sea Res. Part A Oceanogr. Res. Pap.* 35, 473–490. doi: 10.1016/0198-0149(88)90126-4
- Moline, M. A., Claustre, H., Frazer, T. K., Schofield, O., and Vernet, M. (2004). Alteration of the food web along the Antarctic Peninsula in response to a regional warming trend. *Global Change Biol.* 10, 1973–1980. doi: 10.1111/j.1365-2486.2004.00825.x
- Mongin, M. M., Abraham, E. R., and Trull, T. W. (2009). Winter advection of iron can explain the summer phytoplankton bloom that extends 1000 km downstream of the Kerguelen Plateau in the Southern Ocean. *J. Mar. Res.* 67, 225–237. doi: 10.1357/002224009789051218
- Moore, J. K., and Abbott, M. R. (2002). Surface chlorophyll concentrations in relation to the antarctic polar front: seasonal and spatial patterns from satellite observations. *J. Mar. Syst.* 37, 69–86. doi: 10.1016/s0924-7963(02)00196-3
- Morato, T., Hoyle, S. D., Allain, V., and Nicol, S. J. (2010). Seamounts are hotspots of pelagic biodiversity in the open ocean. *Proc. Natl. Acad. Sci. U.S.A.* 107, 9707–9711. doi: 10.1073/pnas.0910290107
- Oliveira, A. P., Coutinho, T. P., Cabeçadas, G., Brogueira, M. J., Coca, J., Ramos, M., et al. (2016). Primary production enhancement in a shallow seamount (Gorringe—Northeast Atlantic). *J. Mar. Syst.* 164, 13–29. doi: 10.1016/j.jmarsys.2016.07.012
- O’Toole, M., Guinet, C., Lea, M. A., and Hindell, M. A. (2017). Marine predators and phytoplankton: how elephant seals use the recurrent Kerguelen plume. *Mar. Ecol. Prog. Ser.* 581, 215–227. doi: 10.3354/meps12312
- Owens, W. B., and Hogg, N. G. (1980). Oceanic observations of stratified Taylor columns near a bump. *Deep Sea Res. Part A Oceanogr. Res. Pap.* 27, 1029–1045. doi: 10.1016/0198-0149(80)90063-1
- Pakhomov, E. A., Henschke, N., Hunt, B. P., Stowasser, G., and Chereil, Y. (2019). Utility of salps as a baseline proxy for food web studies. *J. Plankton Res.* 41, 3–11. doi: 10.1093/plankt/fby051
- Pascual, A., Faugère, Y., Larnicol, G., and Le Traon, P. Y. (2006). Improved description of the ocean mesoscale variability by combining four satellite altimeters. *Geophys. Res. Lett.* 33:L02611. doi: 10.1029/2005GL024633
- Pauly, D., Hood, L., and Stergiou, K. I. (2017). “Tentative von Bertalanffy growth parameters of little-studied fishes,” in *Belated Contributions on the Biology of Fish, Fisheries and Features of Their Ecosystems. Fisheries Centre Research Reports*, Vol. 25, eds D. Pauly, L. Hood, and K. I. Stergiou (Vancouver, BC: Institute for the Oceans and Fisheries), 58–60.
- Perissinotto, R., Laubscher, R. K., and McQuaid, C. D. (1992). Marine productivity enhancement around Bouvet and the South Sandwich Islands (Southern Ocean). *Mar. Ecol. Prog. Ser.* 88, 41–41.
- Perissinotto, R., Lutjeharms, J. R. E., and Van Ballegooyen, R. C. (2000). Biological-physical interactions and pelagic productivity at the Prince Edward Islands. Southern Ocean. *J. Mar. Syst.* 24, 327–341. doi: 10.1016/s0924-7963(99)00093-7
- Perissinotto, R., and Rae, C. D. (1990). Occurrence of anticyclonic eddies on the prince edward plateau (Southern Ocean): effects on phytoplankton biomass and production. *Deep Sea Res. Part A Oceanogr. Res. Pap.* 37, 777–793. doi: 10.1016/0198-0149(90)90006-h
- Pistorius, P., Hindell, M., Crawford, R., Makhado, A., Dyer, B., and Reisinger, R. (2017). At-sea distribution and habitat use in king penguins at sub-Antarctic Marion Island. *Ecol. Evol.* 7, 3894–3903. doi: 10.1002/ece3.2833
- Pitcher, T. J., Morato, T., Hart, P. J. B., Clark, M. R., Haggan, N., and Santos, R. S. (eds) (2007). *Seamounts: Ecology, Fisheries & Conservation. Fish and Aquatic Resources Series 12*. Oxford: Blackwell Publishing, 527.
- Pollard, R. T., Salter, I., Sanders, R. J., Lucas, M. I., Moore, C. M., Mills, R. A., et al. (2009). Southern Ocean deep-water carbon export enhanced by natural iron fertilization. *Nature* 457, 577–580. doi: 10.1038/nature07716
- Queguiner, B. (2013). Iron fertilization and the structure of planktonic communities in high nutrient regions of the Southern Ocean. *Deep Sea Res. Part II Top. Stud. Oceanogr.* 90, 43–54. doi: 10.1016/j.dsr2.2012.07.024
- Read, J., and Pollard, R. (2017). An introduction to the physical oceanography of six seamounts in the southwest Indian Ocean. *Deep Sea Res. Part II Top. Stud. Oceanogr.* 136, 44–58. doi: 10.1016/j.dsr2.2015.06.022
- Reisinger, R., Raymond, B., Hindell, M. A., Bester, M. N., Crawford, R., Davies, D., et al. (2017). Habitat modelling of tracking data from multiple marine predators identifies important areas in the Southern Indian Ocean. *Biodivers. Res.* 24, 535–550. doi: 10.1111/ddi.12702
- Reisinger, R. R., Raymond, B., Hindell, M. A., Bester, M. N., Crawford, R. J., Davies, D., et al. (2018). Habitat modelling of tracking data from multiple marine predators identifies important areas in the Southern Indian Ocean. *Divers. Distrib.* 24, 535–550. doi: 10.1111/ddi.12702
- Rhoads, D. C., and Boyer, L. F. (1982). “The effects of marine benthos on physical properties of sediments,” in *Animal-Sediment Relations*, ed. P. McCall (Boston, MA: Springer), 3–52. doi: 10.1007/978-1-4757-1317-6\_1
- Rintoul, S. R. (2018). The global influence of localized dynamics in the Southern Ocean. *Nature* 558, 209–218. doi: 10.1038/s41586-018-0182-3
- Rogers, A. D., Yesson, C., and Gravestock, P. (eds) (2015). A Biophysical and Economic Profile of South Georgia and the South Sandwich Islands as Potential Large-Scale Antarctic Protected Areas. *Adv. Mar. Biol.* 70, 1–286. doi: 10.1016/bs.amb.2015.06.001
- Sallée, J. B., Lloft, J., Tagliabue, A., and Lévy, M. (2015). Characterization of distinct bloom phenology regimes in the Southern Ocean. *ICES J. Mar. Sci.* 72, 1985–1998. doi: 10.1093/icesjms/fsv069
- Sanial, V., van Beek, P., Lansard, B., d’Ovidio, F., Kestenare, É, Souhaut, M., et al. (2014). Study of the phytoplankton plume dynamics off the Crozet Islands (Southern Ocean): a geochemical-physical coupled approach. *J. Geophys. Res. Oceans* 119, 2227–2237. doi: 10.1002/2013jc009305
- Sanial, V., van Beek, P., Lansard, B., Souhaut, M., Kestenare, E., d’Ovidio, F., et al. (2015). Use of Ra isotopes to deduce rapid transfer of sediment-derived inputs off Kerguelen. *Biogeosciences* 12, 1415–1430. doi: 10.5194/bg-12-1415-2015
- Santora, J. A., Sydeman, W. J., Schroeder, I. D., Field, J. C., Miller, R. R., and Wells, B. K. (2017). Persistence of trophic hotspots and relation to human impacts within an upwelling marine ecosystem. *Ecol. Appl.* 27, 560–574. doi: 10.1002/eap.1466
- Sc-Camlr-XXXVII (2018). *Annex 7: Report of the Meeting of the Workshop on Spatial Management. Report of the Thirty-seven Meeting of the Scientific Committee*. Hobart: Commission for the Conservation of Antarctic Marine Living Resources, 203–245.
- Scheffer, A., Trathan, P. N., and Collins, M. (2010). Foraging behaviour of king penguins (*Aptenodytes patagonicus*) in relation to predictable mesoscale oceanographic features in the Polar Front Zone to the north of South Georgia. *Prog. Oceanogr.* 86, 232–245. doi: 10.1016/j.pocean.2010.04.008
- Schmechtig, C., Claustre, H., Poteau, A., and D’Ortenzio, F. (2014). *Bio-Argo quality control manual for Chlorophyll-A concentration. Version 1.0*. Available at: [http://www.jamstec.go.jp/ARGORC/documents/Bio-Argo%20quality%20control%20manual%20for%20Chlorophyll-A%20concentration\\_v1.0.pdf](http://www.jamstec.go.jp/ARGORC/documents/Bio-Argo%20quality%20control%20manual%20for%20Chlorophyll-A%20concentration_v1.0.pdf) (accessed December 17th 2014).
- Schmechtig, C., Poteau, A., Claustre, H., D’Ortenzio, F., Dall’Olmo, G., and Boss, E. (2018). *Processing BGC-Argo Particle Backscattering at the DAC Level. Version 1.4, 07 March 2018*. France: IFREMER for Argo Data Management Villefranche-sur-Mer.
- Sérazin, G. (2011). *An approximate Neutral Density variable for the World’s Oceans*. France: École Centrale de Lyon.
- Siegelman, L., O’Toole, M., Flexas, M., Rivière, P., and Klein, P. (2019). Submesoscale ocean fronts act as biological hotspot for southern elephant seal. *Sci. Rep.* 9:5588. doi: 10.1038/s41598-019-42117-w
- Smetacek, V., Assmy, P., and Henjes, J. (2004). The role of grazing in structuring Southern Ocean pelagic ecosystems and biogeochemical cycles. *Antarct. Sci.* 16, 541–558. doi: 10.1017/s0954102004002317

- Smetacek, V., De Baar, H. J. W., Bathmann, U. V., Lochte, K., and Van Der Loeff, M. R. (1997). Ecology and biogeochemistry of the Antarctic Circumpolar Current during austral spring: a summary of Southern Ocean JGOFS cruise ANT X/6 of RV Polarstern. *Deep Sea Res. Part II Top. Stud. Oceanogr.* 44, 1–21. doi: 10.1016/s0967-0645(96)00100-2
- Smetacek, V., Scharek, R., and Nöthig, E. M. (1990). “Seasonal and regional variation in the pelagial and its relationship to the life history cycle of krill,” in *Antarctic Ecosystems*, eds D. C. Williams and P. B. Howard-Williams (Berlin: Springer), 103–114. doi: 10.1007/978-3-642-84074-6\_10
- Sohrin, Y., Iwamoto, S. I., Matsui, M., Obata, H., Nakayama, E., Suzuki, K., et al. (2000). The distribution of Fe in the Australian sector of the Southern Ocean. *Deep Sea Res. Part I Oceanogr. Res. Pap.* 47, 55–84. doi: 10.1016/s0967-0637(99)00049-7
- Sokolov, S., and Rintoul, S. R. (2007). On the relationship between fronts of the Antarctic Circumpolar Current and surface chlorophyll concentrations in the Southern Ocean. *J. Geophys. Res. Oceans* 112:C07030.
- Staniland, I. J., Reid, K., and Boyd, I. L. (2004). Comparing individual and spatial influences on foraging behaviour in Antarctic fur seals *Arctocephalus gazella*. *Mar. Ecol. Prog. Ser.* 275, 263–274. doi: 10.3354/meps275263
- Staudigel, H., Koppers, A. A. P., Lavelle, J. W., Pitcher, T. J., and Shank, T. M. (2010). Defining the word “seamount”. *Oceanography* 23, 20–21. doi: 10.5670/oceanog.2010.85
- Sullivan, C. W., Arrigo, K. R., McClain, C. R., Comiso, J. C., and Firestone, J. (1993). Distributions of phytoplankton blooms in the Southern Ocean. *Science* 262, 1832–1837.
- Tagliabue, A., Aumont, O., and Bopp, L. (2014). The impact of different external sources of iron on the global carbon cycle. *Geophys. Res. Lett.* 41, 920–926. doi: 10.1002/2013gl059059
- Tagliabue, A., Mtshali, T., Aumont, O., Bowie, A. R., Klunder, M. B., Roychoudhury, A. N., et al. (2012). A global compilation of dissolved iron measurements: focus on distributions and processes in the Southern Ocean. *Biogeosciences* 9, 2333–2349. doi: 10.5194/bg-9-2333-2012
- Tamsitt, V., Drake, H. F., Morrison, A. K., Talley, L. D., Dufour, C. O., Gray, A. R., et al. (2017). Spiraling pathways of global deep waters to the surface of the Southern Ocean. *Nat. Commun.* 8:172. doi: 10.1038/s41467-017-00197-0
- Taylor, G. I. (1923). Experiments on the motion of solid bodies in rotating fluids. *Proc. R. Soc. Lond. Ser. A* 104, 213–218. doi: 10.1098/rspa.1923.0103
- Thomalla, S. J., Fauchereau, N., Swart, S., and Monteiro, P. M. S. (2011). Regional scale characteristics of the seasonal cycle of chlorophyll in the Southern Ocean. *Biogeosciences* 8, 2849–2866. doi: 10.5194/bg-8-2849-2011
- Thompson, A. F., and Naveira Garabato, A. C. (2014). Equilibration of the Antarctic circumpolar current by standing meanders. *J. Phys. Oceanogr.* 44, 1811–1828. doi: 10.1175/jpo-d-13-0163.1
- Van Bennekom, A. J., Berger, G. W., Van der Gaast, S. J., and De Vries, R. T. P. (1988). Primary productivity and the silica cycle in the Southern Ocean (Atlantic sector). *Palaeogeogr. Palaeoclimatol. Palaeoecol.* 67, 19–30. doi: 10.1016/0031-0182(88)90120-4
- Venables, H., Meredith, M. P., Atkinson, A., and Ward, P. (2012). Fronts and habitat zones in the Scotia Sea. *Deep Sea Res. Part II Top. Stud. Oceanogr.* 59, 14–24. doi: 10.1016/j.dsr2.2011.08.012
- Venables, H. J., and Meredith, M. P. (2009). Theory and observations of Ekman flux in the chlorophyll distribution downstream of South Georgia. *Geophys. Res. Lett.* 36:L23610. doi: 10.1029/2009GL04137
- Venables, W. N., and Ripley, B. D. (2002). *Modern Applied Statistics with S-PLUS*, 4th Edn. New York, NY: Springer.
- Venrick, E. L. (1991). Mid-ocean ridges and their influence on the large-scale patterns of chlorophyll and production in the North Pacific. *Deep Sea Res. Part A Oceanogr. Res. Pap.* 38, S83–S102.
- Viglione, G. A., and Thompson, A. F. (2016). Lagrangian pathways of upwelling in the Southern Ocean. *J. Geophys. Res. Oceans* 121, 6295–6309. doi: 10.1002/2016jc011773
- Viljoen, J. J., Philibert, R., Van Horsten, N., Mtshali, T., Roychoudhury, A. N., Thomalla, S., et al. (2018). Phytoplankton response in growth, photophysiology and community structure to iron and light in the Polar Frontal Zone and Antarctic waters. *Deep Sea Res. Part I Oceanogr. Res. Pap.* 141, 118–129. doi: 10.1016/j.dsr.2018.09.006
- Watson, A. J., Ledwell, J. R., Messias, M. J., King, B. A., Mackay, N., Meredith, M. P., et al. (2013). Rapid cross-density ocean mixing at mid-depths in the Drake Passage measured by tracer release. *Nature* 501, 408–411. doi: 10.1038/nature12432
- Whitehead, T. O., Kato, A., Ropert-Coudert, Y., and Ryan, P. G. (2016). Habitat use and diving behaviour of macaroni Eudyptes chrysolophus and eastern rockhopper E. chrysocome filholi penguins during the critical pre-moult period. *Mar. Biol.* 163:19.
- Wilson, R. P., Bost, C. A., Pütz, K., Charrassin, J. B., Culik, B. M., and Adelung, D. (1997). Southern rockhopper penguin Eudyptes chrysocome chrysocome foraging at Possession Island. *Polar Biol.* 17, 323–329. doi: 10.1007/pl00013373
- Xing, X., Claustre, H., Blain, S., d’Ortenzio, F., Antoine, D., Ras, J., et al. (2012). Quenching correction for in vivo chlorophyll fluorescence acquired by autonomous platforms: a case study with instrumented elephant seals in the Kerguelen region (Southern Ocean). *Limnol. Oceanogr. Methods* 10, 483–495. doi: 10.4319/lom.2012.10.483
- Yesson, C., Clark, M. R., Taylor, M. L., and Rogers, A. D. (2011). The global distribution of seamounts based on 30 arc seconds bathymetry data. *Deep Sea Res. Part I Oceanogr. Res. Pap.* 58, 442–453. doi: 10.1016/j.dsr.2011.02.004

**Conflict of Interest:** The authors declare that the research was conducted in the absence of any commercial or financial relationships that could be construed as a potential conflict of interest.

Copyright © 2020 Sergi, Baudena, Cotté, Ardyna, Blain and d’Ovidio. This is an open-access article distributed under the terms of the Creative Commons Attribution License (CC BY). The use, distribution or reproduction in other forums is permitted, provided the original author(s) and the copyright owner(s) are credited and that the original publication in this journal is cited, in accordance with accepted academic practice. No use, distribution or reproduction is permitted which does not comply with these terms.



**Supplementary Figure 1: Difference in the Mixed Layer Depth (MLD) between the Indo-Atlantic ACC region and the Kerguelen region (magenta box) in December (a), January (b) and February (c) between 2005 and 2010.** Data are extracted from the GLORYS12V1 reanalysis produced by Mercator Ocean (product id: GLOBAL\_REANALYSIS\_PHY\_001\_030-TDS). Black dashed lines bound the Exclusive Economic Zones around the subantarctic islands. Isobaths of bottom topography of 3000 m and 4100 m depths are showed in black.



## 2.2 Synthesis

### 2.2.1 Summary of key results

Ten-years observations of animal tracking data of Antarctic-Fur Seals (*Arctocephalus gazella*), Southern Elephant Seals (*Mirounga leonina*), King Penguins (*Aptenodytes patagonicus*), Macaroni Penguins (*Eudyptes chrysolophus*) and Southern Rockhopper Penguins (*Eudyptes chrysocome*) breeding at the South African Prince Edward Islands (46 °S 37 °E) reveal an open ocean region of potential important multi-level trophic biomass (Figure 1A in section 2.1). This region includes the upwelling zone identified in the previous Chapter (section 1.2), surfacing deep water masses enriched by hydrothermal iron, but it also extends thousands of kilometres upstream of it. The open ocean region targeted by megafauna species is situated far away from islands or other known iron supply mechanisms. However, it lies downstream of two ridge systems, the Shona Ridge System and the South-West Indian Ridge, characterised by numerous ( $> 60$ ) shallow seamounts (peaking between 2 and 1000 m under the sea level) [Yesson et al., 2011].

The first step of this study consisted in evaluating the phytoplankton biomass of this apparent oligotrophic region and its relation with the shallow seamounts upstream of it. This is investigated with two datasets. Firstly, we looked at the *in-situ* Chlorophyll *a* concentrations (Chl-*a*) measured by profiling observing systems. Two BGC-Argo floats crossed longitudinally the Shona Ridge System and showed an increase in Chl-*a* and backscattering values in the first 100 m of the water column downstream of the seamounts (respectively, about  $1 \text{ mg/m}^3$  and  $3.0 \cdot 10^{-3} \text{ m}^{-1}$ ) compared to the water masses upstream (respectively, about  $0.6 \text{ mg/m}^3$  and  $2.0 \cdot 10^{-3} \text{ m}^{-1}$ ). The late Chl-*a* enhancement observed by the floats, between the middle of January and the middle of February, suggests a possible positive biological effect due to the topographic highs and not simply linked to the seasonal bloom phenology [Sallée et al., 2015; Ardyna et al., 2017].

The enhancement of phytoplankton biomass downstream of seamounts is further inves-

tigated in monthly Ocean Color maps. These data provide higher spatial and temporal coverages compared to profiling floats. In the meanwhile, monthly maps allow us to avoid cloudy coverage and capture occasional mesoscale signals. Distinct Chl-*a* plumes (in excess of  $0.6 \text{ mg/m}^3$  and statistically higher than surrounding waters, about 2-fold) have been found to spread downstream of the shallow seamounts of both the Shona Ridge System and the South-West Indian Ridge. These Chl-*a* plumes spread for thousands of kilometres, similarly to the plumes stemming from islands (Figs. 3 A, B and 4 A). Lagrangian plumes stemming from seamounts are then computed and compared to the Chl-*a* plumes: depending on the study cases the Chl-*a* concentration were between 30 and 50 % higher within the Lagrangian plume than in the surrounding regions (in all the cases the difference was statistically significant with  $p < 0.01$ ). By tracking at mesoscale precision thousands of kilometres long high Chl-*a* water masses (Figs 3 E,F and 4 C), the Lagrangian analyses unambiguously link the Chl-*a* plumes to the seamounts.

Over climatological time scales (2000-2015) the Chl-*a* signals and Lagrangian plumes stemming from the seamounts match at large scale with predators distributions (Figure 5A in section 2.1). The ecological significance of these moderate Chl-*a* signatures is evaluated by investigating its phytoplankton composition with the PHYSAT method [Alvain et al., 2005, 2008]. This analysis demonstrates that bio-optical signatures of the moderate blooms downstream of seamounts are similar to the rich biological systems downstream of islands and different from other oligotrophic waters. More precisely according to PHYSAT, between December and January (2000-2011), the seamount region (and respectively the Kerguelen bloom) is dominated more than 55% (respectively 70%) of the time by diatoms-type and less than 1% (respectively 3%) of the time by Phaeocystis-type. By comparison, in the same period, the oligotrophic region downstream of the Kerguelen bloom is dominated 16% of the time by diatoms-type and 80% of the time by the small Phaeocystis-type.

### 2.2.2 Conclusions

Our approach (based on short time scales and high bathymetric resolution data) allows us to identify novel and significant phytoplankton responses to the seamounts of the Shona Ridge System and the South-West Indian Ridge. Even if temporally intermittent and less predictable and effective than the blooms stemming from islands, these signals cannot be neglected. Indeed, from an ecological point of view, the seamounts effect considered in this study appear closer to the island biological systems, well-known multi-trophic hotspots, than past evaluations. Both phytoplankton blooms spread for thousands of kilometres and have similar bio-optical signatures. Even though islands' blooms are much more intense than the ones identified downstream of seamounts, this difference is potentially overestimated in satellite maps due to the deeper summertime mixed layer in the seamount region compared to the island systems (between 10 and 100% deeper depending on the island system, [Supplementary Figure S1](#)). Seamounts appear then to complement islands mass effect in fuelling pelagic ecosystems.

Two necessary conditions have been proposed by this study for inducing a biological response associated to seamounts. The first one, is the presence of deep iron-enriched hydrographic regions (such as the water masses at intermediate depth, i.e. below the biologic activity, that transited over an island). The second one, is the presence of upwelling dynamics, due to the interaction between the ACC and the seamounts, able to lift iron-laden deep waters. The proposed mechanism, framed by the limiting effect of iron and the structuring effect of horizontal advection, is schematized in Figure 7<sup>1</sup>. Even if more detailed studies should be done for unambiguously understand the mechanisms at the basis of the seamount effect, these results enhance the need to consider the continuity of this ACC region and its biophysical processes, both in science and conservation. By contrast, conservation actions in the ACC region, far away from sea-ice margins, are currently dominated by national programs and consequently display important discontinuities

---

<sup>1</sup>See the Material and Methods and the Discussion parts of [Sergi et al., \(2020\)](#) for a more detailed description of such mechanism.

constrained by the jurisdictional framework (economic exclusive zones).





## Part III

# From the identification of biophysical forcing pathways to the management of marine environment



Since the adoption in 1982 of the United Nations Convention on the Law of the Sea (hereinafter UNCLOS), the marine region is divided between the exclusive economic zones (EEZs), that is the area contained within the 200 nautical miles from the territorial sea baseline, and the high seas, the region beyond them. Following this, the responsibility for the management and conservation of marine resources is under the competences of single countries (territorial waters and exclusive economic zones)<sup>1</sup> or falls into the international law domain (high seas)<sup>2</sup>. Indeed, despite the principle of freedom of the high seas<sup>3</sup>, States have the duties to protect and preserve the marine environment and to cooperate for the conservation and management of the living resources included in this international space too<sup>2</sup>. Consequently, several trans-boundary agreements have been established since the beginning of the 20th century, in order to respond to these conservation duties (Brown, 2016).

As introduced in chapter 1 of Part I, the conservation of marine living resources in the Southern Ocean is under the responsibility of several States with overseas territories there (islands under the national jurisdiction of United-Kingdom, Norway, South-Africa, France or Australia) and an international body, the CCAMLR. However, the fragmentation of legal conservation competences in the Southern Ocean is smoothed. From a jurisdictional point of view, all the States having sovereignty on overseas territories in the CAMLR Convention Area are original signatories of CCAMLR and contracting parties of the Antarctic Treaty System (Antarctic Treaty and related agreements), of which CCAMLR is part, since its establishment in 1959. Moreover the EEZs of these territories are completely or almost completely included in the Convention Area. Yet, at the time of the negotiation of the CAMLR Convention, the EEZ had not been formally adopted by any international legally-binding agreement<sup>4</sup>. This historical context has led to particular interactions between national and CCAMLR's measures in this region. As example, conservation measures concerning the EEZs here considered are also discussed at the CCAMLR meetings,

---

<sup>1</sup>UNCLOS (1982), Art. 56.

<sup>2</sup>UNCLOS (1982), Art. 118.

<sup>3</sup>UNCLOS (1982), Art. 87.

<sup>4</sup>The CAMLR Convention has been adopted in 1980, two years before the UNCLOS.

some measures are then jointly managed by CCAMLR members and sovereign States. More broadly, efforts are made for ensuring continuity in conservation actions in the circumpolar Southern Ocean between EEZs and CCAMLR<sup>5</sup>, and beyond them with adjacent international bodies<sup>6</sup>.

This Part illustrates similarities and differences of the conservation approach and more specifically, of the scientific contribution to such policies, adopted in the CCAMLR and in the French Southern Overseas Lands frameworks. Indeed, in both frameworks the conservation and management of living resources shall be done under scientific advice and based on “best available science”<sup>7</sup>. However, conservation policies can adopt different forms and so can the scientific contributions to them. Chapter 1 summarises how the results contained in Part II supports CCAMLR conservation efforts in the Antarctic Circumpolar Current region. Thereafter, Chapter 2 further develops the concept of “end-to-end” marine ecology providing a more comprehensive view of the contribution of scientific research to a conservation policy: the extension of the French National Natural Reserve of Saint-Paul and Amsterdam islands. This last Chapter firstly explains the role of the scientific community in the MPA extension project and then details the analysis made on the biophysical processes at the basis of the pelagic food web. Finally, it describes how this analysis has been integrated in the official conservation process.

---

<sup>5</sup>e.g. CCAMLR-XXV (2006), Annex 10, §4.

<sup>6</sup>e.g. [Arrangement between the Meeting Parties of the Southern Indian Ocean Fisheries Agreement and the Commission for the Conservation of Antarctic Marine Living Resources \(2018\)](#), which engage these two international bodies to cooperate to harmonise approaches in areas of mutual interest and concern; §2 (iii) of such agreement

<sup>7</sup>CCAMLR Convention (1980), Art. 9 par. 1 and 4 and Art. 14; CCAMLR (2009), Resolution 31/XXVIII; French Decree no. 2006-1211 of October 4<sup>th</sup>, 2006 modified, Art. 4

## Chapter 1

# Conservation of the high seas: the case of the Antarctic Circumpolar Current region

Conservation planning in the Antarctic Circumpolar Current (ACC) region, i.e. elsewhere from the ice-dependent ecosystems, is currently dominated by national programs, and consequently displays important discontinuities constrained by the jurisdictional framework (i.e. Exclusive Economic Zones). However, the analyses contained in this Thesis (Part II) shed new perspectives on bottom-up controls on the pelagic seascape in the ACC region far away from islands and their national maritime spaces. Therefore, this Chapter explores the contribution of the understanding of such bottom-up processes to CCAMLR conservation effort. To this aim, I first introduce CCAMLR's conservation strategy and its scientific basis. Then, I describe present and ongoing conservation efforts made in the ACC region of the CAMLR Convention Area. This is achieved giving a particular attention to two scientific reports submitted to CCAMLR's meetings to which I contributed during my Thesis: [o'Toole et al. \[2018\]](#) and [Sergi et al. \[2019\]](#) (full texts are available in [Appendix A1](#) and [Appendix A2](#), respectively).

## 1.1 Context

### 1.1.1 CCAMLR's structure, functioning and mechanisms for scientific research contribution

As introduced previously, CCAMLR is composed of two bodies, the Commission and an advisory body, the Scientific Committee. Each member, currently 25 States and the European Union, are represented by a political and a scientific delegation belonging to the Commission and the Scientific Committee, respectively. Annual meetings gather Commission and Scientific Committee's members in order to pursue common conservation objectives inscribed in the Convention text. Subsidiary bodies fuel and provide elements to the annual meetings of the Scientific Committee, which in turn advises the Commission for decision-making. These are for instance the three scientific permanent Working Groups which have annual meetings preceding the Scientific Committee's one: the Working Groups on (1) Ecosystem Monitoring and Management, (2) Statistics, Assessments and Modelling and (3) Fish Stock Assessment. In addition, numerous intersessional activities are undertaken by Expert Groups, Workshops or E-Groups and in turn fuel the annual meetings of the permanent Working Groups. Figure 1.1 illustrates the structure of CCAMLR bodies (grey filled boxes) and subsidiary bodies (white filled boxes) leading to conservation measures (political actions). Scientific research contributes to many CCAMLR activities (boxes with green contours). For instance, scientists may contribute to the conservation process by participating to CCAMLR activities with a CCAMLR Member and submitting papers containing relevant scientific information<sup>1</sup>. The part of scientific research, particularly fundamental research, decreases while rising up the structure leaving space to management and conservation actions' discussions (symbolised in Figure 1.1 B by a graduated green transparency). Metaphorically speaking, the conservation process established within CCAMLR can be seen as a tree, it sources at its roots

---

<sup>1</sup>For instance, the two scientific reports listed at the beginning of this chapter were contributions made under the French delegation at the CCAMLR Spatial Management Workshop held in 2018 (o'Toole et al. [2018]) and at the CCAMLR Ecosystem Monitoring and Management annual meeting of 2019 (Sergi et al. [2019]).

which represent the scientific knowledge, the trunk represents CCAMLR bodies and subsidiary bodies, the branches represent the decisions acted during CAMLR Commission and Scientific Committee's annual meetings and, finally, the tree's canopy represents conservation measures (this is illustrated in Figure 1.1 A). The scientific research at the basis of such process is essential, however, conservation measures grow on the advices endorsed by the two CCAMLR bodies. Consequently, in order to explain how the understanding of alternative iron deep pathways can contribute to the CCAMLR conservation effort, it is important to firstly introduce the approach adopted by CCAMLR and the decisions endorsed by CCAMLR on which our contributions are developed.

### 1.1.2 Origin and ingredients of CCAMLR's conservation strategy

Since 2002, CCAMLR has recognized the World Summit for Sustainable Development's commitment to establish a network of MPAs and added this topic to its agenda (Brooks, 2013). However, MPAs have been defined as a key management tool for CCAMLR long before this. Indeed, as its Convention signed in 1980 reports, conservation measures adopted by CCAMLR shall include the establishment of special areas for protection and scientific study<sup>2</sup>. The first CCAMLR Workshop on MPAs took place in 2005. At this time less than 0.2% of the Convention Areas was under protection, essentially represented by measures undertaken by the Antarctic Treaty System or National programs. Following this workshop, a system of ecologically representative protected areas emerged as a key tool for furthering CCAMLRs objectives. The scope was "to provide a comprehensive, adequate and representative system of MPAs to contribute to the long-term ecological viability of marine systems, to maintain ecological processes and systems, and to protect the Antarctic marine biological diversity at all levels"<sup>3</sup>. In addition, the workshop identified potential candidates for MPAs represented by: (1) Scientific areas considered as reference points for distinguishing between the effects of human activities from natural ecosystem changes and studying ecosystem without interferences and (2) Areas potentially vulnerable to impacts

---

<sup>2</sup>CAMLR Convention (1980), Art. 9, §2(g).

<sup>3</sup>SC-CAMLR-XXIV (2005), §3.54.



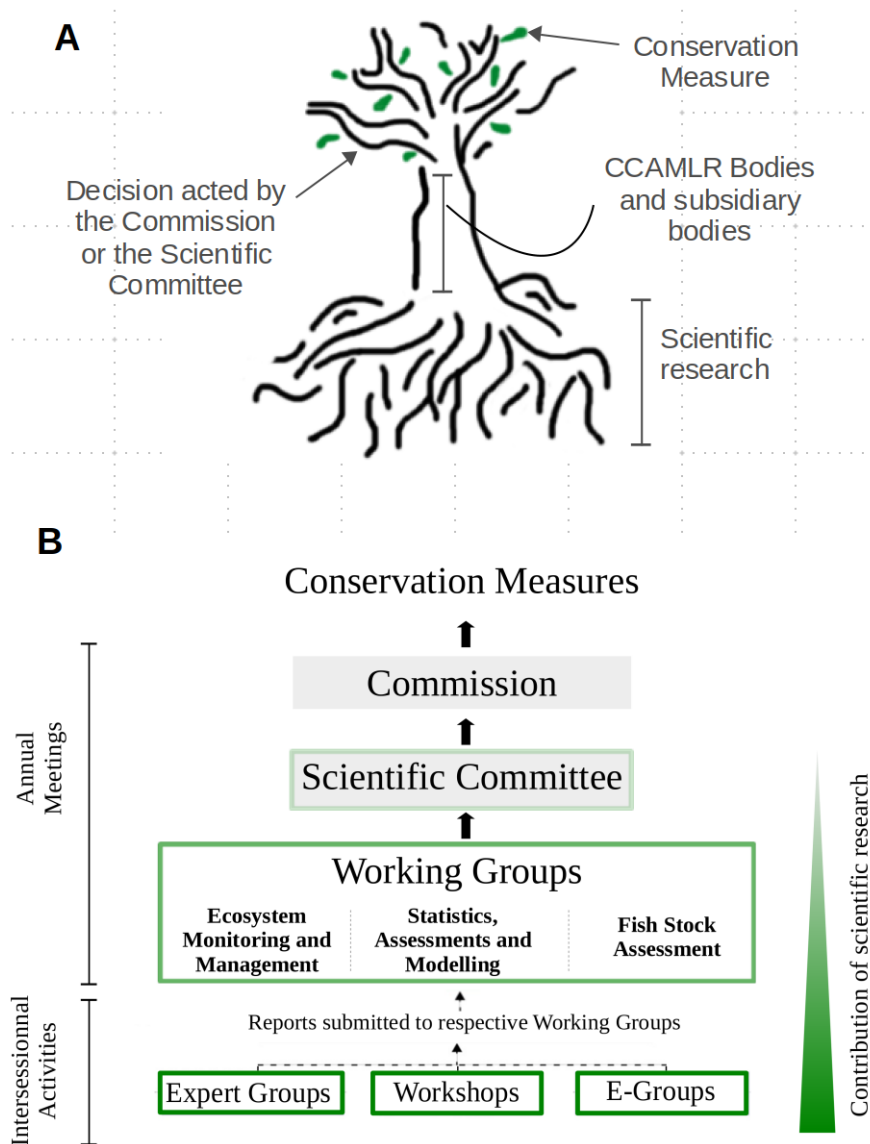


FIGURE 1.1: **Contribution of scientific research in CCAMLR conservation activities.** (A) **Illustration of the conservation process established within CCAMLR.** The conservation process sources at its roots which represent the scientific knowledge, the trunk represents CCAMLR bodies and subsidiary bodies, the branches represent the decisions acted during CAMLR Commission and Scientific Committee’s annual meetings and, finally, the tree’s canopy represents conservation measures. (B) **Structure of CCAMLR and its subsidiary bodies.** From the bottom up, scientist representatives from Member States submit reports to the relevant working groups on interseasonal activities (e.g., workshops, Expert Groups, e-groups). Three permanent Working Groups - WG-SAM (Statistics, Assessments, and Modeling), WG-EMM (Ecosystem Management and Monitoring), and WG-FSA (Fish Stock Assessment) review conclusions provided by these interseasonal activities and additional information. Each October, the Scientific Committee meets to review advice from the three Working Groups and in turn makes advices to the Commission for the decision-making final step. Grey filled boxes represent CCAMLR bodies, the Commission and the Scientific Committee, while white filled boxes represent CCAMLR subsidiary bodies. The decrease of contribution of scientific research, particularly of fundamental research, while rising up the structure which leaves space to management and conservation actions is here represented by green color transparency (from darkest to lightest). Panel B has been adapted from [Sylvester and Brooks \[2020\]](#).

by human activities, in order to mitigate those impacts and/or ensure the sustainability of the rational use of marine living resources. In 2008, the establishment of a representative system of MPAs across the Convention Area became a high priority for the Scientific Committee<sup>4</sup> and the Commission<sup>5</sup> and a legal framework in this aim was adopted in 2011<sup>6</sup>. As evoked previously, to date, two MPAs have been designated in the Convention Area: the South Orkney Islands MPA<sup>7</sup> in the Sub-Antarctic region, close to the Antarctic Peninsula, and the Antarctic MPA in the Ross Sea established in 2016<sup>8</sup>.

Since the first CCAMLR Workshop on MPAs, several key tasks have been identified and endorsed by the Scientific Committee for establishing a representative system of MPAs. These include a bioregionalisation of the Southern Ocean, both at circumpolar scale and at regional scale, and secondly, the identification of areas that might be used to achieve the conservation objectives (representativeness, scientific value, vulnerability)<sup>9</sup>. During the International Polar Year 2007-2009, particular efforts have been undertaken by the scientific community for ameliorating knowledge of these remote regions. In this context, the scientific research program Marine Biodiversity Information Network was launched by the Scientific Committee on Antarctic Research ([SCAR-MarBIN](#)). This vast program aimed to compile, link, integrate and disseminate Antarctic marine biodiversity information for scientific, management, monitoring and conservation purposes. Many studies have been carried out under the catalyst effect of this program [e.g [Griffiths et al., 2011](#); [De Broyer and Danis, 2011](#); [Griffiths, 2010](#); [Grant et al., 2010](#); [Koubbi et al., 2010](#)] including the [Biogeographic Atlas of the Southern Ocean](#) published in 2011 by SCAR. Within CCAMLR, a Southern Ocean Bioregionalisation Workshop was held in 2007 with the primary end-use of the bioregionalisation analysis to assist in achieving the conservation of marine biodiversity, including the development of representative MPAs<sup>10</sup>.

---

<sup>4</sup>SC-CAMLR-XXVII (2008), §3.55.

<sup>5</sup>CCAMLR-XXVII (2008), §7.2.

<sup>6</sup>CCAMLR (2011), Conservation Measure 91-04

<sup>7</sup>CCAMLR (2009), Conservation Measure 91-03.

<sup>8</sup>CCAMLR (2016), Conservation Measure 91-05.

<sup>9</sup>SC-CAMLR-XXIV (2005), §3.64.

<sup>10</sup>SC-CAMLR-XXVI (2007), Annex 9, §8.

A scientific consensus has been reached on the essential role of bioregionalisation analyses in understanding, conserving and managing biodiversity in the marine environment [e.g., [Leathwick et al., 2006](#); [Hogg et al., 2018](#); [Woolley et al., 2020](#)]. Indeed, a major criteria in conservation for designing protected areas, is to select regions representative of biodiversity [[Moilanen et al., 2009](#)]. Ecoregions are often considered as a proxy of biodiversity spatial patterns [[Godet et al., 2020](#); [Dinerstein et al., 2017](#); [Shaw et al., 2014](#)]. In this Thesis, bioregions are regions identified both on abiotic environmental drivers of marine life (mostly in geography, geomorphology and oceanography) and chlorophyll *a* concentration. While ecoregions are based on merged analyses of bioregions and flora and fauna assemblages, considered both by species and functional diversities (trophic web, essential habitats, life history traits, etc.) [[Agostini et al., 2009](#); [Koubbi et al., 2016b,a](#); [Woolley et al., 2020](#)]. Consequently, bioregions are an intermediate step towards the definition of ecoregions, which should be the most complete view of ecosystems. However, when data on species assemblages are not sufficiently available, bioregions are used as proxy of ecoregions [[Godet et al., 2020](#); [Woolley et al., 2020](#)]. Definition of bioregionalisation and ecoregionalisation analyses follow the definitions used for bioregions and ecoregions, respectively.

## 1.2 CCAMLR conservation effort in the ACC region

Following the CCAMLR Bioregionalisation Workshop of 2007, a set of priority areas was pinpointed to be more closely examined for establishing a representative system of protected areas in the Southern Ocean. These were mainly Antarctic adjacent areas and in the ACC region in the areas surrounding islands. Indeed, the first bioregionalisation analyses revealed the open ACC region as a set of meridionally-distributed uniform bioregions punctuated by islands<sup>11</sup>. Rapidly, this view appeared to be largely limited. Indeed, a second CCAMLR Workshop on MPAs held in 2011 highlighted the important gaps in the coverage provided by the “priority areas” for the conservation effort designated during

---

<sup>11</sup>SC-CCAMLR XXVII (2007), Annex 4, Fig. 12.

the Bioregionalisation workshop<sup>12</sup>. Since then, 9 Planning Domains have been identified (represented in Figure 1.3) and have been endorsed by the Scientific Committee<sup>13</sup>. These domains aim to provide a comprehensive coverage of bioregions in the Southern Ocean and should reflect the scale and location of research efforts for bioregionalisation analyses allowing to identify MPAs proposals<sup>14</sup>. Several initiatives have been developed over the regional Planning Domains, here I only summarise the ones that consider the ACC region, hence excluding the area dominated by sea ice.

First of all, a CCAMLR Technical Workshop on Planning Domain 5 (del Cano-Crozet) was held in 2012 aiming at mapping the biodiversity features, determining the biodiversity targets and evaluate pressures in such region. In addition to CCAMLR initiatives, a workshop was held in France in 2016 aiming at gathering the scientific community for an ecoregionalisation process around the Kerguelen and Oceanic zones. The main aim of these ecoregionalisation analyses was to: (1) give orientations for extending the coastal natural reserve of French Southern Lands, (2) evaluate if the process should be extended in the CCAMLR area in the Planning Domains 5 and 6. The results of this workshop provided the scientific basis for the extension of the French National Natural Reserve around Kerguelen and Crozet and highlighted the role of high seas regions that should be considered to cover the whole range of important bird and marine mammal areas for populations living on both islands<sup>15</sup>. Following these steps, the Scientific Committee created an e-group<sup>16</sup> on Indian Ocean sub-Antarctic spatial planning encouraging other Members to “participate in the development of the scientific elements for a proposal for designating future pelagic MPAs in the Indian Ocean sub-Antarctic zone of the Southern Ocean”<sup>17</sup>.

As evoked at the beginning of this Chapter, during my Thesis I contributed to two scientific

---

<sup>12</sup>SC-CAMLR-XXX (2011), Annex 6, §2.19.

<sup>13</sup>SC-CAMLR-XXX (2011), §5.20.

<sup>14</sup>SC-CAMLR-XXX (2011), Annex 6, §6.6.

<sup>15</sup>SC-CAMLR-XXXV (2016), §5.30.

<sup>16</sup>An e-group is a collection of users all having the ability to access and contribute to forum topics as a means of collaborating intersessionally.

<sup>17</sup>SC-CAMLR-XXXV (2016), §5.32.

papers submitted to different CCAMLR's meetings. Both of these works aimed to contribute to CCAMLR conservation effort in the ACC region. In the two following sections I summarise these two works, focusing on my specific contributions. Finally, in the last section of this Chapter, I explain how these contributions fit into the the CCAMLR conservation effort in the ACC and I introduce some future issues for achieving conservation targets in this oceanic region.

### **1.2.1 Predator trophic hotspots in the Indian sector of the subantarctic Southern Ocean: how do they overlap with marine protected areas? CCAMLR-WS-SM-18-07**

Recent scientific campaigns in the Indian sector of the subantarctic Southern Ocean, along with analysis of multi-satellite and bio-logging data, have greatly progressed our understanding of the biophysical mechanisms driving open ocean ecosystems [Koubbi et al., 2016b,a], for different levels of the trophic web ranging from micronutrients, phytoplankton, zooplankton, micronekton and top predator species [Charrassin et al., 2002; Cotté et al., 2007; Bost et al., 2009, 2015]. In particular, predators as pinnipeds and penguins are particularly useful because they disperse over extensive areas, interact with important frontal features, and can carry multiple sensors that record an individual's location and behaviour [Bost et al., 2009]. In the past, several studies have focused on individual megafauna species, and have identified several trophic hotspots in open ocean blooming and post-blooming waters downstream of subantarctic islands. The portion of the trophic hotspots close to the islands have benefited in the recent years of national special protection measures. However, the foraging grounds extending in the international waters have not been considered insofar specifically by conservation plans. The work summarised in this Chapter addressed this issue by revisiting the location of trophic hotspots for subantarctic top predators and assessing their coverage by the network of protected areas existing in this region.

The analyses contained in this work have been achieved within two steps. The first

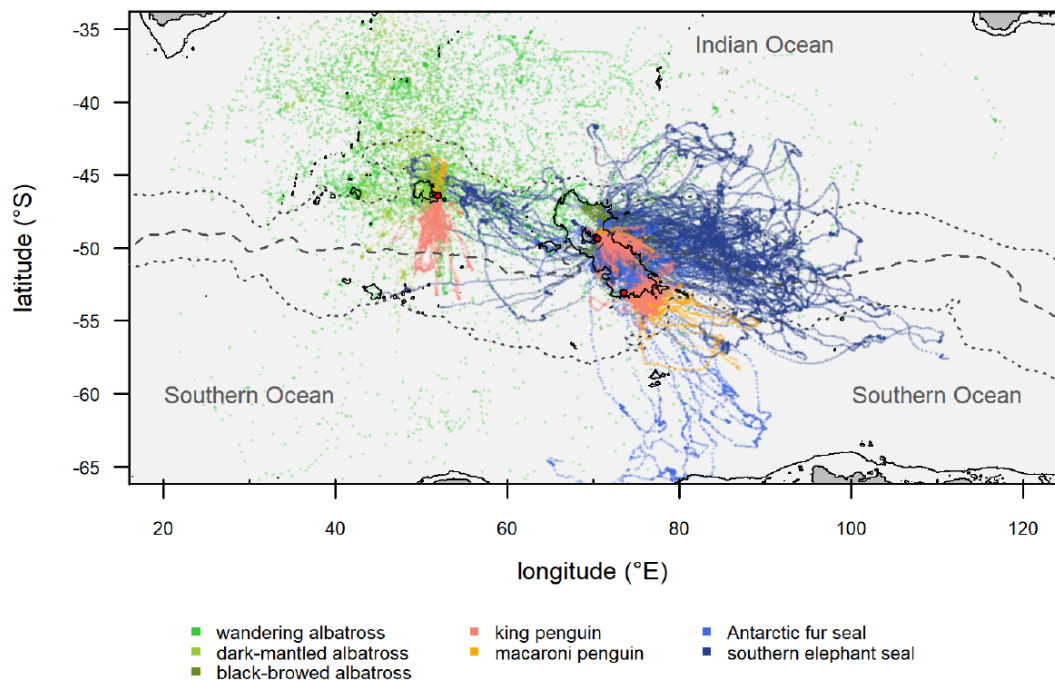


FIGURE 1.2: **Distribution of predator track from the Crozet, Kerguelen and Heard Islands' colonies.** Observed tracks are coloured by species (see key) and include transit (faded) and search locations (bold). Black lines indicate major fronts (from north to south): Subtropical Front (dotted), Polar Front (solid) and Southern Antarctic Circumpolar Current Front (dotted).

step consisted in compiling telemetry tracks of over 800 subantarctic predator tracks collected since 1989 from Antarctic fur seal (*Arctocephalus gazella*), southern elephant seal (*Mirounga leonina*), king penguin (*Aptenodytes patagonicus*), macaroni penguin (*Eudyptes chrysolophus*), wandering albatross (*Diomedea exulans*), black-browed albatross (*Thalassarche melanophris*) and dark-mantled albatross (*Phoebastria fusca*). Data sources included the Centre d'Etudes Biologique de Chizé in France, and Australian institutes; the Australian Antarctic Division and Institute for Marine and Antarctic Studies. At this time, this analysis was, to our knowledge, the most up-to-date and homogeneous map of trophic hotspots for the pelagic top predators studied in this region. The map we have generated shows a network of hotspots connected by the Antarctic Circumpolar Current, with most of the important areas located in the wake of the islands (Figure 1.2). The

second step of this work, which represent my specific contribution to it, aimed to evaluate the distribution of top predators' foraging hotspots contained within the national jurisdictions (French, Australian and South African) and beyond them, in the high seas: within CCAMLR and the Southern Indian Ocean Fishery Agreement (SIOFA), north of it. In order to obtain this, a density plot with the R software package MASS (function `kde2d`) was extracted from the search locations. Next, a k-means classification method (3 clusters) was applied on the density plots for each population. This resulted in 3 classes for each population interpreted as zero density, low density and high density hotspots. Only low and high density hotspots for each population was considered. The distribution of the hotspots in the jurisdictional framework was obtained by calculating the proportion of the foraging hotspots' surface area (without distinction between the higher and lower density classes) included in the French, Australian and South African EEZ and in the CCAMLR and SIOFA areas. Results are shown in Figure 1.3.

Merging our analysis with previous results, we found that the trophic hotspots constitute a network connected by the Antarctic Circumpolar Current (ACC) through a bottom up effect. However, the network of hotspots appeared to be only partly protected in existing MPAs under national jurisdictions. Indeed, even if the national reserves have a large extent, at least 50% of the foraging hotspots areas for half of the populations here analysed were beyond the national jurisdictions and the national MPAs (Figure 1.3). This is the case for several species that are considered threatened (vulnerable or endangered) or near threatened by the IUCN Red list: the endangered dark-mantled albatross from Crozet, the colonies of macaroni penguin on Heard and Kerguelen Islands, the wandering albatross from Crozet and Kerguelen colonies and the black-browed albatross from the Heard colony. In addition of the vulnerability of the species assessed at the present time by IUCN Red List, several studies predict an increasing of the population's vulnerability under the effects of climate change. As an example, the Crozet population of the king penguin - a species presently classified as least concern by IUCN - is expected to decline under climate change forcings [Le Bohec et al., 2008; Bost et al., 2009].



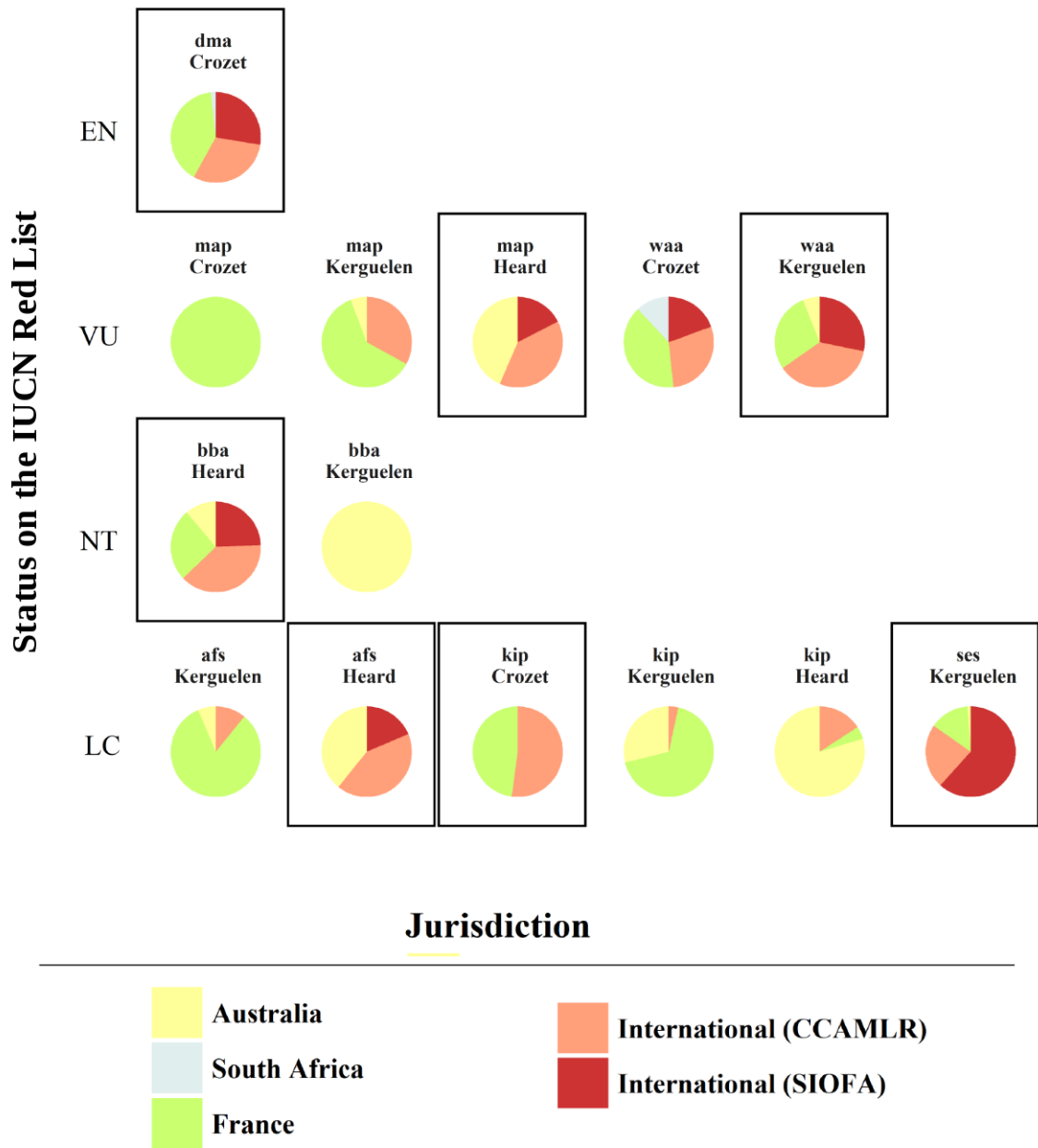


FIGURE 1.3: Proportion of the foraging hotspots' coverage included in each area of competence (different national EEZ, CCAMLR and SIOFA). The distribution of the foraging hotspot defined by a k-means cluster per species and per colony. The 7 species - Antarctic fur seal (afs), black-browed albatross (bba), king penguin (kip), macaroni penguin (map), southern elephant seal (ses), dark-mantled-albatross (dma) and wandering albatross (waa) - are grouped by their category under the IUCN Red List: Endangered (EN), Vulnerable (VU), Near Threatened (NT) and Least Concern (LC).

In conclusion, these analyses showed that adequate protection of a suite of top predators would incorporate high-seas areas, and highlighted that areas both within and beyond the CCAMLR area must be considered in order to afford increased protection. Future perspectives of this work would be to extend this study to the Prince Edward Islands and further West, including other Regional Fisheries Management Organizations than SIOFA as the South East Atlantic Fishery Organization (SEAFO), in order to determine potential pelagic priority areas for designing a future system of subantarctic MPAs.

### **1.2.2 Unfolding the connectivity patterns along the Antarctic Circumpolar Current in the Sub-Antarctic region. CCAMLR-WG-EMM-19-71**

Connectivity progressively emerged as a key component of the relevance and design of conservation measures for the marine environment [e.g. [Salm et al., 2006](#); [Almany et al., 2009](#); [Foley et al., 2010](#)]. Identifying the interconnections between populations, habitats and ecosystems and studying them in the light of climate change becomes a priority [[Andrello et al., 2015](#)]. Generally, these mechanisms are addressed in terms of the ecological connectivity, i.e. the exchange of individuals among geographically separated sub-populations [[Cowen and Sponaugle, 2009](#)]. In this context the analysis of the dynamical connectivity is a key tool to reproduce the Lagrangian dispersal of planktonic organisms [[Lehahn et al., 2018](#)], as fish larvae [e.g. [Christie et al., 2010](#); [Rossi et al., 2014](#)]. In this paper we reviewed the use of satellite-based Lagrangian methods for reproducing connectivity and dispersal patterns induced by the horizontal transport. These are a key tool for identifying ecological important areas in the high seas by taking into account of connectivity due to marine circulation and the biophysical processes associated to it. On the other hand, the identification of dispersal patterns can have larger scopes than ecological studies, because these techniques can map the horizontal pathways to and from any region of interest. Therefore, the second scope of this work was to computing the cross-boundary dispersal patterns of the water within and beyond the EEZs in the sub-Antarctic. These patterns inform on

the incoming and outgoing pathways of tracers transported in the upper layer, like fish larvae and possible pollutants, and may then provide useful information to policymakers.

Horizontal transport has a prominent structuring effect on pelagic ecosystems in the ACC region. The studies contained in Part II of this Thesis provide remarkable examples of the reconstruction of phytoplankton blooms downstream of nutrient sources, such as islands, seamounts and hydrothermal vents, by satellite-based Lagrangian methods. Consequently, the utilisation of such techniques for these applications, which are also reviewed in this scientific report (Sergi et al. [2019]) in order to bring this to the attention of scientists involved in CCAMLR activities, are not detailed in this Thesis' Chapter. On the other hand, the Lagrangian tools used for reproducing phytoplankton biomasses can also provide useful information on higher trophic levels. As an example, in the well-documented island systems, pinnipeds and seabirds are known to intensively forage in the island chlorophyll-a plumes during summer times and, during winter, follow the water masses which supported chlorophyll-a in springtime during their drift along the ACC [Cotté et al., 2015; Bost et al., 2009]. Lagrangian methods are consequently used in ongoing works for disentangling the distribution of top predators after the bloom season (Cotté et al. in prep.; o'Toole et al. in prep.) filling the spatio-temporal lags characterizing the maturation of the pelagic trophic chain. The role of the ACC can be seen as a giant surface conveyor belt of the water masses in the sub-Antarctic ocean. In this regard ecological temporal lags (for instance, the delay between primary and secondary production) are translated into spatial lags (in this example, the distance between a foraging site, the upstream location of a phytoplankton bloom and its nutrient sources, as sketched in Figure 1.4).

Due to the strong ACC, any activity (fishing, seabed mining, marine pollution; but spill-out effects of marine protected areas as well) may have an impact over a large spatial and temporal extent. The second part of the work illustrated the physical connectivity of zones under and beyond national jurisdictions by tracking water masses within the sub-Antarctic EEZs along the ACC. This was achieved by advecting the water masses using altimetry-derived velocities and seeking when they reached the EEZs. The area under

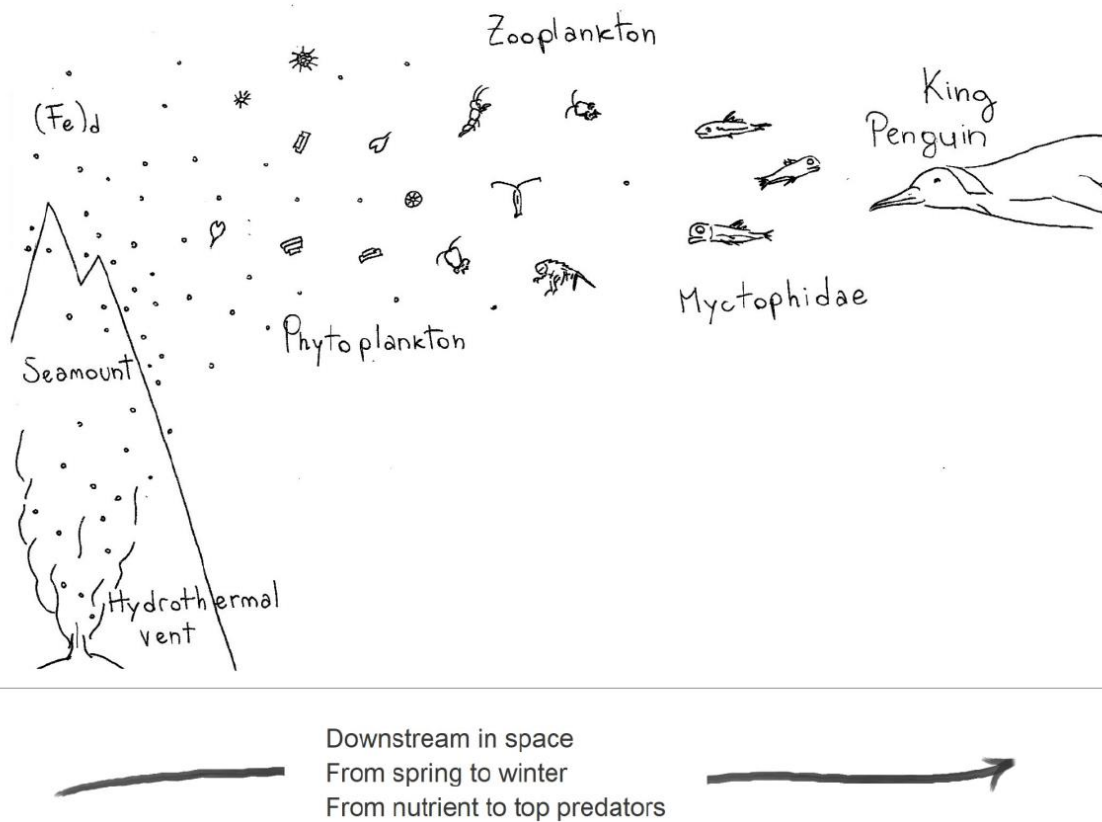


FIGURE 1.4: Schematic representation of the spatial and temporal lags structuring the trophic chain along the ACC. Hydrothermal vents and seamounts are added as iron sources for the primary production.

the influence of the water contained inside the EEZs was similarly identified by advecting water parcels from the EEZs. The aim was to assess the potential spatial and temporal extent of an activity happening within the EEZ of one State and to show how this can affect a huge area extending to the high seas and other national jurisdictions.

Figure 1.5A shows all the water masses that reach an EEZ after a certain period of time since the 1st January, 2015. It represents the area from where an activity or a measure could impact the water under national jurisdiction on a time horizon up to four months. As a complement, Figure 1.5B locates the water masses which were in the last

four months before the 1st January 2015 within the EEZ. It represents the area potentially impacted by an activity or a measure undertaken in the sub-Antarctic EEZs under the same time horizon. The analysis reproduces the distinctive circulation pathways of the region, as the intense branch of the ACC in the Drake Passage. Water masses in the Drake passage reach South Georgia (more than 2000 km away) in less than four months (Figure 1.5A). Indeed the intense jet associate to the Sub-Antarctic Front with typical velocities exceeding 50 cm/s illustrates the amplitude of the eastward surface current in this region [Cunningham and Pavic, 2007; Lenn et al., 2007]. Meanwhile, the analysis highlights some unexpected connections. The divergent pathway upstream of Bouvet Island EEZ indicates an important distant origin of water masses influencing this jurisdictional region (Figure 1.5A). Further analyses over different time period may be undertaken to test the representativeness of this pattern. Although the time period has been chosen arbitrarily, this work could be done for any date and period depending on the question raised. In any case these examples clearly highlight the linkage between the sub-Antarctic EEZ and between the areas under and beyond the national jurisdictions.

Two main outcomes emerge from this review:

1. By drawing attention to the role of seamounts and hydrothermal vents in iron fertilization this review provide examples of processes which challenge the paradigm of the sub-Antarctic as a blue desert with isolated oceanic oases around islands. Indeed, the role of seamounts and hydrothermal vents in influencing phytoplankton distribution and abundance suggests switching to a connected vision of the region, accounting for vertical connectivity - the link between the topographic structures and the water above - as well as horizontal connectivity - due to the strong eastward Antarctic Circumpolar Current-.
2. Methods like Lagrangian tools and observations from high resolution remote sensing appear today as a mature approach for identifying physical connectivity pathways down to resolutions of few tens of kilometres, and could be integrated in ongoing pelagic spatial planning activities for the eastern sub-Antarctic region (e.g. SC-

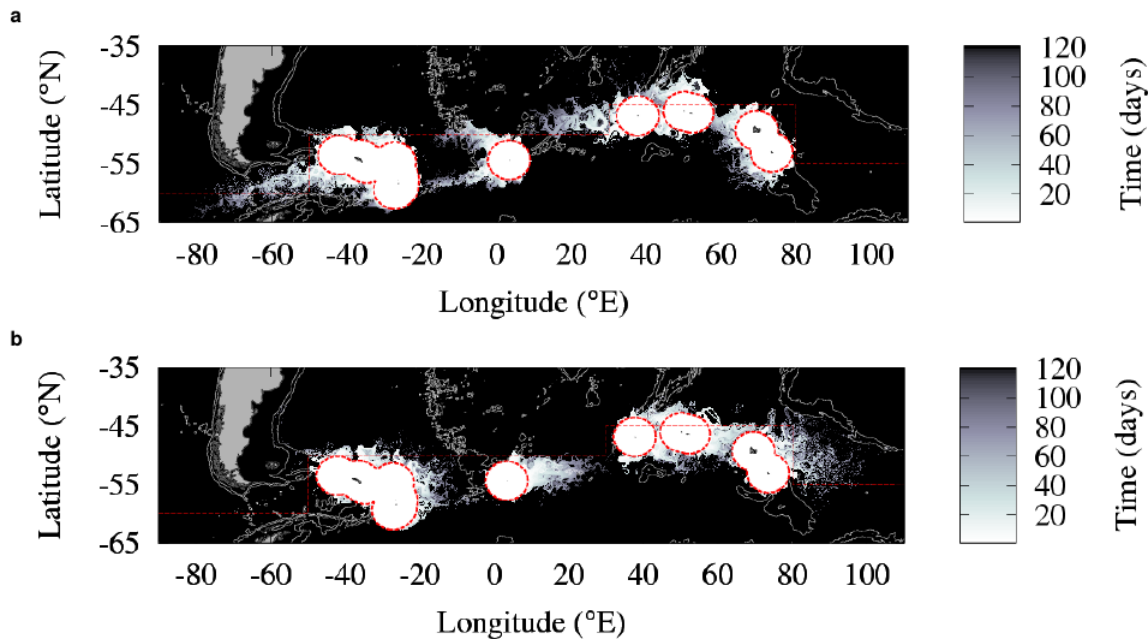


FIGURE 1.5: **Horizontal connectivity between Exclusive Economic Zones in the Southern Ocean.** Distance in time of water masses that will influence the EEZs (a) and of water masses influenced by the EEZs (b). The advection of particle are computed forward in time from the 1st of January, 2015 (a) and back in time since 1st January, 2015 (b). Red dashed lines delimit the Convention Area of CCAMLR and the EEZs (bold lines). Isobaths at 1000 and 3000 m depth are shown in white. As a first approximation, we considered the 200 nautical mile disk around the center of the islands under national jurisdiction as the EEZ.

CAMLR-XXXVII, §6.60 to 6.62).

### 1.2.3 Future issues for achieving conservation targets in the ACC region

The two scientific reports summarised in the previous sections was submitted to CCAMLR meetings with the French scientific delegation, in order to bring their conclusions to the attention of scientists involved in CCAMLR activities. o'Toole et al. [2018], was submitted during the CCAMLR Spatial Management workshop, reinforcing the need to incorporate high-seas areas for adequate protection of a suite of high predators<sup>18</sup>. Following the

<sup>18</sup>SC-CAMLR (2018), Annex 7, §3.74.

scientific information submitted during it, the workshop recommended to the Scientific Committee to consider the creation of an Expert Group in order to continue the development of MPAs Planning Domains 4, 5 and 6, similarly to the process occurring around the Antarctic Peninsula (planning Domain 1)<sup>19</sup>. Indeed, while an e-group mainly represents a technical facility, the adoption of an Expert Group is essential for pursuing the conservation process in order to achieve CCAMLR objectives. The adoption of an Expert Group can be interpreted as the recognition by CCAMLR bodies that sufficient scientific knowledge has been brought to light in order to achieve ecoregionalisation analyses of a given region and propose relevant areas for achieving a representative system of MPAs. The second scientific report described in this Chapter, [Sergi et al. \[2019\]](#), was submitted during the annual CCAMLR meeting of the Working Group on Ecosystem Monitoring and Management in 2019. This aimed to demonstrate that bottom-up processes can have important structuring effects in the pelagic ACC region and that techniques for identifying dynamical pathways of such processes are now mature. [Figure 1.6](#) contextualizes these two scientific contributions to CCAMLR working efforts in the ACC region.

The achievement of a representative system of MPAs within the Convention Area was initially fixed by the Commission for 2012 following international commitments<sup>20</sup>. Despite the multiple workshops made by scientists, independent experts and conservation organizations for pursuing such objective [e.g., see summaries included in [Brooks, 2013](#); [Brooks et al., 2020b](#)], this goal is far from being achieved [[Sylvester and Brooks, 2020](#)]. Several MPAs proposals around Antarctica are currently under negotiation at the CCAMLR, but this is not the case for the ACC region. Indeed, despite the vast scientific knowledge on ecosystems in these regions, the creation of an Expert Group is still considered not required at this stage by the Scientific Committee<sup>21</sup>. Be that as it may, the efficiency

---

<sup>19</sup>SC-CAMLR (2018), Annex 7, §3.81

<sup>20</sup>CCAMLR, XXVIII, §7.19.

<sup>21</sup>SC-CAMLR-XXXVII, §6.61.



of the CCAMLR process in more advanced projects, such as MPAs proposals around Antarctica, may also be questioned. For instance, a recent analysis of the Antarctic Peninsula MPA proposal process, which was initiated in 2011 and is still negotiated at CCAMLR, highlights that science-policy best practices may not be sufficient to drive consensus [Sylvester and Brooks, 2020]. Authors demonstrate the ultimate need for political will in the decision-making underpinning MPAs' designation in the Southern Ocean, similarly to what has already been observed in other study cases within CCAMLR [Sylvester and Brooks, 2020; Liu and Brooks, 2018; Brooks et al., 2020b].

Concerning the ACC region, current scientific effort in pursuing ecoregionalisation works of this zone is mainly undertaken outside of the CCAMLR official framework. For instance, the Expert Workshop for Pelagic Spatial Planning in Eastern subantarctic region held in 2019 in South Africa was not an official CCAMLR Workshop, even if it was organised by researchers of CCAMLR delegations. The working plan emerged from the workshop has not been recognised either as an official CCAMLR position<sup>22</sup>. From a scientific point of view, the analyses contained in this Thesis demonstrate the presence of deep bottom-up forcing pathways in the ACC region far away from islands undetected previously. Such studies will integrate future regionalisation analyses at the basis of conservation process in this region (e.g. scientific working plan of Expert Workshop on Pelagic Spatial Planning for the eastern sub-Antarctic region<sup>22</sup>).

---

<sup>22</sup>This is summarised in SC-CCAMLR-XXXVIII (2019) §6.76.

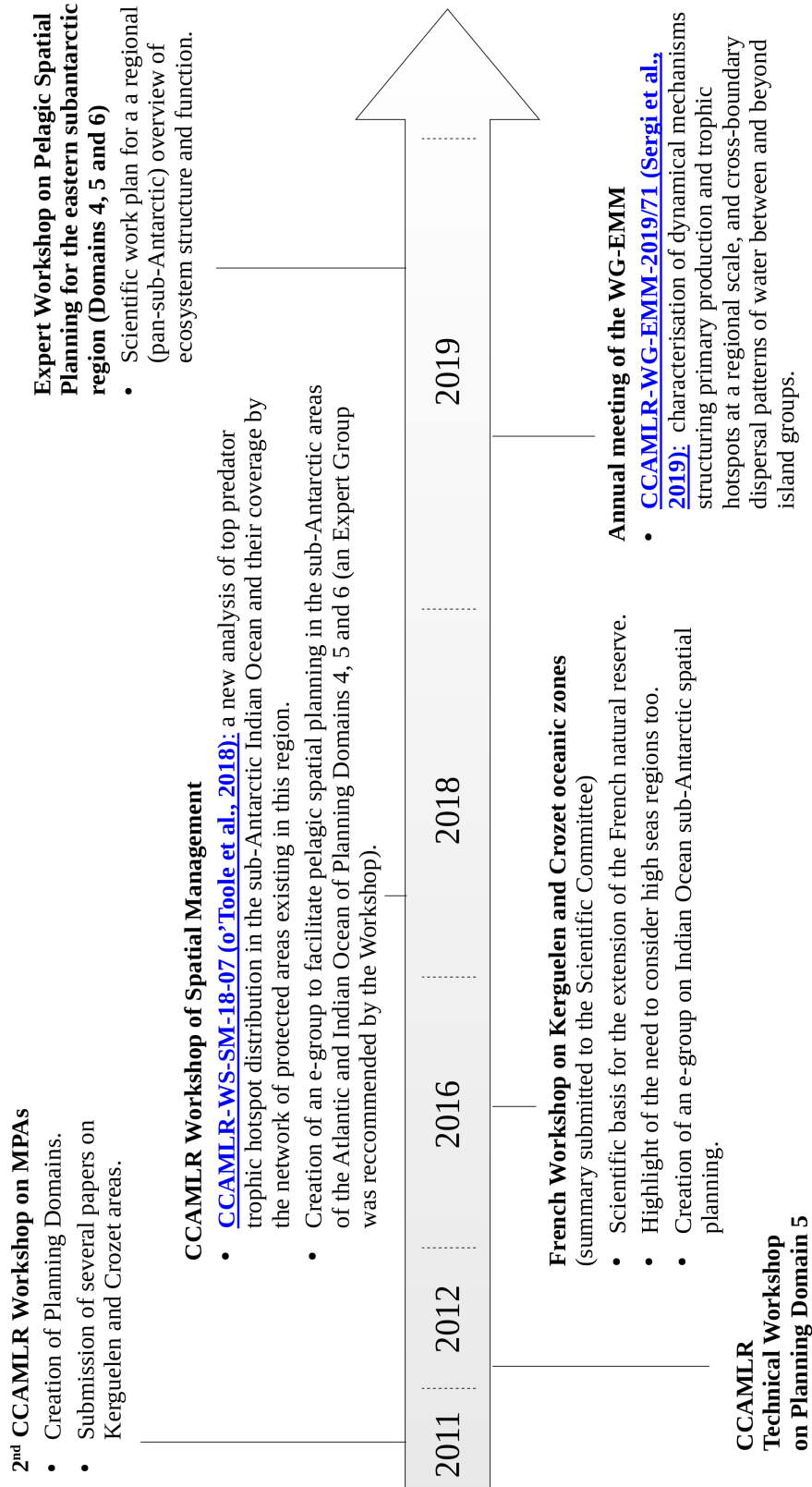


FIGURE 1.6: Timeline of spatial planning effort in the Antarctic Circumpolar Current region and contextualisation of the scientific contribution considered in this thesis (underlined blue text).



## Chapter 2

# “End-to-end” marine ecology: the case of the Saint Paul and Amsterdam Islands Marine Protected Area

This chapter includes contributions published in:

Sergi et al 2021: Océanographie biologique autour des îles de Saint-Paul et Amsterdam; *Chapitre dans un volume de la collection Patrimoines naturels MNHN* (in press)

### 2.1 Context

#### 2.1.1 National Natural Reserves of the French Southern Lands

The French Southern Lands are located between the 37th and 50th parallels south in the Indian sector of the Southern Ocean and are composed of three districts: the Crozet,

Kerguelen and Saint-Paul and Amsterdam Islands (Figure 2.1). These terrestrial and marine environments are recognized as productivity hotspots in an otherwise nutrient-poor ocean, supporting one of the highest concentrations of birds and marine mammals in the world (e.g. world largest population of King Penguins and Yellow-nosed albatrosses<sup>1</sup>). The islands are extremely well-preserved showcases of biological evolution and a unique terrain for scientific research<sup>1</sup>. These ecosystems are currently managed by the National Natural Reserve of the French Southern Lands (thereafter RNN following the French acronym Réserve Naturelle Nationale). The RNN has been created in 2006 covering the whole terrestrial lands of the islands and a part of their territorial seas (12 nautical miles from the coast). Ten years later, the marine part of the RNN has been extended around Crozet's and Kerguelen's archipelagos to protect the marine ecosystems of these oceanic regions and their role in the climate change attenuation<sup>2</sup>. In 2017, in order to support the development and the implementation of a concerted strategy in favour of a network of MPAs in the CAMLR Convention Area, a protection perimeter has been proclaimed beyond the RNN, covering the whole EEZs in the three districts<sup>3,4</sup>. Figure 2.1 shows current perimeters and protections levels of the RNN in the three districts. The universal value of the French Southern Lands has been recognized in 2019 by UNESCO by inscribing them in its World Heritage list<sup>5</sup>.

A close link connects the RNN and the scientific community. This can be summarised along three axes. Firstly, there is a long-term collaboration between the scientific community and the RNN, with about 200 research by year on the research bases at the islands and more than 25 research programs<sup>6</sup>. Secondly, similarly to CCAMLR, the scientific knowledge

---

<sup>1</sup> Refer to the UNESCO's description of the French Austral Lands and Seas, which are now inscribed to the World Heritage List, <https://whc.unesco.org/en/list/1603/>

<sup>2</sup> French Decree no. 2016-1700 of December 12, 2016.

<sup>3</sup> French Ministerial Order, no. 2017-28 of March 31<sup>st</sup>, 2017, Art. 5.

<sup>4</sup> The protection perimeter allows to extend some regulation of the RNN outside of it. For instance, as for the RNN, the advisory council of the French Southern Lands also includes members designated by the Ministry of Ecology when managing activities included in the protection perimeter region. In addition, the regulation of dumping wastes, tourism, sporting and the introduction or the deterioration of flora resources is managed in a similar way within the RNN and the protection perimeter region. Refers to the legal texts for a more comprehensive comparison of the protection levels within and beyond the RNN.

<sup>5</sup> Five sites inscribed on UNESCO's World Heritage List. UNESCO. 5 July 2019

<sup>6</sup> e.g., [https://www.senat.fr/rap/r11-208/r11-208\\_mono.html](https://www.senat.fr/rap/r11-208/r11-208_mono.html)

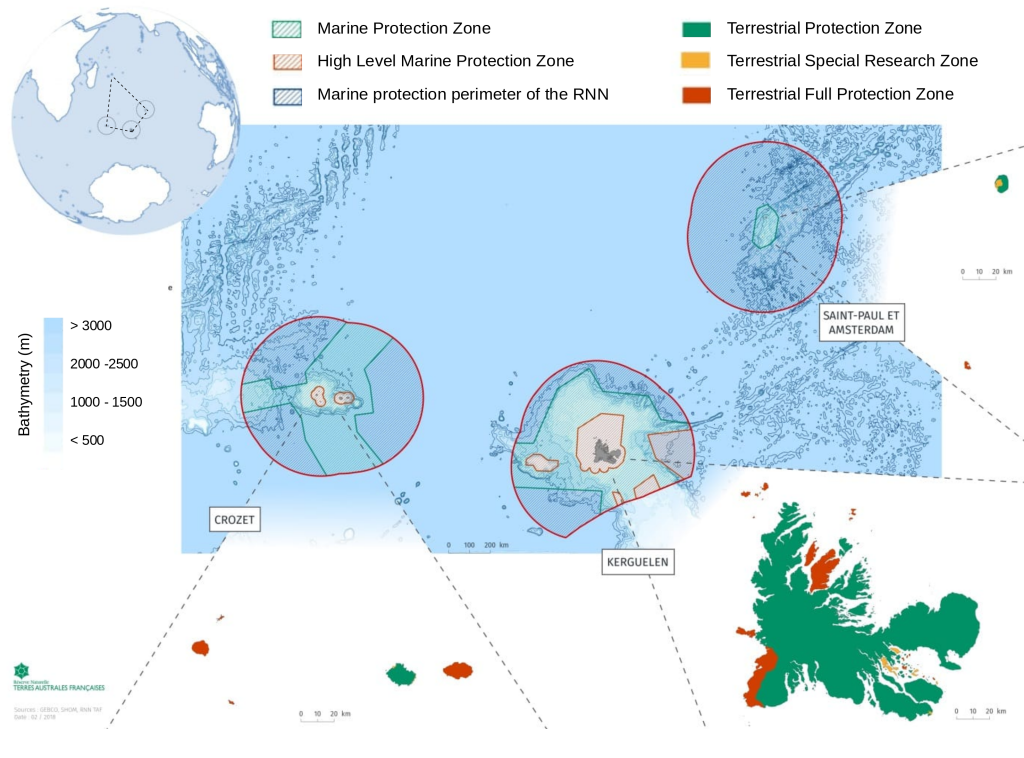


FIGURE 2.1: **National Natural Reserves under the French Southern and Antarctic Lands (RNN)**. Three archipelagos constitute the RNN: these are from the west to the east the Crozet, Kerguelen and Saint-Paul and Amsterdam Islands. Red contours in the ocean region displays the Exclusive Economic Zones Boundaries. In the Marine part of the RNN the dashed green and red zones represent respectively the limit of the RNN and the limits of the high protection zones within it. For other elements refer to the figure’s legend. The figure has been adapted from the Natural National Reserve of French Southern Territories.

is at the basis of the processes leading to the definition of the RNN perimeter. Thirdly, the scientific community largely contribute to the RNN managements plans, both in the definition and achievement of some targets. The example detailed in this thesis belongs to the second type of scientific contribution: the support to the establishment of a MPA. In the French Southern Lands this can be summarised in three steps schematised in Figure 2.2: (1) Characterisation of ecosystems’ patterns and processes; (2) Ecoregionalisation process aiming at characterizing and hierarchizing ecological issues (consultation between the different specialists of the scientific community); (3) Adoption of MPA and specific conservation measures within it (political step). Similarly to the CCAMLR framework (see

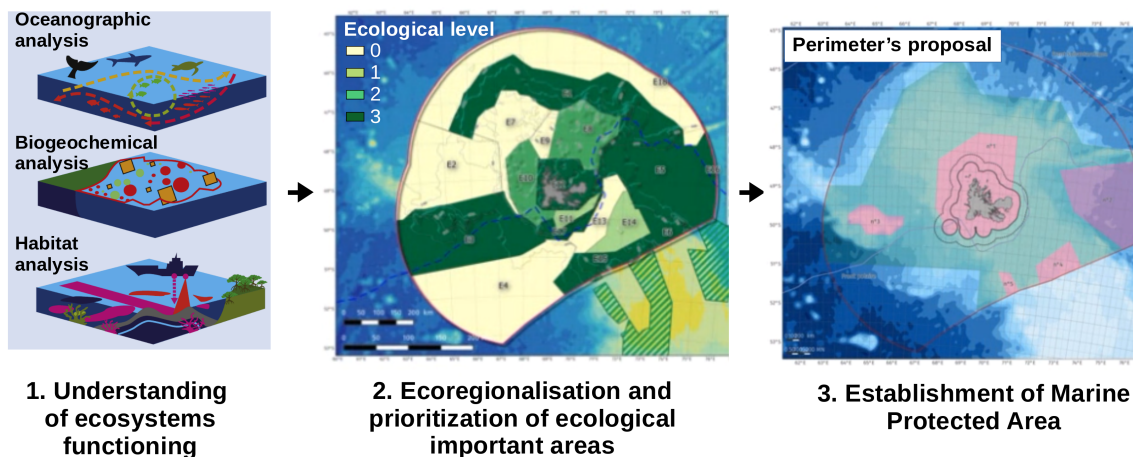


FIGURE 2.2: Schematic representation of steps leading to the establishment of a Marine Protected Area in the French Southern Territories. The definition of a MPA in the TAAF can be summarised in three steps: (1) Characterisation of ecosystems' patterns and processes; (2) Ecogionalisation process aiming at characterizing and hierarchizing ecological issues (concertation between the different specialists of the scientific community); (3) Adoption of MPA and specific conservation measures within it. Scientists are the main actors of steps (1) and (2), while step (3) is under the responsibility of policy maker after the consultation of other relevant actors (e.g. socio-economic actors). This schematic process depicts here the study case of the Kerguelen region: the middle panel represents the hierarchisation of ecological issues in the Kerguelen EEZ after the scientific consultation held in 2016 (colors from light yellow to dark green represent a growing level ecological issues), and the right panel represents the perimeter of the Kerguelen RNN adopted in 2016 (pink regions are areas proposed for high level of protection and green regions the extent of the RNN<sup>2</sup>). Figure sources: (1) Caldow et al. [2015], (2) and (3) Natural National Reserve of French Southern Lands.

Chapter 1), the ecoregionalisation analysis is a cornerstone of the scientific basis supporting conservation measures. As mentioned in the previous Chapter, ecoregionalisation analyses have been conducted in 2016 on the Kerguelen and Crozet oceanic zones allowing to extend the RNN there [Koubbi et al. [2016b,a]; Figure 2.2 B represents the scientific basis of the Kerguelen RNN extension in 2016]. However, the Saint Paul and Amsterdam Islands region has not been considered during such works due to the poor scientific knowledge on its marine habitats and ecosystems, compared to the well-known Crozet and Kerguelen oceanic environments.



### 2.1.2 Conservation process at the Saint Paul and Amsterdam region

Current conservation activities around the Saint Paul and Amsterdam (SPA) region result from a particular political window. Indeed, following the disclosure of the critical status of marine biodiversity in the [IPBES](#) Global Assessment Report on Biodiversity and Ecosystem Services report and in the [IPCC](#) Special Report on the Ocean and Cryosphere in a Changing Climate published both in 2019, the French government has undertaken several engagements in the domain of conservation policy. Among them, the French National Strategy for Protected Areas 2030 launched in January 2021 aims at improving performance and efficiencies of national Protected Areas and more largely increasing international cooperation for biodiversity conservation. The SPA region is considered as a potential contribution to two key measures of such action plan: (1) covering at least 30% of the national terrestrial and marine spaces under French jurisdiction or sovereignty with protected areas and (2) establishing high-level protection for 10% of them. For the SPA region the political engagement consists in: (1) extending the SPA RNN until the EEZ limits and (2) defining high protection level zones within it<sup>7</sup>.

Following this favourable political momentum and in collaboration with the scientific community, the RNN engaged itself in 2020 in gathering and ameliorating knowledge on marine ecosystems in the SPA region (this corresponds to step 1 in the schematic of [Figure 2.2](#)). In 2021, similarly to the approach adopted for the extension of the Kerguelen and Crozet RNN in 2016, a consultation process between the scientific community and the RNN took place in April 2021 and June 2021 in order to achieve the second step of the schema [2.2](#). More precisely, the two workshops had the following specific objectives: (1) characterise, spatialise and prioritise conservation issues in the SPA region and (2) define ecologically important zones, depending on the conservation priority, in the SPA region. Overall, the final scope of the workshop was to construct the scientific basis for the definition of the high protection zones in the future RNN perimeter.

---

<sup>7</sup>Ministry of the Ecological Transition (2021), [Action plan 2021-2023 for the National Strategy For Protected Areas 2030](#), Measures 1 and 2

The workshops assembled researchers from multiple laboratories<sup>8</sup> in order to gather all available information on the marine ecosystems of the study region (e.g. distribution of habitats or communities). The description of the methodologies adopted is largely beyond the scope of this thesis. Briefly, the aim was to identify ecological priority regions for the pelagic and benthic compartments following three criteria identified in the literature: Comprehensiveness, Adequacy and Representativeness.

Concerning the pelagic compartment, the SPA region is known to host several seabirds and marine mammal colonies, including globally threatened species of seabirds showing alarming population trends [Heerah et al., 2019; Delord et al., 2021]. In addition, this oceanic region is known to be targeted by numerous migratory marine species [Samaran et al., 2013]. However, the pelagic productivity of this region and the bio-physical processes at its basis have been little investigated in the literature and the definition of oceanic bioregions is a key step of the ecoregionalisation process [e.g., Koubbi et al., 2016b,a].

This Chapter addresses this pelagic knowledge gap in order to contribute to the scientific basis for the extension of the RNN in the SPA region. More precisely, Section 2.2 analyses the spatio-temporal dynamics of the phytoplankton biomass in the SPA region, examines the physical drivers of such dynamics and finally makes a regionalisation of the pelagic environment based on the identified bio-physical drivers. The contribution of such bio-physical analyses to the consulting process with the RNN and the scientific community is reported in the last section of this Chapter (Section 2.3).

## 2.2 Analysis of bottom-up controls at the basis of the pelagic food-web

The SPA region lies in the South Indian Ocean. In terms of primary production, this is a transition environment between the Antarctic Circumpolar Current and the Agulhas

---

<sup>8</sup>MNHN, ENSTA Bretagne, CEBC, LOCEAN (with which I was affiliated during the two workshops), Sorbonne University, Ifremer, IRD and UBFC

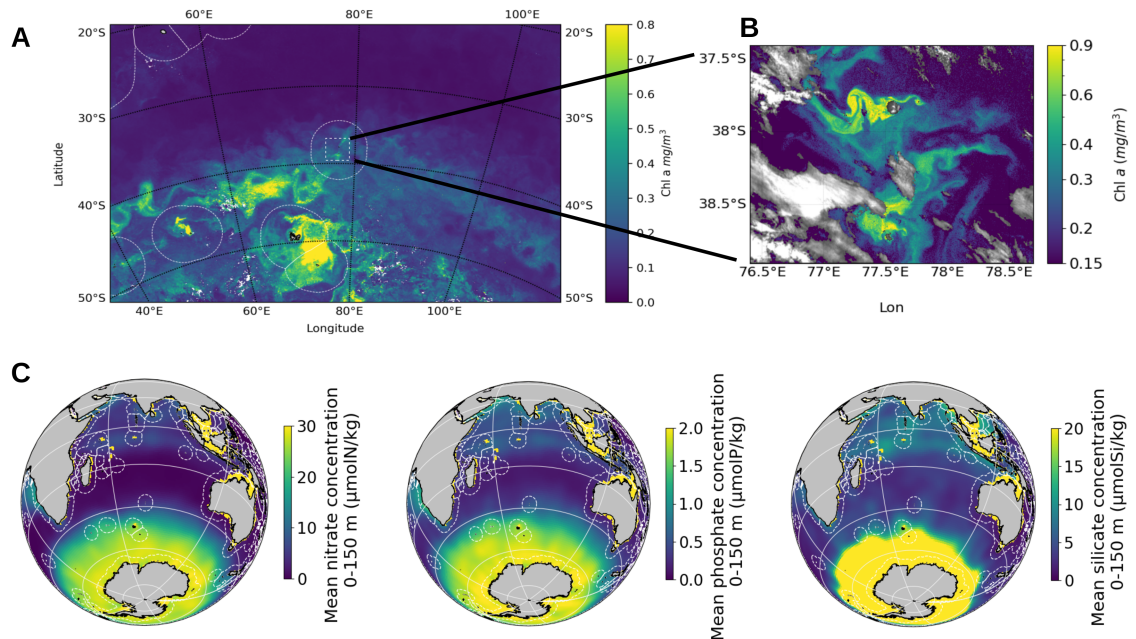


**FIGURE 2.3: Phytoplankton and nutrient distribution in the South Indian Ocean.** (A, B) Spatial distribution of Chlorophyll *a* concentration in the South Indian Ocean in December 2000 (A) and close to the Saint-Paul Islands on the March 13<sup>th</sup>, 2020 (B). (C) Climatological distribution of Nitrate, Phosphate and Silicate concentrations averaged between 0 and 150 m in the South Indian Ocean. Exclusive Economic Zones are shown in white (A, B). White and grey regions in panels A and C shows data absence due to the clouds coverage. Data sources: (A) Monthly mean data from de GlobColour product produced by ACRI-ST and distributed by CMEMS (product id: OCEANCOLOUR\_GLO\_CHL\_L4\_REP\_OBSERVATIONS\_009\_082). (B) Chlorophyll *a* concentration represents Level2 data of European Spatial Agency's program Sentinel 3A distributed by the Copernicus Online Data Access service of the European Organisation for the Exploitation of Meteorological Satellites. Cloud coverage has been estimated by Level1 data of the Sentinel 3A service distributed by the NASA Ocean Biology Processing Group. (C) World Ocean Atlas 2018.

Return Current regions in the South, rich in phytoplankton biomass, and the oligotrophic Subtropical Indian Ocean Gyre in the North, a nutrient and phytoplankton depleted region [Visser et al., 2015; Gandhi et al., 2012; Jasmine et al., 2009]. This dominant North-South gradient in phytoplankton and surface nutrient concentrations is evident in large scale maps (Figure 2.3 A and C). In the SPA EEZ, the annual maximum Chlorophyll *a* concentration (Chl-*a*) is about 0.45 mg/m<sup>3</sup> south of 38 °S and 0.15 mg/m<sup>3</sup> north of it, with a smooth latitudinal gradient. In addition, a large scale zonal gradient in phytoplankton

biomass decreases from west to east, due to nutrient transport by large scale circulation downstream of the African continental shelf [Machu et al., 2005]. The oceanographic cruise Galathea 3 documented this double gradient in nutrient and primary production across the South Indian Ocean in spring 2006. Factors of about 100 and 5 in inorganic nitrogen and phosphorus concentrations' respectively, have been measured between the high productive waters of the South-Western sector ( $> 35^{\circ}\text{S}$  et  $< 80^{\circ}\text{E}$ ) and the ones in the oligotrophic sector in the North-Eastern region [Visser et al., 2015]. The transition between these two systems, identified close to the French Islands ( $37^{\circ}\text{S}$ ;  $73^{\circ}\text{E}$ ), was characterised by a dial primary production of about  $180 \text{ mgC}\cdot\text{m}^{-2}\cdot\text{d}^{-1}$  [Visser et al., 2015]. The SPA region, considered here at the EEZ scale, stands out from the large scale gradients with a positive anomaly in phytoplankton biomass close to the islands. A high resolution satellite image shows an episodical augmentation of the phytoplankton biomass around the SPA islands (Figure 2.3C). This phenomenon, referred to the island mass effect, consists in a phytoplankton growth stimulated by multiple mechanisms allowing to intensify the nutrient input in the surface ocean associated to the presence of an island [Doty and Oguri, 1956]. Contrary to the Southern Ocean islands, as the Kerguelen and Crozet Islands, the island mass effect associated to the SPA Islands is spatially limited and less intense (a comparison can be observed in Figure 2.3A during December 2000).

### **2.2.1 Spatial and seasonal variability modes of phytoplankton biomass in the SPA region**

The seasonal variability of the phytoplankton biomass averaged over the SPA region is very low. It peaks between November and December ( $0.20 \pm 0.03 \text{ mg}/\text{m}^3$ , followed by a lower local maximum in autumn) and falls in march (with  $0.15 \pm 0.05 \text{ mg}/\text{m}^3$ ). The spatial and temporal variability of the climatological (1997-2018) seasonal Chl *a* cycle is analysed with an Empirical Orthogonal Function analysis (EOF, also known as Principal Component Analysis, depending on the field of application). This method aims at identifying coherent spatial and temporal variability, by analysing the distribution of the variance of a subset

of time series spatially distributed, and is largely used in oceanography [e.g. Talley et al., 2011]. The analysis translates the time series  $\psi_m(t)$  associated to the spatial point  $m$  as the sum of orthogonal spatial functions  $\phi_i$ , as following:

$$\psi_m(t) = \sum_{i=1}^M (a_i(t)\phi_i(m)) \quad (1)$$

where  $m \in [1; M]$ , with  $M$  the total number of spatial points and each spatial point  $m$  is defined by two coordinates  $(x,y)$ .  $a_i(t)$  represent the temporal amplitudes of the  $\phi_i(m)$  spatial modes. Because the modes are independent of each other, the modes can be interpreted individually in terms of physical process.

Here, the EOF analysis, computed using the `eofs.xarray` function from Python, is performed over the climatological seasonal time series associated to each point of the SPA region. For each point of the space, the seasonal climatologies of Chl  $a$  are computed from the monthly mean data measured by satellite between 1997 and 2018 (GlobColour product produced by ACRI-ST and distributed by CMEMS<sup>9</sup>).

The two first EOFs identified by the analysis, thereafter referred to as spatial variability modes, together represent more than 95% of the internal variability of the dataset. The first spatial variability mode reproduces 67% of the internal inertia and represents a North-South dipole, characterised by negative anomalies North of 38 °S and positive anomalies South of it (Figure 2.4A). The second spatial variability mode reproduces 28% of the internal inertia and represents an intensification of the Chl- $a$  concentration on the oceanic shelf around the two islands (about 2000 m depth) compared to the rest of the SPA region (Figure 2.4B). This second variability mode can be interpreted as the island mass effect associated to Amsterdam and Saint-Paul Islands. The seasonal variability of the two modes, represented by the coefficients contained in  $a_1(t)$  and  $a_2(t)$ , is reproduced in Figure 2.4C (the y-axis is normalized between the minima and the maxima of each time series  $a_i(t)$ ). As showed in Figure 2.4C, the two spatial modes display different seasonal

<sup>9</sup>product id: OCEANCOLOUR\_GLO\_CHL\_L4\_REP\_OBSERVATIONS\_009\_082

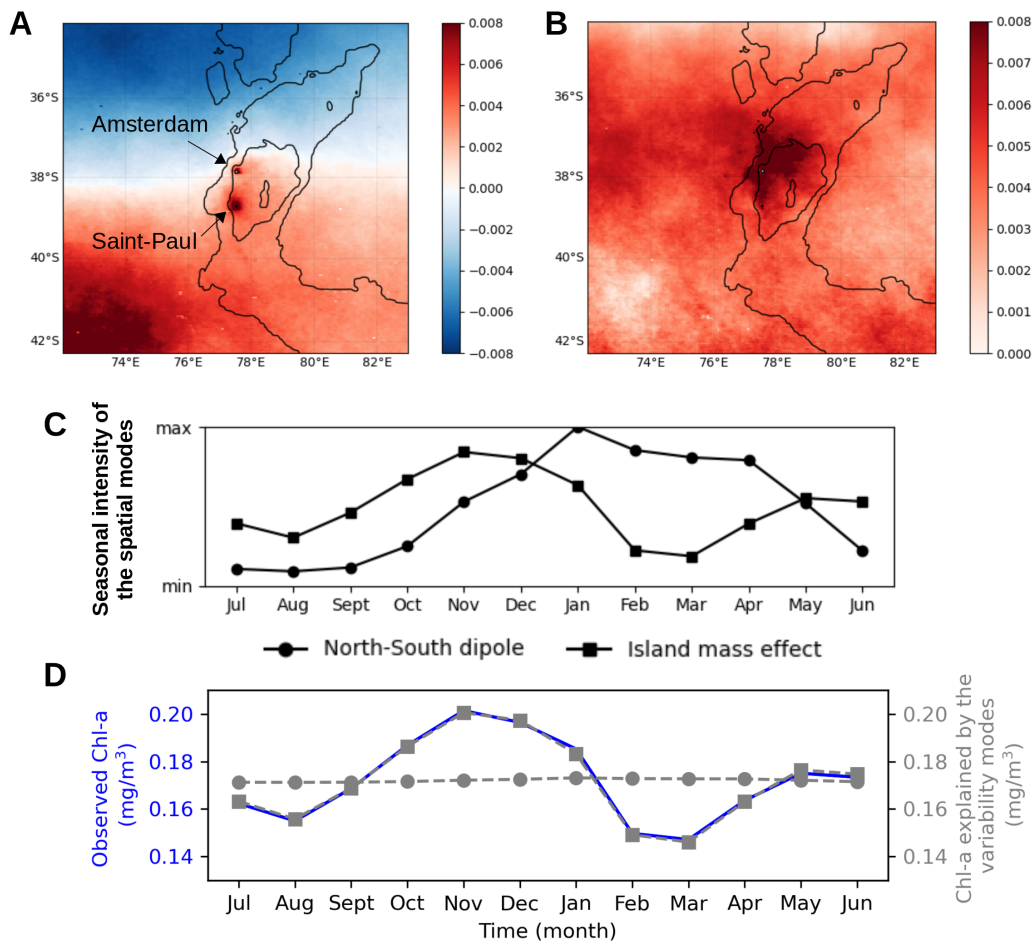


FIGURE 2.4: **Variability modes of the seasonal phytoplankton biomass in the SPA region.** (A-B) Spatial distribution of the two first EOFs identified: North South dipole (A) and island mass effect (B). (C-D) Seasonal variability of the spatial modes in terms of their amplitude (C) and in terms of their contribution to the Chl-*a* concentration in the SPA region (D). Chl-*a* contribution of the spatial modes (grey lines) are compared to the Chl-*a* averaged over the whole SPA (blue line, D). Lines with circle and square symbols represent the North-South dipole and the island mass effect, respectively.

variations. The amplitude of the North-South dipole peaks in January, meaning that at this time of the year the contrast between the South and the North regions is maximal. By contrast, the second variability mode, representing the island mass effect, peaks in November and May, meaning that the contrast between the islands shelf (about 2000 m deep) and the rest of the region is higher during these two periods. This seasonal cycle

is typical of the island mass effect in the Southern Ocean. Indeed, it is characterised by a first bloom, due to the springtime stratification, followed by a minor bloom in late summer, due to the regeneration of organic material [Borrione and Schlitzer, 2013].

The EOF analysis separates the spatial and temporal patterns of the mean-removed data. Consequently the contribution of each mode  $i$ , in terms of chlorophyll  $a$  concentration to the dataset, named  $Chl_{mode.i}(t)$ , can be reconstructed as following:

$$Chl_{mode.i}(t) = \left[ \frac{1}{M} \sum_{m=1}^M \phi_i(m) \right] a_i(t) + \frac{1}{M} \frac{1}{T} \sum_{m=1}^M \sum_{t=1}^T Chla(m, t) \quad (2)$$

Where  $T=12$  representing the 12 months.  $Chl_{NS\_Dipole}$  and  $Chl_{Island\_mass\_effect}$  are largely uneven (Figure 2.4D). Indeed, the seasonal variability of the island mass effect alone explains the variability of the Chl- $a$  averaged over the SPA region all along the year (respectively grey line with square symbols and blue line in Figure 2.4D). By contrast, the contribution of the North-South dipole to the Chl- $a$  of the SPA region does not display seasonal variations (grey line with circle symbols in 2.4 D). Indeed, when spatially averaged over the SPA region, the opposite anomalies of the South and North regions offset each other and clear the signal observed in Figure 2.4C from its seasonal variability.

### 2.2.2 Modulation of the phytoplankton biomass by physical drivers

The phytoplankton biomass observed in satellite images needs a consequent supply of macronutrients, notably nitrates, phosphates and silicates, which limits the SPA region [Gouretski and Koltermann, 2004; Shiozaki et al., 2014] into the euphotic layer. Due to the weak horizontal currents in the region and its distance from continents, two processes are potentially able to penetrate into the nutricline and surface deep nutrients: the entrainment associated to the winter deepening of the mixed layer depth and the turbulent mixing generated by internal waves. These two mechanisms are described in the following paragraphs.



Spatial and temporal dynamics of the mixed layer depth are a potential primary driver of phytoplankton biomass variations observed in the SPA region [Tagliabue et al., 2014]. Nutrient entrainment in the euphotic layer from the deep ocean is stimulated by winter mixing due to the wind stress and the seasonal decrease of the solar heat flux. Similarly to the phytoplankton biomass, the winter mixing layer depth shows an intense latitudinal gradient in the SPA region, with important differences between the sectors North and South of 38 °. Figure 2.5 illustrates this contrast in reanalysis data, however this contrast is also visible when looking at *in situ* estimations of the mixed layer depth only (regional analysis of the database published in [Holte et al., 2017], figure not shown). In August, when the mixed layer is the deepest regardless the study region, it penetrates deeper than 300 m in the South, while it doesn't reach the 100 m depth horizon in the North sector (Figure 2.5A). This contrast can be explained by the intense westerlies at high latitudes (40-50 ° S) and a higher solar heat flux at low latitudes. Indeed, in the North of the SPA region, the association of the very low winter mixing and an all year around important heat flux stratifies the water column. This induces a low variability of the phytoplankton biomass and a low phytoplankton maximum during the winter mixing [Morel et al., 2010; Signorini et al., 2015].

Dynamics of internal waves are the second physical mechanism susceptible to explain the phytoplankton biomass contrasts observed in the SPA region. Indeed, the dissipation of energy due to the interaction of internal waves with rough topographies, may enhance diapycnal mixing and subsequent nutrient transfer from deep waters to the surface ocean [Melet et al., 2014]. Due to the weak circulation of the SPA region, the dissipation of energy from tidal waves is possibly dominant compared to the energy generated by lee waves [Melet et al., 2014; Garrett and Kunze, 2007]. This second hypothesis is corroborated by a recent cartography of turbulence produced by internal tides [Lavergne et al., 2020]. In the region close to the SPA Islands, the analysis identifies a hotspot of internal waves breaking (generated turbulence ranging between  $10^{-9}$  and  $10^{-8}$  W/kg) over the whole water column, from bottom to surface ocean (Figure 2.5B). This feature is unique in a region larger than 1500 km around the islands (turbulence is between one and two order

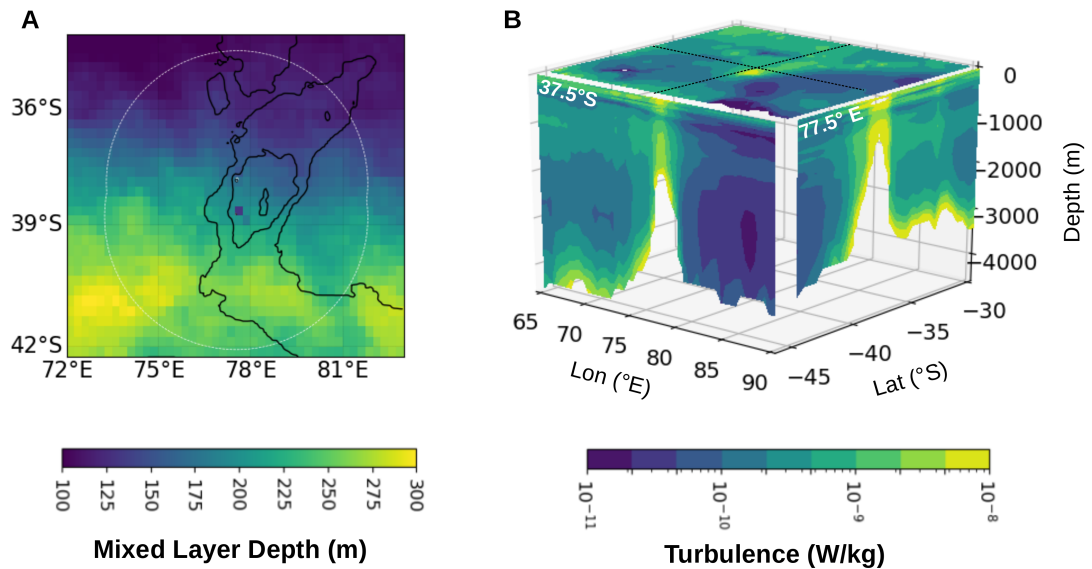


FIGURE 2.5: **Spatial distribution of physical drivers of deep nutrient into the SPA euphotic layer: winter mixing and turbulent mixing induced by internal waves.** (A) Climatological winter mixing depth, computed as the annual monthly-mean maximum of the climatological (2003-2018) mixed layer depth. (B) Mean turbulence produced by internal tidal waves and represented in three sections: close to the surface (185 m; top layer), on the zonal section at 37.5 °S (left layer) and on the meridian section at 77.5 °E (right layer). The mixed layer depth is estimated by the monthly data of the GLORYS12V1 reanalysis produced by Mercator Ocean and distributed by CMEMS (product id: GLOBAL\_REANALYSIS\_PHY\_001\_030). The turbulence generated by internal waves is reproduced from [Lavergne et al. \[2020\]](#)

of magnitude less intense elsewhere, 2.5B). In the Mid-Atlantic Ridge internal tides have already been observed to drive intense diapycnal nitrate fluxes to the euphotic layer and subsequent Chl-*a* enhancements [[Tuerena et al., 2019](#)]. Consequently, the intense tidally induced diapycnal mixing localised around SPA islands may induce a potential important diffusive transfer of nitrates and phosphates to the euphotic layer and drives the island mass effect observed in Ocean Color maps. However, the seasonal modulation of the island mass effect observed in Figure 2.4C may be linked to other forcing, such as the mixing and stratification processes linked to air-sea interactions.

According to World Ocean Atlas climatologies, maximal amounts of nitrates and phosphates are found in the study region between 1 and 2 kilometres deep [[Gouretski and](#)

Koltermann, 2004]. In order to further investigate our hypothesis, further *in situ* measurements of nutrient concentrations are needed to identify the nutricline depth and estimate nutrient fluxes induced respectively from vertical entrainment, due to winter mixing, and from dypicnal mixing, due to internal tides [Rigby et al., 2020; Tuerena et al., 2019].

### 2.2.3 Identification of pelagic bioregions

Environmental regions with similar characteristics but distinct from each other can be identified with a clustering method as the K-means analysis [Macqueen, 1967]. This clustering analysis has already been successfully applied for identifying bioregions at both large scales, such as the whole Southern Ocean [Ardyna et al., 2017; D’Ortenzio et al., 2012], or regional scales [D’Ortenzio, 2009; Mayot et al., 2016; Lacour et al., 2015]. Here, I perform the K-means analysis over the climatological (2000-2015) annual mean Chl-*a* data and three parameters showing important spatial contrast in the study region and identified for their potential effect on phytoplankton distribution: (1) the bathymetry, (2) the mean turbulence produced by internal tide waves cumulated over the water column; and (3) the winter mixing intensity, computed as the annual monthly-mean maximum of the climatological (2000-2015) mixed layer depth as previously computed.

The clustering method delimits and characterises the three regions previously described: two regions in the deeper oceanic sector, a subtropical one North of 38 °S (region A) and a subantarctic one South of this limit (region B), and a region over the island shelf dominated by the island mass effect (region C; Figure 2.6A). The three regions display different characteristics in the four variables used for the clustering (Figure 2.6B). For instance, during the winter mixing, the mixing layer depth is in average 70 et 52 % deeper in the subantarctic zone than in the subtropical and shelf zones, respectively. The shelf region (region C) is distinguished by its intense energy dissipation induced by internal tides ( $8.11 \pm 4.9 \cdot 10^{-3} \text{ W/m}^2$  compared to the  $1.5 \pm 1.1 \cdot 10^{-3}$  and  $1.8 \pm 1.1 \cdot 10^{-3} \text{ W/m}^2$  estimated in the subantarctic and subtropical bioregions, respectively) and

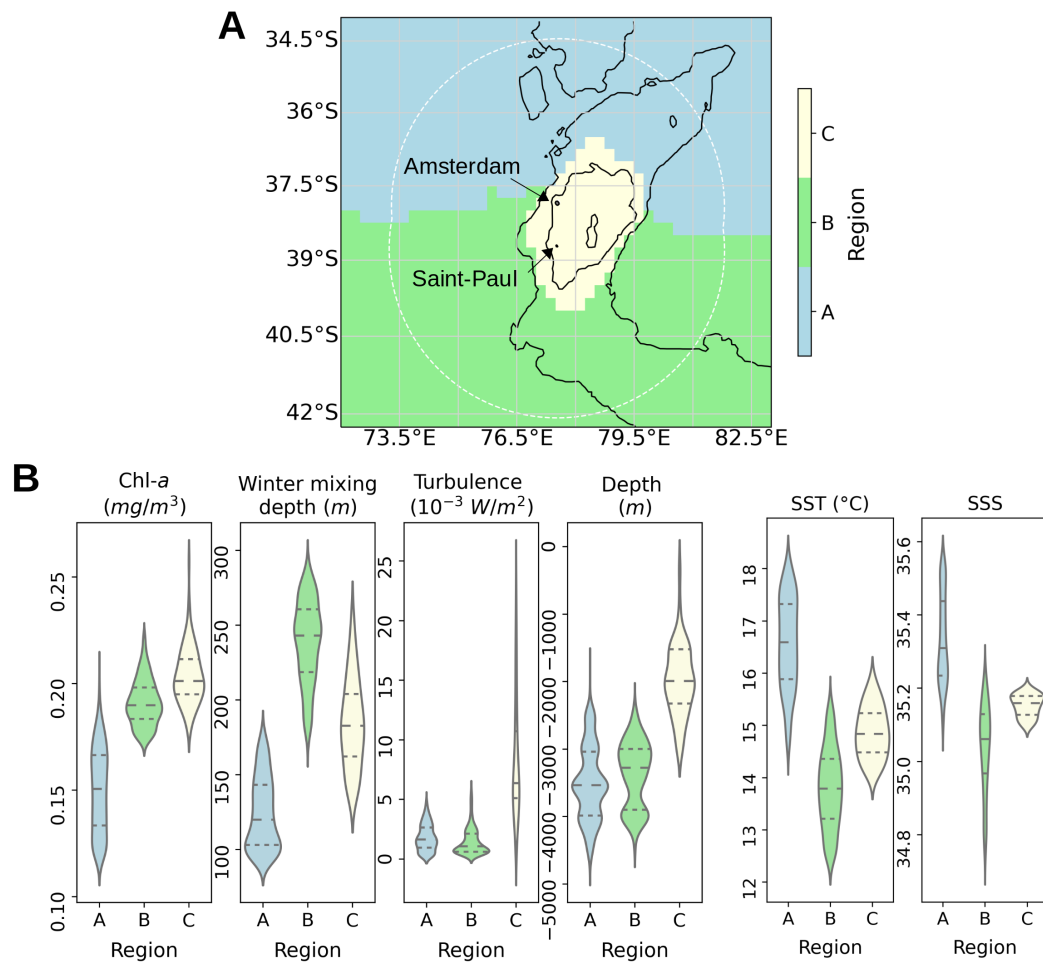


**FIGURE 2.6: Pelagic bioregionalisation of the Saint-Paul and Amsterdam oceanic environment under the physical drivers of phytoplankton biomass. (A, B) Spatial distribution of pelagic bioregions (A) and distribution of annual mean Chl-*a*, annual maximal mixed layer depth, annual mean turbulence, ocean depth, mean sea surface temperature and mean surface salinity in the pelagic bioregions (B). Surface temperature and salinity data have not been used for the clustering but has been projected in identified bioregions. In order to give the same weight to all the variables, the extent of each variable has been normalized by deducing the spatial minimum and dividing it by the spatial maximum.**

a slightly higher distribution of Chl-*a* values (Figure 2.6B). Surface temperature<sup>10</sup> and

<sup>10</sup>Mean sea surface temperature computed from monthly data between 2000-2015 from the OSTIA product, produced by the UK Met Office and distributed by CMEMS, product id: SST\_GLO\_SST\_L4\_NRT\_OBSERVATIONS\_010\_011

salinity<sup>11</sup> are projected in the regions identified by the clustering (Figure 2.6B) due to their possible important role in structuring the pelagic ecosystems. However, clustering results including or excluding these two variables do not change. This is due to the diffuse gradient of these physical properties.

In conclusion, the SPA region is characterised by two pelagic environment with contrasted phytoplankton biomass. One of them is a subtropical environment, with very low winter mixing (<100 m deep) and phytoplankton biomass (mean annual Chl-*a* maximum of about 0.2 mg/m<sup>3</sup>). The other one is subantarctic one, dominated by the intense westerlies winds mixing water masses (maximum winter mixing up to 300 m depth) and surfacing nutrients which in turn sustains the phytoplankton growth (mean annual Chl-*a* maximum of about 0.45 mg/m<sup>3</sup>). The island mass effect dominates such large scale variations, possibly due to the intense vertical mixing induced by internal waves. The SPA marine environment differs from Kerguelen and Crozet subantarctic islands by its weak circulation (values) and different availabilities in macronutrients. Indeed, Southern Ocean Islands are in High Nutrient (iron-depleted) Low Chlorophyll environment, whereas the SPA region is closer to the oligotrophic environment, depleted in both macro and micro-nutriments, and strongly limited in nitrates [Boyd et al., 2000; Blain et al., 2001; Shiozaki et al., 2014]. Despite its small size, the island mass effect associated to SPA is likely a critical contribution of phytoplankton biomass for pelagic ecosystems. This would concern the numerous seabirds and marine mammal colonies breeding at these islands [Heerah et al., 2019] as well as the potential pelagic visitors (cetaceans) which seasonally feed on these waters during their migrations [Samaran et al., 2013].

---

<sup>11</sup>Mean surface salinity obtained from the World Ocean Atlas Climatology 2006-2015

## 2.3 Integration of the pelagic analysis in the consultation process with the scientific community and the RNN

The contrast between the South and the North sectors identified in our analyses corresponds to boundaries between two biogeochemical provinces, the South subtropical convergence in the North and the Subantarctic water ring in the South, defined by the global analyses of Longhurst [2010] and Reygondeau et al. [2013]. The island shelf region does not appear on these global analyses, due to their large scale, but it is visible in our high resolution study. Consequently, the pelagic bioregions identified above have been retained as a comprehensive description of the pelagic environment. The distribution of several pelagic compartments appears to follow bioregions identified in the previous section: significant differences between bioregions were found by colleagues in zooplankton, micro-nekton, fish and predators (birds) depending on the bioregions and on the communities. In addition, due to the structuring role of these bioregions, some of the biotic layers were extrapolated from discreet observations to the bioregions. This was the case for the seabirds distributions patterns observed from boat during the regular rotations of the Marion Dufresne between the three districts<sup>12</sup>.

Despite the significant differences found in several compartments of the pelagic food web between the North and the South of the SPA region, from an ecological view point, no information is currently available for characterizing this transition region in the open ocean. Indeed, most of the observations, from plankton and nekton sampling to direct observations of seabirds or mammals, have been obtained during the rotation track of the Marion Dufresne, which crosses the SPA region from South to North, but always transiting over the shallow plateau. Consequently, in the open ocean, the transition between the subtropical and subantarctic environments has not been sampled. From an oceanographic view point, no sharp boundary has been found (as for instance the transition in Chl-*a*

---

<sup>12</sup>The typical rotation of the Marion Dufresne is represented in the large scale global map of Figure 2.1 (black dashed line): it sails from La Réunion to Crozet Islands, then from Crozet Islands to Kerguelen Islands, then from Kerguelen Islands to Saint-Paul and Amsterdam Islands, and next back to La Réunion.

appears as a smooth gradient). Conversely, in the subantarctic region the Polar Front creates strong contrast in the biogeography of the pelagic environment [De Broyer et al., 2014; González-Wevar et al., 2021, e.g.]. The different phytoplankton phenologies found in satellite maps, revealing the co-existence of subtropical and subantarctic conditions within the EEZ, appears then a key tool for better characterising this transition zone in the open ocean region.

### 2.3.1 Characterisation of the transition zone

In order to assess the variability of the transition zone between subtropical and subantarctic conditions, the position of this boundary has been analysed over the last 20 years (1997-2017 period). Here, the transition zone is defined as the boundary between two regions characterised by different seasonal cycles in phytoplankton biomasses, i.e. different phenologies. To maintain consistency in the seasonal data availability, the annual cycle is defined between July and June of the following year. Following Ardyna et al. [2017], a k-means analysis is applied on the normalized annual Chl-*a* time series (i.e. deducted by the annual minimum and divided by the annual maximum). The k-means algorithm classifies the normalized time series into two groups which are similar within them (minimization of the intra-group variance) and distinctive between them (maximisation of the inter-group variance). Each group is then representative of a phenological characteristic regime: the subantarctic or the subtropical one. Successively, the annual results of the k-means analyses (containing binary values in function of the two regions) are averaged over the 20-years period. The resulting map represents the probability to be in the subtropical regime (which is complementary to the probability to be in the subantarctic one) over the 20-years period. A Transition Zone Index is finally computed by calculating the spatial gradient of this probability map. This Transition Zone Index represents the variation of probability to belong to a region (between the 20-year period) by kilometres (expressed in  $\Delta\%/km$ ). Therefore, when the Transition Zone Index equals to zero it means that two narrow points during the 20-y period had exactly the same probability to belong to the



same region (more likely, this probability was 1 for both due to the long analysed period). On the opposite, the higher the Transition Zone Index is, the more this point was at the interface of two different regions (subtropical vs subantarctic).

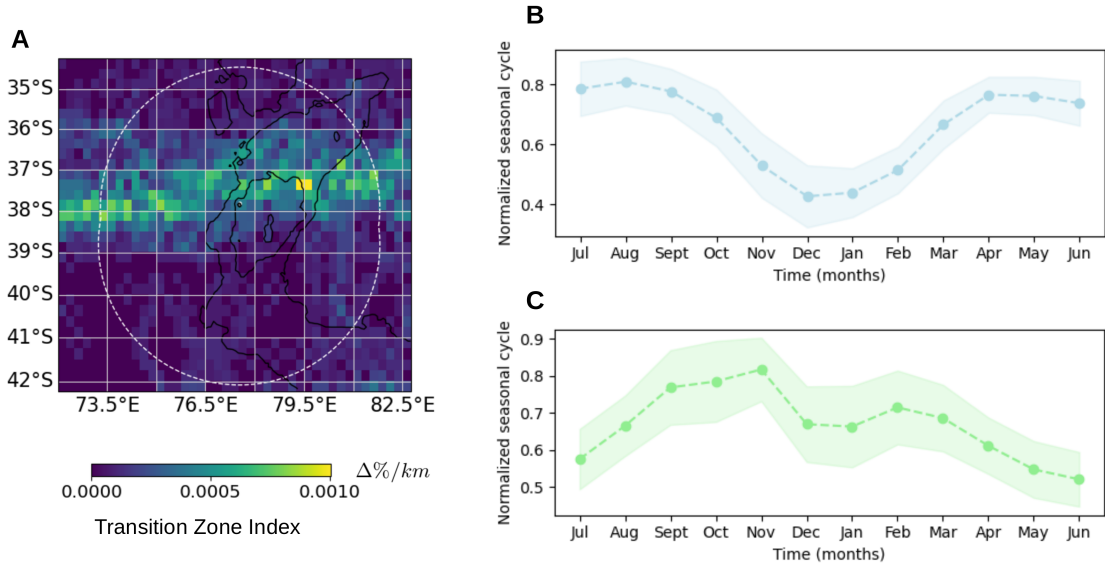


FIGURE 2.7: **Transition zone between the Subantarctic and Subtropical environments in the Saint-Paul and Amsterdam region during the period 1997-2017.** (A) Transition Zone Index ( $\Delta\%/km$ ) between the Subantarctic and Subtropical environments between 1997 and 2017. (B) Mean (line) and standard deviation (filled region) of normalized chlorophyll *a* seasonal cycle over the years 1997-2017 in the subtropical region computed with the k-means method. (C) same as (B) but for the subantarctic region.

The distribution of the Transition Zone Index is shown in Figure 2.7A. The normalized seasonal cycles (mean  $\pm$  standard deviation) of the Subtropical and Subantarctic regimes identified by the annual k-means over the 20-years period are shown in Fig 2 A and B, respectively. These time series confirm the presence of distinct phenological regimes all over the two decades representative of the Subantarctic and subtropical conditions. In conclusion, this analysis demonstrates that in the SPA region and over the period 1997-2017, the transition zone between the subantarctic and subtropical condition was mostly found in the latitudinal band between 39 and 37 °S with more poleward position in the west compared to the east (Figure 2.7A).

As described previously, no direct biological observation of this pelagic Transition Zone is available. Consequently, the analysis of Ocean Color maps provides the only biological information on this region. The distinct phenological regimes identified by the analysis can be indicative of distinct physical and biological habitats. Consequently, organisms populating this zone are potentially accustomed to a high environmental variability. Even if no ecological information is available on these communities, the particularity of this environment and the representativeness criteria justify to include a part of this unique habitat in the prioritisation regions defined by the scientific community.

### 2.3.2 Long term variability under climate change

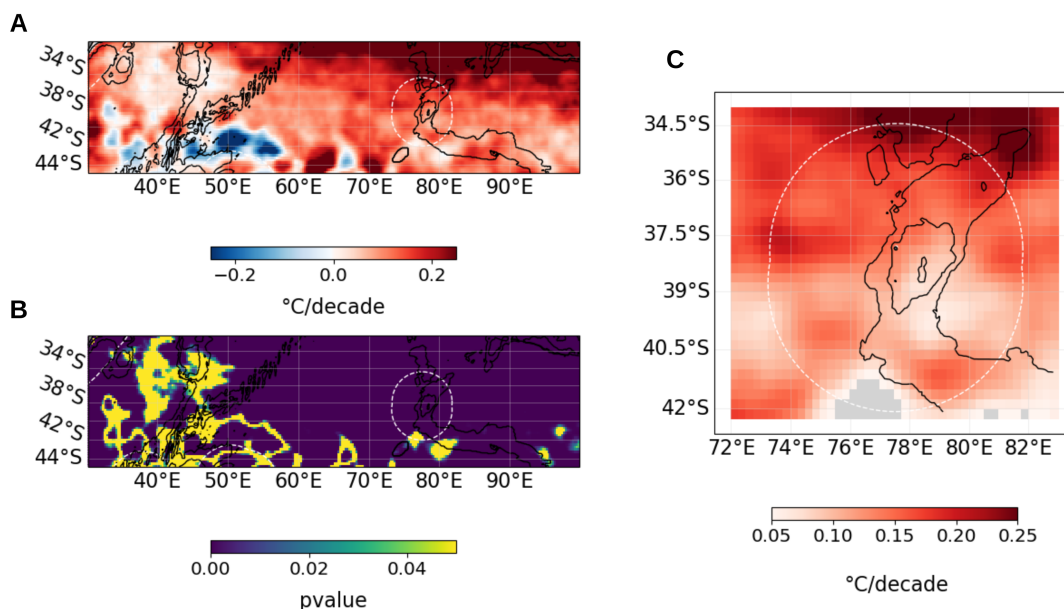


FIGURE 2.8: **Surface warming trends estimated from sea surface temperature between 1985 and 2017 in the South Indian Ocean.** (A) Surface warming trends and (B) p-value associated to these trends at the regional scale. (C) Significant surface warming trends in the SPA region (no significant trends ( $p < 0.05$ ) are shaded in grey).

The spatial contrast identified in climatologies (section 2.2.3) are likely to evolve in function of the considered time scales. The low number of historical vertical profiles of stratification since the middle of the 2000s prevents us from found any significant long term changes.

Similarly, no long-term trend in the evolution of the Transition Zone has been identified in the 1997-2017 OceanColor maps due to an important interannual variability. However, time series of sea surface temperature obtained by satellite since 1985 provide some insights on the historical velocity changes in the physical properties of the surface ocean of the SPA region. Figure 2.8 shows surface warming trends computed with an Ordinary Least Squares regression on the monthly data between 1985-2017 from the OSTIA product, produced by the UK Met Office and distributed by CMEMS<sup>13</sup>. A large scale gradient in the sea surface warming trends is observed in the South Indian Ocean, with higher warming trends in the oligotrophic gyre and lower trends south of it (Figure 2.8A). These observations are in line with past large scales analyses [e.g., Dunstan et al., 2018]. In the SPA region, warming trends range between 0.05 et 0.15 °C per decade in the southern part of the EEZ and between 0.15 et 0.25 °C per decade in the northern sector (Figure 2.8C). By computing the gradient and the trends we can estimate the velocity evolution of the marine environment. The regional analysis of sea surface warming trends over the period 1985-2019 shows a poleward migration of temperature conditions of about 20 kilometres per decade (figure not shown).

A global poleward migration of habitats is expected under climate change, however impacts may be largely more complex depending on the region and the interplay of multiple bio-geo-physical processes. In the study region, historical trends in the spatial expansion of the Subtropical Gyre of the South Indian Ocean and a decrease of Indian subtropical Chl-*a* concentration have been documented in the literature [Jena et al., 2013; Signorini et al., 2015]. This corroborated a potential poleward migration of the transition zone between the pelagic subtropical and subantarctic conditions. Reygondeau et al. [2020] projected the spatial distribution of global biogeochemical provinces from 1950 to 2100 under climate change forcing. This work estimates an average poleward shift of biogeochemical provinces of 18.4 Km per decade, close to the poleward velocity trends calculated in the study region from sea surface temperature data (about 20 Km per decade). Consequently, in order to take account future environmental changes in the next 50 years, during the consulting

<sup>13</sup>Product id: SST\_GLO\_SST\_L4\_NRT\_OBSERVATIONS\_010\_011

process with the scientific community and the RNN, a latitudinal range of 1° has been retained as a reasonable spatial range buffering some particular regions. For instance, a latitudinal range of 1° was considered for representing the transition Zone in the priority areas. Furthermore, a particular biogeochemical province (the Indian South subtropical gyre defined by Longhurst [2010] and Reygondeau et al. [2013]), has been identified during the workshop in the top north of the region. This biogeochemical province, distinct from the rest of the French Southern Lands' marine regions, is supposed to further enter into the SPA zone in the following decades [Reygondeau et al., 2020]. Therefore, a latitudinal band of 1° was also defined around this small portion of the biogeochemical province included in the EEZ during the ecoregionalisation analyses.

## Part IV

# Conclusions and perspectives



# Summary of main findings

Since the formulation of the famous [Martin's Iron hypothesis](#)<sup>1</sup>, sources and delivery pathways of this micronutrient to the surface Southern Ocean have become a topic of active research for the scientific community. Iron limitation in the Southern Ocean was primarily thought to be linked to the low windblown dust deposition, due to the lack of continental lands beside the ice-covered Antarctica, whereas elsewhere this is a dominant iron source to the surface ocean [[Mahowald et al., 2006](#)]. Dust deposition in open ocean areas and ice sheet melt-back, which releases aeolian iron deposited during winter, have been proposed to primarily control Southern Ocean primary production and global atmospheric CO<sub>2</sub> concentration [[Martin, 1990](#), and references therein]. Since the 2000s, the injection of iron-rich deep water to the surface ocean has progressively appeared as a major input, exceeding aeolian sources [[Latimer and Filippelli, 2001](#); [Tagliabue et al., 2017](#)]. Lithogenic iron, transferred to the water column from islands' and continental shelves, surfaces due to important vertical mixing at these regions and winter entrainment, and is advected offshore [[Blain et al., 2007](#); [Mongin et al., 2009](#); [Planquette et al., 2011](#); [Boyd et al., 2012](#); [Bowie et al., 2015](#); [d'Ovidio et al., 2015](#)]. The description of such mechanisms was an important step showing a direct delivery pathway of iron from the ocean interior to the surface ocean. Thereafter, further alternative iron pathways from the ocean interior have been investigated due to their important implications for biogeochemistry and climate issues. This thesis studies these processes, here referred as “deep” processes, in order to differentiate them to the processes linked to the atmosphere, ice and coastal margins,

---

<sup>1</sup>“Give me a half tanker of iron, and I will give you an ice age.” J. Martin (1988)



focusing on their ecological effect over the pelagic food-webs.

A first question is then raised: ***What is the ecological role of deep iron sources and how do they influence the pelagic seascape in the Southern Ocean?***

This question is addressed in Part II of this thesis. Under the structuring effect of the Antarctic Circumpolar Current (ACC), the Lagrangian analysis of geostrophic currents is used for reproducing the surface expression of phytoplankton biomasses in the open ocean ACC region driven by previously unknown deep iron supplies. Figure 1.1 schematises and compares these novel deep iron supplies to the surface Southern Ocean to well-known shallower supplies, the ones close to ice and continental (and islands) margins. In this thesis, an iron supply represents either an iron source, i.e. an external nutrient input to the Southern Ocean reservoir, such as hydrothermal iron (Chapter 1), either a delivery mechanism allowing to reinject iron in the productive layer, this is the case for seamounts (Chapter 2). Here, I summarise key results of the analyses of previously unknown deep iron supplies contained in Part II of this thesis, and how do they challenge our understanding of the pelagic seascape in the Southern Ocean.

Hydrothermalism is now accepted as a new source of iron to the ocean reservoir [e.g., Tagliabue et al., 2010]. Studies presented in Chapter 1 of Part II are the first observational evidences of its intense impact on surface primary production in the iron-depleted Southern Ocean. Intense biological responses have been observed with *in situ* profiling floats (maximum depth-integrated biomass superior to 80 mg Chla m<sup>-2</sup> in both Indian and Pacific sector) and satellite derived estimations of Net Primary Production (up to 45 gC m<sup>-2</sup> y<sup>-1</sup> in the Pacific sector). The reconstruction of the Lagrangian plumes connects the intense phytoplankton signals to hydrothermal iron. These phytoplankton responses were located in regions that have been documented as important for large predators (seabirds and marine mammals) [for instance see Nel et al., 2001 and Andrews-Goff et al., 2018 for the regions targeted in the Indian and Pacific sector, respectively]. Hydrothermal iron therefore emerges as a new iron source to the surface ocean shaping the pelagic seascape of the Southern Ocean (yellow box in Figure 1.1).

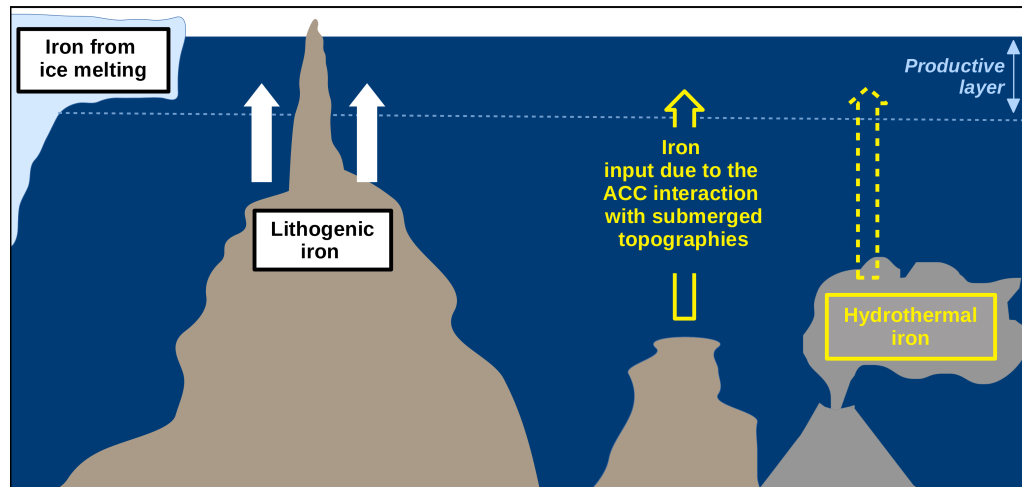


FIGURE 1.1: **Fertilizing from below: schematic representation of iron sources and delivery mechanisms to the euphotic layer driving major phytoplankton contrasts in the Southern Ocean.** Deep iron supplies (sources and delivery mechanisms) considered in this thesis (yellow) are compared to shallower supplies known from the literature (white). Iron nutrient sources (boxes): iron from sea-ice melting, lithogenic iron and hydrothermal iron. Delivery mechanisms of iron sources to the productive layer from the ocean interior (arrow): injection at shelves of emerged lands (continents or islands) and over submerged topographic features. Dashed yellow arrow linking deep hydrothermal iron to the productive layer schematises vertical delivery mechanisms little understood, although the impact of hydrothermal iron in the productive layer has been demonstrated. Proportions are not respected in order to represent processes with different spatial scales in the same schema.

Compared to the intense and efficient phytoplankton responses to hydrothermal iron, Chapter 2 of Part II explores weak phytoplankton signals ( $0.6 \text{ mg/m}^3$  in monthly averaged OceanColor maps) but consistently targeted by multiple predators (ten-year tracking data of 6 species of seabirds and pinnipeds). The analyses presented in Chapter 2 identify phytoplankton blooms associated to the water masses that transited over shallow topographic highs ( $\leq 1000 \text{ m}$ ) and provide a detailed description of them. These results challenged past assumptions which considered the biological effect of seamounts as negligible [Graham et al., 2015; Ardyna et al., 2017] or very localised [Oliveira et al., 2016; Lemos et al., 2018]. Moreover, despite their lower intensity, the study argues that the biological production inferred from land-based predators and stemming from seamounts

provides the same ecological function than the biologically-rich islands systems. This is supported by: (1) the large spatial extent of the phytoplankton blooms detected in Ocean Color maps (thousands of kilometres wide, contrary to past studies) and (2) their similarity to Southern Ocean' island blooms in terms of phytoplankton dominant communities estimated from satellite-based spectral analyses, which are more likely to support pelagic ecosystems that include large predators [Cushing, 1989; Moline et al., 2004; Pakhomov et al., 2019]. Therefore, the interaction of the ACC with submerged topographies appears also as a novel nutrient delivery mechanisms shaping the pelagic seascape from phytoplankton production to upper trophic levels in the open Southern Ocean (yellow arrow in Figure 1.1).

The deep nutrient supplies unravelled in this thesis are not mutually exclusive. For instance, the analysis of seamounts systems suggests that the introduction of nutrients at these regions is mostly linked to the lifting of iron-laden deep waters (Chap. 2), rather to the transfer of lithogenic iron to the water column from the topography, as for shelves of continents and islands [e.g., Planquette et al., 2011; Blain et al., 2007]. Consequently, hydrothermal iron injected in the ocean reservoir is also potentially introduced in the euphotic layer where the ACC interacts with submerged topographies, such as seamounts. Indeed, the vertical mechanisms allowing to introduce deep hydrothermal iron to the euphotic layer are still little understood: several processes are susceptible to occur but the dominant one has not been identified yet (this uncertainty is schematised by a dashed arrow in Figure 1.1). For instance, in function of the depth at which the hydrothermal plume reaches its neutral buoyancy [Morton et al., 1956; Turner, 1979], deep winter mixing may efficiently introduce deep nutrients in the euphotic layer or not, requiring further vertical mechanisms. Overall, further studies are need to elucidate the dynamical mechanisms controlling these bottom-up processes linking the deep ocean to the surface layer. However, it is clear that the mechanisms driving the biological production in the ACC region are largely more connected than previously thought and that ecologically important contrasts may appear far away from islands, challenging past paradigm of the ACC region as an oceanic desert punctuated by oasis around islands, at least from an ecological point

of view.

The following question is then addressed in this thesis: *How can the analysis of deep bottom-up forcings on pelagic ecosystems be used to inform marine conservation policies?*

International law spreads responsibilities for the conservation of marine ecosystems between single States (territorial seas and exclusives and economic zones) and the international community (high seas). In the Southern Ocean, in both the national and international domains similar approaches for achieving conservation objectives have been adopted. This concerns in particular the process for establishing Marine Protected Areas (MPAs), a key conservation tool, which is considered for the case-studies undertaken by this thesis. Ecoregionalisation analysis is the central core of the scientific basis supporting the establishment of MPAs in the study region [e.g., Koubbi et al., 2016b,a]. This analysis aims to gather scientific knowledge on the marine environment and on all the compartments of the food-webs. It should represent the most exhaustive understanding of the marine ecosystems and the distribution of ecological values within them (e.g., life-history habitats, sites targetted by vulnerable species, etc.).

The deep nutrient pathways studied in Part II are localised in the ACC region under CCAMLR competence. Consequently, Chapter 1 of Part III explores how the understanding of these novel bottom-up processes may contribute to the conservation effort undertaken under CCAMLR there. In order to pursue CCAMLR's objective to establish a representative system of MPAs<sup>2</sup>, ecoregionalisation analyses are performed for identifying MPA proposals<sup>3</sup>. From a scientific point of view, our understanding of the pelagic seascape in the ACC region has largely evolved in past decades. The conclusions of the CCAMLR Bioregionalisation workshop held in 2007, which identified priority regions for MPAs in the ACC region only close to islands, have been recognized largely insufficient<sup>4</sup>. However, to our knowledge, to date no bioregionalisation analysis has identified the biore-

---

<sup>2</sup>CCAMLR-XXVII (2008), §7.2.

<sup>3</sup>For a more comprehensive description of such process please refer to Chapter 1 of Part III.

<sup>4</sup>SC-CAMLR-XXX (2011), Annex 6, §2.19.

gions sustained by the biophysical mechanisms evidenced in this thesis (large scale effects of seamounts and hydrothermal iron in the Indian and Pacific sectors of the Southern Ocean). Indeed, from a biogeochemical point of view, pelagic regionalisations depict the ACC as a series of homogeneous zonal bands punctuated by islands shelves and locally by seamounts [see for instance the recent analysis of the CCAMLR's MPAs' overlap with pelagic bioregions made by [Brooks et al., 2020a](#)]. Regionalisations undertaken on climatological phytoplankton's biomass and phenology shape a more heterogeneous space, but still do not identify the intense phytoplankton plumes associated to hydrothermal vents [e.g., [Ardyna et al., 2017](#)]. This highlights the need to include analyses of biophysical mechanisms unravelled by circulation connectivity patterns at regional scale for a comprehensive understanding of the pelagic seascape and sub-sequential identifications of ecoregions<sup>5</sup>.

In Chapter 2 of Part III, the study region is expanded towards lower latitudes, while considering an important actor for conservation policies in the Southern Ocean: the French Southern Lands. This Chapter analyses the scientific contribution to the current expansion project of the National Natural Reserve of the French Southern Lands in the South Indian Ocean, around the Saint-Paul and Amsterdam Islands (38 °S 77.5 °E). The methodology applied by the French National Natural Reserve in this subtropical area is the same that the one applied in past years in other oceanic regions under its competence in the Southern Ocean (Crozet and Kerguelen archipelagos). However, from a scientific point of view, the Southern Ocean and the South Indian Ocean regions are well distinct. First of all, north of the ACC, geostrophic flows are reduced and the surface ocean is depleted in both macro- and micro-nutrients [e.g., [Estrada et al., 2016](#); [Visser et al., 2015](#)]. Secondly, while the Kerguelen and Crozet oceanic zones have been the object of intense research since several decades [e.g., [Koubbi et al., 2016b,a](#)], scientific knowledge around the Saint-Paul Islands is much more scarce. In order to address this pelagic knowledge gap, Chapter 2 of Part III evaluates variability patterns in phytoplankton biomass and their possible drivers. Our analysis identifies two bioregions, differentiated by phytoplankton's phenology, biomass

---

<sup>5</sup>e.g., The working plan emerged from the Expert Workshop for Pelagic Spatial Planning in Eastern subantarctic region held in 2019 and summarised in SC-CCAMLR-XXXVIII (2019) §6.76.

and mixed layer depth: a subantarctic zone, south of the islands, and a subtropical one, north of them. Despite its small extent, the seasonal increasing in phytoplankton biomass around Saint-Paul and Amsterdam Islands dominates phytoplankton biomass seasonality at the large scale (hundreds of kilometres) and is possibly linked to enhanced diapycnal mixing induced from tidal waves' breaking (the generated turbulence ranges between  $10^{-9}$  and  $10^{-8}$  W/kg over the whole water column). This bioregionalisation appears to structure the distributions of different compartments of the trophic chain and the definition of the transition zone between the subantarctic and subtropical environments provides an interesting region for scientific evaluation of future environment evolution under climate change.

In the next section I discuss three caveats and following perspectives for the analyses contained in this thesis. These concern: (1) limits and way forward of the analysis of nutrients pathways from the deep to the upper ocean; (2) some perspectives for a more comprehensive analysis of the Antarctic Circumpolar Current trophic web; and (3) implications for future conservation policies.





# Perspectives

## 2.1 Nutrients pathways from the deep to the upper ocean: limits of this work and way forward

The Lagrangian analyses contained in this thesis are based on the calculation of trajectories from the two-dimensional horizontal (2D) altimetry-derived data. Representation of ocean velocity field by altimetry is associated with several approximations and errors, ranging from bias caused by interpolation computations to the omission of some components of ocean dynamics, such as ageostrophic currents and Ekman transport [for a larger discussion of limits of Lagrangian analyses based on altimetry-derived velocity fields refer to [Lehahn et al., 2018](#)]. Despite these limitations, Lagrangian analyses of altimetry-derived information have provided valuable information on phytoplankton dynamics and bottom-up mechanisms affecting higher-trophic-level organisms [e.g. [d'Ovidio et al., 2010](#); [cotté et al., 2011](#); [Della Penna et al., 2015, 2017](#); [Lehahn et al., 2018](#)]. Another key caveat of the analysis of altimetry velocity field is the neglect of ocean vertical velocities. The analysis of the 2D velocity field is usually justified by the lower intensity of oceanic vertical velocities compared to the horizontal ones (typically  $10^{-5}$  vs  $10^{-1}$   $m/s$ ; [[d'Ovidio et al., 2004](#)]). However, the exclusion of the vertical dimension is even more challenging in the study-cases contained in this thesis, which consider the link between deep nutrient sources and the euphotic layer. For instance, Chapter 2 of Part II investigates the effect of seamounts between 0 and 1000 m depth on surface phytoplankton biomass. In

the [Introduction](#), the utilisation of altimetry-derived geostrophic currents for reproducing the ocean transport over the first hundreds of kilometers of the water column has been justified by the quasi-barotropic structure of the Antarctic Circumpolar Current (ACC) [[Phillips and Bindoff, 2014](#)]. More precisely, the equivalent barotropic assumption is a common first-order approximation to the time-mean ACC, stating that the deep flow is parallel (i.e. shows a small rotation angle) and proportional to the surface flow over an e-folding spatial scale. Studies have concluded that the time-mean ACC has an equivalent barotropic behaviour down to an e-folding scale ranging between 500 and 1000 m [e.g., [Karsten and Marshall, 2002](#); [Gille et al., 2004](#); [Firing et al., 2011](#); [Phillips and Bindoff, 2014](#)]. The equivalent barotropic behaviour of the ACC varies depending on the region. For instance, [Phillips and Bindoff \[2014\]](#) analysed the ACC circulation patterns in the northern Kerguelen plateau with profiling floats and found a non-equivalent barotropic behaviour most of the time (60%). However, the equivalent barotropic assumption was still valid for the mean flow (null mean rotation) [[Phillips and Bindoff, 2014](#)]. Even though the analysis of vertical motions would provide valuable information to our understanding of connectivity pathways linking the deep nutrients to the surface layer, the analysis of horizontal velocity fields assuming the equivalent barotropic model appears reasonable for exploring dynamics linked to deep structures ( $< 1000$  m) too.

Location of active vent systems and shallow seamounts ( $\leq 1000$  m deep) in the Southern Ocean, represented respectively by red dots and black triangles, is illustrated in [Figure 2.1](#). This thesis has evaluated the influence of hydrothermal iron and/or seamount effects over the pelagic seascape in study-regions located by the yellow boxes labelled A and C. However, similar processes are susceptible to act in many other regions. Here I provide some arguments for considering two regions for analysing the role of these deep iron supplies in the Southern Ocean (dashed yellow boxes in [Figure 2.1](#)). The first one is the Kerguelen bloom zone, which is surrounded by numerous active vents of the South-East Indian Ridge and some shallow ( $\leq 1000$  m deep) seamounts (box B in [Figure 2.1](#)). In this region, the phytoplankton bloom stemming from the Kerguelen shelf is possible to be re-enhanced when the current interacts with seamounts, similarly to the effect of

seamounts of the South West Indian Ridge on the Bouvet Island's bloom (Chapter 2 of Part II). Distinct phytoplankton plumes more than 1000 km downstream of the Kerguelen bloom and potentially separated from it can be observed in Ocean Color maps [e.g., see Figure 4A in [Robinson et al., 2016](#)]. In addition, the interannual extension of the Kerguelen phytoplankton bloom cannot be explained with the advection of water masses that were in contact with the Kerguelen shelf only [[Robinson et al., 2016](#)], suggesting that other mechanisms are possibly controlling the extension of the Kerguelen's bloom. Another potential interesting zone for investigating regional processes driving deep iron supplies is located in the Pacific sector of the Southern Ocean (box D in Figure 2.1). This region, the Udintsev Fracture Zone, represents the narrowest choke point of the ACC (see the narrow Northern and Southern limits of the ACC in Figure 2.1). This particular region has been identified as a hotspots of both energy flux into lee waves and upwelling [[Park et al., 2019](#); [Melet et al., 2014](#); [Tamsitt et al., 2017](#)]. Consequently, the Udintsev Fracture Zone appears as an interesting candidate for evaluating hydrothermal iron lifting from both local and remote systems, similarly to the processes analysed in Chapter 1 of Part II. Similarly to this, the region downstream of the Drake Passage, could also be an interesting candidate due to the intense ACC transport there (see for instance section 1.2.2 in Part III) and to the numerous seamounts and hydrothermal vents there (Figure 2.1).

In addition to future regional studies, some mechanisms need to be better constrained to improve our understanding of deep iron supplies pathways. More precisely, a key component of the utilisation of horizontal advective pathways for reproducing iron fertilization is the residence time of this micro-nutrient in the upper ocean. Indeed, iron is a scavenged element, meaning that it is absorbed by suspended particles in the ocean, iron-complexing ligands, and is subsequently removed from the surface ocean by sinking down in the water column. Therefore, the interplay between iron scavenging fluxes, driven by organic iron-complexing ligands cycles, and iron regeneration regulates ocean iron cycle [[Tagliabue et al., 2017, 2019](#)]. The residence time of bioavailable iron is thought to vary between 10 and 100 days in the ocean mixed layer waters [[Black et al., 2020](#)] and to increase up to 100 years in the ocean interior (<1500 m depth) [[Bruland et al., 1994](#); [Bergquist and](#)

Boyle, 2006; Weber, 2020]. On another hand, studies considering iron transport from ocean circulation demonstrated that the iron transferred to the ocean from continental margins during winter remains available in the upper ocean and stimulates blooms in the summer months [Mongin et al., 2009; d'Ovidio et al., 2015; Robinson et al., 2016]. Multiple processes can alter iron bioavailability and its transport during the advection period, such as the dilution of iron by physical mixing or iron luxury uptake by biota (refer to Mongin et al. [2008] for a larger discussion). The complexity of mechanisms regulating iron residence in the upper ocean layer and its bioavailability is reflected in the analysis of horizontal circulation by the different advection periods of water masses downstream of continental shelves in function of the study-region. For instance, the Crozet bloom has a maximum overlap with the water masses that left the continental shelf within the 2-3 months before the bloom, while this period is extended up to 6 months for the Kerguelen and South Georgia's blooms [Robinson et al., 2016]. Consequently, it appears important to better understand both dynamical and biogeochemical mechanisms controlling iron outcome and its impact on biological production [Boyd et al., 2012; d'Ovidio et al., 2015; Wadley et al., 2014]. This is particularly relevant for hydrothermal iron for which numerous processes are unconstrained (refer to Tagliabue and Resing [2016] for a description of them). Progress made under the GEOTRACES program has already revolutionned our understanding of ocean micro-nutrient cycling, however the impact of hydrothermal iron on the Southern Ocean biological carbon pump appears to be dominated by the poorly explored southern ridge systems [Tagliabue and Resing, 2016]. Consequently, future explorations of the Southern Ocean region are expected to provide invaluable contributions to our understanding of iron cycle and its impact on the pelagic seascape [Tagliabue and Resing, 2016].

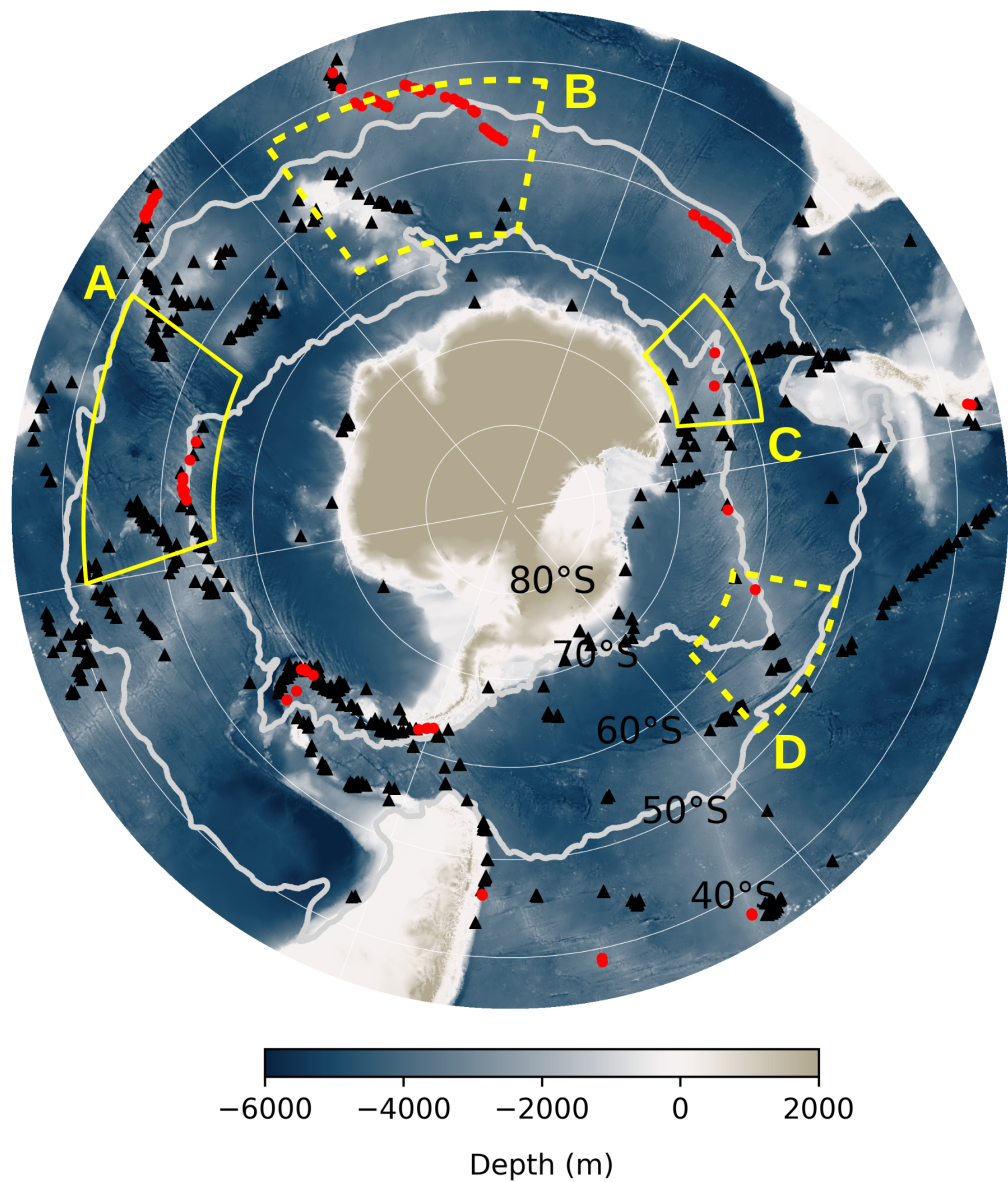


FIGURE 2.1: **Distribution of shallow seamounts ( $\leq 1000$  m deep; black triangles) and active hydrothermal vents (red dots) in the Southern Ocean.** Solid yellow boxes locate the research regions considered in this thesis: (A) downstream of the Shonda Ridge System and the South West Indian Ridge (Chapters 1 and 2 of Part II) and (C) over the Australian-Antarctic Ridge (Chapter 1 of Part II). Yellow dashed boxes locate potentially interesting research region for analysing deep iron supply mechanisms: (B) downstream of the Kerguelen's bloom and (D) on the Udintsev Fracture Zone. Refer to the text for more details on such regions. Light gray lines are the Northern Boundary and the Southern Boundary of the Antarctic Circumpolar Current defined by [Park et al. \[2019\]](#). Data sources: etopo for the bathymetry, [Yesson et al. \[2011\]](#) for the seamounts, hydrothermal vents from the InterRidge Vents Database Version 3.4 [[Beaulieu and Szafranski, 2020](#)].

## 2.2 Towards a comprehensive analysis of the Antarctic Circumpolar Current trophic web: including the mesopelagic community and gelatinous organisms

This thesis aims to adopt a particular perspective for the analysis of deep nutrient supplies: it adopts an ecological perspective and not a common biogeochemical one. Due to the strong iron limitation of the Southern Ocean, which drives major contrasts in phytoplankton distribution [Martin, 1990; Sullivan et al., 1993; Boyd et al., 2000; Thomalla et al., 2011; Ardyna et al., 2017], our approach consisted in analysing phytoplankton signals and their drivers. The analysis of phytoplankton dominant communities of studied blooms and their spatial overlap with megafauna species provides us some insights on bottom-up effects for higher-trophic-level organisms. However, the lack of observations of mid trophic levels, which make link between primary production and predators, is an important limitation of our studies. More generally, the under-researched mesopelagic layer is a common obstacle for the understanding of structure and functioning of the pelagic ecosystem [e.g., Robison, 2009; Tittensor et al., 2010].

During this thesis, I participated to a study aiming at identifying predators trophic niches through two physical drivers used as proxies of predators' prey fields in the Indian sector of the Southern Ocean (o'Toole, Baudena, Sergi et al., [in prep.]). Figure 2.2 represents the distribution of the two physical drivers and their overlap with the foraging hotspots of seven predators' species (seabirds and pinnipeds). The two physical drivers are: (1) the climatological distribution of the post-bloom waters - through which I provided my contribution to the study - which was estimated by the advection of water masses from iron sources (shallow topographies and upwelled hydrothermally-influenced deep waters, as evaluated in Ardyna et al., [2019]) (panel A); (2) the climatological presence of Winter Waters (panel B). While the post-bloom water are used as an indicator of the "maturation" of the pelagic ecosystem inside the drifting water masses, the presence of Winter Waters is used for evaluating the accessibility of the preys. Indeed, this cold water mass is known to



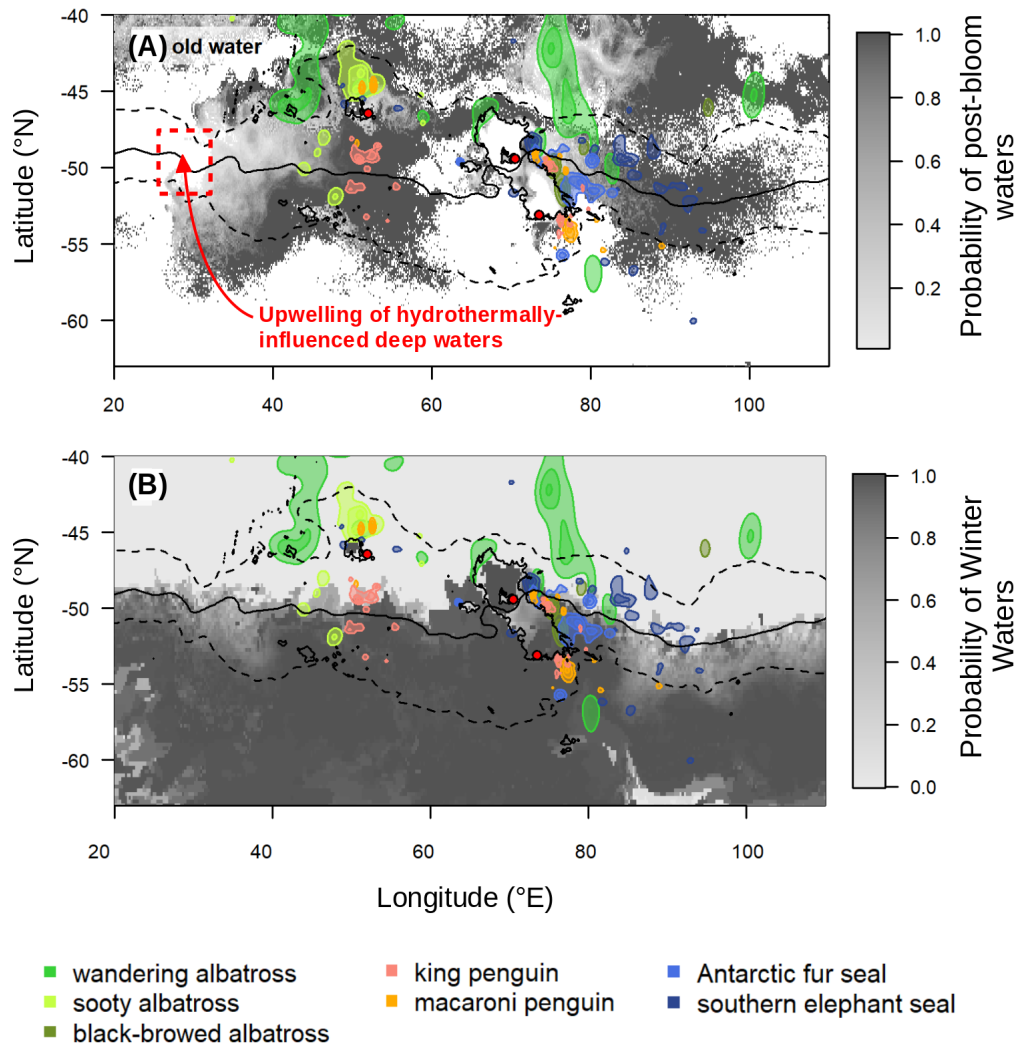


FIGURE 2.2: **Distribution of predator hotspots and climatology of physical drivers in the Indian sector of the Southern Ocean.** Predator hotspots include king penguins (salmon), macaroni penguin (orange), Antarctic fur seal (blue), southern elephant seal (dark blue), dark-mantled albatross (light green), wandering albatross (green) and black-browed albatross (dark green). Antarctic Circumpolar Current fronts (North to South) include the sub-Antarctic Front, Polar Front and southern Antarctic Circumpolar Current Front. Red dots represent predator colonies (North to South) Crozet, Kerguelen and Heard. Shelf break (1000 m bathymetric contour) is represented by a solid black line. Predator hotspots generated from kernel density values. Source: collaboration with o'Toole et al., [in prep.].



modulate the vertical distribution of mesopelagic fishes [Collins et al., 2008]. The statistical preference of the predators species for the two drivers is then evaluated comparing the selected habitat of each species to its available habitat defined by simulated animal track [Raymond et al., 2018]. These analyses demonstrate that the two physical drivers unfold the trophic niches of the regional top predators in a remarkably consistent way (result not shown).

In addition to the critical need to better understand the distribution and temporal variability of the mesopelagic layer’s hotspots [Hazen et al., 2013; Benoit-Bird and McManus, 2012] other component of the trophic chain would benefit from further investigations. For instance, salps are generally assumed to belong to an alternative trophic web, the microbial food web, and considered as a “dead end” of the pelagic food-web [Verity and Smetacek, 1996; Sommer et al., 2002; Pakhomov et al., 2019; Trebilco et al., 2020]. Indeed, low-trophic foragers (such as penguins) and mesopelagic foragers (pinnipeds) feed preferentially on krill and/or mesopelagic fishes or squids [see chapter 2 for more details and Trebilco et al., 2020]. Consequently, in this thesis I adopted the same view, looking at the pelagic trophic chain extending from diatoms (which are a very rare prey item for salps [e.g., Trebilco et al., 2020]) up to megafauna species (see section 2). However, salps are a key element of carbon biological pump and their potential prey value is still debated [Henschke et al., 2016]. When considering the future ocean in which salps are projected to proliferate, our simplistic view of the pelagic food-web could be re-evaluated [Trebilco et al., 2020]. Similarly, the pelagic trophic chain considered in this thesis neglects benthic-pelagic coupling, although important trophic links can exist between sessile benthos and large pelagic predators. For instance, the phytoplankton blooms of the Prince Edward Islands (Indian sector of the Southern Ocean) sustain benthic habitats and, in turn, benthic suspension- and deposit-feeders feed shrimps which contribute on average 25% by mass to the annual food consumed by penguins and flying seabirds [Louise Allan et al., 2013].

## 2.3 Implications for future conservation policies

From an ecological view-point, the dynamical pathways for bottom-up controls analysed in this thesis sustain several pelagic hotspots located in the Southern Ocean and in the South Indian Ocean. Figure 2.3 localises the processes evaluated in this thesis and contextualises them within the distribution of the Important Marine Mammals Areas (IMMAs) recently identified by the scientific community<sup>1</sup>. Analyses contained in this thesis concern: (1) “Amsterdam Island, Saint Paul and Associated Waters IMMA” (Chapter 2 of Part III), (2) “Prince Edward Islands and Western Oceanic Waters IMMA” (Chapters 1 and 2 of Part II), and (3) a region straddling between IMMAs and IMMAs’ candidates (Chapter 2 of Part II) (Figure 2.3).

While not an endpoint in themselves, IMMAs are indicators of marine mammal’s preys’ locations and provide key information to conservation bodies [Corrigan et al., 2014; Sciara et al., 2016; Bonizzoni et al., 2019]. In this thesis I analysed the current conservation process undergoing in the Saint-Paul and Amsterdam region, in the context of the extension project of the French National Natural Reserve, and in the Southern Ocean within the CCAMLR. Despite the science-based management approach adopted by policy-makers in both areas, the case studies highlight a limiting factor to the scientific contribution to conservation action: the ultimate need for political will in decision-making. In the less studied Saint-Paul and Amsterdam Islands region, the development of scientific knowledge and its contribution to conservation actions were stimulated by a favourable political momentum (Chapter 2 of Part III). By contrast, in the international Southern Ocean, despite the production of actionable science, CCAMLR’s MPAs’ process appears particularly slow and numerous political blocking points have been identified [e.g., Sylvester and Brooks, 2020; Liu and Brooks, 2018; Brooks et al., 2020b]. Currently, an international legally binding agreement on the conservation and sustainable use of marine biodiversity in areas beyond national jurisdiction (BBNJ agreement) is negotiated under the United Nations umbrella.

---

<sup>1</sup>IUCN Marine Mammal Protected Areas Task Force, 2020. List of Areas of Interest (AoI), candidate Important Marine Mammal Area (cIMMA) and IMMA (Important Marine Mammal Area) for the Extended Southern Ocean, May 2020. Unpublished report.

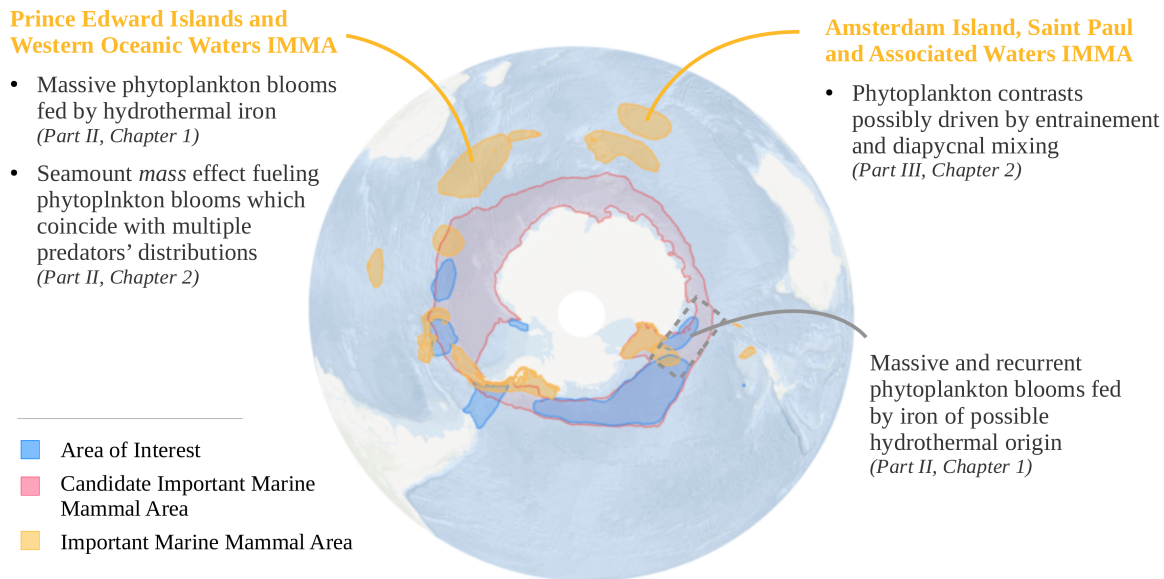


**FIGURE 2.3: Distribution of Important Marine Mammals Areas in the Southern Ocean and bottom-up processes analysed in this thesis.** Recognized Important Marine Mammals Areas (IMMAs) (orange), IMMAs candidates (red) and Areas of Interest (blue) established by the scientific community in November 2020. Figure adapted from the IUCN Marine Mammal Protected Areas Task Force 2020.

This agreement will implement the United Nations Convention on the Law of the Sea (UNCLOS, 1982) and will cover both the high seas and the seabed beyond States' Continental Shelf. The BBNJ process provides an opportunity for the international community to contribute to the transformative change necessary to reverse marine biodiversity loss<sup>2</sup> and to facilitate our ability to respond to climate change threats<sup>3</sup>.

MPAs can have multiple roles in buffering ecosystems against climate change impacts and increasing their resilience [Roberts et al., 2017]. However the ability of current MPAs to meet their conservation objectives under future environmental threats looks poor [e.g.

<sup>2</sup>IISD (2019), Summary of the Third Session of the Intergovernmental Conference on the Conservation and Sustainable Use of Marine Biodiversity of Areas Beyond National Jurisdiction: 19-30 August 2019

<sup>3</sup>IPCC (2019), Special Report on the Ocean and Cryosphere in a Changing Climate, Summary for Policymakers, SPM.C C3.5

Johnson, 2018]. The identification of MPAs networks more effective and robust to climate change impacts is a major challenge for marine conservation policies [McLeod et al., 2009]. In order to face to climate change threats, conservations programs need to consider future species' range shifts [O'Leary et al., 2018], ecosystems' stressors, as well identify regions that seems to be less impacted from future threats<sup>4</sup> [e.g., Lourenço et al., 2016; Bruno et al., 2018; Roberts et al., 2017; O'Leary et al., 2018].

The incorporation of climate change information in conservation policies is all the more challenging as scientific understanding of future ecosystems' responses to climate change is severely limited. Ecosystems can have different sensitivities to climate change and the projection of biological response to future stressors is particularly challenging [e.g., Trebilco et al., 2020; Gattuso et al., 2018; Crain et al., 2008]. By contrast, climate change scenarios of ocean physical conditions are much better constrained. For this reason, the identification of physical drivers of hotspots' formation is a key way forward for considering climate change scenarios and get some insights on possible future vulnerabilities of pelagic ecosystems [Hazen et al., 2013; van Gennip et al., 2017; McMahon et al., 2019]. Consequently, an important perspectives to the studies contained in this thesis is to analyse future projections of the physical drivers that appear to structure the ecological hotspots in the region, including the dynamical pathways controlling the ecological effects of hydrothermal iron and seamounts. From a management point of view, major challenges concern the development of instruments able to integrate climate change information in all the steps of conservation actions, from the definition of MPAs' perimeters, trough a strong precautionary principle, to the time adaptation of management policies according to environmental and biological evolutions.

---

<sup>4</sup>In the literature these are referred to as *climate refugia*: "potential safe havens that enhance environmental diversity by buffering the effects of large scale change, facilitating species persistence at regional scales and conserving unique genetic diversity", following the definition from Lourenço et al. [2016]



# Appendix







CCAMLR

Commission for the Conservation of Antarctic Marine Living Resources  
Commission pour la conservation de la faune et la flore marines de l'Antarctique  
Комиссия по сохранению морских живых ресурсов Антарктики  
Comisión para la Conservación de los Recursos Vivos Marinos Antárticos

WS-SM-18/07

16 June 2018

Original: English

**Predator trophic hotspots in the Indian sector of the subantarctic Southern Ocean: how do they overlap with marine protected areas?**

WS-SM

---

M. O'Toole, S. Sergi, A. Baudena, C. Cotté, C. Bost, C. Guinet, H. Weimerskirch, M.A. Hindell, P. Koubbi and F. d'Ovidio



This paper is presented for consideration by CCAMLR and may contain unpublished data, analyses, and/or conclusions subject to change. Data in this paper shall not be cited or used for purposes other than the work of the CAMLR Commission, Scientific Committee or their subsidiary bodies without the permission of the originators and/or owners of the data.

## **Predator trophic hotspots in the Indian sector of the subantarctic Southern Ocean: how do they overlap with marine protected areas?**

Malcolm O'Toole<sup>1</sup>, Sara Sergi<sup>1</sup>, Alberto Baudena<sup>1</sup>, Cedric Cotté<sup>1</sup>, Charles Bost<sup>2</sup>, Christophe Guinet<sup>3</sup>, Henri Weimerskirch<sup>3</sup>, Mark A Hindell<sup>4</sup>, Philippe Koubbi<sup>5</sup>, Francesco d'Ovidio<sup>1,\*</sup>

<sup>1</sup>Sorbonne Université, Laboratoire d'Océanographie et du Climat (LOCEAN-IPSL), CNRS/MNHN, Université Pierre et Marie Curie, Paris 75252, France | <sup>2</sup>Centre d'études biologiques de Chizé, Villiers-en-Bois 79360, France | <sup>3</sup>Institute for Marine and Antarctic Studies, University of Tasmania, Hobart, TAS 7001, Australia | <sup>4</sup>Antarctic Climate and Ecosystems CRC, Hobart, TAS 7001, Australia | <sup>5</sup>UMR Biologie des Organismes et des Ecosystèmes Aquatiques, MNHN/CNRS-7208 Sorbonne Université/IRD-207/UCN/UA, 43 rue Cuvier, Paris 75005, France

\* Corresponding author: francesco.dovidio@locean-ipsl.upmc.fr

**Synopsis.** The Indian sector of the subantarctic region hosts large populations of top predators which are listed at various level of vulnerability by the IUCN and which are monitored by several bio-logging programs since the late 1980s. Here we analyze more than 800 individuals from seven different pelagic species of albatross, penguins and pinnipeds. Merging our analysis with previous results, we find that the trophic hotspots constitute a network connected by the Antarctic Circumpolar Current (ACC) through a bottom up effect. When mapped on jurisdictions, this network of hotspots appears to be only partly protected in existing MPAs under national jurisdictions. This study suggests that some High seas areas need to be considered within the CCAMLR area but also the SIOFA.

## CONTEXT OF THE STUDY

### Environmental context.

The environment of the open Southern Ocean is populated by strongly contrasted physical features, whose lifetime occurs on ecologically-relevant spatial and temporal scales (McGillicuddy 2016). This dynamical landscape (Lévy et al. 2015) has a primary structuring role on the marine ecosystem, in particular in the pelagic region (d'Ovidio et al. 2015), where constraints of the topography and bathymetry interact with time-dependent features like filaments and eddies. Understanding the dynamical nature of the pelagic environment is especially relevant to conservation activities such as defining the boundaries of pelagic bioregions (Grant et al. 2006; Raymond 2014), one of the preliminary step towards designing Marine Protected Areas (MPAs). Recent scientific campaigns in the Indian sector of the subantarctic Southern Ocean (refers to the Supplementary Information for a non-exclusive list), along with analysis of multi-satellite and bio-logging data, have greatly progressed our understanding of the biophysical mechanisms driving open ocean ecosystems (Koubbi et al. 2011; 2012; 2016a and b), for different levels of the trophic web ranging from micronutrients, phytoplankton, zooplankton, micronekton and top predator species (Charrassin et al. 2002, Cotte et al. 2007, Bost et al. 2009, 2015, Hindell et al. 2011, Peron et al. 2012, d'Ovidio et al. 2013, Cotté et al. 2015, Koubbi et al. 2016a and b). Here the shallow bathymetric features like the Kerguelen and Crozet plateaux each form a major bathymetric barrier to the deep-reaching Antarctic Circumpolar Current (ACC), with important implications for the surrounding pelagic ecosystem. The surface waters in particular present very strong contrasts in primary production, which in general reflects contrasts in the availability of the main limiting nutrient of this region: iron. Iron sources are mainly located on shallow bathymetric features like the continental plateaux around the subantarctic archipelagos where internal tide mixing suspend iron from the sediments (Park et al. 2008, van Beek et al. 2008, Tagliabue et al. 2014). From these sources, iron is spread downstream of the ACC during wintertime and recharges the mixed layer, where in this season consumption by phytoplankton is inhibited by light limitation (Mongin et al. 2009). These iron plumes, stemming for hundreds of kilometres in the wake of the subantarctic islands (Ardyna et al. 2017), then fuel dramatic blooms during springtime (Fig. 1). The phytoplankton biomass is then transferred to intermediate trophic levels, and eventually

reach top predators, which are known to feed in bloom and post-bloom areas (Cotte et al. 2011, Bon et al. 2015, Della Penna et al. 2015).

Syntheses of these results have led to eco-regional studies for supporting conservation plans in subantarctic exclusive economic zones (EEZs) (e.g. Koubbi et al. 2011a and b, 2012, 2016a and b).

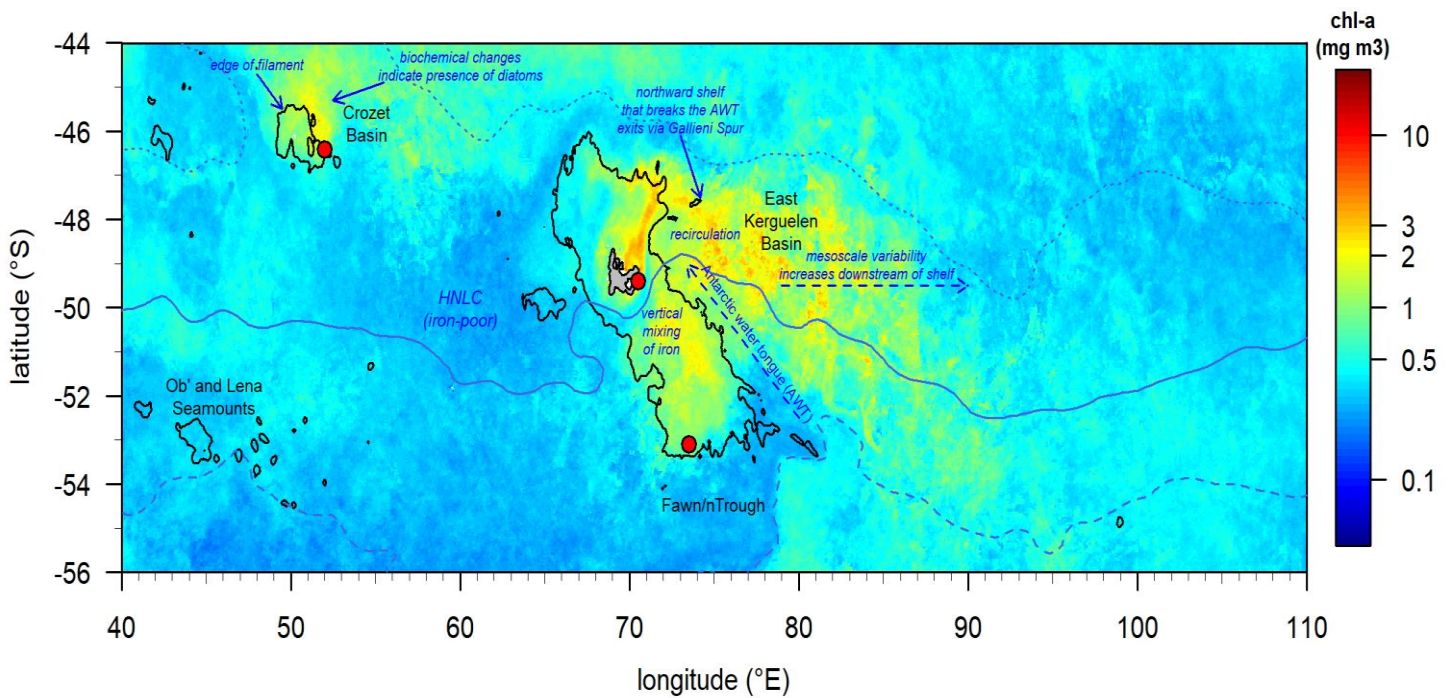


**Fig 1.** A schematic of the austral summer chlorophyll bloom, and physical features and processes in the Indian sector of the subantarctic Southern Ocean. Blue lines indicate major fronts: STF (dotted), PF (solid) and sACCF (dashed). Oceanic features include (in black from west to east) the Ob'and Lena Seamounts (Sergi unpublished data), Crozet Basin, Fawn Trough and East Kerguelen Basin (Park et al. 2008). Ocean processes include (in blue from west to east) the edge of a filament (Read et al. 2007), presence of diatoms (Seeyave et al. 2007), high-nutrient low-chlorophyll water (HNLC) (Tagliabue et al. 2012), vertical mixing of iron (Park et al. 2008), where the shelf breaks the Antarctic water tongue (Zhou et al. 2014), recirculation (Trull et al. 2015), the iron-rich Antarctic water tongue (Blain et al. 2001) and increasing downstream mesoscale variability (Moore & Abbott 2000). The black line represents the 1000 m bathymetric contour. Red dots represent island colonies in this study (from north to south): Crozet, Kerguelen and Heard. Note the two major bloom events north-east of Crozet Island and east of Kerguelen Islands

### **Jurisdictional context.**

The Indian sector of the Southern Ocean, surrounding the Antarctic Convergence, is straddling on a complex jurisdictional framework (Fig. 4) (Koubbi et al., 2012). Several

archipelagos are under national jurisdiction: French Crozet's and Kerguelen's archipelagos, the South African Prince Edward Islands and the Australians Heard and McDonald Islands. In the high seas different international organizations are responsible for the management of the living resources among the main ones for our study: the Commission for the Conservation of Marine Living Resources (CCAMLR) and the Southern Indian Ocean Fishery Agreement (SIOFA), north of it. In addition other intergovernmental organizations are responsible for the management of specific species in the same region: the Commission for the Conservation of Southern Bluefin Tuna (CCSBT) is responsible for the management of the southern bluefin tuna (*Thunnus maccoyii*) throughout its distribution and the Indian Ocean Tuna Commission (IOTC) is responsible for the management of all other tuna or tuna-like species in the Indian Ocean.

The subantarctic islands of the Indian sector of the Southern Ocean and the marine areas surrounding them have experienced an increasing conservation effort in accordance with CCAMLR conservation measures.

The Heard Island and McDonald Islands Marine Reserve was proclaimed by Australia in 2002 to protect the conservation values of the islands and the adjacent unique and vulnerable marine ecosystems (Environment Protection and Biodiversity Conservation (Heard Island and McDonald Islands Marine Reserve) Proclamation 2002). The Marine Reserve was then extended in 2014. Meanwhile the South African Prince Edward and Marion Islands was classed as a Special Nature Reserve in 2003 to make the area primarily available for scientific research or environmental monitoring (South African Environmental Management: Protected Areas Act, No. 57 of 2003, par. 18). Ten years later a Marine Protected Area (MPA) has been proclaimed within the surrounding waters to provide protection for unique species habitats and ecosystem processes as specified in the Article 2 of the Government Gazette No. 36572 (2013). In 2006 France created natural reserves in the regions surrounding the Saint Paul - Amsterdam, Crozet and Kerguelen archipelagos which has been extended in 2016 to protect the ecosystems and their role in the climate change attenuation (Décret n. 2016-1700 du 12 décembre 2016). The following year a protection perimeter has been proclaimed to complete protection in the whole French EEZ (Arreté n. 2017-28 du 31 mars 2017, art. 5).

## **Objectives of the study.**

Here we aim at revisiting the location of trophic hotspots for subantarctic top predators on the basis of the more extended multi-species bio-logging data now available, and at assessing their coverage by the network of protected areas existing in this region. In order to achieve this, we have compiled telemetry tracks of over 800 subantarctic predator tracks collected since 1989 from Antarctic fur seal (*Arctocephalus gazella*), southern elephant seal (*Mirounga leonina*), king penguin (*Aptenodytes patagonicus*), macaroni penguin (*Eudyptes chrysolophus*), wandering albatross (*Diomedea exulans*), black-browed albatross (*Thalassarche melanophris*) and dark-mantled albatross (*Phoebastria fusca*). Data sources include the Centre d'Etudes Biologique de Chizé (CEBC) in France, and Australian institutes; the Australian Antarctic Division (AAD) and Institute for Marine and Antarctic Studies (IMAS). These species are particularly useful because they disperse over extensive areas, interact with important frontal features, and can carry multiple sensors that record an individual's location and behaviour (Bost et al. 2009).

## **MARINE PREDATORS**

### **Bio-logging dataset.**

Telemetry devices recorded 821 tracks of seven marine predator species in the Indian sector of the Southern Ocean from 1989 to 2015. Deployments were made between October and March at Kerguelen, Crozet and Heard Islands to coincide with recurrent phytoplankton bloom events that occur during the austral spring and summer. Track locations were recorded by either Argos or GPS devices at intervals < 6h. If individual animals made multiple foraging trips from their colony, tracks were partitioned into separate trips. These animals spent the majority of their time (> 50 percent) in pelagic waters (> 1000 m deep) north of 60°S. A full list of marine predator species and their trip number is presented in Table 1. Device specifications and details of deployments are provided in Methods SI.

**Table 1. Instrumentation of seven marine predators.** Deployments were made on three colonies in the study region between 1989 and 2016 during the austral summer months (Oct-Mar).

colony	species	no. of tracks	deployment years
Crozet	dark-mantled albatross	42	2007-2009
	wandering albatross	161	1989; 1990-1992; 1994; 1998-2003; 2007-2010
	king penguin	38	2011-2016
	macaroni penguin	4	2009-2010
Heard	black-browed albatross	28	2003-2004
	king penguin	67	2002-2004
	macaroni penguin	28	2003-2004
	Antarctic fur seal	65	2000-2001; 2003-2004
Kerguelen	black-browed albatross	18	1994-1995; 1999
	wandering albatross	24	2002; 2007-2009
	king penguin	48	1998-2004; 2006
	macaroni penguin	10	2011; 2014-2015
	Antarctic fur seal	52	1998-2000; 2006-2008; 2012
	southern elephant seal	236	2002; 2004-2016

Observed GPS measurement error seldom exceeded a few tens of kilometres (Lopez et al. 2014) but Argos are associated with varying classes of error. Consequently, all locations were fitted (by species) to a hierarchical first difference correlated random walk state-space model (hDCRW SSM) using the R software package *bsam* (function *ssm\_fit*) (Bestley et al. 2015) to estimate locations. We extracted all posterior location estimates from the *ssm\_fit* output to account for location uncertainty inherent in Argos data. These processed tracks

were then checked for errors prior to further analyses. Fig. 2 include all location estimates from these models (coloured by species). We used a time-spent metric known as first-passage time to identify areas most visited by predator species (search locations; Fauchald & Tveraa 2003), which we use in subsequent analysis of predator foraging hotspots.

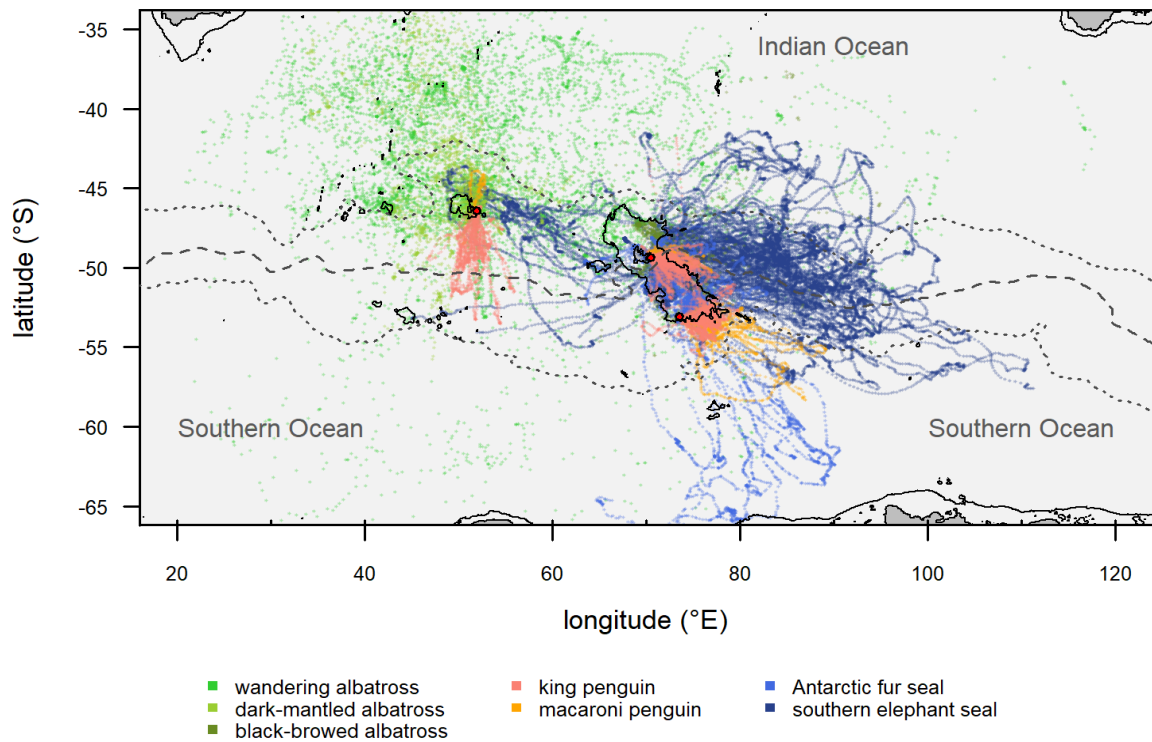


**Fig 2. Predator track distribution.** Observed tracks are coloured by species (see key) and include transit (faded) and search locations (bold). Black lines indicate major fronts (from north to south): Subtropical Front (dotted), Polar Front (solid) and Southern Antarctic Circumpolar Current Front (dotted).

### Predator foraging ecology.

To help interpret physical ocean mechanisms driving important species' foraging grounds it was necessary to summarise what is already known about predator diet and dive behaviour in the region. Here, the feeding ecology of predator species was based on numerical values from the literature (summaries provided in Methods SI). Diet composition was derived from stable isotope analyses and stomach content mass and dive behaviour was recorded from pressure sensors deployed on the animals, or from observations for flying seabirds (values were taken from Delord et al. 2013 and references within unless otherwise stated in Methods SI). Fig. 3 provides a visual summary of diet and dive depth values.



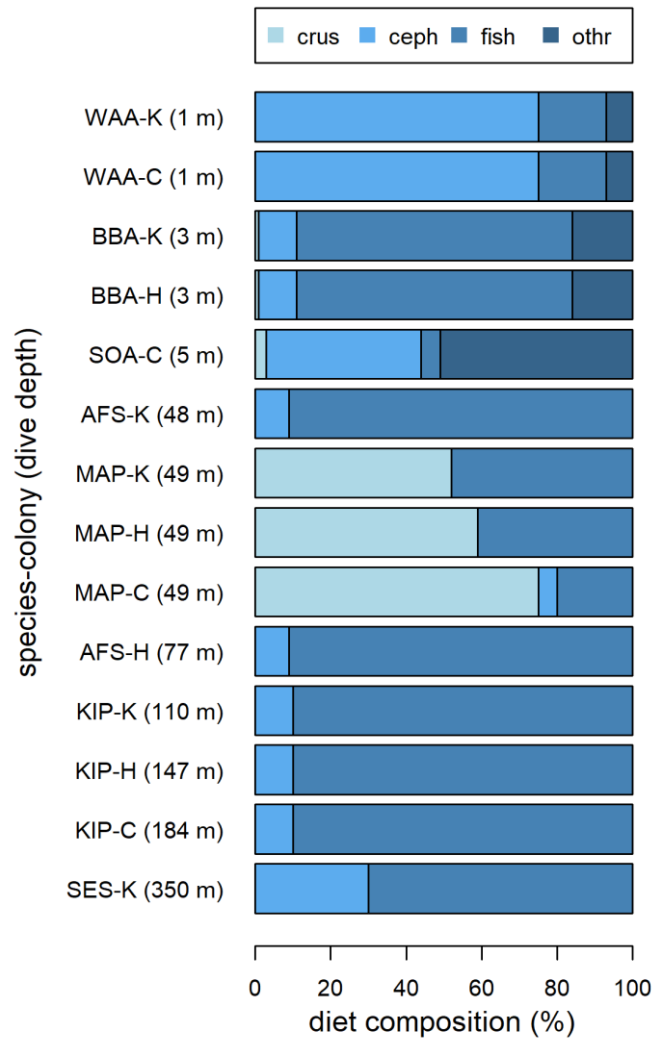


**Fig 3. Predator feeding ecology.** Diet composition (x-axis) and dive depth (y-axis) were derived from numerical data in the literature for predator species from each colony. Predator species include wandering albatross (WAA), black-browed albatross (BBA), dark-mantled albatross (SOA), king penguin (KIP), macaroni penguin (MAP), Antarctic fur seal (AFS) and southern elephant seal (SES). Deployment sites include Crozet (C), Kerguelen (K) and Heard (H). Diet components include crustacean (crus), cephalopod (ceph), myctophid (fish) and other (e.g. bird carrion; othr).

## DISTRIBUTION OF THE FORAGING HOTSPOTS IN THE JURISDICTIONAL FRAMEWORK

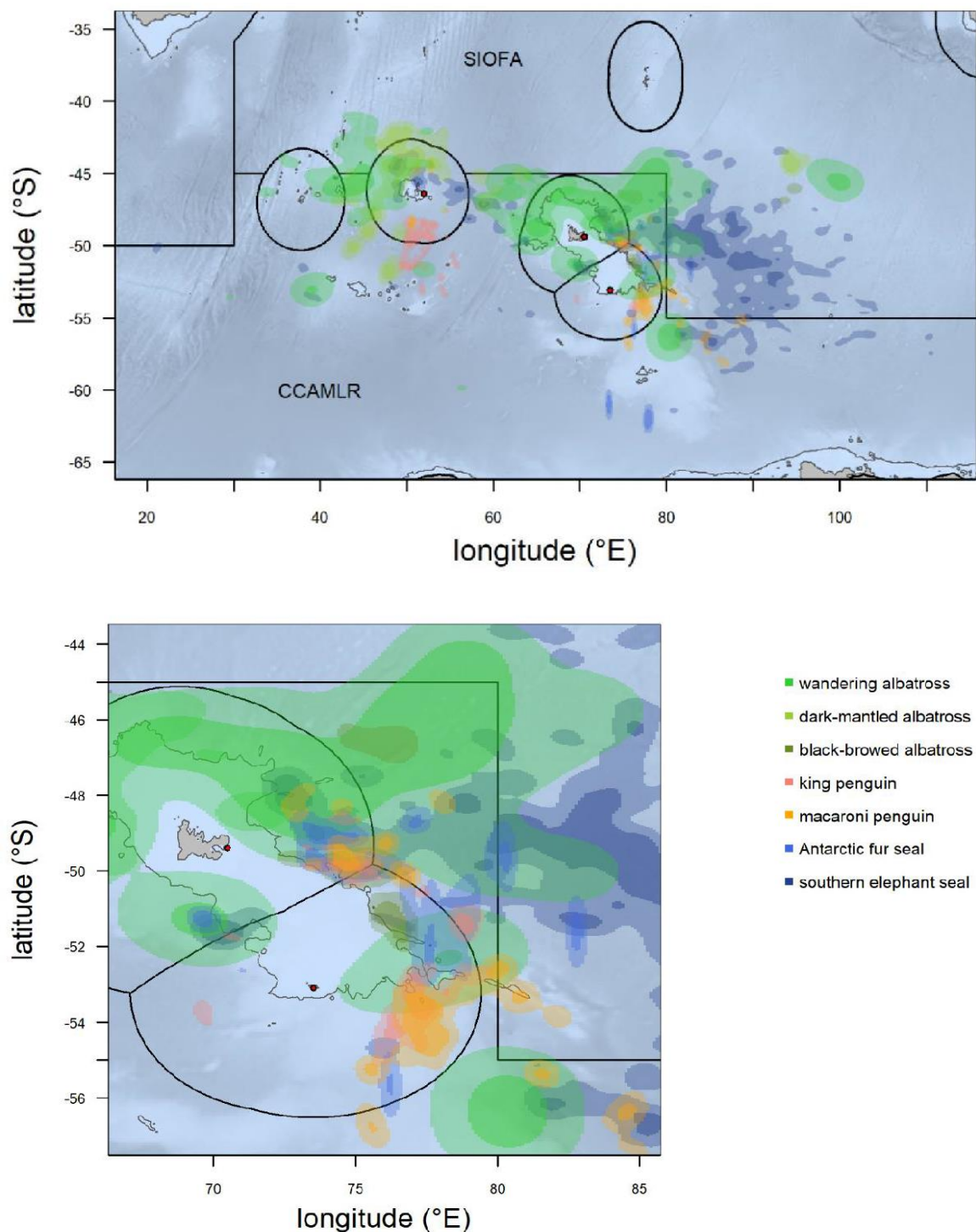


**Fig 4. Distribution of the foraging hotspots in the subantarctic Indian Ocean (A) and eastward of the Kerguelen Plateau (B).** Hotspots are coloured by species and shaded by their intensity (obtained with a k-means classification). Red dots locate the top predators' colonies here analysed. The bathymetry is issued from NOAA, the institutional boundaries (EEZ, SIOFA and CCAMLR) are issued from MarineRegions, FAO and CCAMLR websites.

The marine protected areas established under the national jurisdictions provide protection for the terrestrial and marine environments surrounding the islands, and in particular the breeding colonies of the top predators here studied.

Nevertheless, these predators have an extended foraging range. Here we analysed the distribution of top predators' foraging hotspots in the national jurisdictions (French, Australian and South African) and beyond them, in the high seas : within the CCAMLR's and SIOFA's Areas of Competence. In order to obtain this we extract a density plot with the R software package MASS (function *kde2d*) from the search locations. Next, we use a k-means classification method (3 clusters) on the density plots for each population. This resulted in 3 classes for each population which we interpret as zero density, low density and high density hotspots. We only consider low and high density hotspots for each population (Fig. 4).

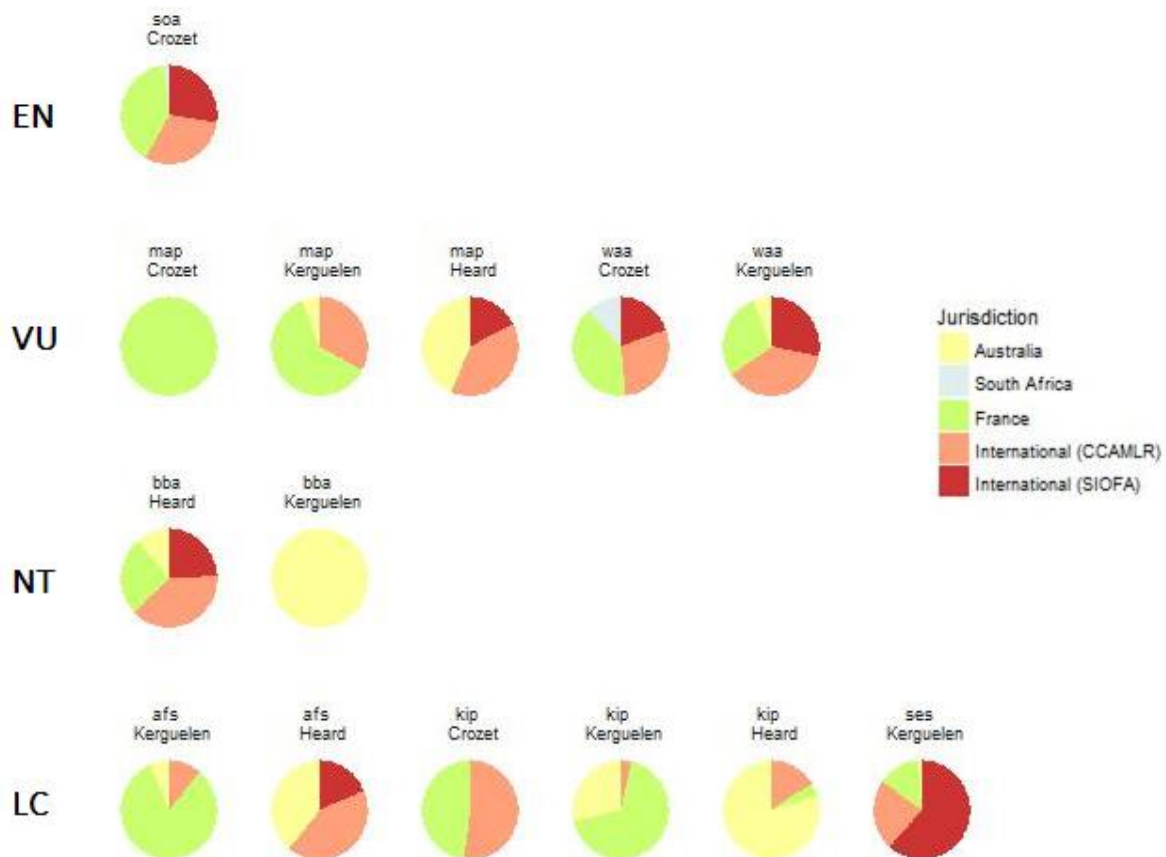


**Fig 5. Proportion of the foraging hotspots' coverage included in each area of competence (different national EEZ, CCAMLR and SIOFA).** The distribution of the foraging hotspot defined by a k-means cluster per species and per colony. The 7 species - Antarctic fur seal (afs), black-browed albatross (bba), king penguin (kip), macaroni penguin (map), southern elephant seal (ses), dark-mantled-albatross (soa) and wandering albatross (waa) – are grouped by their category under the IUCN Red List: Endangered (EN), Vulnerable (VU), Near Threatened (NT) and Least Concern (LC).

To assess quantitatively the distribution of the hotspots in the jurisdictional framework we calculated the proportion of the foraging hotspots' surface area (without distinction between the higher and lower density classes) included in the French, Australian and South African EEZ and in the CCAMLR and SIOFA areas. For this part of the analysis we decided to not include the RFMOs responsible for the management of tuna or tuna-like species (IOTC and CCSBT) according to their sphere of competence and due to the spatial overlapping of these commissions with the areas under national jurisdictions and, beyond them, with the other intergovernmental organizations here considered. Nevertheless, these commission still have an important role, especially in terms of incidental seabird mortality associated with fishing activities.

Even if the national reserves have a large extent, at least 50 % of the foraging hotspots areas for half of the populations here analysed are beyond the national jurisdictions and the national MPAs (Fig. 5). This is the case for several species considered threatened (vulnerable or endangered) or near threatened by the IUCN Red list: the endangered dark-mantled albatross from Crozet, the colonies of macaroni penguin on Heard and Kerguelen Islands, the wandering albatross from Crozet and Kerguelen colonies and the black-browed albatross from the Heard colony. In addition of the vulnerability of the species assessed at the present time by IUCN Red List, several studies predict an increasing of the population's vulnerability under the effects of climate change. As an example, the Crozet population of the king penguin - a species presently classified as least concern by IUCN – is expected to decline under climate change forcings (Le Bohec et al. 2008, Bost et al. 2015).

## **CONCLUSIONS**

The archipelagos located in the subantarctic Indian ocean have a prominent ecological role. They host important colonies of pelagic top predators and act at the same time as sources of micronutrients for phytoplankton. Due to the presence of the Antarctic Circumpolar Current, lithogenic micronutrients are dispersed eastward for hundreds of km and give rise to massive phytoplanktonic blooms during springtime. In the past, several studies have focused on individual species, and have identified several trophic hotspots in these open ocean blooming and post-blooming waters. The portion of the trophic hotspots close to the islands have benefited in the recent years of national special protection measures. However, the foraging grounds extending in the international waters have not been considered

insofar specifically by conservation plans. Here we have addressed this issue by revisiting the location of trophic hotspots for several pelagic predators. In order to achieve this we have considered over 800 biologging tracks collected since 1989 from Antarctic fur seal (*Arctocephalus gazella*), southern elephant seal (*Mirounga leonina*), king penguin (*Aptenodytes patagonicus*), macaroni penguin (*Eudyptes chrysolophus*), wandering albatross (*Diomedea exulans*), black-browed albatross (*Thalassarche melanophris*) and dark-mantled albatross (*Phoebastria fusca*). This analysis is, to our knowledge, the most up-to-date and homogeneous map of trophic hotspots for the pelagic top predators studied in this region. The map we have generated shows a network of hotspots connected by the Antarctic Circumpolar Current, with most of the important areas located in the wake of the islands. We have then overlapped this map onto jurisdictional regions. Among endangered and vulnerable species, Crozet dark-mantled albatrosses, Heard and Kerguelen macaroni penguins and wandering albatrosses have the majority of their foraging grounds outside national protected areas but inside CCAMLR division 58.5.1 and subareas 58.6 and 58.7. Other albatross hotspots and most of the subantarctic foraging areas for elephant seals (listed as Least Concern by IUCN) fall instead in the SIOFA Area of Competence. We propose that this work should be extended to PEI and more West, including other RFMOs than SIOFA as the South East Atlantic Fishery Organization (SEAFO), to determine potential pelagic priority areas for designing a future system of subantarctic MPAs.

### **Acknowledgements**

This work is a contribution to the Cnes Tosca/OSTST LAECOS project. The authors wish to thank the Institut polaire français Paul-Emile Victor for its essential support to the research presented here, in particular to the IPEV programs 109 and 394.

## References

- Ardyna M, Claustre H, Sallée J, D'Ovidio F, Gentili B, Dijken G, D'Ortenzio F, Arrigo KR (2017) Delineating environmental control of phytoplankton biomass and phenology in the Southern Ocean. *Geophys Res Lett* 44:5016–5024
- Beek P van, Bourquin M, Reyss J-L, Souhaut M, Charette MA, Jeandel C (2008) Radium isotopes to investigate the water mass pathways on the Kerguelen Plateau (Southern Ocean). *Deep Sea Res Part II Top Stud Oceanogr* 55:622–637
- Bestley S, Jonsen ID, Hindell MA, Harcourt RG, Gales NJ (2015) Taking animal tracking to new depths: synthesizing horizontal–vertical movement relationships for four marine predators. *Ecology* 96
- Blain S, Tréguer P, Belviso S, Bucciarelli E, Denis M, Desabre S, Fiala M, Martin Jézéquel V, Fèvre J Le, Mayzaud P, Marty JC, Razouls S (2001) A biogeochemical study of the island mass effect in the context of the iron hypothesis: Kerguelen Islands, Southern Ocean. *Deep Res Part I Oceanogr Res Pap* 48:163–187
- Bohec C Le, Durant JM, Gauthier-Clerc M, Stenseth NC, Park Y-H, Pradel R, Grémillet D, Gendner J-P, Maho Y Le (2008) King penguin population threatened by Southern Ocean warming. *Proc Natl Acad Sci* 105:2493 LP-2497
- Bon C, Penna A Della, d'Ovidio F, Y.P. Arnould J, Poupart T, Bost C-A (2015) Influence of oceanographic structures on foraging strategies: Macaroni penguins at Crozet Islands. *Mov Ecol* 3:32
- Bost CA, Cotté C, Bailleul F, Cherel Y, Charrassin JB, Guinet C, Ainley DG, Weimerskirch H (2009) The importance of oceanographic fronts to marine birds and mammals of the southern oceans. *J Mar Syst* 78:363–376
- Bost CA, Cotté C, Terray P, Barbraud C, Bon C, Delord K, Gimenez O, Handrich Y, Naito Y, Guinet C, Weimerskirch H (2015) Large-scale climatic anomalies affect marine predator foraging behaviour and demography. *Nat Commun* 6:8220
- Charrassin JB, Park YH, Maho Y Le, Bost CA (2002) Penguins as oceanographers unravel hidden mechanisms of marine productivity. *Ecol Lett* 5:317–319
- Cotte C, d'Ovidio F, Chaigneau A, Lèvy M, Taupier-Letage I, Mate B, Guinet C (2011). Scale-dependent interactions of Mediterranean whales with marine dynamics. *Limnol Oceanogr* 56:219–232
- Cotté C, d'Ovidio F, Dragon AC, Guinet C, Lévy M (2015). Flexible preference of southern elephant seals for distinct mesoscale features within the Antarctic Circumpolar Current. *Prog Oceanogr* 131:46–58
- Cotte C, Park Y-H, Guinet C, Bost C-A (2007). Movements of foraging king penguins through marine mesoscale eddies. *Proc R Soc B Biol Sci* 274:2385–2391
- Delord K, Barbraud C, Bost CA, Cherel Y, Guinet C, Weimerskirch H (2014). Atlas of top predators from French Southern Territories in the Southern Indian Ocean (Doctoral dissertation, CNRS).
- d'Ovidio F, Monte S De, Penna A Della, Cotté C, Guinet C (2013) Ecological implications of eddy retention in the open ocean: a Lagrangian approach. *J Phys A Math Theor* 46:254023
- d'Ovidio F, Penna A Della, Trull TW, Nencioli F, Pujol MI, Rio MH, Park YH, Cotté C, Zhou M, Blain S (2015) The biogeochemical structuring role of horizontal stirring: Lagrangian perspectives on iron delivery downstream of the Kerguelen Plateau. *Biogeosciences* 12:5567–5581
- Fauchald, P. & Tveraa, T. (2003). Using first-passage time in the analysis of area-restricted search and habitat selection. *Ecology*, 84, 282–288
- Grant, S., Constable, A., Raymond, B., Doust, S., 2006. Bioregionalisation of the Southern Ocean: Report of Experts Workshop (Hobart, September 2006): ACE-CRC and WWF Australia, 45 p.
- Hindell M, Lea M-A, Bost C-A, Charrassin J-B, Gales N, Goldsworthy S, Page B, Robertson G, Wienecke B, O'Toole M, Guinet C (2011) Foraging habitats of top predators, and areas of ecological significance, on

- the Kerguelen Plateau. In: *The Kerguelen Plateau: marine ecosystem and fisheries*.p 203–215
- Koubbi P, Moteki M, Duhamel G, Goarant A, Hulley P-A, O’Driscoll R, Ishimaru T, Pruvost P, Tavernier E, Hosie G (2011a) Ecoregionalization of myctophid fish in the Indian sector of the Southern Ocean: Results from generalized dissimilarity models. *Deep Sea Res Part II Top Stud Oceanogr* 58:170–180
- Koubbi P, Hulley PA, Raymond B, Penot F, Gasparini S, Labat JP, Pruvost P, Mormède S, Irisson JO, Duhamel G, Mayzaud P (2011b). Estimating the biodiversity of the sub-Antarctic Indian part for ecoregionalisation: Part I. Pelagic realm of CCAMLR areas 58.5.1 and 58.6. CCAMLR. WS-MPA-11/11.
- Koubbi P, Crawford R, Alloncle N, Ameziane N, Barbraud C, Besson D, Bost C, Delord K, Duhamel G, Douglass L, Guinet C, Hosie G, Hulley P, Irisson J. O., Kovacs K, Erwann Lagabriele, Leslie R, Lombard AT, Makhado A, Martinez C, Mormède S, Penot F, Pistorius P, Pruvost P, Raymond R, Reuillard E, Ringelstein J, Samaai T, Tixier P, Verheye HM, Vigetta S, Von Quillfeldt C, Weimerskirch H (2012). Estimating the biodiversity of Planning Domain 5 (Marion and Prince Edward Islands–Del Cano–Crozet) for ecoregionalisation (Doctoral dissertation, Commission for the Conservation of Antarctic Marine Living Resources).
- Koubbi P, Guinet C, Alloncle N, Ameziane N, Azam CS, Baudena A, Bost CA, Causse R, Chazeau C, Coste G, Cotté C, D’Ovidio F, Delord K, Duhamel G, Forget A, Gasco N, Hauteceur M, Lehodey P, Monaco C Lo, Marteau C, Martin A, Mignard C, Pruvost P, Saucède T, Sinigre R, Thellier T, Verdier AG, Weimerskirch H (2016). Ecoregionalisation of the Kerguelen and Crozet islands oceanic zone. Part I: Introduction and Kerguelen oceanic zone. CCAMLR Document WG-EMM-16/43.
- Koubbi P, Mignard C, Causse R, Da Silva O, Baudena A, Bost C, Cotté C, d’Ovidio F, Della Penna A, Delord K, Fabri-Ruiz S, Ferrieux M, Guinet C, Lo Monaco C, Saucède T, Weimerskirch H (2016). Ecoregionalisation of the Kerguelen and Crozet islands oceanic zone. Part II: The Crozet oceanic zone. WG-EMM-16/54.
- Lea MA, Cherel Y, Guinet C, Nichols PD (2002) Antarctic fur seals foraging in the Polar Frontal Zone: Inter-annual shifts in diet as shown from fecal and fatty acid analyses. *Mar Ecol Prog Ser* 245:281–297
- Lévy M, Jahn O, Dutkiewicz S, Follows MJ, d’Ovidio F (2015) The dynamical landscape of marine phytoplankton diversity. *J R Soc Interface* 12:20150481
- Lopez R, Malardé JP, Royer F, Gaspar P (2014) Improving argos doppler location using multiple-model kalman filtering. *IEEE Trans Geosci Remote Sens* 52:4744–4755
- McGillicuddy DJ (2016) Mechanisms of Physical-Biological-Biogeochemical Interaction at the Oceanic Mesoscale. *Ann Rev Mar Sci* 8:125–159
- Mongin MM, Abraham ER, Trull TW (2009) Winter advection of iron can explain the summer phytoplankton bloom that extends 1000 km downstream of the Kerguelen Plateau in the Southern Ocean. *J Mar Res* 67:225–237
- Moore JK, Abbott MR (2000) Phytoplankton chlorophyll distributions and primary production in the Southern Ocean. *J Geophys Res Ocean* 105:28709–28722
- Park Y-H, Fuda J-L, Durand I, Garabato ACN (2008) Internal tides and vertical mixing over the Kerguelen Plateau. *Deep Sea Res Part II Top Stud Oceanogr* 55:582–593
- Penna A Della, Monte S De, Kestenare E, Guinet C, d’Ovidio F (2015) Quasi-planktonic behavior of foraging top marine predators. *Sci Rep* 5:18063
- Peron C, Weimerskirch H, Bost C-A (2012) Projected poleward shift of king penguins’ (*Aptenodytes patagonicus*) foraging range at the Crozet Islands, southern Indian Ocean. *Proc R Soc B Biol Sci* 279:2515–2523
- Read JF, Pollard RT, Allen JT (2007) Sub-mesoscale structure and the development of an eddy in the Subantarctic Front north of the Crozet Islands. *Deep Sea Res Part II Top Stud Oceanogr* 54:1930–1948
- Roquet F, Williams G, Hindell MA, Harcourt R, McMahon C, Guinet C, Charrassin J-B, Reverdin G, Boehme L, Lovell P, Fedak M (2014) A Southern Indian Ocean database of hydrographic profiles obtained with instrumented elephant seals. *Sci Data* 1:140028

- Seeyave S, Lucas MI, Moore CM, Poulton AJ (2007) Phytoplankton productivity and community structure in the vicinity of the Crozet Plateau during austral summer 2004/2005. *Deep Sea Res Part II Top Stud Oceanogr* 54:2020–2044
- Tagliabue A, Mtshali T, Aumont O, Bowie AR, Klunder MB, Roychoudhury AN, Swart S (2012) A global compilation of dissolved iron measurements: focus on distributions and processes in the Southern Ocean. *Biogeosciences* 9:2333–2349
- Tagliabue A, Sallée J-B, Bowie AR, Lévy M, Swart S, Boyd PW (2014) Surface-water iron supplies in the Southern Ocean sustained by deep winter mixing. *Nat Geosci* 7:314
- Trull TW, Davies DM, Dehairs F, Cavagna A-J, Lasbleiz M, Laurenceau-Cornec EC, d’Ovidio F, Planchon F, Leblanc K, Quéguiner B, Blain S (2015) Chemometric perspectives on plankton community responses to natural iron fertilisation over and downstream of the Kerguelen Plateau in the Southern Ocean. *Biogeosciences* 12:1029–1056
- Zhou M, Zhu Y, d’Ovidio F, Park Y-H, Durand I, Kestenare E, Sanial V, Van-Beek P, Queguiner B, Carlotti F, Blain S (2014) Surface currents and upwelling in Kerguelen Plateau regions. *Biogeosciences Discuss* 11:6845–6876

## Websites

CCAMLR online GIS, [accessed in March 2018] <https://gis.ccamlr.org/>  
FAO GeoNetwork, [accessed in March 2018] <http://www.fao.org/geonetwork/srv/en/main.home?uuid=fao-rfb-map-siofa>  
Marine Regions’ Database, [accessed in March 2018] <http://www.marineregions.org/eezsearch.php>



## SI. Non-exclusive list of scientific ship cruise in the study area

Year	Campaign	Reference
2017-2018	REPCCOAI (Réponses de l'Écosystème Pélagique aux Changements Climatiques dans l'Océan Austral – Indien)	KOUBBI Philippe (2018) VT 159 / REPCCOAI cruise, RV Marion Dufresne, <a href="http://dx.doi.org/10.17600/18000383">http://dx.doi.org/10.17600/18000383</a> TOULLEC Jean-Yves, KOUBBI Philippe (2017) VT 155 / REPCCOAI cruise, RV Marion Dufresne, <a href="http://dx.doi.org/10.17600/17017100">http://dx.doi.org/10.17600/17017100</a>
2016-2017	THEMISTO (Towards Hydroacoustics and Ecology of Mid-trophic levels in Indian and Southern Ocean)	COTTE Cédric (2017) VT 154 / THEMISTO cruise, RV Marion Dufresne, <a href="http://dx.doi.org/10.17600/17017000">http://dx.doi.org/10.17600/17017000</a> COTTE Cédric (2016) VT 149 / THEMISTO cruise, Marion Dufresne R/V <a href="https://doi.org/10.17600/16016100">https://doi.org/10.17600/16016100</a>
2013-2015	MyctO-3D-MAP (Myctophid assessment in relation to Oceanographic conditions: a three Dimension Density Distribution approach combining Modelling-, Acoustic- and Predators' data)	ROUDAUT Gildas (2015) VT 144 / MYCTO cruise, RV Marion Dufresne, <a href="http://dx.doi.org/10.17600/15003200">http://dx.doi.org/10.17600/15003200</a> CHEREL Yves (2014) MD 197 / MYCTO cruise, RV Marion Dufresne, <a href="http://dx.doi.org/10.17600/14002500">http://dx.doi.org/10.17600/14002500</a> CHEREL Yves. (2014). VT 139 / MYCTO cruise, Marion Dufresne R/V. Sismar. <a href="https://doi.org/10.17600/14004300">https://doi.org/10.17600/14004300</a> JOSSE Erwan (2013) VT 124 / MYCTO cruise, RV Marion Dufresne, <a href="http://dx.doi.org/10.17600/13200060">http://dx.doi.org/10.17600/13200060</a> JOSSE Erwan. (2013). VT 134 / MYCTO cruise, Marion Dufresne R/V. Sismar. <a href="https://doi.org/10.17600/13200110">https://doi.org/10.17600/13200110</a>
2013-2016	MDCPR (Marion Dufresne Continuous Plankton Recorder)	PRUVOST Patrice (2016) VT 148 / MDCPR cruise, RV Marion Dufresne, <a href="http://dx.doi.org/10.17600/16000200">http://dx.doi.org/10.17600/16000200</a> KOUBBI Philippe (2015) VT 143 / MDCPR cruise, RV Marion Dufresne, <a href="http://dx.doi.org/10.17600/15002900">http://dx.doi.org/10.17600/15002900</a> KOUBBI Philippe (2014) VT 137 / MDCPR cruise, RV Marion Dufresne, <a href="http://dx.doi.org/10.17600/14002800">http://dx.doi.org/10.17600/14002800</a> KOUBBI Philippe (2013) VT 126 / MDCPR cruise, RV Marion Dufresne, <a href="http://dx.doi.org/10.17600/13200080">http://dx.doi.org/10.17600/13200080</a>
2011	KEOPS2 (KErguelen Ocean and Plateau compared Study)	QUEGUINER Bernard (2011) MD 188 / KEOPS 2 cruise, Marion Dufresne R/V. Sismar. <a href="https://doi.org/10.17600/11200050">https://doi.org/10.17600/11200050</a>
2007	KEOPS (KErguelen Ocean and Plateau compared Study)	BLAIN Stéphane (2007) VT 86 / KEOPS cruise, Marion Dufresne R/V. Sismar. <a href="https://doi.org/10.17600/7200040">https://doi.org/10.17600/7200040</a>
2004	EIFEX (European Iron Fertilization Experiment)	R/V Polarstern cruise ANT XXI/3
1998-2018	OISO (Océan Indien Service d'Observation)	METZL Nicolas, LO MONACO Claire (2018) VT 157 / OISO-28 cruise, RV Marion Dufresne, <a href="http://dx.doi.org/10.17600/18000005">http://dx.doi.org/10.17600/18000005</a> METZL Nicolas, LO MONACO Claire (2017) VT 153 / OISO-27 cruise, RV Marion Dufresne, <a href="http://dx.doi.org/10.17600/17009700">http://dx.doi.org/10.17600/17009700</a> METZL Nicolas, LO MONACO Claire (2016) VT 147 / OISO-25 cruise, RV Marion Dufresne, <a href="http://dx.doi.org/10.17600/16010000">http://dx.doi.org/10.17600/16010000</a> METZL Nicolas, LO MONACO Claire (2015) VT 142 / OISO-24 cruise, RV Marion Dufresne, <a href="http://dx.doi.org/10.17600/15003000">http://dx.doi.org/10.17600/15003000</a> LO MONACO Claire, METZL Nicolas (2014) VT 136 / OISO-23 cruise, RV Marion Dufresne, <a href="http://dx.doi.org/10.17600/14002700">http://dx.doi.org/10.17600/14002700</a> LO MONACO Claire (2013) VT 127 / OISO-22 cruise, RV Marion Dufresne, <a href="http://dx.doi.org/10.17600/13200090">http://dx.doi.org/10.17600/13200090</a> METZL Nicolas, LO MONACO Claire (2012) VT 120 / OISO-21 cruise, RV Marion Dufresne, <a href="http://dx.doi.org/10.17600/12200030">http://dx.doi.org/10.17600/12200030</a>

		<p>METZL Nicolas, LO MONACO Claire (2011) VT 117 / OISO-20 cruise, RV Marion Dufresne, <a href="http://dx.doi.org/10.17600/11200070">http://dx.doi.org/10.17600/11200070</a></p> <p>METZL Nicolas, LO MONACO Claire (2011) VT 114 / OISO-19 cruise, RV Marion Dufresne, <a href="http://dx.doi.org/10.17600/11200010">http://dx.doi.org/10.17600/11200010</a></p> <p>METZL Nicolas, LO MONACO Claire (2009) VT 108 / OISO-18 cruise, RV Marion Dufresne, <a href="http://dx.doi.org/10.17600/9200090">http://dx.doi.org/10.17600/9200090</a></p> <p>METZL Nicolas, LO MONACO Claire (2009) VT 105 / OISO 17 cruise, RV Marion Dufresne, <a href="http://dx.doi.org/10.17600/9200040">http://dx.doi.org/10.17600/9200040</a></p> <p>BRUNET Christian, METZL Nicolas (2008) VT 94 / OISO 16 cruise, RV Marion Dufresne, <a href="http://dx.doi.org/10.17600/8200080">http://dx.doi.org/10.17600/8200080</a></p> <p>METZL Nicolas (2007) VT 85 / OISO 15 cruise, RV Marion Dufresne, <a href="http://dx.doi.org/10.17600/7200030">http://dx.doi.org/10.17600/7200030</a></p> <p>BRUNET Christian, METZL Nicolas (2006) VT 81 / OISO 14 cruise, RV Marion Dufresne, <a href="http://dx.doi.org/10.17600/6200030">http://dx.doi.org/10.17600/6200030</a></p> <p>BRUNET Christian, METZL Nicolas (2005) VT 80 / OISO 13 cruise, RV Marion Dufresne, <a href="http://dx.doi.org/10.17600/5200070">http://dx.doi.org/10.17600/5200070</a></p> <p>BRUNET Christian, METZL Nicolas, QUEGUINER Bernard (2005) VT 79 / OISO 12 cruise, RV Marion Dufresne, <a href="http://dx.doi.org/10.17600/5200040">http://dx.doi.org/10.17600/5200040</a></p> <p>METZL Nicolas (2004) VT 62 / CARAUS - OISO 11 cruise, RV Marion Dufresne, <a href="http://dx.doi.org/10.17600/4200010">http://dx.doi.org/10.17600/4200010</a></p> <p>METZL Nicolas (2003) VT 60 / CARAUS - OISO 10 cruise, RV Marion Dufresne, <a href="http://dx.doi.org/10.17600/3200030">http://dx.doi.org/10.17600/3200030</a></p> <p>BRUNET Christian, METZL Nicolas (2002) VT 57 / OISO 9 cruise, RV Marion Dufresne, <a href="http://dx.doi.org/10.17600/2200070">http://dx.doi.org/10.17600/2200070</a></p> <p>METZL Nicolas (2002) OISO 8 cruise, RV Marion Dufresne, <a href="http://dx.doi.org/10.17600/2200010">http://dx.doi.org/10.17600/2200010</a></p> <p>BRUNET Christian, METZL Nicolas (2001) OISO 7 cruise, RV Marion Dufresne, <a href="http://dx.doi.org/10.17600/1200070">http://dx.doi.org/10.17600/1200070</a></p> <p>METZL Nicolas, PIERRE Catherine (2001) VT 51 / OISO 6 cruise, Marion Dufresne R/V. Sismer. <a href="https://doi.org/10.17600/1200010">https://doi.org/10.17600/1200010</a></p> <p>METZL Nicolas (2000) OISO5 (VT 49) cruise, Marion Dufresne R/V. Sismer. <a href="https://doi.org/10.17600/200100">https://doi.org/10.17600/200100</a></p> <p>METZL Nicolas (2000) OISO4 (VT 46) cruise, Marion Dufresne R/V. Sismer. <a href="https://doi.org/10.17600/200050">https://doi.org/10.17600/200050</a></p> <p>METZL Nicolas, LEFEVRE Fabien (1998) OISO3-NIVMER98 cruise, Marion Dufresne R/V. Sismer. <a href="https://doi.org/10.17600/98200080">https://doi.org/10.17600/98200080</a></p> <p>METZL Nicolas (1998) OISO2 cruise, Marion Dufresne R/V. Sismer. <a href="https://doi.org/10.17600/98200070">https://doi.org/10.17600/98200070</a></p> <p>METZL Nicolas (1998) OISO1 cruise, Marion Dufresne R/V. Sismer. <a href="https://doi.org/10.17600/98200060">https://doi.org/10.17600/98200060</a></p>
--	--	---

## **Methods SI.** Deployments and device details

Two types of bio-logging devices were used to obtain the tracking data used in this study: global positioning system loggers (GPS) and platform terminal transmitters, which obtained their satellite fixes via the Argos system (Argos). GPS obtain their location fixes from orbiting satellites and store them in an on-board flash memory card. These devices are very accurate (typically less than 5 m) and are able to record positional fixes as frequently as every second. However, power consumption is high and need to be retrieved in order to download the track data (though recent loggers can now upload data via satellite). Argos, although not as accurate as GPS (accuracy varies from a few kilometres to tens of kilometres), have a longer battery life and track data can be sent to a receiving station for download. Argos therefore allows for real-time tracking of animals by providing several locations (up to 20) per day.

Devices were fixed to the feathers of the back with cyanolycrate adhesive securely fastened with cable-ties for birds, and head with two-part epoxy adhesive for pinnipeds. For further details about capture and tag specifications refer to (Lea et al. 2002, Roquet et al. 2014, Bost et al. 2015).

## Methods SI. Diet description

Species	Colony	Diet description	Diet composition (%) <sup>^</sup>			
			crus	ceph	fish	othr
King penguin	Crozet	Chick food is dominated by <i>Kreffichthys anderssoni</i> , <i>Electrona carlsbergi</i> and <i>Protomyctophum tenisoni</i> ; cephalopod makes up the remainder of the diet.	0	10	90	0
	Kerguelen	Chick food is dominated by <i>Kreffichthys anderssoni</i> (myctophid) and the pelagic stage of the eel-cod <i>Muraenolepis marmoratus</i> is an important item in some years. Cephalopod make up the remainder of the diet.	0	10	90	0
Macaroni penguin	Heard	We assume diet is similar to birds from Kerguelen	0	10	90	0
	Crozet	The main crustacean prey is the subantarctic krill <i>Euphausia vallentini</i> and hyperiids including <i>Themisto gaudichaudii</i> . <i>Myctophid Kreffichthys anderssoni</i> is the major fish prey (caught in colder waters)	75	5	20	0
	Kerguelen	The main crustacean prey is the subantarctic krill <i>Euphausia vallentini</i> . <i>Myctophid Kreffichthys anderssoni</i> is the major fish prey	52	0	48	0
Wandering albatross	Heard	Chick food is dominated by crustacean prey, including the subantarctic krill <i>Euphausia vallentini</i> and hyperiids <i>Themisto gaudichaudii</i> (Green et al 1998, Deagle et al 2007, 2008). The proportion of crustacean prey in the diet falls steadily over the chick-rearing period and is replaced by myctophid, mostly <i>K. anderssoni</i> (Green et al 1998, Deagle et al 2008).	59	0	41	0
	Crozet	Chick food is dominated by adult cephalopod onychoteuthids <i>Kondakovia longimana</i> . Fish prey are mostly Patagonian toothfish <i>Dissostichus eleginoides</i>	0	75	18	7
Black-browed albatross	Kerguelen	We assume diet is similar to birds from Crozet. However, in 1998, cephalopod (46%) and toothfish (48%) were equally important; dominated by adult cephalopod onychoteuthids <i>Kondakovia longimana</i> and Patagonian toothfish <i>Dissostichus eleginoides</i> .	0	75	18	7
	Kerguelen	Chick food is dominated by fish that are neritic and slope species, followed by macaroni penguin carrion and juvenile ommastrephid cephalopod. Please note, how demersal prey are caught remains a mystery.	1	10	73	14
Dark-mantled albatross	Crozet	Fish, cephalopod and crustacean prey are pelagic. Bird carrions include crested penguins ( <i>Eudyptes</i> sp.) and prions ( <i>Pachyptila</i> sp.).	3	41	5	51
Antarctic fur seal	Kerguelen	Scat analysis show females feed mainly on myctophid including <i>Gymnoscopelus piabilis</i> , <i>Electrona subaspera</i> and <i>G. nicholsi</i> . In warmer years, myctophid consumption decreases, with a shift to the netric icefish <i>Champscephalus gunnari</i> . The main cephalopod prey is the ommastrephid <i>Martialia hyadesi</i> .	0	9	91	0
	Heard	We assume diet is similar to seals from Kerguelen	0	9	91	0
Southern elephant seal	Kerguelen	Blubber fatty acid profiles indicate that females likely feed on myctophid, and to a lesser extent, cephalopod (Newland et al. 2009). Feed on myctophid in deep water (isotope analysis indicate myctophid feed on crustacean; Cherel MEPS 2008).	0	30	70	0

<sup>^</sup> crus=crustacean, ceph=cephalopod, fish=fish, othr=other (often carrion)

Green, K., Williams, R. & Green, M. (1998). Foraging ecology and diving behaviour of macaroni penguins *Eudyptes chrysolophus* at Heard Island. *Mar. Ornithol.*, 26, 27–34

Deagle, B.E., Gales, N.J. & Hindell, M.A. (2008). Variability in foraging behaviour of chick-rearing macaroni penguins *Eudyptes chrysolophus* and its relation to diet. *Mar. Ecol. Prog. Ser.*, 359, 295–309

Newland, C., IC, F., PD, N. & CJA, B. (2009). Blubber fatty acid profiles indicate dietary resource partitioning between adult and juvenile southern elephant seals. *Mar. Ecol. Prog. Ser.*, 384, 303–312

Cherel Y, Ducatez S, Fontaine C, Richard P, Guinet C (2008) Stable isotopes reveal the trophic position and mesopelagic fish diet of female southern elephant seals breeding on the Kerguelen Islands. *Mar Ecol Prog Ser* 370:239–247

## Methods SI. Dive depth

		Daytime				Nocturnal			
Species	Colony	Description	min	max	mean	Description	min	max	mean
Wandering albatross	Kerguelen	Birds from South Georgia dive < 1 m (dives are rare) (Prince et al. 1994)	-	1	1		-	-	-
Black-browed albatross	Kerguelen	Birds from South Georgia dive to 2 m (1.5 dives day-1) (Sakamoto et al. 2009); $3 \pm 1$ m, 1 – 5 m (Feb-Aug 1993) (Prince et al. 1994); Prey capture observed at 48°S,57°W (2 mins) (Cobley 1996)	1	5	3	Birds from South Georgia dive up to 4 m (Sakamoto et al. 2009)	-	4	3
Dark-mantled albatross	Crozet	Light-mantled albatross from Kerguelen dive $5 \pm 3$ , 1 – 12 m (Nov-Dec 1992) (Prince et al. 1994)	1	12	5		-	-	-
Macaroni penguin	Crozet	15 – 70 m, max. 100 m	15	100	43	3 – 6 m	3	6	5
	Heard	10 – 60 m, max. 100 m (Nov-Feb 1992-93) (Green et al. 1998); $36 \pm 13$ m, 13 – 55 m (Guard, Dec-Jan 2003-04) (Deagle et al. 2008); $46 \pm 8$ m, 36 – 59 m (Crèche, Jan-Feb 2003-04) (Deagle et al. 2008). Birds dive predominately during daylight hours (Green et al 2005).	10	100	41	Only 2% dives > 10 m (i.e. foraging dives) occur 21h – 03h (Deagle et al. 2008)	-	10	6
	Kerguelen	Assume dive data from Crozet and Heard	13	100	42		3	8	5
Fur seal	Heard	Only 10% dives performed during the day; dive activity peaks around dawn and dusk (Goldsworthy et al. 2010)	-	-	-	$124 \pm 30$ m (deep); $30 \pm 4$ m (shallow) (Dec 2000 – Feb 2001) (Goldsworthy et al. 2010)	30	124	77

	Kerguelen	Only 10% dives performed during the day; dive activity peaks around dawn and dusk (Lea et al. 2002)	-	-	-	53 ± 17 m, 117 – 240 m (Dec-Mar, 1997-2000) (Lea et al. 2002); 56 ± 5 m, 11 – 99 m (warm, deep water, Feb 2000) (Lea & Dubroca 2003); 35 ± 3 m, 20 – 57 m (cool, shallow water, Feb 2000) (Lea & Dubroca 2003)	11	240	48
King penguin	Crozet	1995-96 breeding season (N=21) (Charrassin 2001): 204 ± 18 m (autumn crèche in transit); 204 ± 16 m (winter crèche in central phase); 161 ± 13 m (incubation in central phase); 167 ± 12 m (autumn crèche in central phase); 192 ± 9 m (brooding in central phase); 177 ± 16 m (PM in transit); 183 ± 11 m (PM in central phase)	-	-	184		-	-	-
	Kerguelen	148 ± 32 m, max. 272 m (Feb-Mar 1998-2001) (Charrassin et al. 2002); 131 ± 3 m (incubation), 148 ± 7 m (brood) (Jan-Mar 2005-06, 2010-11) (Scheffer et al. 2016)	-	272	142	med. 12 m, max. 60 m (Mar 1995) (Bost et al. 2002)	-	60	12
Southern elephant seal	Kerguelen	Dive data from post-breeding females from Macquarie Island: 382 ± 166 (max. 991), 589 ± 175 (max. 1152), 384 ± 166 (max. 911), 490 ± 169 (max. 1100), 347 ± 154 (max. 918), 395 ± 216 (max. 1256), 439 ± 216 (max. 1152), 423 ± 200 (max. 1256) (Hindell et al 1991)	-	1092	431	Dives from post-breeding females from Macquarie Island were 200-400 m deeper at night (Hindell et al 1991)	-	1392	731

Bost CA, Zorn T, Maho Y Le, Duhamel G (2002) Feeding of diving predators and diel vertical migration of prey: King penguins' diet versus trawl sampling at Kerguelen Islands. *Mar Ecol Prog Ser* 227:51–61

Charrassin J-B (2001) Utilisation of the oceanic habitat by king penguins over the annual cycle. *Mar Ecol Prog Ser* 221:285–298

Charrassin JB, Park YH, Maho Y Le, Bost CA (2002) Penguins as oceanographers unravel hidden mechanisms of marine productivity. *Ecol Lett* 5:317–319

- Cobley ND (1996) An observation of live prey capture by a black-browed albatross *Diomedea melanophrys*. *Mar Ornithol* 24:45–46
- Deagle BE, Gales NJ, Hindell MA (2008) Variability in foraging behaviour of chick-rearing macaroni penguins *Eudyptes chrysolophus* and its relation to diet. *Mar Ecol Prog Ser* 359:295–309
- Goldsworthy SD, Page B, Welling A, Chambellant M, Bradshaw CJA (2010) Selection of diving strategy by Antarctic fur seals depends on where and when foraging takes place. *Mar Ecol Prog Ser* 409:255-U273
- Green K, Williams R, Green M (1998) Foraging ecology and diving behaviour of macaroni penguins *Eudyptes chrysolophus* at Heard Island. *Mar Ornithol* 26:27–34
- Lea M-A, Dubroca L (2003) Fine-scale linkages between the diving behaviour of Antarctic fur seals and oceanographic features in the southern Indian Ocean. *ICES J Mar Sci* 60:990–1002
- Lea MA, Hindell M, Guinet C, Goldsworthy SD (2002) Variability in the diving activity of Antarctic fur seals, *Arctocephalus gazella*, at Iles Kerguelen. *Polar Biol* 25:269–279
- Prince PA, Huin N, Weimerskirch H (1994) Diving depths of albatrosses. *Antarct Sci* 6:353–354
- Sakamoto KQ, Takahashi A, Iwata T, Trathan PN (2009) From the Eye of the Albatrosses: A Bird-Borne Camera Shows an Association between Albatrosses and a Killer Whale in the Southern Ocean. *PLoS One* 4:1–4
- Scheffer A, Trathan PN, Edmonston JG, Bost CA (2016) Combined influence of meso-scale circulation and bathymetry on the foraging behaviour of a diving predator, the king penguin (*Aptenodytes patagonicus*). *Prog Oceanogr* 141:1–16



CCAMLR

Commission for the Conservation of Antarctic Marine Living Resources  
Commission pour la conservation de la faune et la flore marines de l'Antarctique  
Комиссия по сохранению морских живых ресурсов Антарктики  
Comisión para la Conservación de los Recursos Vivos Marinos Antárticos

WG-EMM-2019/71

10 juin 2019

Original: Français

WG-EMM

## Unfolding connectivity patterns along the Antarctic Circumpolar Current in the sub-Antarctic region

---

S. Sergi, G. Grizaud, C. Cotté and F. d'Ovidio



This paper is presented for consideration by CCAMLR and may contain unpublished data, analyses, and/or conclusions subject to change. Data in this paper shall not be cited or used for purposes other than the work of the CAMLR Commission, Scientific Committee or their subsidiary bodies without the permission of the originators and/or owners of the data.



# Unfolding connectivity patterns along the Antarctic Circumpolar Current in the sub-Antarctic region

Sara Sergi<sup>1</sup>, Guilhem Grizaud<sup>1,2,3</sup>, Cédric Cotté<sup>1</sup>, Francesco d'Ovidio<sup>1</sup>

<sup>1</sup> *Laboratoire d'Océanographie et du Climat (LOCEAN-IPSL), Sorbonne Université, Paris 75252, France*

<sup>2</sup> *Master Sciences de l'Océan, de l'Atmosphère et du Climat, Sorbonne Université, 4 place de Jussieu, Paris 75005, France*

<sup>3</sup> *Master in Environmental Policy, Paris School of International Affairs (SciencesPo), 28 rue des Saints-Pères, Paris 75007, France*

## **Abstract**

The sub-Antarctic region - here considered between the sub-Antarctic Front and the southern boundary of the Antarctic Circumpolar Current (ACC) - falls under many distinct jurisdictions, including Exclusive Economic Zones (EEZs) of several countries, as well as the areas of competence of several international bodies as the SEAFO, SIOFA and CCAMLR. However, in oceanographic terms, these zones appear mostly as a continuum, due to the connecting effect of the ACC. In this paper we review some techniques which have been developed recently in order to trace connectivity and dispersal patterns induced by the horizontal transport. These are satellite-based Lagrangian methods, which predict remarkably well the extent of phytoplanktonic blooms occurring for hundreds of kilometres in the wake of nutrient sources like islands, seamounts, and hydrothermal vents. These quantitative methods can be applied as well to areas under and beyond national jurisdictions. As an example, we show here the cross-boundary dispersal patterns of the water within and beyond the EEZs in the sub-Antarctic. These patterns inform on the incoming and outgoing pathways of tracers transported in the upper layer, like fish larvae and possible pollutants. The high connection of the physical and biological processes and the cross-boundary physical linkage suggests a geographically integrated evaluation of the sub-Antarctic region.

## **Executive Summary**

1. By drawing attention to the role of seamounts and hydrothermal vents in iron-fertilization (Fig. 4-5) we provide examples of processes which encompass the paradigm of the sub-Antarctic as a blue desert with isolated oceanic oases around islands. Indeed, the role of seamounts and hydrothermal vents in influencing phytoplankton distribution and abundance suggests switching to a connected vision of the region, accounting for vertical connectivity - the link between the topographic structures and the water above - as well as horizontal connectivity - due to the strong eastward Antarctic Circumpolar Current-.
2. Methods like Lagrangian tools and observations from high resolution remote sensing appear today as a mature approach for identifying physical connectivity pathways down to resolutions of few tens of km, and could be integrated in ongoing pelagic spatial planning activities for the eastern sub-Antarctic region (e.g. SC-CAMLR-XXXVII, paragraphs 6.60 to 6.62).

## Introduction

The physics of the Southern Ocean plays different roles on the flow of the biomass all along the food chain and on the organisation of biodiversity patterns. Hosting one of the strongest currents of world – the Antarctic Circumpolar Current (ACC) – the Southern Ocean presents a case in which horizontal transport links coastal and offshore areas and has a prominent structuring effect on the pelagic ecosystem. One of the most notable effects of horizontal advection is in the patterns of phytoplankton production. Pelagic primary production in the Southern Ocean in general has large availability of micronutrients (carbon, nitrogen and phosphorus compounds), but is limited in micro-nutrients, and notably iron (Martin, 1990; De Baar et al., 1995a; Sohrin et al., 2000; Boyd et al., 2000, 2010). In the sub-Antarctic region, when the eastward ACC encounters topographic features, it is enriched by iron which is then dispersed downstream in the open ocean for hundreds, and sometimes thousands, of kilometres. In springtime, when the mixed layer shallows and light is available to phytoplankton, massive blooms arise in the wake of islands and continental plateaus persisting for hundreds and thousands of kilometres (e.g. Bakker et al., 2007; Mongin et al., 2009; Sullivan et al., 1993; Lancelot et al., 2009; Ardyna et al., 2017). Studies combining multi-satellite data, circulation modelling, lithogenic isotopes, iron measurements, and drifters have highlight the predominant role of horizontal advection in these island mass effects (Borrione et al., 2014; d’Ovidio et al., 2015; Mongin et al., 2009; Ardyna et al., 2017).

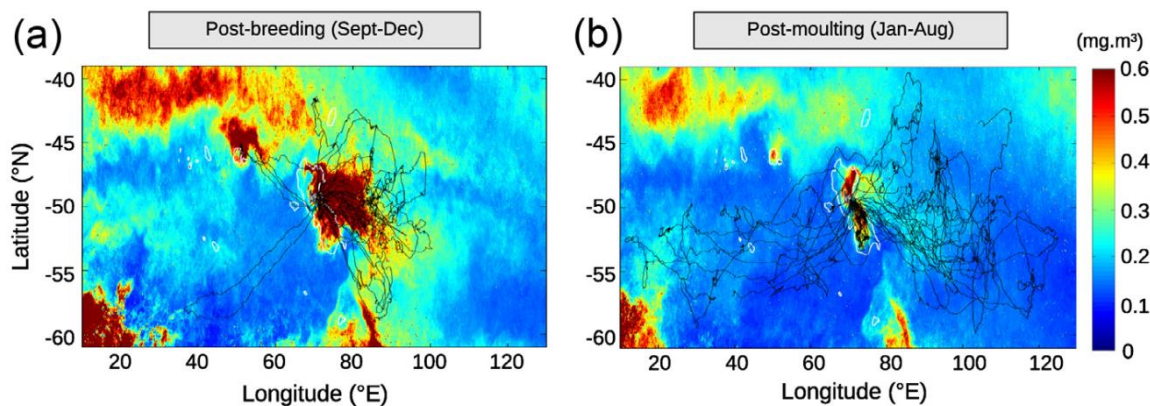


**Figure 1: Biological oases downstream of islands: the case of the Kerguelen plume.** During the bloom period a large scale chlorophyll plume spreads downstream of the Kerguelen plateau and elephant seals intensively forage in this area (a). In the post-bloom period, chlorophyll concentration are much lower and elephant seals forage further east downstream of the ACC (b). Elephant seal distribution and chlorophyll concentration climatologies are analysed between 2005 and 2011. Figure adapted from Cotté et al., (2015).

The biological oases downstream of sub-Antarctic islands contrast with an otherwise mostly oligotrophic environment (fig. 1). This large phytoplankton biomass in turn sustains numerous colonies of top predators breeding in the islands (De Broyer et al., 2014). Pinnipeds and seabirds intensively forage in the chlorophyll-a plumes downstream of the Kerguelen plateau (o'Toole et al., 2017; Lea et al., 2006; Cotté et al., 2015; Guinet et al., 2001), the Crozet archipelago (Bon et al., 2015; Koubbi et al., 2016) and South Georgia (Scheffer et al., 2010; Barlow and Croxall, 2002; Staniland et al., 2004; Rogers et al., 2015). Animals not only feeds in the chlorophyll plumes during summer times, but they also follow during winter the water masses which supported chlorophyll-a in springtime drifting along the ACC as observed for the Southern elephant seals (Cotté et al. 2015, see also fig. 1). Similarly, Macaroni penguins forage further east downstream of the spring chlorophyll plume in winter compared to the summer foraging grounds (Bost et al., 2009).

This document has two aims. The first is to summarize past studies and briefly show where the main dispersal patterns of ecological relevance induced by the ACC occur. In this regard, horizontal advection is a useful tool to integrate spatial and temporal lags reproducing the development and maturation of the pelagic trophic chain along the ACC. The identification of dispersal patterns however has a larger scope than ecological studies, because these techniques can map the horizontal pathways to and from any region of interest. The second aim of this document is to develop an example of this more general application by showing how the Exclusive Economic Zone (EEZ) surface water masses are connected by the ACC and can be tracked from information about the surface circulation. This information may be useful when estimating fish larval connectivity or pollutant dispersal among zones under different jurisdictions.

## **Drifting along the ACC: unraveling connectivity of the biological production in the sub-Antarctic**

Marine phytoplankton production drives marine ecosystem trophic-structures (Frederiksen et al., 2006; Iverson, 1990; Boersma et al., 2009; Block et al., 2011) and ecosystem services, as carbon export into the deep ocean (Michaels and Silver, 1988; Legendre and Rassoulzadegan, 1995) or fisheries production (Chassot et al., 2010). Consequently, delineating the control of algal productivity has major implications for modelling activities, as the parameterization of nutrient input adopted in biogeochemical models (Tagliabue et al., 2014; Lancelot et al., 2009; Aumont and Bopp, 2006), for the identification of biological hotspots and for the management and conservation of marine living resources (Santora et al., 2017; Gove et al., 2016). In this section we describe the main connectivity patterns driving phytoplankton production in the sub-Antarctic, both in terms of horizontal and vertical connectivity, focusing on processes that have been underestimated in the past years.

## 1. Horizontal connectivity: islands and seamounts

At the circumpolar scale, northern from the ice margin, phytoplankton blooms are triggered by the interaction of the ACC with the topography (e.g. Sullivan et al., 1993; Lancelot et al., 2009; Ardyna et al., 2017). As described above, the effect of islands and continental lands in structuring the primary production and successively the trophic chain has been largely documented. In particular, the advection of particles from shallow topography has been validated in several studies as a representation of the island mass effect (e.g. d'Ovidio et al., 2015; Sanial et al., 2014, 2015; Mongin et al., 2009). As for instance, figure 2 shows a circumpolar distribution of iron delivery downstream of islands and continental lands by applying an exponential scavenging relation - based on in situ iron measurements - to the time of the contact of the water parcels with the topographic features (for more details refer to Ardyna et al., 2017).

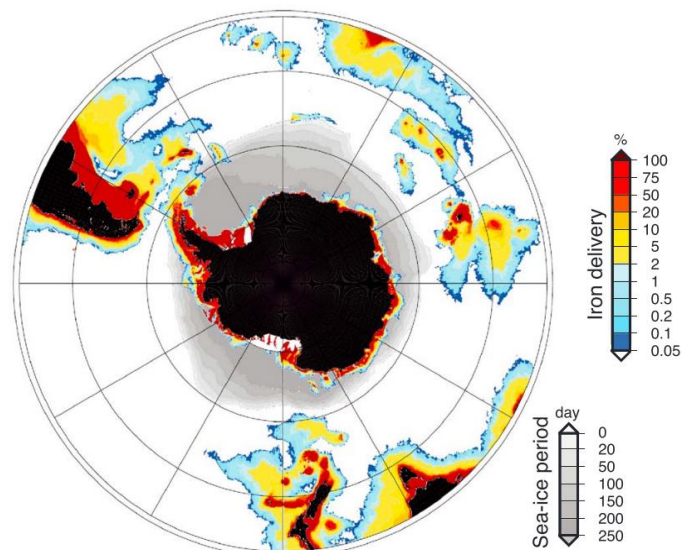


**Figure 2: Lagrangian estimation of continental and island control of phytoplankton in the Southern Ocean.** Use of a Lagrangian model based on altimetry for estimating the iron delivery downstream of shallow topography (%; percent of iron remaining in a water parcel after scavenging in respect to its initial concentration acquired in shallow areas; red to blue). Red areas shows the shallow areas (<500 m). Note that areas characterized by a seasonal sea ice cover are also shown (grey). Figure adapted from Ardyna et al., (2017).

These Lagrangian analyses (Lehahn et al., 2018) are then used to reconstruct the chlorophyll plume downstream of islands. As for instance figure 3 shows two examples where the extension and the shapes of the chlorophyll plumes downstream of Crozet (a) and Kerguelen (b) are reconstructed with the horizontal advection (respectively c and d). These methods allows not only to reconstruct the chlorophyll pathway, but also to assess the rates and time scales for the offshore transport of surface waters, identify the different flows of water feeding the phytoplankton plume and guide adaptive sampling strategies for biogeochemical campaigns (Sanial et al., 2014, d'Ovidio et al., 2015). In the following we present ongoing



results identifying connectivity patterns between deeper structures - as seamounts - and the shallow primary production.

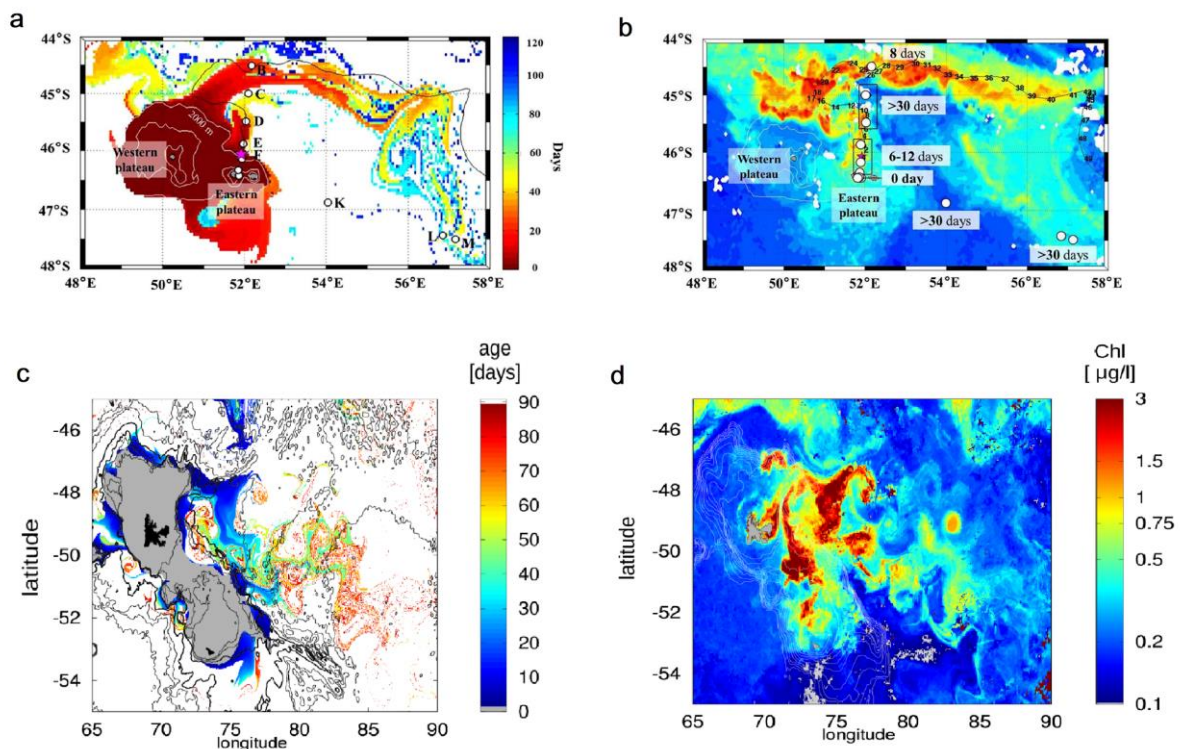


**Figure 3:** Lagrangian prediction of the chlorophyll plumes downstream of the Crozet shelf (a-b) and the Kerguelen plateau (c-d). The number of days since a water parcel has left the plateau, here called “age”, (a-c) is compared with the chlorophyll-a concentration measured by satellite (b-d). For the Crozet chlorophyll plume, the ages of surface waters derived from the Lagrangian model based on altimetry are compared with isotope measurements (apparent radium ages derived from the  $^{224}\text{Ra}/^{228}\text{Ra}$  ratios; stations are located by white dots) and the equivalent transit time of a drifter (black line) since its deployment location (magenta star) (a-b). Figures are adapted from Sanial et al., 2014 (a-b) and d’Ovidio et al., 2015 (c-d).

Differently to the role of islands and continental lands, the relationship between chlorophyll and submerged topographic highs is still debated. On one hand the theory in biology on “seamount effects” has been supported by numerous observations of local increased primary and secondary production close to the seamounts (Fock et al., 2002; Comeau et al., 1995) and recent analyses of very high resolution bathymetric data have permitted to identify numerous seamounts at shallow depth (<1000 m) including in the sub-Antarctic region (Yesson et al., 2011). On the other hand, the past analyses conducted in this region concluded that the shallow seamounts does not seem to fertilize the surrounding waters (e.g. Graham et al., 2015; Ardyna et al., 2017). Here we use the Lagrangian model with the high resolution seamounts dataset provided by Yesson et al. (2011) to reproduce chlorophyll patterns from the seamounts shallower of 1000 m depth of the Shona Ridge System (CCAMLR sub-region 48.6) following the ongoing analyses from Sergi et al. *in prep* (Fig. 4).

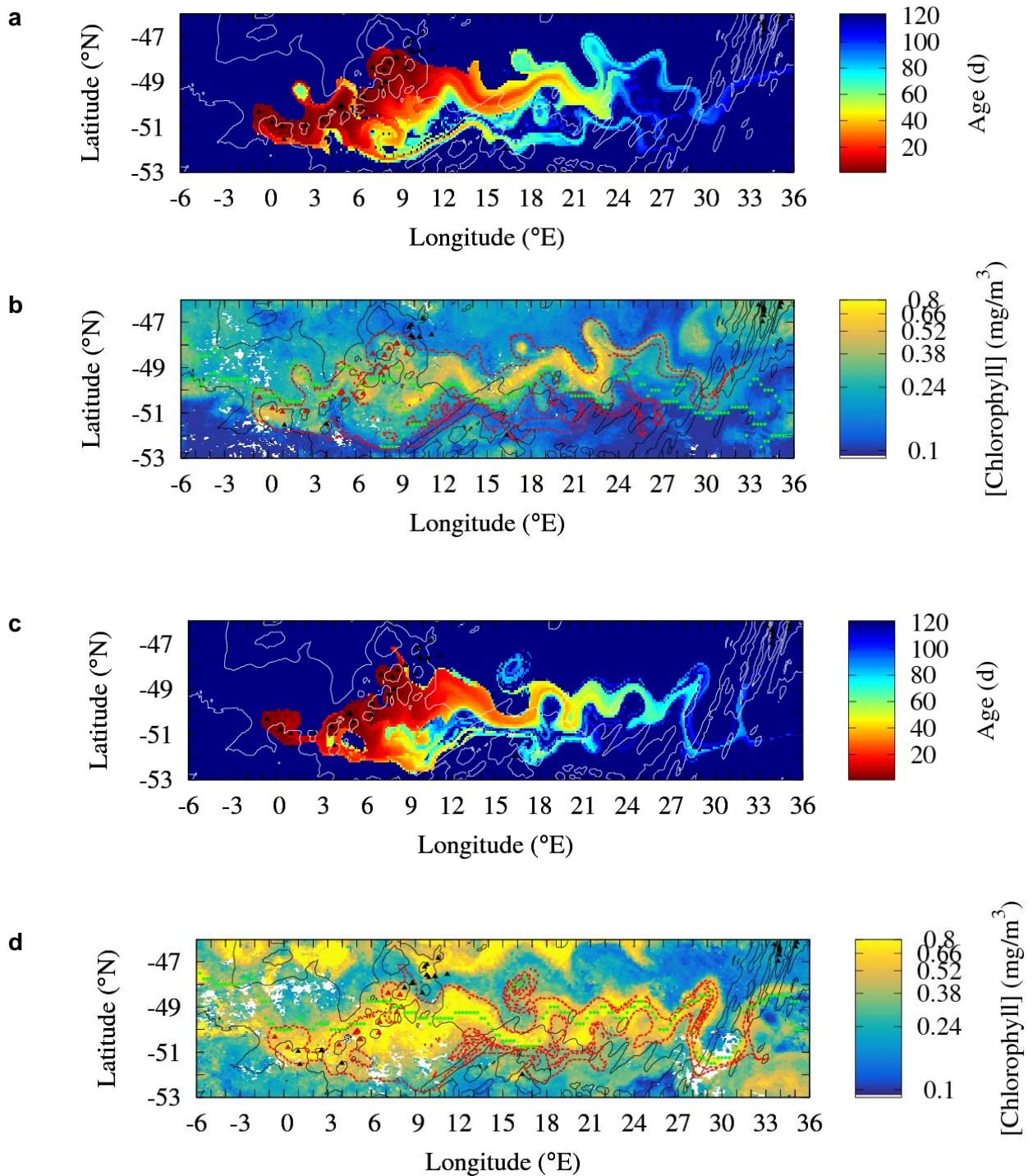


**Figure 4: Observation of the seamount mass effect on the Shona Ridge system in the summer seasons 2003/2004 (a-b) and 2004/2005 (c-d).** The chlorophyll-a concentration in February 2004 (a) and December 2004 (c) are respectively compared with the age of particle horizontally advected from the seamounts selected of the Shona Ridge systems on the 2004/2/15 (b) and 2004/12/15 (d). Shallow seamounts (<1000 m depth) are located by triangles in all the panels. Among these the red ones indicates the "possible fertilizing seamounts" selected with a distance of 90 km from the PF position (b-d). Red contours indicates the water masses that have been in contact in the 100 days before the blooms event with the "possible fertilizing seamounts" (b-d). Isobaths of bottom topography of 3000 m and 4100 m depths are showed in black (b-d) and in white (a-c). PF position during February 2004 period is shown with the green dots (b-d).

The analysis of the Shona Ridge System (Fig. 4) is a remarkable example of the important role of horizontal advection in the structuring of primary production. The chlorophyll pathway are stretched in February 2004 and December 2004 along the intense current branch (Fig. 4 b and d respectively). The Lagrangian model estimates that in 100 days water masses are advected longitudinally, for a mean latitude of 49° S, for almost 2000 km (Fig. 4 a and c). The model identify here the time, in days, since the particles left the “fertilizing seamounts” (here defined as seamounts in a distance of 90 km from the PF location, for more details on methods refer to Sergi et al. in prep). In particular the water masses within the red contour (Fig. 4 b and d) were in contact with the seamounts "touched" by the enriched plume (here definite as the "fertilizing seamounts") in the last 100 days before each bloom period.

In both cases pattern of the Lagrangian model reproduce the pattern of chlorophyll, in terms of extension and shape, reproducing meanders and mesoscale features, like the chlorophyll patch trapped by a mesoscale eddy around 17°E 48.5 °S in February 2004 (fig. 4a). During the two studied periods the mean chlorophyll concentration is about 40% higher in the water masses that were in contact in the last 100 days with the "fertilizing seamounts" rather than elsewhere in the maps. These analyses provides the first observational evidence of seamount mass effect associated to the Shona Ridge System. Similar analyses are computed for the seamounts of the South-West Indian Ridge, east of Bouvet (here not shown). Lagrangian altimetry (Lehahn et al. 2018) is successfully used to translate spatial and temporal lags between the seamounts location and primary production and thus identify fertilizing processes undetected in past studies.

In the next section we resume recent scientific advances on a second iron source that has also been largely underestimated in the past and that identify new connectivity patterns for the sub-Antarctic region.

## **2. Vertical connectivity: from deep hydrothermal vents to subsurface chlorophyll blooms**

In addition to the classic iron inputs, as the fertilization from shallow topography or the nutrient input from the season variability of the mixed layer depth (e.g. Ardyna et al., 2017), an additional iron source is emerging as a possible new actor: the hydrothermal iron. The interest in hydrothermal iron as a possible important nutrient input for the Southern Ocean primary production has been supported by scientific advances in three main directions. Firstly, a modelling study has demonstrated that observation of dissolved iron in the Southern ocean can be replicated in simulations only including hydrothermal sources (Tagliabue et al., 2010). Secondly, observations have shown important deep iron's input and the stabilization of the iron plumes kilometers far away from active venting sites (Wu et al., 2011; Bennett et al., 2008; Resing et al., 2015). Thirdly, these discoveries are justified by recent discoveries in biochemistry: differently to what was previously believed, the iron input from hydrothermal vent does not completely precipitate at the proximity of the vent. On the contrary, the iron's



complexation with ligand makes it more bioavailable and keeps it in a stable form (Sander and Koschinsky, 2011; Bennett et al., 2008). In addition, about 10% of dissolved iron (<200 nm) input from the hydrothermal vents to the deep ocean is in the form of nanoparticulate pyrite which has been suggested to be more resistant to oxidation than dissolved Fe(II) and FeS (Yucel et al., 2011). At the same time, studies highlight that intense upward movements generated from the interaction of the ACC, and its fronts, with large and deep (> 2500 m depth) topographic features all over the Southern Ocean may introduce deep iron in the upper ocean and sustain the phytoplankton productivity (Sokolov and Rintoul, 2007).

In this context, Ardyna et collaborators (2019) linked the important vertical motion and the hydrothermal iron availability, by providing the first observations of intense phytoplankton blooms in the Southern Ocean supported by upwelled hydrothermally influenced deep waters. Their conclusions are supported by observations of intense chlorophyll blooms from BGC-Argo floats, in situ measurement of the hydrothermal tracer helium-3 ( $^3\text{He}$ ) (Fitzsimmons et al., 2014) which is correlated to hydrothermal iron (Resing et al., 2015), and connectivity pathways, linked both to the identification of vertical isopycnal displacement - suggesting the upwelling downstream of the mid-ocean ridge - and to the Lagrangian dispersal of iron in the upper ocean. The ocean-ridge influenced blooms, their frequencies and their biomass is there included to the assessment of the environmental forcing on phytoplankton production in the Southern Ocean (Fig.5).

By connecting the hydrothermal vents along the South-West Indian Ridge, East from Bouvet, to intense chlorophyll blooms in the Enderby Basin, south of the Del Cano Rise (CCAMLR sub-areas 58.4.4a and 58.7), these results identify a new bio-physical connectivity pathway for the pelagic sub-Antarctic. In complement to this non-exhaustive review of connectivity processes structuring the phytoplankton production from islands, seamounts and deep hydrothermal vents, in the next section we apply the Lagrangian model previously described to the geopolitical boundaries of the sub-Antarctic region.

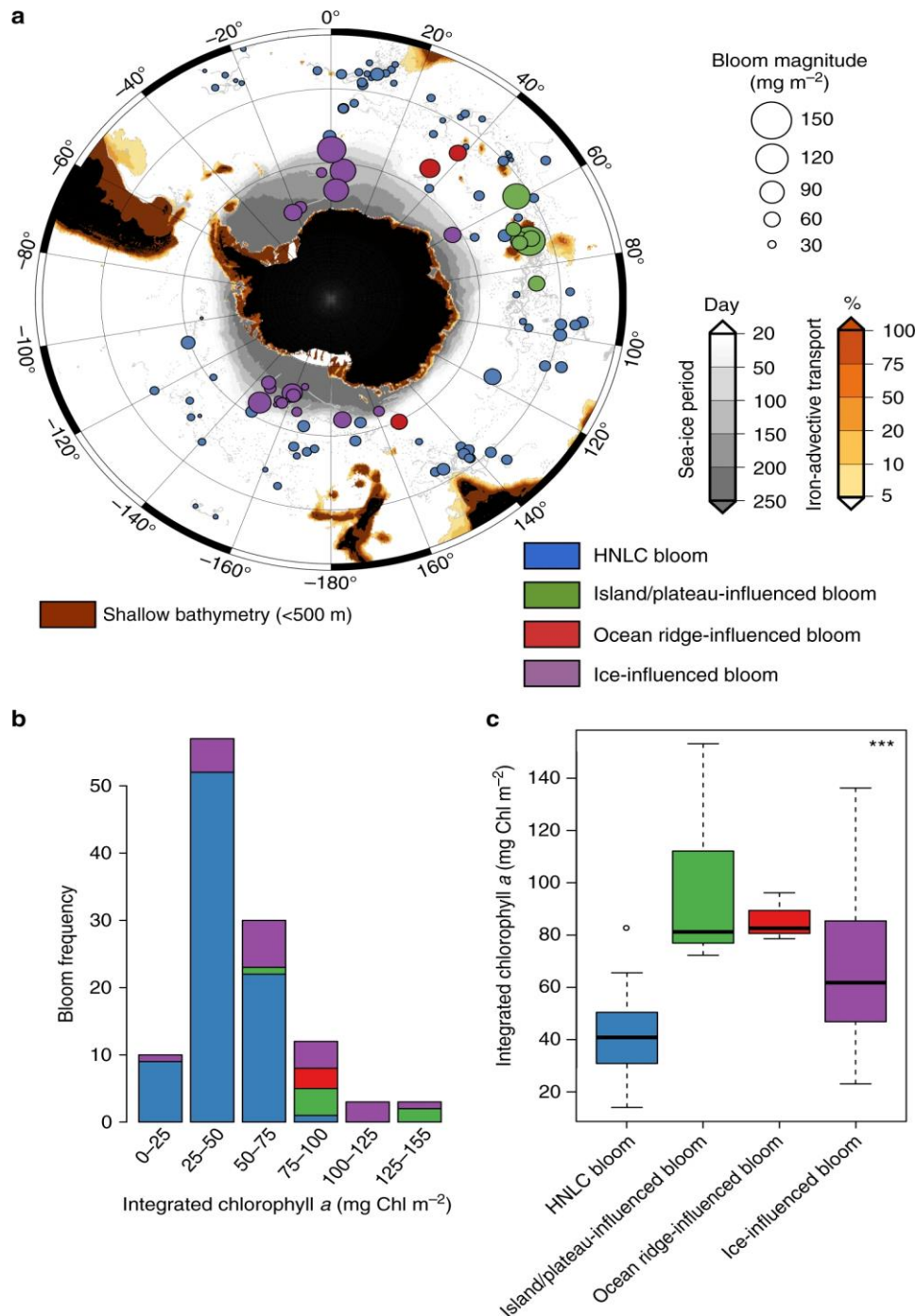


**Figure 5: Environmental control of phytoplankton blooms observed by BGC-Argo in the Southern Ocean: island/plateau influenced blooms (green), HNLC blooms (blue), ice-influenced blooms (purple) and ocean ridge-influenced blooms (red).** Map of the different bloom types sampled (a). The magnitude of the bloom (i.e., the maximum depth-integrated biomass) is related to the size of the colored circles. The gray dots indicate the individual float profiles. Similarly to fig. 2 shallow areas (<500m) are shown in red, areas characterized by a seasonal sea ice cover are shown in grey and the Lagrangian model based on altimetry is used for estimating the iron delivery downstream of shallow topography (%; percent of iron remaining in a water parcel after scavenging in respect to its initial concentration acquired in shallow areas). Histograms of the bloom frequency (b) and boxplot of the bloom magnitude (c) are also shown depending on the environmental control. The figure has been extracted from Ardyna et al., (2019), refer to the paper for more details.

## Connectivity of water masses under national jurisdictions

Due to the strong ACC, any activity (fishing, seabed mining, marine pollution; but spill-out effects of marine protected areas as well) may have an impact over a large spatial and temporal extent. Here we illustrate the physical connectivity of zones under and beyond national jurisdictions by tracking water masses within the sub-Antarctic EEZs along the ACC. For this we advect the water masses using altimetry-derived velocities and seeking when they reach the EEZs. The area under the influence of the water contained inside the EEZs can be similarly identified by advecting water parcels from the EEZs. This is the same Lagrangian model used in figure 4. As a first approximation, we considered the 200 nautical mile disk around the center of the islands under national jurisdiction as the EEZ. The aim is to assess the potential spatial and temporal extent of an activity happening within the EEZ of one State and to show how this can affect a huge area extending to the high seas and other national jurisdictions.

Figure 6a shows all the water masses that reach an EEZ after a certain period of time since the 1st January, 2015. It represents the area from where an activity or a measure could impact the water under national jurisdiction on a time horizon up to four months. As a complement, figure 5b locates the water masses which were in the last four months before the 1st January 2015 within the EEZ. It represents the area potentially impacted by an activity or a measure undertaken in the sub-Antarctic EEZs under the same time horizon. The analysis reproduces the distinctive circulation pathways of the region, as the intense branch of the ACC in the Drake Passage. Water masses in the Drake passage reach South Georgia (more than 2000 km away) in less than four months (Fig. 6a). Indeed the intense jet associated to the SAF with typical velocities exceeding 50 cm/s illustrates the amplitude of the eastward surface current in this region (Cunningham and Pavic, 2007; Lenn et al., 2007). Meanwhile, the analysis highlights some unexpected connections. The divergent pathway upstream of Bouvet Island EEZ indicates an important distant origin of water masses influencing this jurisdictional region (fig. 6a). Further analyses over different time period may be undertaken to test the representativeness of this pattern. Although the time period has been chosen arbitrarily, this work could be done for any date and period depending on the question raised. In any case these examples clearly highlight the linkage between the sub-Antarctic EEZ and between the areas under and beyond the national jurisdictions.

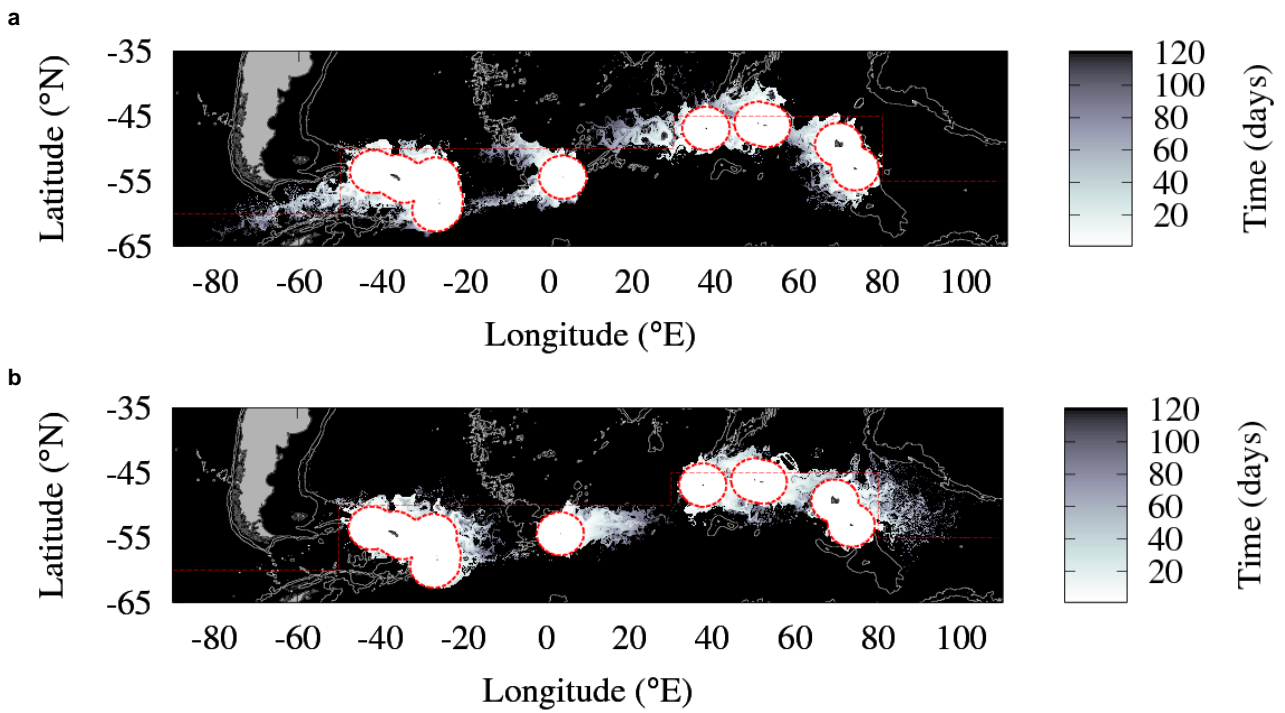


**Figure 6: Connectivity between the EEZ.** Distance in time of water masses that will influence the EEZs (a) and of water masses influenced by the EEZs (b). The advection of particle are computed forward in time from the 1st of January, 2015 (a) and back in time since 1st January, 2015 (b). Red dashed lines delimit the Convention Area of CCAMLR and the EEZs (bold lines). Isobaths at 1000 and 3000 m depth are shown in white.

## Discussion

Connectivity progressively emerged as a key component of the relevance and design of conservation measures for the marine environment (e.g. Roberts et al., 2006; Salm et al., 2006; Almany et al., 2009; Foley et al., 2010). Identifying the interconnections between populations, habitats and ecosystems and studying them in the light of climate change becomes a priority (e.g. Andrello et al., 2015; Magris et al., 2014). Generally, these mechanisms are addressed in terms of the ecological connectivity, i.e. the exchange of individuals among geographically separated sub-populations (Cowen and Sponaugle, 2009). In this context the analysis of the dynamical connectivity is a key tool to reproduce the Lagrangian dispersal of planktonic organisms (Lehahn et al. 2018), as fish larvae (e.g. Christie et al., 2010, Rossi et al., 2014). Here we focus on some dynamical mechanisms structuring the primary production and ultimately some trophic hotspots at a regional scale. More specifically, as a first step, we review the horizontal transport pathways present in the sub-Antarctic and the Lagrangian tools used to predict them from satellite data (Fig. 1, 2 and 3). In a second step, we remark some interconnections processes between underwater features like seamounts and hydrothermal vents, far away from the islands, and near-surface primary production (Fig. 4 and 5). The strong connectivity of the physical and biological processes over a large spatial and temporal extent is then further explored by looking at the dynamical connectivity patterns between the different jurisdictional frameworks (Fig. 6).

The sub-Antarctic provide an interesting study case where several trophic levels aggregate in the same areas, downstream of islands, which appear as marine biological oases. Indeed the local advective and iron supply processes from islands and continents mainly drives the zonally asymmetries in the phytoplankton biomass (Ardyna et al., 2017) and the higher trophic levels aggregate on the large scale phytoplankton high (e.g. Cotté et al., 2015; Toole et al., 2017; Lea et al., 2006; Bon et al., 2015; Koubbi et al., 2016; Scheffer et al., 2010; Barlow and Croxall, 2002; Rogers et al., 2015; De Broyer et al., 2014). In this particular context, the advection of water parcels enriched in nutrients by the topography has been validated in several studies as a representation of the island mass effect (e.g. d'Ovidio et al., 2015; Sanial et al., 2014, 2015; Ardyna et al., 2017; Mongin et al., 2009) and this method is used in ongoing works for disentangling the distribution of top predators after the bloom season (Cotté et al. in prep.; o'Toole et al. in rev.) filling the spatio-temporal lags characterizing the maturation of the pelagic trophic chain. The role of the ACC can be seen as a giant surface conveyor belt of the water masses in the sub-Antarctic ocean. In this regard ecological temporal lags (for instance, the delay between primary and secondary production) are translated into spatial lags (in this example, the distance between a foraging site, the upstream location of a phytoplanktonic bloom and its nutrient sources, as sketched in Fig. 7).

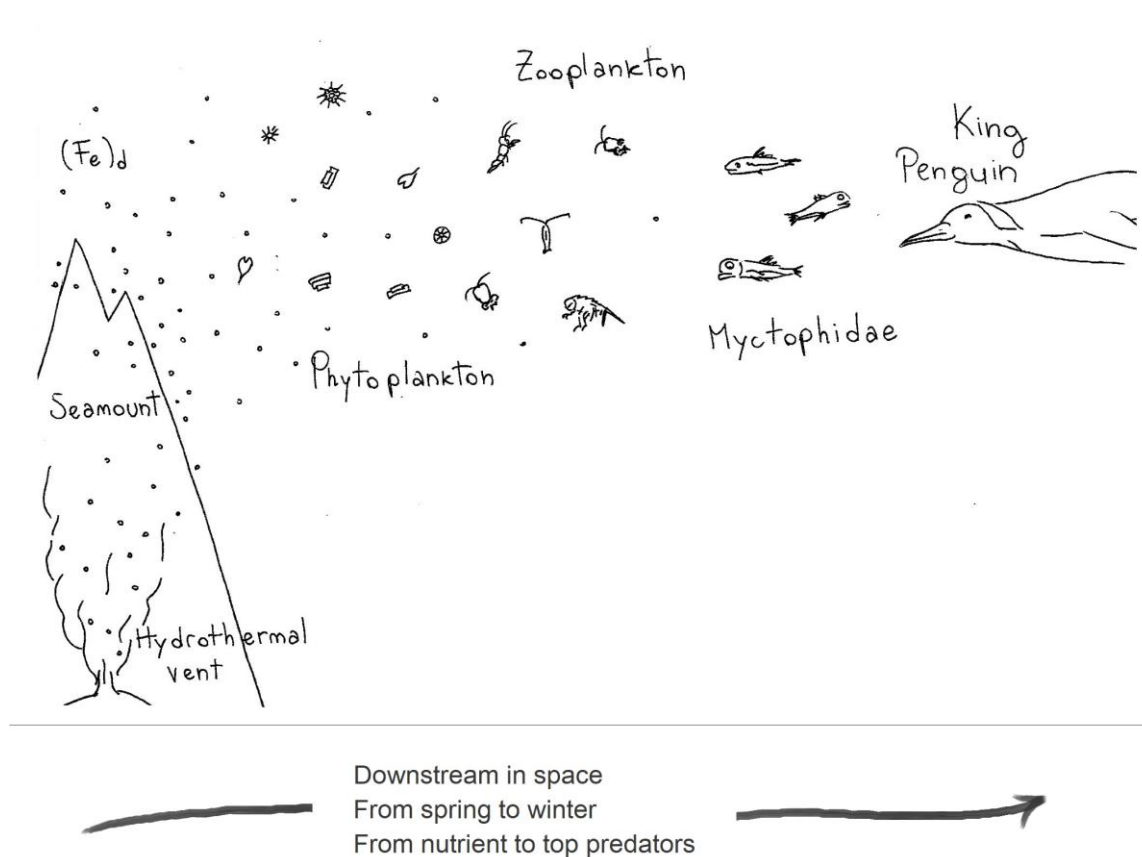


**Figure 7: Schematic representation of the spatial and temporal lags structuring the trophic chain along the ACC.** Hydrothermal vents and seamounts are added as iron sources for the primary production.

For the case of seamounts and hydrothermal vents we limited our synthesis in this document to primary production, which is the aspect most explored by the scientific literature. However recent observations suggest that several foraging hotspots are located downstream of these submerged features, in analogy to what has been found in the wake of sub-Antarctic islands. A notable example is the region south of the Crozet Islands (CCAMLR sub-areas 58.6 and 58.4.4b) which feed the highest colony of king penguin of the Southern Ocean (Bost et al., 2015; Le Bohec et al., 2008; Péron et al., 2012). A second interesting area is located in the sub-Antarctic region between 0 and 40°E. There, increased studies evidence that numerous predators breeding at the Prince Edward Islands, still forage in the Polar region but in this case undertow of the ACC, in the southern Agulhas Basin (Pistorius et al., 2017; Arthur et al., 2017; Reisinger et al., 2018). Our understanding of the distribution of these foraging hotspots may be revisited in the light of mechanisms here described for the sub-Antarctic region: the seamount effect of the Shona Ridge System in the Southern Agulhas Basin and the blooms influenced by hydrothermal vents in the Enderby Basin.

## References

- Almany, G. R., Connolly, S. R., Heath, D. D., Hogan, J. D., Jones, G. P., McCook, L. J., ... & Williamson, D. H. (2009). Connectivity, biodiversity conservation and the design of marine reserve networks for coral reefs. *Coral Reefs*, 28(2), 339-351.
- Andrello, M., Mouillot, D., Somot, S., Thuiller, W., & Manel, S. (2015). Additive effects of climate change on connectivity between marine protected areas and larval supply to fished areas. *Diversity and Distributions*, 21(2), 139-150.
- Ardyna, M., Claustre, H., Sallée, J. B., D'Ovidio, F., Gentili, B., Van Dijken, G., ... & Arrigo, K. R. (2017). Delineating environmental control of phytoplankton biomass and phenology in the Southern Ocean. *Geophysical Research Letters*, 44(10), 5016-5024.
- Ardyna, M., Lacour, L., Sergi, S., d'Ovidio, F., Sallée, J. B., Rembauville, M., ... & Claustre, H. (2019). Hydrothermal vents trigger massive phytoplankton blooms in the Southern Ocean. *Nature communications*, 10, 2451.
- Arthur, B., Hindell, M., Bester, M., De Bruyn, P. N., Trathan, P., Goebel, M., & Lea, M. A. (2017). Winter habitat predictions of a key Southern Ocean predator, the Antarctic fur seal (*Arctocephalus gazella*). *Deep Sea Research Part II: Topical Studies in Oceanography*, 140, 171-181.
- Aumont, O., & Bopp, L. (2006). Globalizing results from ocean in situ iron fertilization studies. *Global Biogeochemical Cycles*, 20(2).
- Bakker, D. C., Nielsdóttir, M. C., Morris, P. J., Venables, H. J., & Watson, A. J. (2007). The island mass effect and biological carbon uptake for the subantarctic Crozet Archipelago. *Deep Sea Research Part II: Topical Studies in Oceanography*, 54(18-20), 2174-2190.
- Barlow, K. E., & Croxall, J. P. (2002). Seasonal and interannual variation in foraging range and habitat of macaroni penguins *Eudyptes chrysolophus* at South Georgia. *Marine Ecology Progress Series*, 232, 291-304.
- Bennett, S. A., Achterberg, E. P., Connelly, D. P., Statham, P. J., Fones, G. R., & German, C. R. (2008). The distribution and stabilisation of dissolved Fe in deep-sea hydrothermal plumes. *Earth and Planetary Science Letters*, 270(3-4), 157-167.
- Block, B. A., Jonsen, I. D., Jorgensen, S. J., Winship, A. J., Shaffer, S. A., Bograd, S. J., ... & Ganong, J. E. (2011). Tracking apex marine predator movements in a dynamic ocean. *Nature*, 475(7354), 86.
- Boersma, P. D., Rebstock, G. A., Frere, E., & Moore, S. E. (2009). Following the fish: penguins and productivity in the South Atlantic. *Ecological Monographs*, 79(1), 59-76.
- Bon, C., Della Penna, A., d'Ovidio, F., Arnould, J. Y., Poupart, T., & Bost, C. A. (2015). Influence of oceanographic structures on foraging strategies: Macaroni penguins at Crozet Islands. *Movement ecology*, 3(1), 32.
- Borrione, I., Aumont, O., Nielsdóttir, M. C., & Schlitzer, R. (2014). Sedimentary and atmospheric sources of iron around South Georgia, Southern Ocean: a modelling perspective. *Biogeosciences*, 11(7), 1981-2001.
- Bost, C. A., Cotté, C., Bailleul, F., Cherel, Y., Charrassin, J. B., Guinet, C., ... & Weimerskirch, H. (2009). The importance of oceanographic fronts to marine birds and mammals of the southern oceans. *Journal of Marine Systems*, 78(3), 363-376.
- Bost, C. A., Cotté, C., Terray, P., Barbraud, C., Bon, C., Delord, K., ... & Weimerskirch, H. (2015). Large-scale climatic anomalies affect marine predator foraging behaviour and demography. *Nature communications*, 6, 8220.
- Boyd, P. W., Watson, A. J., Law, C. S., Abraham, E. R., Trull, T., Murdoch, R., ... & Charette, M. (2000). A mesoscale phytoplankton bloom in the polar Southern Ocean stimulated by iron fertilization. *Nature*, 407(6805), 695.
- Boyd, P. W., & Ellwood, M. J. (2010). The biogeochemical cycle of iron in the ocean. *Nature Geoscience*, 3(10), 675.



- Chassot, E., Bonhommeau, S., Dulvy, N. K., Mélin, F., Watson, R., Gascuel, D., & Le Pape, O. (2010). Global marine primary production constrains fisheries catches. *Ecology letters*, 13(4), 495-505.
- Christie, M. R., Tissot, B. N., Albins, M. A., Beets, J. P., Jia, Y., Ortiz, D. M., ... & Hixon, M. A. (2010). Larval connectivity in an effective network of marine protected areas. *PloS one*, 5(12), e15715.
- Comeau, L. A., Vézina, A. F., Bourgeois, M., & Juniper, S. K. (1995). Relationship between phytoplankton production and the physical structure of the water column near Cobb Seamount, northeast Pacific. *Deep Sea Research Part I: Oceanographic Research Papers*, 42(6), 993-1005.
- Cotté, C., d'Ovidio, F., Dragon, A. C., Guinet, C., & Lévy, M. (2015). Flexible preference of southern elephant seals for distinct mesoscale features within the Antarctic Circumpolar Current. *Progress in Oceanography*, 131, 46-58.
- Cowen, R. K., & Sponaugle, S. (2009). Larval dispersal and marine population connectivity. *Annual review of marine science*, 1, 443-466.
- Cunningham, S., & Pavic, M. (2007). Surface geostrophic currents across the Antarctic circumpolar current in Drake Passage from 1992 to 2004. *Progress in Oceanography*, 73(3-4), 296-310.
- d'Ovidio, F., Della Penna, A., Trull, T. W., Nencioli, F., Pujol, M. I., Rio, M. H., ... & Blain, S. (2015). The biogeochemical structuring role of horizontal stirring: Lagrangian perspectives on iron delivery downstream of the Kerguelen plateau. *Biogeosciences*, 12(19), 5567-5581.
- De Baar, H. J., De Jong, J. T., Bakker, D. C., Löscher, B. M., Veth, C., Bathmann, U., & Smetacek, V. (1995). Importance of iron for plankton blooms and carbon dioxide drawdown in the Southern Ocean. *Nature*, 373(6513), 412.
- De Broyer, C., Koubbi, P., Griffiths, H., & Grant, S. A. (2014). *Biogeographic atlas of the Southern Ocean* (p. 498). Cambridge: Scientific Committee on Antarctic Research.
- Fitzsimmons, J. N., Boyle, E. A., & Jenkins, W. J. (2014). Distal transport of dissolved hydrothermal iron in the deep South Pacific Ocean. *Proceedings of the National Academy of Sciences*, 111(47), 16654-16661.
- Fock, H., Uiblein, F., Köster, F., & Von Westernhagen, H. (2002). Biodiversity and species–environment relationships of the demersal fish assemblage at the Great Meteor Seamount (subtropical NE Atlantic), sampled by different trawls. *Marine Biology*, 141(1), 185-199.
- Foley, M. M., Halpern, B. S., Micheli, F., Armsby, M. H., Caldwell, M. R., Crain, C. M., ... & Carr, M. H. (2010). Guiding ecological principles for marine spatial planning. *Marine Policy*, 34(5), 955-966.
- Frederiksen, M., Edwards, M., Richardson, A. J., Halliday, N. C., & Wanless, S. (2006). From plankton to top predators: bottom- up control of a marine food web across four trophic levels. *Journal of Animal Ecology*, 75(6), 1259-1268.
- Gove, J. M., McManus, M. A., Neuheimer, A. B., Polovina, J. J., Drazen, J. C., Smith, C. R., ... & Dillon, A. K. (2016). Near-island biological hotspots in barren ocean basins. *Nature communications*, 7, 10581.
- Graham, R. M., De Boer, A. M., van Sebille, E., Kohfeld, K. E., & Schlosser, C. (2015). Inferring source regions and supply mechanisms of iron in the Southern Ocean from satellite chlorophyll data. *Deep Sea Research Part I: Oceanographic Research Papers*, 104, 9-25.
- Guinet, C., Dubroca, L., Lea, M. A., Goldsworthy, S., Cherel, Y., Duhamel, G., ... & Donnay, J. P. (2001). Spatial distribution of foraging in female Antarctic fur seals *Arctocephalus gazella* in relation to oceanographic variables: a scale-dependent approach using geographic information systems. *Marine Ecology Progress Series*, 219, 251-264.
- Iverson, R. L. (1990). Control of marine fish production. *Limnology and Oceanography*, 35(7), 1593-1604.
- Koubbi, P., Mignard, C., Causse, R., Da Silva, O., Baudena, A., Bost, C., & Fabri-Ruiz, S. (2016). Ecoregionalisation of the Kerguelen and Crozet islands oceanic zone. Part II: The Crozet oceanic zone. *CCAMLR Report*, 1-50.
- Lehahn, Y., d'Ovidio, F., & Koren, I. (2018). A satellite-based Lagrangian view on phytoplankton dynamics. *Annual review of marine science*, 10, 99-119.



- Lancelot, C., Montety, A. D., Goosse, H., Becquevort, S., Schoemann, V., Pasquer, B., & Vancoppenolle, M. (2009). Spatial distribution of the iron supply to phytoplankton in the Southern Ocean: a model study. *Biogeosciences*, 6(12), 2861-2878.
- Le Bohec, C., Durant, J. M., Gauthier-Clerc, M., Stenseth, N. C., Park, Y. H., Pradel, R., ... & Le Maho, Y. (2008). King penguin population threatened by Southern Ocean warming. *Proceedings of the National Academy of Sciences*, 105(7), 2493-2497.
- Lea, M. A., Guinet, C., Cherel, Y., Duhamel, G., Dubroca, L., Pruvost, P., & Hindell, M. (2006). Impacts of climatic anomalies on provisioning strategies of a Southern Ocean predator. *Marine Ecology Progress Series*, 310, 77-94.
- Legendre, L., & Rassoulzadegan, F. (1995). Plankton and nutrient dynamics in marine waters. *Ophelia*, 41(1), 153-172.
- Lenn, Y. D., Chereskin, T. K., Sprintall, J., & Firing, E. (2007). Mean jets, mesoscale variability and eddy momentum fluxes in the surface layer of the Antarctic Circumpolar Current in Drake Passage. *Journal of Marine Research*, 65(1), 27-58.
- Magris, R. A., Pressey, R. L., Weeks, R., & Ban, N. C. (2014). Integrating connectivity and climate change into marine conservation planning. *Biological Conservation*, 170, 207-221.
- Martin, J. H. (1990). Glacial- interglacial CO<sub>2</sub> change: The iron hypothesis. *Paleoceanography*, 5(1), 1-13.
- Michaels, A. F., & Silver, M. W. (1988). Primary production, sinking fluxes and the microbial food web. *Deep Sea Research Part A. Oceanographic Research Papers*, 35(4), 473-490.
- Mongin, M. M., Abraham, E. R., & Trull, T. W. (2009). Winter advection of iron can explain the summer phytoplankton bloom that extends 1000 km downstream of the Kerguelen Plateau in the Southern Ocean. *Journal of Marine Research*, 67(2), 225-237.
- Péron, C., Weimerskirch, H., & Bost, C. A. (2012). Projected poleward shift of king penguins (*Aptenodytes patagonicus*) foraging range at the Crozet Islands, southern Indian Ocean. *Proceedings of the Royal Society B: Biological Sciences*, 279(1738), 2515-2523.
- Pistorius, P., Hindell, M., Crawford, R., Makhado, A., Dyer, B., & Reisinger, R. (2017). At- sea distribution and habitat use in king penguins at sub- Antarctic Marion Island. *Ecology and evolution*, 7(11), 3894-3903.
- Toole, M. O., Guinet, C., Lea, M. A., & Hindell, M. A. (2017). Marine predators and phytoplankton: how elephant seals use the recurrent Kerguelen plume. *Marine Ecology Progress Series*, 581, 215-227.
- Toole, M. O., Baudena, A., Sergi, S., Cotté, C., Bost, C., Guinet, C., ... & d'Óvidio, F. (in rev.). Underlying physical mechanisms driving trophic niches in the open ocean. *Journal of the Royal Society Interface*
- Reisinger, R. R., Raymond, B., Hindell, M. A., Bester, M. N., Crawford, R. J., Davies, D., ... & Ryan, P. G. (2018). Habitat modelling of tracking data from multiple marine predators identifies important areas in the Southern Indian Ocean. *Diversity and Distributions*, 24(4), 535-550.
- Resing, J. A., Sedwick, P. N., German, C. R., Jenkins, W. J., Moffett, J. W., Sohst, B. M., & Tagliabue, A. (2015). Basin-scale transport of hydrothermal dissolved metals across the South Pacific Ocean. *Nature*, 523(7559), 200.
- Roberts, C. M., Reynolds, J. D., Cote, I. M., & Hawkins, J. P. (2006). Redesigning coral reef conservation. *Conservation Biology Series-Cambridge*, 13, 515.
- Rogers, A. D., Yesson, C., & Gravestock, P. (2015). A Biophysical and Economic Profile of South Georgia and the South Sandwich Islands as Potential Large-Scale Antarctic Protected Areas. In *Advances in marine biology* (Vol. 70, pp. 1-286). Academic Press.
- Rossi, V., Ser- Giacomi, E., López, C., & Hernández- García, E. (2014). Hydrodynamic provinces and oceanic connectivity from a transport network help designing marine reserves. *Geophysical Research Letters*, 41(8), 2883-2891.
- Salm, R. V., Done, T., & McLeod, E. (2006). Marine protected area planning in a changing climate. *Coral reefs and climate change: science and management. American Geophysical Union, Washington, DC*, 207-221.

- Sander, S. G., & Koschinsky, A. (2011). Metal flux from hydrothermal vents increased by organic complexation. *Nature Geoscience*, 4(3), 145.
- Sanial, V., van Beek, P., Lansard, B., d'Ovidio, F., Kestenare, E., Souhaut, M., ... & Blain, S. (2014). Study of the phytoplankton plume dynamics off the Crozet Islands (Southern Ocean): A geochemical- physical coupled approach. *Journal of Geophysical Research: Oceans*, 119(4), 2227-2237.
- Sanial, V., Van Beek, P., Lansard, B., Souhaut, M., Kestenare, É., D'Ovidio, F., ... & Blain, S. (2015). Use of Ra isotopes to deduce rapid transfer of sediment-derived inputs off Kerguelen. *Biogeosciences*, 12(5), 1415-1430.
- Santora, J. A., Sydeman, W. J., Schroeder, I. D., Field, J. C., Miller, R. R., & Wells, B. K. (2017). Persistence of trophic hotspots and relation to human impacts within an upwelling marine ecosystem. *Ecological applications*, 27(2), 560-574.
- Scheffer, A., Trathan, P. N., & Collins, M. (2010). Foraging behaviour of king penguins (*Aptenodytes patagonicus*) in relation to predictable mesoscale oceanographic features in the Polar Front Zone to the north of South Georgia. *Progress in Oceanography*, 86(1-2), 232-245.
- Sohrin, Y., Iwamoto, S. I., Matsui, M., Obata, H., Nakayama, E., Suzuki, K., ... & Ishii, M. (2000). The distribution of Fe in the Australian sector of the Southern Ocean. *Deep Sea Research Part I: Oceanographic Research Papers*, 47(1), 55-84.
- Sokolov, S., & Rintoul, S. R. (2007). On the relationship between fronts of the Antarctic Circumpolar Current and surface chlorophyll concentrations in the Southern Ocean. *Journal of Geophysical Research: Oceans*, 112(C7).
- Staniland, I. J., Reid, K., & Boyd, I. L. (2004). Comparing individual and spatial influences on foraging behaviour in Antarctic fur seals *Arctocephalus gazella*. *Marine Ecology Progress Series*, 275, 263-274.
- Sullivan, C. W., Arrigo, K. R., McClain, C. R., Comiso, J. C., & Firestone, J. (1993). Distributions of phytoplankton blooms in the Southern Ocean. *Science*, 262(5141), 1832-1837.
- Tagliabue, A., Bopp, L., Dutay, J. C., Bowie, A. R., Chever, F., Jean-Baptiste, P., ... & Aumont, O. (2010). Hydrothermal contribution to the oceanic dissolved iron inventory. *Nature Geoscience*, 3, 252-256.
- Tagliabue, A., Aumont, O., & Bopp, L. (2014). The impact of different external sources of iron on the global carbon cycle. *Geophysical Research Letters*, 41(3), 920-926.
- Yesson, C., Clark, M. R., Taylor, M. L., & Rogers, A. D. (2011). The global distribution of seamounts based on 30 arc seconds bathymetry data. *Deep Sea Research Part I: Oceanographic Research Papers*, 58(4), 442-453.
- Wu, J., Wells, M. L., & Rember, R. (2011). Dissolved iron anomaly in the deep tropical–subtropical Pacific: Evidence for long-range transport of hydrothermal iron. *Geochimica et Cosmochimica Acta*, 75, 460-468.
- Zainuddin, M., Kiyofuji, H., Saitoh, K. & Saitoh, S.I. (2006) Using multi- sensor satellite remote sensing and catch data to detect ocean hot spots for albacore (*Thunnus alalunga*) in the northwestern North Pacific. *Deep-Sea Research Part, II*, 419–431.

Contents lists available at [ScienceDirect](https://www.sciencedirect.com)

## Deep-Sea Research Part I

journal homepage: <http://www.elsevier.com/locate/dsr>

## Matching zooplankton abundance and environment in the South Indian Ocean and Southern Ocean

Claire Godet<sup>a</sup>, Marine Robuchon<sup>a,b,c,\*</sup>, Boris Leroy<sup>a</sup>, Cédric Cotté<sup>d</sup>, Alberto Baudena<sup>d,e</sup>,  
Ophélie Da Silva<sup>e,f</sup>, Salomé Fabri-Ruiz<sup>e</sup>, Claire Lo Monaco<sup>d</sup>, Sara Sergi<sup>d</sup>, Philippe Koubbi<sup>g,h</sup>

<sup>a</sup> Laboratoire de Biologie des Organismes et écosystèmes Aquatiques (BOREA), Muséum National d'Histoire Naturelle, CNRS, IRD, Sorbonne Université, Université de Caen Normandie, Université des Antilles, CP 26, 57 Rue Cuvier, 75005, Paris, France

<sup>b</sup> Centre d'Ecologie et des Sciences de la Conservation (CESCO), Muséum National d'Histoire Naturelle, CNRS, Sorbonne Université, CP 135, 57 Rue Cuvier, 75005, Paris, France

<sup>c</sup> Joint Research Centre (JRC) of the European Commission, Directorate for Sustainable Resources, Ispra, Italy

<sup>d</sup> Sorbonne Université UMR 7159 CNRS-IRD-MNHN, LOCEAN-IPSL, 75005, Paris, France

<sup>e</sup> Laboratoire D'Océanographie de Villefranche-sur-Mer, UMR 7093 - CNRS/UPMC, 181 Chemin Du Lazaret, 06230, Villefranche-sur-Mer Cedex, France

<sup>f</sup> Institut de Systématique, Evolution, Biodiversité (ISYEB), Muséum National d'Histoire Naturelle, CNRS, Sorbonne Université, EPHE, Université des Antilles, CP 50, 57 Rue Cuvier, 75005, Paris, France

<sup>g</sup> UFR918 Terre, Environnement, Biodiversité. Sorbonne Université, 4 Place Jussieu, 75252, PARIS Cedex 05, France

<sup>h</sup> IFREMER Centre Manche Mer Du Nord - 150, Quai Gambetta, 62200, Boulogne-sur-Mer, France

## ARTICLE INFO

## Keywords:

Bioregionalization  
Southern Ocean  
Indian Ocean  
Pelagic ecosystem  
Zooplankton  
Continuous plankton recorder

## ABSTRACT

Distinguishing regions based on the geographic distribution of both abiotic factors and living organisms is an old but still actual central issue for biogeographers. In the Southern Ocean, the few existing regionalization studies have been carried out either at very large scales or on the relatively small region around the Sub-Antarctic islands of Kerguelen and the Crozet archipelagos. However, regionalization studies at meso-scales (100–300 km) covering the Indian part of the Southern Ocean and adjacent South Indian Ocean are scarce. These waters, ranging from the Subtropical to the polar region, are home to large populations of well-studied top predators that depend on the biomass of less known mid-trophic level species such as zooplankton. To fill those gaps, our study aims at conducting bioregional analyses of this transition area at the meso-scale based on the distribution of abiotic factors and chlorophyll-*a*, and to investigate how the abundance of zooplankton varies across the bioregions identified. To that end, we first characterized epipelagic bioregions 30°S in the South Indian Ocean to 65°S in the Southern Ocean and from 40° to 85°E including the islands of Crozet, Kerguelen, Saint-Paul and New Amsterdam. We then determined whether these bioregions correspond to variations in the abundance of zooplankton collected by a Continuous Plankton Recorder. Finally, we analyzed which environmental parameters influence zooplankton abundance. Our analyses evidenced six regions, providing a synthetic overview of a contrasting environment. The spatial variability of zooplankton abundance was explained by most of the environmental variables used in the bioregionalisation and, to a lesser extent, by the bioregions. Copepods are abundant in the colder and physically-energetic regions associated with the Antarctic Circumpolar Current (ACC). *Limacina* and euphausiids are both abundant in regions characterized by a high concentration of chlorophyll-*a*, although euphausiids are also abundant in the subtropical region. This work represents a crucial step forward in the integration of living organism distribution in the regionalization of the Indian part of Southern Ocean and adjacent South Indian Ocean. This can, ultimately contribute to the optimization of marine conservation strategies.

\* Corresponding author. Joint Research Centre (JRC) of the European Commission, Directorate for Sustainable Resources, Via E. Fermi 2749, 21027 Ispra, VA, Italy.

E-mail address: [marine.robuchon@ec.europa.eu](mailto:marine.robuchon@ec.europa.eu) (M. Robuchon).

<https://doi.org/10.1016/j.dsr.2020.103347>

Received 4 July 2019; Received in revised form 16 June 2020; Accepted 30 June 2020

Available online 1 August 2020

0967-0637/© 2020 Elsevier Ltd. All rights reserved.

## 1. Introduction

Marine ecoregionalization is a process that aims to divide oceanic areas into distinct spatial regions, using a range of abiotic and biotic – such as chlorophyll-*a* and species assemblages – information (Foster et al., 2017; Hill et al., 2017; Koubbi et al., 2010, 2011; Spalding et al., 2007). When data on species assemblages are not sufficiently available to identify ecoregions accurately, bioregions (Grant et al., 2006) or biogeochemical regions (Longhurst, 2010) can be identified based on the distribution of abiotic factors and chlorophyll-*a* only, i.e. available satellite gridded products. The process results in a set of bioregions, each with relatively homogeneous and predictable ecosystem properties (Grant et al., 2006). Bioregions can be divided at different spatial scales, depending on their physical and environmental characteristics. Bioregions are considered as a proxy of biodiversity spatial patterns through an objective zoning. They constitute a basis for understanding, conserving and managing activities in the marine environment (Grant et al., 2006; Ainley et al., 2010; Hogg et al., 2018).

Several studies have proposed regionalizations based on the biogeochemical, hydrological or physical and geographical characteristics of the oceans including the Southern Ocean (Grant et al., 2006; Longhurst, 2010; Raymond, 2014; Reygondeau and Huettmann, 2014). Four biogeochemical provinces have been identified in the Southern Ocean (Longhurst, 2010) from publications on satellite observations, oceanographic and biotic observations on chlorophyll-*a*, phytoplankton or zooplankton collected during oceanographic surveys. Major changes in these biogeochemical provinces are projected by modeling studies, including southward shifts of the provinces and changes in their areas (Reygondeau and Huettmann, 2014). Changes in the Southern Ocean are mainly imputed to the consequences of human activities, both direct (exploitation of living resources by fishing) and indirect (increase in temperature, seasonality of sea ice, ocean acidification; Constable et al., 2014; Turner et al., 2014; IPCC, 2019). These alter the functioning of marine systems and food webs because they induce habitat modifications, which affect primary producers up to top predators, coastal organisms down to deep species, and the Sub-Antarctic Zone up to the sea ice zone (Constable et al., 2014; Gutt et al., 2015).

However, the existing Southern Ocean regionalizations (Grant et al., 2006; Raymond, 2014) did not consider regional features such as phytoplankton plumes linked to island effects and did not include seasonality. In addition, their northern limit (40°S) excluded the Subtropical zone. This paper proposes to delimit bioregions for the South Indian Ocean and the Southern Ocean covering the area between 40°E and 85°E; 30°S and 65°S. These include the islands of Crozet, Kerguelen, Saint Paul and New Amsterdam. These islands are linked to important topographic features, the ridges of southwest and southeast Indian Del Cano elevation, Crozet Islands' shelf (archipelago) and the Kerguelen Plateau. The occurrence of different water masses and the interaction of the intense ACC with these bathymetric features contribute to the heterogeneity of the region, both from an hydrodynamical point of view and for the subsequent distribution of biogeochemical properties (Roquet et al., 2009; Sokolov and Rintoul, 2007). In this area, the large-scale distribution of primary production and top predators are well known, respectively from remote sensing and biologging data (Cotté et al., 2007; Bost et al., 2009; De Monte et al., 2012; Gandhi et al., 2012; Ropert Coudert et al., 2014). However, very few studies have examined the regional distribution of zooplankton and intermediate trophic levels such as micronekton which includes small organisms (~1–20 cm or g) that can swim (Koubbi, 1993; Handegard et al., 2013; Duhamel et al., 2014; Lehodey et al., 2015; Béhagle et al., 2016; Venkataramana et al., 2019). In addition, the main studies on plankton have been mostly conducted in around Kerguelen, either in the coastal zone, above the island shelf or on the eastern edge of the plateau (Blain et al., 2007; Pollard et al., 2007; Sanial et al., 2014).

Sampling devices gathering large scale zooplankton information, like the Continuous Plankton Recorder (CPR), can survey vast geographical

region to study zooplankton distribution (Batten et al., 2019). This plankton sampling device continuously collects organisms all along a cruise track at the sub-surface and has already been deployed in the Southern Ocean for past studies (Hosie et al., 2003, 2014). The CPR was deployed for the first time in the South Indian Ocean and the Southern Ocean in 2013 on board the R/V “Marion Dufresne” (Meilland et al., 2016) and since then the surveys have been carried out every year between January and February (Fig. 1). These new samples at high spatial resolution fill a geographic gap in both the South Indian Ocean and the Southern Ocean.

Therefore, the objectives of this study were (i) to delimit and characterize bioregions in this area and (ii) to verify whether variations in the abundance of zooplankton can be explained by the environmental characteristics of the bioregions. Specifically, we wanted to define these bioregions at the mesoscale (100–300 km) to provide a better representation of oceanographic features, such as water mass dynamics and fronts. To attain our general objectives, we first delimited summer pelagic bioregions on the basis of environmental parameters (sea surface temperature, chlorophyll-*a* concentration, kinetic energy and bathymetry) describing the main characteristics of the region analyzed. Then, we determined whether these bioregions were precise predictors of variations in zooplankton abundance in the Southern Ocean and the South Indian Ocean by using samples collected by the CPR. Finally, we investigated the extent to which changes in zooplankton abundance were explained by the environmental characteristics of bioregions.

## 2. Materials and methods

### 2.1. Bioregionalization

#### 2.1.1. Study area

Our study area lies between 40°E and 85°E; 30°S and 65°S (Fig. 1) and includes large latitudinal gradients in water masses properties with different fronts separating the subtropical waters from the polar waters (Orsi et al., 1995). These fronts are associated with the ACC which is very intense in this area. Some of these fronts depict drastic changes in temperature and salinity (Post et al., 2014; Park et al., 1991, 1993) and delimit large oceanographic regions. The Subtropical Front (STF) defines the southern limit of warm and oligotrophic waters that characterize the subtropical gyre. Further south lies the Sub-Antarctic Front (SAF) associated to the main core of the ACC (Park et al., 2002, 2008), followed by the Antarctic Polar Front (PF). The Sub-Antarctic Zone extends between the STF and the SAF, while the Polar Frontal Zone extends between the SAF and the PF. The Subtropical Zone is located to the north of the STF. In this area, the Sub-Antarctic Zone corresponds to a narrow band of about 2° of latitude (between 44°S and 46°S) that is formed by the convergence of the SAF and STF, in the East of the Kerguelen shelf the PF is also close to the other fronts (Park et al., 1991, 1993). The largest extent of the Polar Frontal Zone is found to the south of Crozet (between 45°S and 52°S), while it covers only a few degrees in latitude to the north-east of Kerguelen (Sokolov and Rintoul, 2009). The Subtropical Zone also includes the Agulhas Return Current, current which influences species assemblages in the western subtropical part of the area (Koubbi, 1993). On a longitudinal scale, several shallow island shelves and seamounts diversify the geomorphological landscape and shape the ocean circulation. The Kerguelen plateau is a major bathymetric feature extending from the Kerguelen island shelf towards the Antarctic shelf. It deeply, influences the hydrology of the area. It acts as a barrier deflecting the ACC which flows continuously through the Southern Ocean due to the absence of continental lands (Roquet et al., 2009). The study area is also highly heterogeneous in terms of biological productivity. Most of the ice-free polar waters in the Permanent Open Ocean Zone (zone between 50° and 60°S; Pondaven et al., 1998) are characterized by High Nutrient Low Chlorophyll (HNLC; i.e. phytoplankton are not abundant whereas there are high macronutrient levels) conditions due to iron limitation. This trace element limits the primary



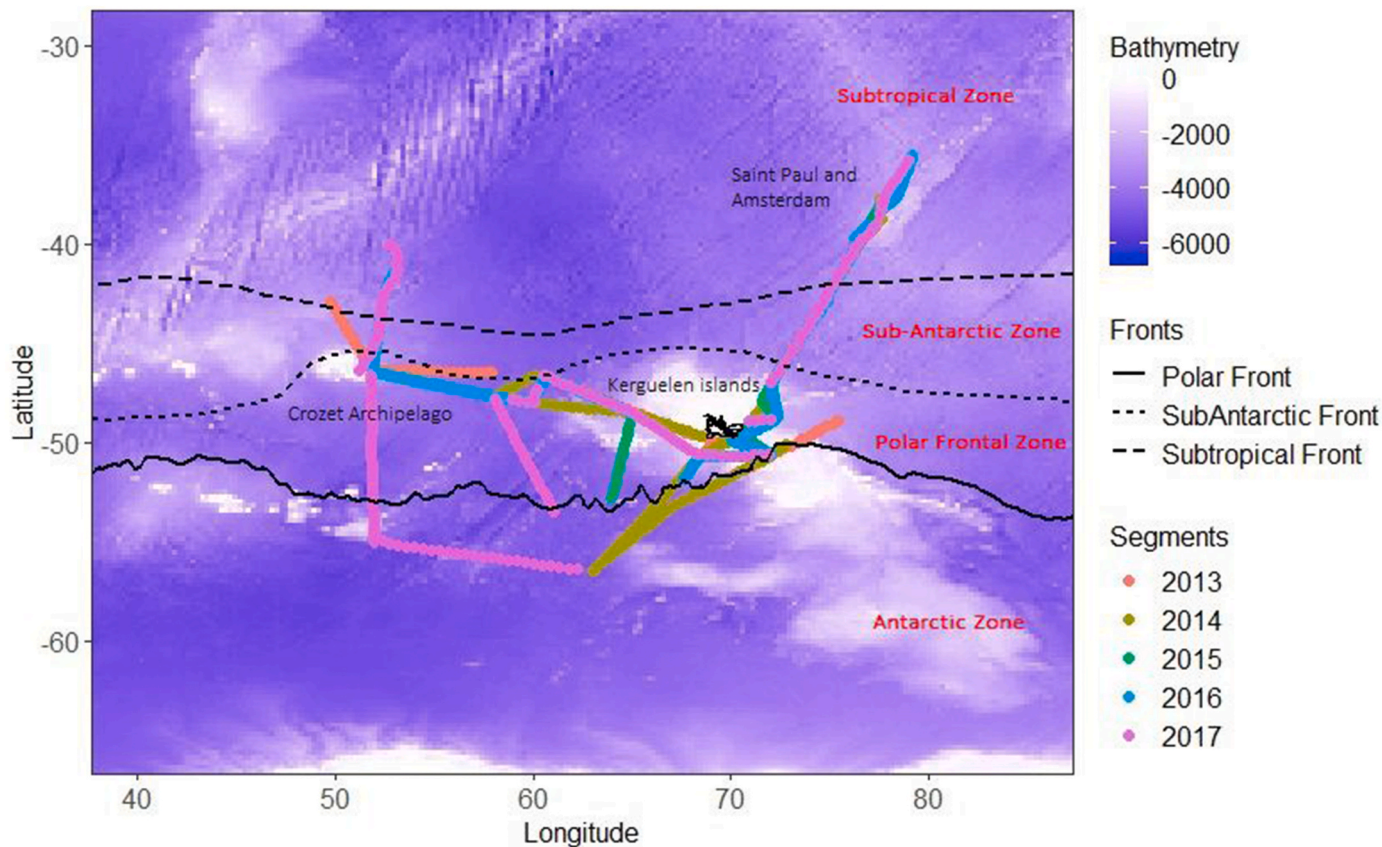


**Fig. 1.** Map of the study area showing the routes of the oceanographic vessel for each year (2013–2017), the different fronts of the represented area (Subtropical Front, Sub-Antarctic Front and Polar Front) and the different zones of the area (Subtropical Zone, Sub-Antarctic Zone, Polar Frontal Zone and Antarctic Zone). The position of the fronts follows Post et al. (2014).

production in the study area (Martin, 1990; De Baar et al., 2005). The HNLC region contrasts with the intense phytoplankton blooms occurring close to iron sources, notably around the Sub-Antarctic islands. There, the iron is delivered by the interaction of the flow and the shallow topography (Boyd and Ellwood, 2010). This physical and biogeochemical process supports recurrent phytoplankton blooms, occurring during spring over the plateau between Kerguelen and Heard Islands (southeast of Kerguelen), north and east of Kerguelen (Blain et al., 2007; Park et al., 2008), as well as north and east of Crozet (Pollard et al., 2007; Sanial et al., 2014). Conversely, the upstream waters of Kerguelen and Crozet are generally less productive.

2.1.2. Environmental data

Our first objective was to delineate bioregions on the basis of four environmental parameters: (i) sea surface temperature, which varies

latitudinally in the study area, (ii) chlorophyll-*a* concentration, which is an indicator of phytoplankton abundance and iron enrichment zones, (iii) kinetic energy, which identifies physically-energetic zones associated with the ACC and (iv) bathymetry, which distinguish shelf from open ocean zones.

Oceanographic data were obtained from satellite measurements from 2013 to 2017 for the period from November to March (i.e. during Austral summer). The parameters studied were sea surface temperature (SST, in °C), chlorophyll-*a* concentration (Chl-*a*, in mg.m<sup>-3</sup>), kinetic energy (KE, in m<sup>2</sup>.s<sup>-2</sup>) and bathymetry (Bat, in m) (Table 1). Each environmental parameter had a different spatial resolution. In order to manage these differences, we carried out bioregionalization at the lowest resolution of the environmental parameters, i.e. the spatial resolution of the kinetic energy at 0.25°.

The KE was calculated from the altimetry-based horizontal current

**Table 1**  
Description of environmental parameters used in this study.

Environmental parameters	Abbreviations	Source and products	Spatial Resolution	Daily resolution
[Chlorophyll- <i>a</i> ] (mg.m <sup>-3</sup> )	Chl- <i>a</i>	Copernicus Marine Environmental Monitoring Service website ( <a href="http://marine.copernicus.eu/">http://marine.copernicus.eu/</a> ): "OCEANCOLOUR_GLO_CHL_L4_REP_OBSERVATIONS_009_082" for 2013 and 2014 data and "OCEANCOLOUR_GLO_CHL_L4_NRT_OBSERVATIONS_009_033" (satellite products).	0.04°	8 days mean
Sea Surface Temperature (°C)	SST	Copernicus Marine Environmental Monitoring Service website ( <a href="http://marine.copernicus.eu/">http://marine.copernicus.eu/</a> ): "SST_GLO_SST_L4_NRT_OBSERVATIONS_010_001" (satellite products).	0.05°	Daily mean
Kinetic Energy (m <sup>2</sup> .s <sup>-2</sup> ).	KE	KE data were obtained from the zonal and southern velocity (U and V, respectively) which estimate surface currents derived from altimetry through a geostrophic approximation. U and V are provided in the "SEALEVEL_GLO_PHY_L4_REP_OBSERVATIONS_008_047" product which was downloaded from the E.U. Copernicus Marine Environment Monitoring Service (CMEMS, <a href="http://marine.copernicus.eu/">http://marine.copernicus.eu/</a> ) for the period 2013–2017. In this way, an estimation of the total kinetic energy is obtained.	0.25°	Daily mean
Bathymetry (m)	Bat	<a href="http://www.gebco.net">http://www.gebco.net</a> (satellite products)	0.008°	/

velocities, using the following formula:

$$KE = 0.5 \cdot (U^2 + V^2) / 1000$$

where U and V are the zonal (i.e. longitude) and meridional (i.e. latitude) velocities. The bathymetry of the study area was downloaded from the General Bathymetric Chart of the Oceans website ([www.gebco.net](http://www.gebco.net)).

Oceanographic data were downloaded for the period November to March for the years 2013, 2014, 2015, 2016 and 2017. The raw data correspond to daily averages for the SST and KE parameters and weekly averages for the Chl-a parameter, due to the very high cloud cover in the study area. Data were then analyzed using the mean value calculated over the summer period (November to March).

### 2.1.3. Zooplankton sampling and identification

Zooplankton was sampled using a CPR on board the R/V “Marion Dufresne” every summer, between January and February, from 2013 to 2017, for a total of 1282 samples corresponding to 6410 nautical miles. The CPR is a mechanical device that allows continuous sampling of plankton while being towed in the subsurface behind the vessel (at a speed from 10 to 15 knots). The CPR was towed approximately 100 m behind the vessel at a depth varying between 10 and 30 m. The CPR works as follows: water enters through a square opening (1.62 cm<sup>2</sup>: 1.27 × 1.27 cm) into a collecting tunnel (10 × 5 cm). The plankton then reaches a moving silk band (filter silk) with an average mesh size of 270 µm. A second strip of silk (covering silk) covers the filtering silk and is then wound in the fixing tank, which contains diluted formaldehyde. Regardless of the speed of the vessel, the silk advances at a speed of about 1 cm per nautical mile during towing (Hunt and Hosie, 2003; Hosie et al., 2014).

In the laboratory, each set of silk is unwound and cut by segments of 5 nautical miles. The entire content of each sample is identified at a coarse taxonomic resolution and assigned to one of the following groups: copepods, euphausiids, amphipods, *Limacina*, chaetognaths and ostracods, which are counted under a stereomicroscope. For each major taxon, the individuals are counted in the fraction where at least 100 individuals of that taxon are found. For this a Folsom splitter was used.

Zooplankton abundance data obtained by the CPR (2013–2017) for each taxon and silk sample and the corresponding metadata (GPS coordinates) were stored in a table. The abundances were calculated (number of individuals per nautical mile) and each sample was assigned to the time of day (Day, Dusk, Night, Dawn) which was calculated using the solar angle (“RAtmosphere” package; Biavati, 2014). The number of samples is 552 during the day, 167 at dusk, 338 at night and 225 at dawn.

## 2.2. Data processing and statistical analyses

All statistical analyses were done using R (R Core Team., 2018) and the maps were realized using either R or using a Geographic Information System (ArcGIS v. 10.5.1.).

### 2.2.1. Bioregionalization

The first step in the bioregionalization procedure was to conduct a principal component analysis (PCA, Legendre and Legendre, package “FactoMineR”, 1998; Lê et al., 2008) on environmental parameters (SST, KE, Bat and Chl-a) to eliminate noise before classification (concentration of information on the first components), resulting in a more stable classification. The second step consisted of clustering sites by applying the method of K-means (MacQueen, 1967) on the coordinates of site on the two first PCA axes. The optimal number of clusters (in this study, the environmental envelopes of bioregions) was chosen using the index of Calinsky and Harabasz, 1974 and the elbow method (Kodinariya and Makwana, 2013). The final step was to create a map of bioregions based on the clusters obtained.

### 2.2.2. Characterization of zooplankton sampling

To study variations in zooplankton abundance (log(abundance+1)) between the different taxa, a Kruskal-Wallis analysis was conducted. The same analysis was performed without zero values of abundance for each taxon, to take into account the fact that some taxa live in schools in the Southern Ocean. After each Kruskal-Wallis analysis, post-hoc pairwise Wilcoxon rank sum tests were carried out. This consisted of a multiple comparison test with correction by the Holm method (1979) between each pair of taxa to unravel the differences between them.

### 2.2.3. Analyses of variation in plankton abundance

The following analyses were carried out on the total abundance of zooplankton (including data with zero values). To investigate how zooplankton abundance (log(abundance+1)) varied according to the period of the day, a Kruskal-Wallis analysis was performed. The same analysis was performed to test differences in abundances between years. Post-hoc pairwise Wilcoxon rank sum tests were also carried out to unravel the differences between each pair of periods of the day.

These analyses focused on copepods, euphausiids and *Limacina*, which were the most abundant taxa. Night samples were used for this analysis because at night, zooplankton abundance and diversity are higher due to nocturnal migrations. A Kruskal-Wallis test was used to study variations in the abundance of copepods, euphausiids and *Limacina* between the different bioregions. A Kruskal-Wallis test was used to study variations in the abundance of copepods, euphausiids and *Limacina* in the different bioregions. Subsequent post-hoc pairwise Wilcoxon rank sum tests were carried out to reveal the differences between each pair of bioregions regarding the abundance of each taxon. Then, a generalized linear model (with Poisson distribution) was used to study the fluctuations in the abundance of the different taxa as a function of different environmental parameters (SST, the log of KE, the log of Chl-a and the log of Bat).

## 3. Results

### 3.1. Characterization of bioregions

The first two axes of the PCA on environmental variables explained 70% of the total variance (Fig. 2). Axis 1 permitted to discriminate sites according to KE and SST while axis 2 permitted to discriminate sites according to Bat and Chl-a. The clustering on the first two axes of the PCA on environmental variables identified six distinct bioregions, a number of clusters that allowed us also to describe the study area with sufficient detail to make sense from an ecological point of view (Fig. 2). Indeed, Axis 1 opposes bioregions with relatively high KE and SST (Bioregions 3, 5 and 6) to bioregions with lower KE and SST (Bioregions 4 and 2) and axis 2 further opposes one bioregion with high Chl-a and Bat (Bioregion 1) to the others (Fig. 2). The 6 bioregions are mapped and their environmental variability described in Fig. 3, while Table 2 provides a synthetic overview of their localization and environmental characteristics.

### 3.2. Characterization of zooplankton sampling

The Kruskal-Wallis test showed that the abundance of zooplankton sampled in the surface layer varied significantly between the different taxa (Fig. 4a). Specifically, we found that (i) copepods were more abundant than the other taxa, (ii) the abundance of copepods was not significantly different from the total abundance, (iii) *Limacina* and amphipod taxa present similar abundances.

In addition, when performing the same analyses without the zero abundance values of the different taxa, we found that the abundance of copepods, euphausiids and *Limacina* differed significantly from each other (Fig. 4b). As the abundance of euphausiids and *Limacina* was significantly higher than the abundance of ostracods, chaetognaths and amphipods (Fig. 4b) and represent the vast majority of the zooplankton

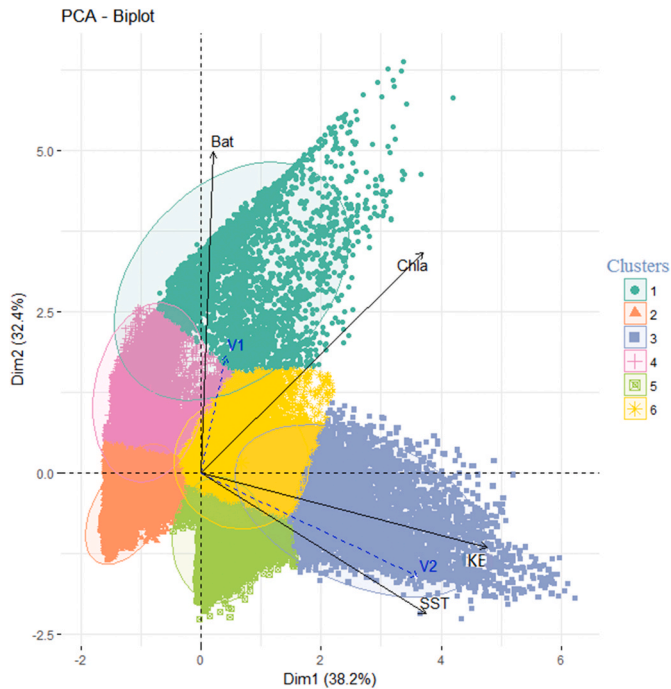


**Fig. 2.** Principal Component Analysis (PCA) of environmental parameters (SST: Sea Surface Temperature (°C); KE: Kinetic Energy ( $m^2 \cdot s^{-2}$ ); Chl-a: concentration of Chlorophyll-a ( $mg \cdot m^{-3}$ ) and Bat: Bathymetry (m)) on the two first significant axes of the PCA (Dim1, Dim2)). V1 = longitude and V2 = latitude are supplementary variables that do not influence the PCA. The colour of the 6 clusters is represented on the observations and concentration ellipses. (For interpretation of the references to colour in this figure legend, the reader is referred to the Web version of this article.)

sampled, we decided to focus the following statistical analyses only on copepods, euphausiids and *Limacina*.

### 3.3. Temporal variations in zooplankton abundance

Kruskal-Wallis analyses and the post-hoc tests of Wilcoxon generally showed that the abundance of zooplankton sampled in the surface layer was significantly higher at night and lower during the day (Fig. 5a). Kruskal-Wallis analyses showed that the abundance of zooplankton sampled in the surface layer did not vary significantly from year to year (Fig. 5b).

### 3.4. Variations in zooplankton abundances across bioregions

The copepod, *Limacina* and total night abundances did not differ significantly between Bioregions 1 to 5 (Fig. 6). Nonetheless, copepod, *Limacina* and total night abundances were the lowest in Bioregion 6, with significant differences with Bioregions 1, 2, and 4 depending on the group (Fig. 6). Euphausiid abundance did not differ significantly among Bioregions 1 and 3 to 6, but was significantly lower in Bioregion 2 than in Bioregions 1 and 6 (Fig. 6).

The bioregions identified in the cluster analysis are differently represented by the zooplankton samples. In particular, Bioregion 3 and Bioregion 5 are largely under-sampled with respectively 3 and 11 samples collected within the five campaigns. This may explain why the zooplankton abundance found there did not differ significantly from any bioregion (Fig. 6).

### 3.5. Variations in zooplankton abundance with environmental parameters

The first GLM model showed that the night abundance of copepods was significantly related to mean SST and KE. Specifically, the

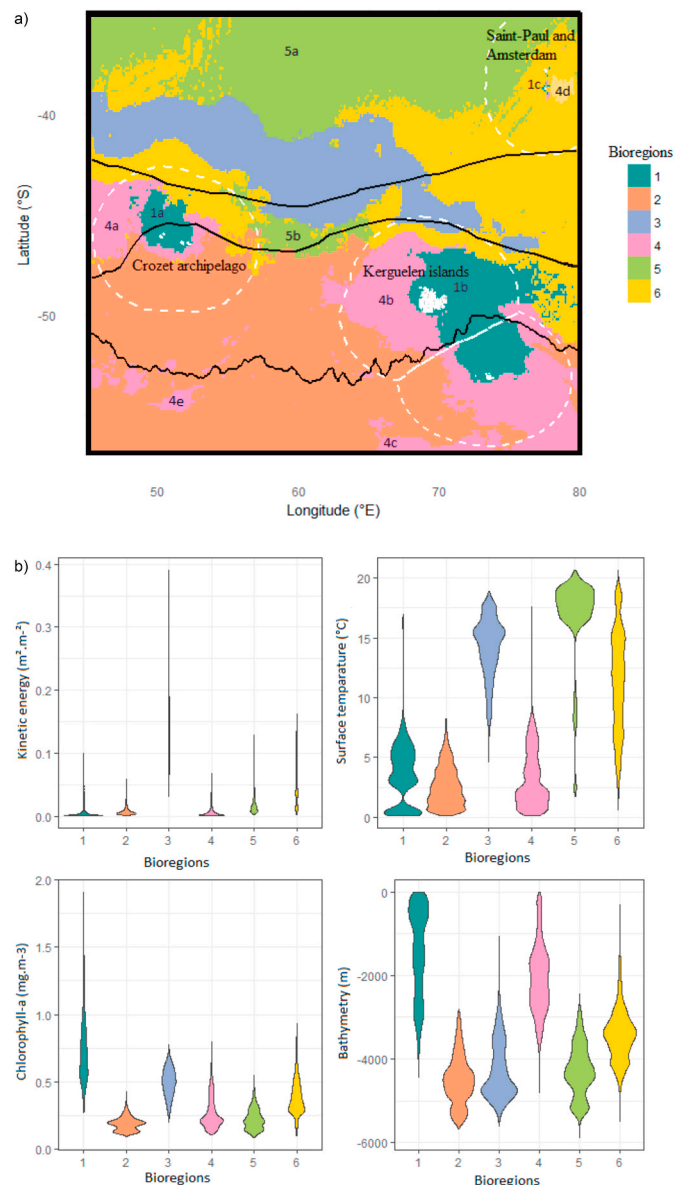


**Fig. 3.** Bioregions defined by SST, KE, Chl-a and Bat (SST: Sea Surface Temperature; KE: Kinetic Energy; Chl-a: concentration of Chlorophyll-a and Bat: Bathymetry). Map of the six bioregions and position of the 3 main hydrological fronts (from north to south: STF, SAF and PF), the white dashed lines correspond to the exclusive economic zones (a). Violin plots of environmental parameters (SST, KE, Chl-a and Bat) according to the six bioregions (b).

abundance of copepods decreased as the mean SST increase, whereas it slightly increased as the mean KE increased (Fig. 7).

The second GLM model showed that the night abundance of euphausiids was significantly related to the mean Chl-a concentration. Specifically, the abundance of euphausiids increased as the mean Chl-a increased (Fig. 7).

The third GLM model showed that the night abundance of *Limacina* was significantly related to mean Chl-a and Bat. Specifically, the abundance of *Limacina* increased as the mean Chl-a increased and decreased as the mean Bat increased (Fig. 7).

## 4. Discussion

In this study, we provided a new set of epipelagic bioregions for the South Indian Ocean and the Indian part of the Southern Ocean at macro- and meso-scale according to their environmental characteristics.



**Table 2**  
Descriptions of the six bioregions identified in the study area and shown in Figs. 2 and 3.

Bioregions	Localization	Characteristics
1	Shelf and high productivity off-shelf waters	<ul style="list-style-type: none"> <li>- Cold SST (min = 0.11 °C, mean = 3.57 °C, max = 16.96 °C)</li> <li>- Low KE (min = 0.00 m<sup>2</sup>.s<sup>-2</sup>, mean = 0.00 m<sup>2</sup>.s<sup>-2</sup>, max = 0.09 m<sup>2</sup>.s<sup>-2</sup>)</li> <li>- High Chl-<i>a</i> (min = 0.27 mg.m<sup>-3</sup>, mean = 0.73 mg.m<sup>-3</sup>, max = 1.91 mg.m<sup>-3</sup>)</li> <li>- Shallow sea (min = -4443.0m, mean = -1434.7m, max = -2.0m)</li> </ul>
2	Deep Eastern Part of the Enderby basin	<ul style="list-style-type: none"> <li>- Cold SST (min = 0.19 °C, mean = 2.59 °C, max = 8.21 °C)</li> <li>- Low KE (min = 0.00 m<sup>2</sup>.s<sup>-2</sup>, mean = 0.01 m<sup>2</sup>.s<sup>-2</sup>, max = 0.05 m<sup>2</sup>.s<sup>-2</sup>)</li> <li>- Low Chl-<i>a</i> (min = 0.09 mg.m<sup>-3</sup>, mean = 0.19 mg.m<sup>-3</sup>, max = 0.42 mg.m<sup>-3</sup>)</li> <li>- Deep sea (min = -5680m, mean = -4499m, max = -2801m)</li> </ul>
3	High turbulence areas of SAF and SFT	<ul style="list-style-type: none"> <li>- Hot SST (min = 4.66 °C, mean = 14.29 °C, max = 18.93 °C)</li> <li>- High KE (min = 0.03 m<sup>2</sup>.s<sup>-2</sup>, mean = 0.15 m<sup>2</sup>.s<sup>-2</sup>, max = 0.39 m<sup>2</sup>.s<sup>-2</sup>)</li> <li>- Moderate Chl-<i>a</i> (min = 0.20 mg.m<sup>-3</sup>, mean = 0.50 mg.m<sup>-3</sup>, max = 0.77 mg.m<sup>-3</sup>)</li> <li>- Deep sea (min = -5595m, mean = -4271m, max = -1072m)</li> </ul> <p>This ecoregion is highly influenced by KE</p>
4	Island shelves less productive areas and seamounts	<ul style="list-style-type: none"> <li>- Cold SST (min = 0.18 °C, mean = 3.16 °C, max = 17.62 °C)</li> <li>- Low KE (min = 0.00 m<sup>2</sup>.s<sup>-2</sup>, mean = 0.01 m<sup>2</sup>.s<sup>-2</sup>, max = 0.06 m<sup>2</sup>.s<sup>-2</sup>)</li> <li>- Low Chl-<i>a</i> (min = 0.10 mg.m<sup>-3</sup>, mean = 0.26 mg.m<sup>-3</sup>, max = 0.80 mg.m<sup>-3</sup>)</li> <li>- Shallow sea (min = -4791m, mean = -2087m, max = -13m)</li> </ul>
5	Indian Ocean Deep	<ul style="list-style-type: none"> <li>- High SST (min = 1.74 °C, mean = 17.01 °C, max = 20.69 °C)</li> <li>- Low KE (min = 0.00 m<sup>2</sup>.s<sup>-2</sup>, mean = 0.02 m<sup>2</sup>.s<sup>-2</sup>, max = 0.12 m<sup>2</sup>.s<sup>-2</sup>)</li> <li>- Low Chl-<i>a</i> (min = 0.08 mg.m<sup>-3</sup>, mean = 0.22 mg.m<sup>-3</sup>, max = 0.55 mg.m<sup>-3</sup>)</li> <li>- Deep sea (min = -5887m, mean = -4283m, max = -2437m)</li> </ul>
6	Indian ridges subtropical	<ul style="list-style-type: none"> <li>- High SST (min = 0.62 °C, mean = 7.98 °C, max = 20.69 °C)</li> <li>- Low KE (min = 0.00 m<sup>2</sup>.s<sup>-2</sup>, mean = 0.05 m<sup>2</sup>.s<sup>-2</sup>, max = 0.16 m<sup>2</sup>.s<sup>-2</sup>)</li> <li>- Low Chl-<i>a</i> (min = 0.10 mg.m<sup>-3</sup>, mean = 0.38 mg.m<sup>-3</sup>, max = 0.93 mg.m<sup>-3</sup>)</li> <li>- Deep sea (min = -5497m, mean = -3433m, max = -319m)</li> </ul>

Furthermore, we highlighted how the abundance of the different zooplankton taxa varied spatially with environmental conditions.

#### 4.1. Bioregionalization of the Indian part of the Southern Ocean and adjacent South Indian Ocean

The six bioregions were determined according to three physical environmental parameters (sea surface temperature, kinetic energy, bathymetry) and chlorophyll-*a* concentration which is considered as a proxy of the surface primary production. These bioregions provide a synthetic and integrated overview of contrasting environments characterized by different biophysical processes (Table 2). In accordance with previous studies by Grant et al. (2006) and Raymond (2014), the six bioregions we identified follow a latitudinal pattern. However, our study included the Southern part of the Indian Ocean (Bioregions 3, 5 and 6 and the islands of Saint Paul and Amsterdam) in addition to the Southern Ocean (Bioregions 1, 2 and 4). Therefore, this study provides details about the transition between these two oceans which are separated by different major fronts, mainly the Sub-Antarctic and the Subtropical Fronts. The main characteristics of the six bioregions are described below.

Bioregion 1 is mainly located to the east of the Kerguelen Plateau and north of the Heard Plateau, on the central and northern part of the Crozet Plateau and in a small extent, around the St. Paul Islands and the New Amsterdam Plateau. This region corresponds to areas with high chlorophyll-*a* concentrations (Fig. 3). Indeed, the distribution of chlorophyll-*a* in the Southern Ocean is dominated by a number of recurrent blooms observed downstream of islands (Sokolov and Rintoul, 2007). These blooms are sustained by the iron enrichment of water masses from the Sub-Antarctic Islands and their plateaus (Blain et al., 2001; Sanial et al., 2014; Graham et al., 2015; d'Ovidio et al., 2015).

Bioregion 2 is located in the deep eastern part of the Enderby Basin in the Southern Ocean, south of SAF. The kinetic energy is low, as well as the sea surface temperature and chlorophyll-*a* concentration, thus representing a typical HNLC zone. South of Crozet, the PF at about 50° S has a low current velocity (Park et al., 1993; Pollard and Read, 2001; Pollard et al., 2002, 2007). The low chlorophyll-*a* concentrations are a consequence of iron deficiency (Boyd et al., 2000, 2007; Pollard et al., 2007; De Baar et al., 2005). Indeed, this area is very deep and remote from islands, shallow plateaus or seamounts (which are the main source of

iron in the region) (e.g. Ardyna et al., 2017).

Bioregion 3 corresponds to the physically-energetic areas of the Indian Ocean characterized by high kinetic energy (Fig. 3). The ACC flows mainly to the north of the Crozet and Kerguelen plateau, the latter being a major obstacle to the eastward flow of the ACC (Roquet et al., 2009). High kinetic energies in this region indicate intense horizontal velocities generated by the ACC and the Agulhas Current. After Bioregion 1, Bioregion 3 is the area with the higher chlorophyll-*a* concentration. Indeed, the intense horizontal velocities allow the transport of nutrient from the shallow topographies around the African coasts into the open ocean for thousands of kilometers sustaining the phytoplankton productivity (e.g. Ardyna et al., 2017). In addition, this area is characterized by an intense mesoscale activity associate to meanders, eddies, filaments and fronts which may also enhance the primary production (e.g. Flierl and Davis, 1993; Oschlies and Garçon, 1998; Machu and Garçon, 2001; Lévy, 2008).

Bioregion 4 is characterized by shallow to mid bathymetry and low chlorophyll-*a* concentrations and is located either in the deepest parts of the island shelves, mainly in the western part of these shelves, and over complex seamounts (Figs. 2 and 3). The relative low chlorophyll-*a* concentration in the western part of the shelf areas (Fig. 3b) may be explained by the zonal location of this bioregion relatively to the plateau. Indeed, due to the main eastward circulation of the ACC, the iron enrichment of the water masses is more intense in the eastern part of the shelves and offshore, generating a longitudinal chlorophyll-*a* gradient upstream and downstream of the plateau (e.g. Sanial et al., 2014; d'Ovidio et al., 2015). This difference can be observed with contrasted chlorophyll-*a* concentrations between Bioregion 4 (western flank, lower chlorophyll-*a* concentration) and Bioregion 1 (eastern flank, higher chlorophyll-*a* concentration). The relative shallow depth of the areas of the Bioregion 4 which are located offshore from the islands is explained by the numerous seamounts included in these areas. These are the large Skif bank to the south-west of Kerguelen and the Elan Bank south-west of Heard at the limit of the study area (Bioregion 4b in Fig. 3). South of Crozet, different seamounts of smaller size such as Ob, Lena and Marion Dufresne are located near the PF (Bioregion 4e in Fig. 3). The presence of shallow seamounts may also stimulate the nutrient input in the euphotic layer thus sustaining higher chlorophyll-*a* concentrations compared to the surrounding water of the abyssal plain (Bioregion 2) (e.g. Pitcher et al., 2008).



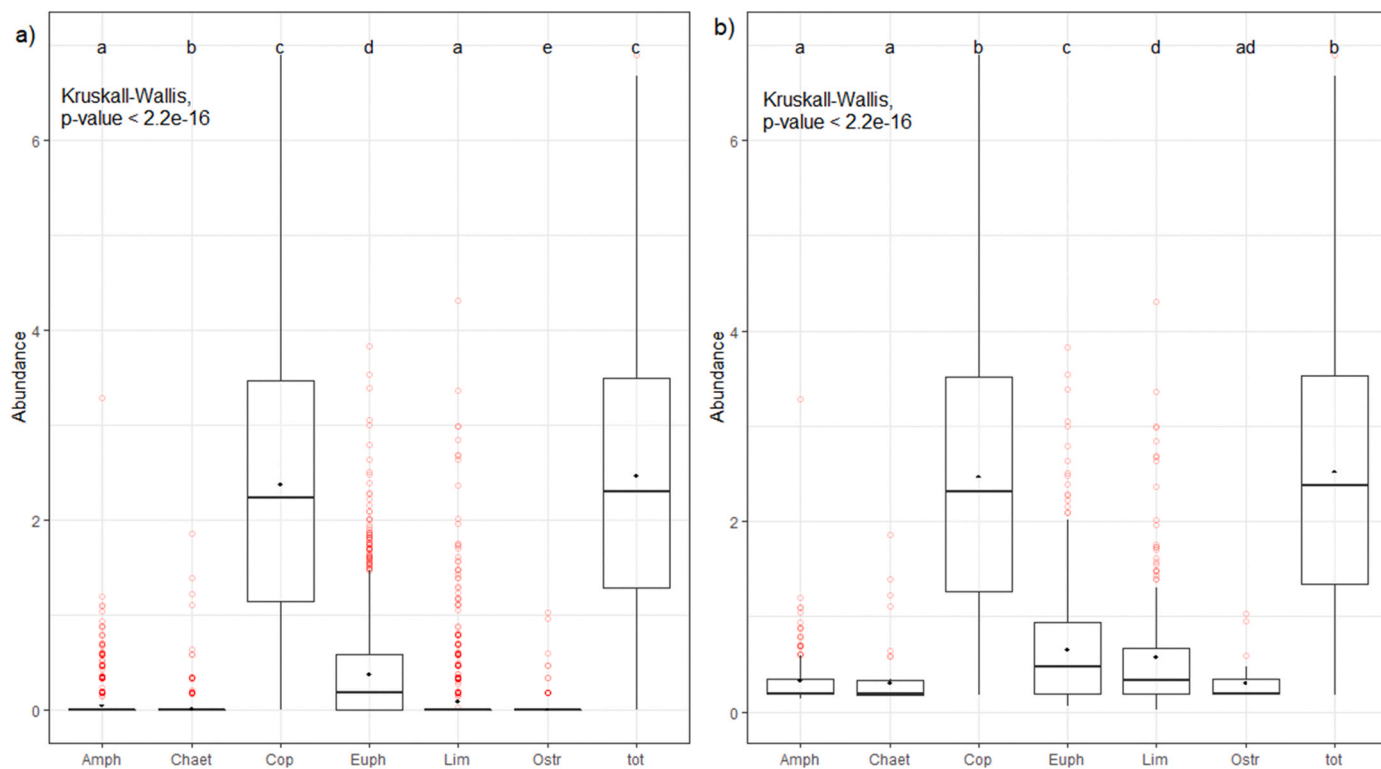


**Fig. 4.** Distribution of values of abundance by taxon (number of individuals per nautical mile) (Amph = Amphipods, Chaet = Chaetognaths, Cop = Copepods, Euph = Euphausiids, Lim = *Limacina*, Ostr = Ostracods, tot = total zooplankton abundance). On the left the abundance values are transformed into  $\log(x+1)$  (a) and on the right the abundance values are transformed into  $\log(x+1)$  and without the zero values (b). The outliers are in red. Following the Wilcoxon post-hoc tests, the letters (a, b, c, d, e) correspond to the representation of significance. If two taxa share the same letter then they are not significantly different, and on the contrary, if two taxa do not share the same letter, then they are significantly different. (For interpretation of the references to colour in this figure legend, the reader is referred to the Web version of this article.)

Bioregion 5 is located in the Subtropical Indian Ocean (5a) and to the north of the STF (5b), two areas of abyssal plains or hills (Harris et al., 2014). They are characterized by higher temperatures and represent the deepest zones of the Indian Ocean. Bioregion 5a is the warmest region and Bioregion 5b is the deepest region (Fig. 3) (Harris et al., 2014). The low chlorophyll-*a* concentrations found in Bioregion 5 are typical of the hyperoligotrophic waters of the subtropical gyres (e.g. McClain et al., 2004; Morel et al., 2010).

Bioregion 6 is characterized by a large thermal amplitude and can be considered as an Indian Subtropical region with deep bathymetry and low kinetic energy. This area also includes shallower seamounts at the mid-ocean ridges (Harris et al., 2014). This area is divided into two sub-areas by Bioregion 3. However, the main part is located to the northeast of the study area, around the St Paul and Amsterdam Islands, and includes part of the Southeast Indian Ridge. The northwestern part includes part of the Southwest Indian Ridge in Indian Ocean.

#### 4.2. Spatial variations in zooplankton abundance

Consistent with previous CPR studies conducted in various regions of the Southern Ocean, we found that copepods account for most of the zooplankton biomass (Hunt and Hosie, 2003, 2006a, 2006b; Hosie et al., 2003; Takahashi et al., 2002, 2010, 2011). Our analyses of copepods, euphausiids and *Limacina* sampled at night permitted to reveal the spatial patterns in the abundance of the different taxa across our study area encompassing the Southern Ocean and the South Indian Ocean. These spatial patterns are explained by (i) the high dependence of copepod abundance on sea surface temperature and, to a lesser extent, kinetic energy; (ii) the high dependence of euphausiid abundance on chlorophyll-*a* concentration; (iii) the high dependence of *Limacina* abundance on chlorophyll-*a* concentration and shallow bathymetry.

The GLM models indicate that the copepods were most abundant in the cold waters of the Southern Ocean. Accordingly, the abundance of copepods was significantly highest in Bioregions 1, 2 and 4, which are located in the southern part of the study area and correspond to the coldest zones in the Permanent Open Ocean Zones, than in Bioregion 6. This is because temperature has major effects on the physiology of zooplankton in Antarctic and is therefore one of the main factors defining its biogeographic distributions (Pörtner et al., 2007). Furthermore, the GLM models revealed a greater abundance of copepods in physically-energetic waters. Although copepods are quite abundant in Bioregion 3, i.e. the most physically-energetic zone of our study area located in the Subtropical and Sub-Antarctic regions, their abundance in this under-sampled bioregion does not differ significantly from the others. Further *in situ* analysis of zooplankton abundance in this high turbulent region could allow us testing this relationship within pelagic bioregions.

The GLM models also revealed that euphausiids were more abundant in chlorophyll-*a* rich areas. Specifically, they were significantly less abundant in low productive open ocean waters of Bioregion 2 compared to the shelf and off-shelf high productivity areas of Bioregion 1. The higher abundance of euphausiids in the Indian ridges subtropical waters of Bioregion 6 could also be related to the higher chlorophyll-*a* found there. This positive relationship between the abundance of euphausiids and chlorophyll-*a* is not surprising because primary production corresponds to phytoplankton, the main food of zooplankton. This further supports previous studies showing that zooplankton biomass is globally found to be positively related to the phytoplankton biomass (Irigoien et al., 2004).

The GLM models also identify a positive relationship between *Limacina* abundance and chlorophyll-*a*, and a positive relationship of *Limacina* abundance with bathymetry. Consequently, the higher

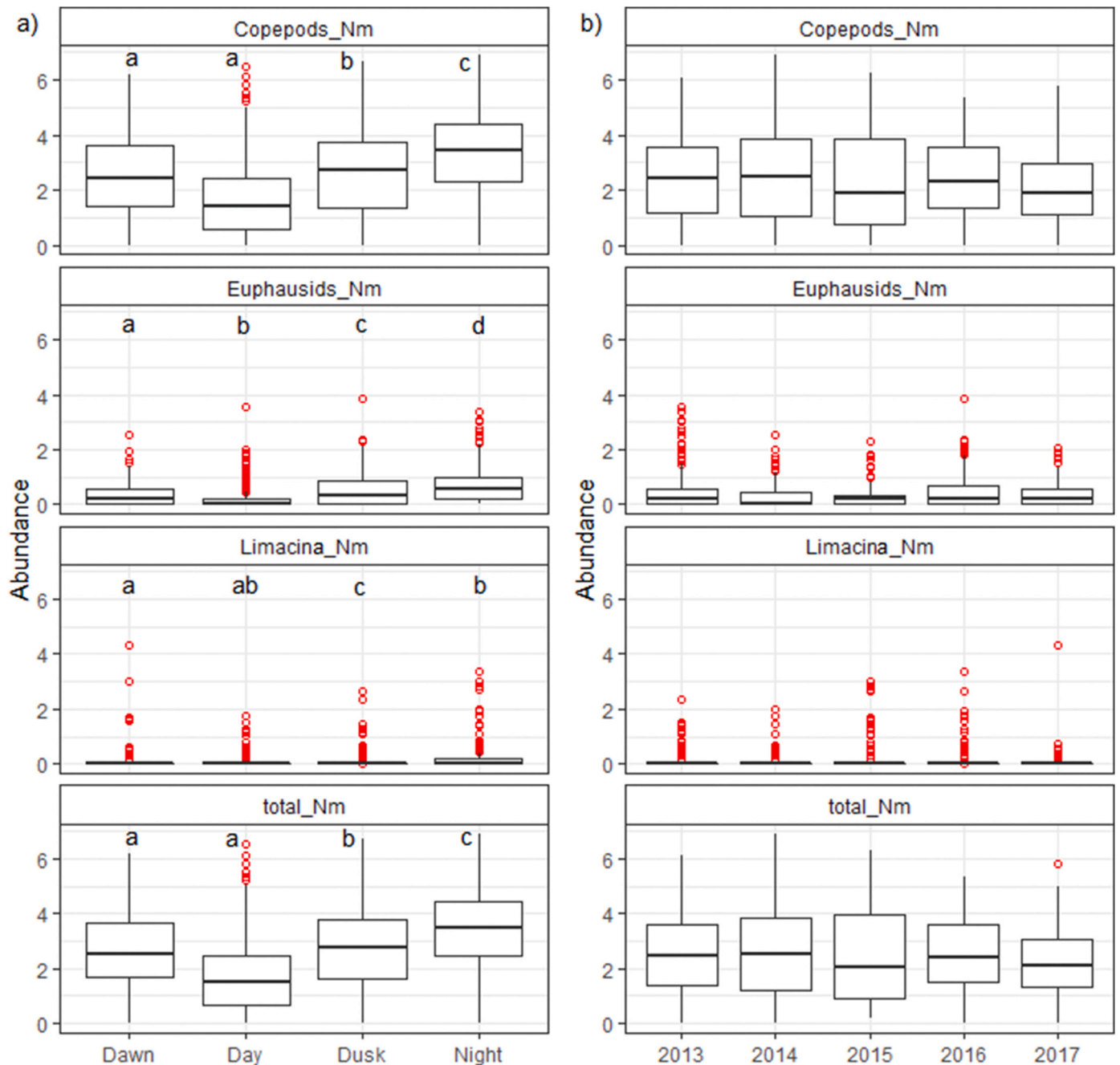


**Fig. 5.** Distribution of abundance value of copepods, euphausiids, *Limacina* and total abundance of zooplankton transformed into a log (x+1) (number of individuals per nautical mile (Nm)) according to different periods of the day (a). Distribution of abundance values of copepods, euphausiids, *Limacina* and total abundance of zooplankton transformed into a log (x+1) (number of individuals per nautical mile) according to different years (b). The outliers are in red. Following the Wilcoxon post-hoc tests, the letters (a, b, c, d, e) correspond to the representation of significance. If two periods of the day share the same letter, then they are not significantly different, and, on the contrary, if two periods of the day do not share the same letter, then they are significantly different. (For interpretation of the references to colour in this figure legend, the reader is referred to the Web version of this article.)

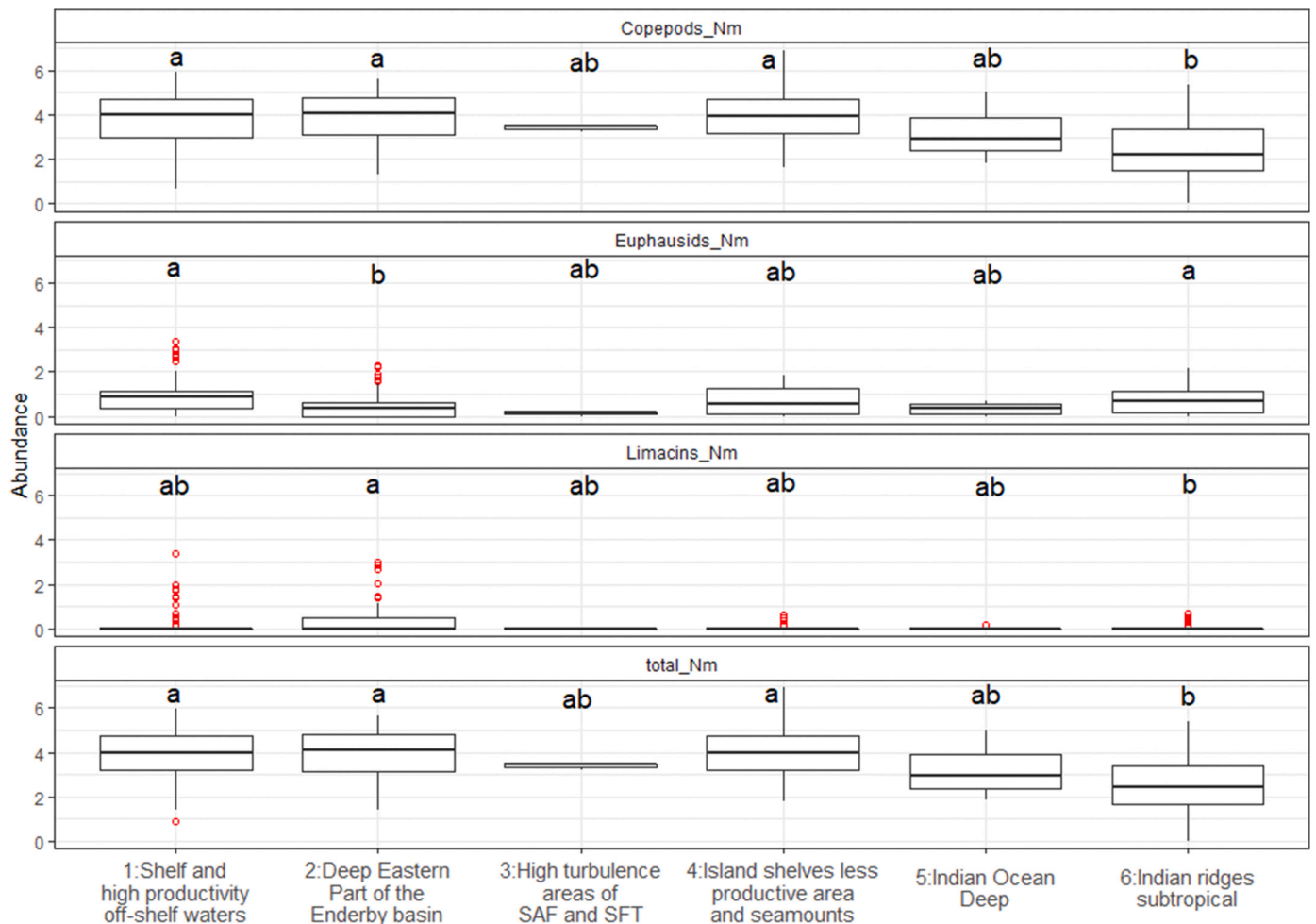


**Fig. 6.** Distribution of values of night abundances of copepods, euphausiids and *Limacina* transformed into a log ( $x+1$ ) (number of individuals per nautical mile (Nm)) according to the different bioregions (the sample sizes for each Bioregion: Bioregion 1: 77 samples; Bioregion 2: 84 samples; Bioregion 3: 3 samples; Bioregion 4: 43 samples; Bioregion 5: 11 samples; Bioregion 6: 120 samples). Following the Wilcoxon post-hoc tests, the letters (a, b, c, d, e) correspond to the representation of significance. If two bioregions share the same letter then they are not significantly different, and, on the contrary, if two bioregions do not share the same letter, then they are significantly different.

abundance of *Limacina* in Bioregion 2 could be related to the more important depths found there. Although not significantly, the shallow shelves of Bioregion 1 also display lower *Limacina* abundance. Further investigations should be done in order to confirm the relationship between *Limacina* abundance and shallow topographies, poorly covered by the existing literature.

Overall, although there are correlations between the three groups of zooplankton and environmental conditions, the different zooplankton groups do not map very well onto the bioregions. Several causes could explain this. Firstly, some key transition bioregions essential for understanding the variability of the studied region - such as Bioregion 3, the high turbulent area between the SAF and the STF - have been under-sampled. Secondly, the coarse taxonomic resolution used in this study could have hampered the identification of clear differences between bioregions. As suggested by previous studies, and given the large temperature gradient sampled, species level data would likely better reveal differences between bioregions in our study area (e.g. Hunt et al., 2011).

#### 4.3. Limits and perspectives

The environmental parameters used in this study come from satellite observations averaged over time and space. Due to their large spatial coverage, these data can be used to distinguish spatial environmental

variations between areas in two dimensions (latitude and longitude) and to explain surface variation in zooplankton abundance. However, these measurements do not take into account how environmental conditions and zooplankton abundance vary according to the vertical dimension, i. e. the depth of the zone. The environmental properties of the water column can influence the ecology of many species along the trophic webs, including top predators (Bost et al., 2009). In addition, we did not consider all the environmental parameters that can affect the abundance of zooplankton. Future studies may consider delineating bioregions in three dimensions and integrating other potentially harmful environmental parameters for zooplankton (e.g. ocean acidification, UV or nutrient levels) to better anticipate the impact of environmental changes on zooplankton in each bioregion.

#### 4.4. Conclusion

In this study, we first characterized bioregions based on physical parameters and chlorophyll-*a*. We then investigated the variations in zooplankton abundance across these bioregions in order to move from a bioregionalization procedure towards an ecoregionalization procedure by progressively integrating species assemblages. Initially, the temporal variations in surface abundance are explained by nocturnal migrations, i.e. zooplankton is more abundant at night in the surface layer. The

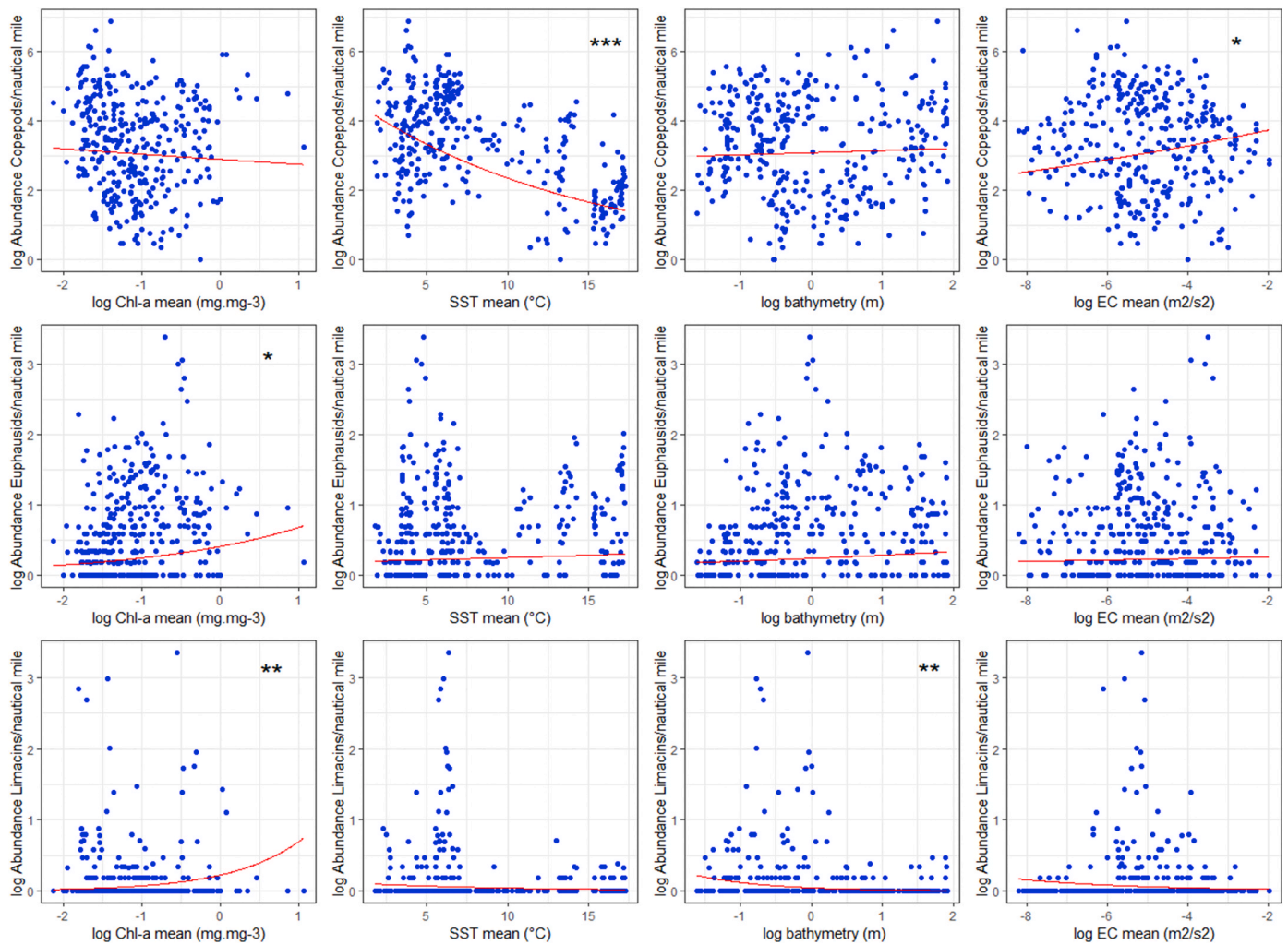


Fig. 7. Log(x+1) of night abundances of the different taxa (TOP: copepods, MIDDLE: euphausiids, BOTTOM: Limacina, all represented as the number of individuals per nautical mile) as a function of the log of Chl-a: chlorophyll-a concentration ( $\text{mg}\cdot\text{m}^{-3}$ ), SST: sea surface temperature ( $^{\circ}\text{C}$ ), Bat: bathymetry (m) and the log of KE: kinetic energy ( $\text{m}^2\cdot\text{s}^{-2}$ ). \* =  $p < 0.05$ , \*\* =  $p < 0.01$ , \*\*\* =  $p < 0.001$  (GLM).

variations in zooplankton abundance are also explained spatially by environmental parameters and, to a lesser degree, by the bioregions. Future campaigns in the under-sampled transition bioregions are needed to determine whether the observed variations could be explained more consistently by the bioregionalization at the meso- and macro-scale, or whether other spatial scales should be considered for their representation.

This study complements previous ecoregionalization work (Koubbi et al., 2016a, 2016b) carried out at smaller spatial scales in the ocean zone around Kerguelen and/or Crozet on the pelagic realm, including seabirds and marine mammals. This work is therefore a further step towards the identification of coherent ecoregions. Once constructed and characterized, these ecoregions will serve as a basis for optimizing marine biodiversity conservation strategies in this part of the Southern Ocean where marine reserves around Crozet, Kerguelen and St-Paul/New Amsterdam were declared by France in 2016 (Koubbi et al., 2016a, 2016b).

An important step forward in ecoregionalization would be the integration of all species in the food web - from phytoplankton to zooplankton, fish and top predators. Indeed, as the different trophic groups do not respond in the same way to spatiotemporal variations in their environment (Koubbi et al., 2011), the way forward to an ecoregionalization of this area is to identify indicator or assemblages from

distinct trophic levels. Future work should therefore investigate further regionalization of less studied mesopelagic fish. Then, it would be interesting to integrate the regionalizations of the different trophic levels in order to obtain a comprehensive regionalization.

#### Declaration of competing interest

None to declare.

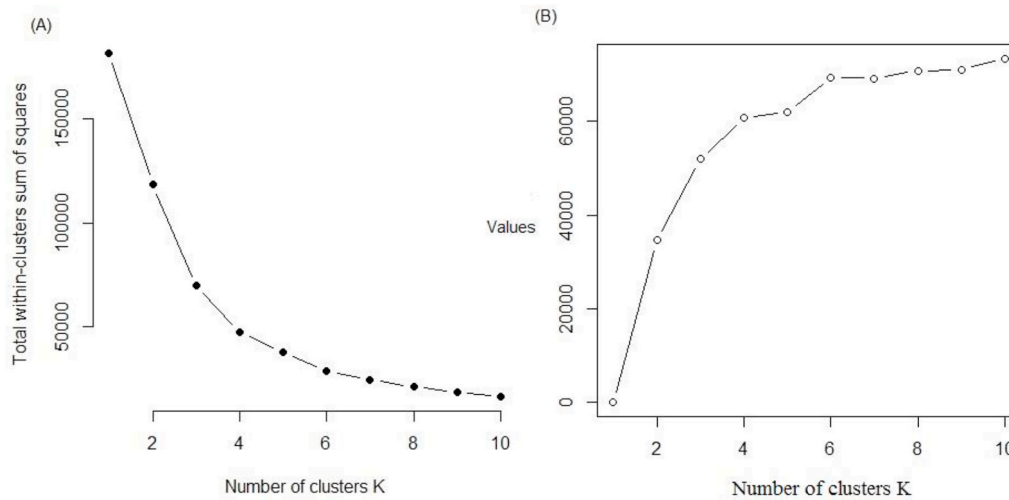
#### Acknowledgements

This work was supported by IPEV, the Flotte Océanographique Française, Zone Atelier Antarctique - CNRS, the European H2020 International Cooperation project MESOPP [grant number 692173] and the TAAF (Southern Lands and Antarctic French Territories) natural reserve. It is related to the SCAR Southern Ocean CPR programme and the Global Alliance CPR Surveys We thank the IPEV teams who were in charge of logistics during the oceanographic surveys, as well as the crew members of the R/V “Marion Dufresne”. We warmly thank Chloé Mignard and Baptiste Sérandour for participating in processing and identification of samples, and Patrice Pruvost for taking in charge the zooplankton sampling during the 2016 survey.



## Appendix A

Outputs of the elbow method (A) and the method of the Calinski Harabasz index (B) which were used to choose the optimal number of clusters and determined the 6 bioregions of our study.



## References

- Ainley, D.G., Ballard, G., Weller, J., 2010. Ross Sea bioregionalization, part I: validation of the 2007 CCAMLR bioregionalization workshop results towards including the Ross Sea in a representative network of marine protected areas in the Southern Ocean. CCAMLR. Document WG-EMM-10/11.
- Ardyna, M., Claustre, H., Sallée, J.B., D'Ovidio, F., Gentili, B., Van Dijken, G., et al., 2017. Delineating environmental control of phytoplankton biomass and phenology in the Southern Ocean. *Geophys. Res. Lett.* 44 (10), 5016–5024. <https://doi.org/10.1002/2016GL072428>.
- Batten, S.D., Abu-Alhija, R., Chiba, S., Edwards, M., Graham, G., Jiyothibabu, R., et al., 2019. A global plankton diversity monitoring program. *Front. Mar. Sci.* 6, 321.
- Béhagle, N., Cotté, C., Ryan, T.E., 2016. Acoustic micronektonic distribution is structured by macroscale oceanographic processes across 20–50°S latitudes in the South-Western Indian Ocean. *Deep-Sea Res. Part I Oceanogr. Res. Pap.* 110, 20–32. <https://doi.org/10.1016/j.dsr.2015.12.007>.
- Biaavati, G., 2014. RAtmosphere: standard Atmospheric profiles. Retrieved from. <http://cran.r-project.org/package=RAtmosphere>.
- Blain, S., Tréguer, P., Belviso, S., Bucciarelli, E., Denis, M., Desabre, S., et al., 2001. A biogeochemical study of the island mass effect in the context of the iron hypothesis: Kerguelen Islands, Southern Ocean. *Deep Sea Res. Oceanogr. Res. Pap.* 48 (1), 163–187. [https://doi.org/10.1016/S0967-0637\(00\)00047-9](https://doi.org/10.1016/S0967-0637(00)00047-9).
- Blain, S., Quéguiner, B., Armand, L., Belviso, S., Bombled, B., Bopp, L., et al., 2007. Effect of natural iron fertilization on carbon sequestration in the Southern Ocean. *Nature* 446 (7139), 1070–1074. <https://doi.org/10.1038/nature05700>.
- Bost, C.A., Cotté, C., Bailleul, F., Cherel, Y., Charrassin, J.B., Guinet, C., et al., 2009. The importance of oceanographic fronts to marine birds and mammals of the southern oceans. *J. Mar. Syst.* 78 (3), 363–376. <https://doi.org/10.1016/j.jmarsys.2008.11.022>.
- Boyd, P.W., Ellwood, M.J., 2010. The biogeochemical cycle of iron in the ocean. *Nat. Geosci.* 3 (10), 675. <https://doi.org/10.1038/ngeo964>.
- Boyd, P.W., Watson, A.J., Law, C.S., Abraham, E.R., Trull, T., Murdoch, R., et al., 2000. A mesoscale phytoplankton bloom in the polar Southern Ocean stimulated by iron fertilization. *Nature* 407 (6805), 695–702. <https://doi.org/10.1038/35037500>.
- Boyd, P.W., Jickells, T., Law, C.S., Blain, S., Boyle, E.A., Buesseler, K.O., et al., 2007. Mesoscale iron enrichment experiments 1993–2005: synthesis and future directions. *Science* 315 (5812), 612–617. <https://doi.org/10.1126/science.1131669>.
- Calinsky, T., Harabasz, J., 1974. A dendrite method for cluster analysis. *Commun. Stat. Theor. Methods* 3 (1), 1–27. Retrieved from. [www.bogucki.com.pl](http://www.bogucki.com.pl).
- Constable, A.J., Melbourne-Thomas, J., Corney, S.P., Arrigo, K.R., Barbraud, C., Barnes, D.K.A., et al., 2014. Climate change and Southern Ocean ecosystems I: how changes in physical habitats directly affect marine biota. *Global Change Biol.* 20 (10), 3004–3025. <https://doi.org/10.1111/gcb.12623>.
- Cotté, C., Park, Y.H., Guinet, C., Bost, C.A., 2007. Movements of foraging king penguins through marine mesoscale eddies. *Proc. Biol. Sci.* 274 (1624), 2385–2391. <https://doi.org/10.1098/rspb.2007.0775>.
- De Baar, H.J.W., Boyd, P.W., Coale, K.H., Landry, M.R., Tsuda, A., Assmy, P., et al., 2005. Synthesis of iron fertilization experiments: from the iron age in the age of enlightenment. *J. Geophys. Res. C Oceans* 110 (9), 1–24. <https://doi.org/10.1029/2004JC002601>.
- De Monte, S., Cotté, C., D'Ovidio, F., Lévy, M., Le Corre, M., Weimerskirch, H., 2012. Frigatebird behaviour at the ocean-atmosphere interface: integrating animal behaviour with multi-satellite data. *J. R. Soc. Interface* 9 (77), 3351–3358. <https://doi.org/10.1098/rsif.2012.0509>.
- Duhamel, G., Hulley, P.A., Causse, R., Koubbi, P., Vacchi, M., Pruvost, P., et al., 2014. Biogeographic patterns of fish. In: *Biogeographic Atlas of the Southern Ocean*, pp. 418–421.
- D'Ovidio, F., Della Penna, A., Trull, T.W., Nencioli, F., Pujol, M.I., Rio, M.H., et al., 2015. The biogeochemical structuring role of horizontal stirring: Lagrangian perspectives on iron delivery downstream of the Kerguelen Plateau. *Biogeosciences* 12 (19), 5567–5581. <https://doi.org/10.5194/bg-12-5567-2015>.
- Flierl, G.R., Davis, C.S., 1993. Biological effects of gulf stream meandering. *J. Mar. Res.* 51 (3), 529–560. <https://doi.org/10.1357/0022240933224016>.
- Foster, S.D., Hill, N.A., Lyons, M., 2017. Ecological grouping of survey sites when sampling artefacts are present. *J. Roy. Stat. Soc. Series C Appl. Stat.* 66 (5), 1031–1047. <https://doi.org/10.1111/rssc.12211>.
- Gandhi, N., Ramesh, R., Laskar, A.H., Sheshshayee, M.S., Shetye, S., Anilkumar, N., et al., 2012. Zonal variability in primary production and nitrogen uptake rates in the southwestern Indian Ocean and the Southern Ocean. *Deep-Sea Res. Part I Oceanogr. Res. Pap.* 67, 32–43. <https://doi.org/10.1016/j.dsr.2012.05.003>.
- Graham, R.M., De Boer, A.M., van Sebille, E., Kohfeld, K.E., Schlosser, C., 2015. Inferring source regions and supply mechanisms of iron in the Southern Ocean from satellite chlorophyll data. *Deep-Sea Res. Part I Oceanogr. Res. Pap.* 104, 9–25. <https://doi.org/10.1016/j.dsr.2015.05.007>.
- Grant, S., Constable, A., Raymond, B., Doust, S., 2006. *Bioregionalisation of the Southern Ocean*. Hobart.
- Gutt, J., Bertler, N., Bracegirdle, T.J., Buschmann, A., Comiso, J., Hosie, G., et al., 2015. The Southern Ocean ecosystem under multiple climate change stresses - an integrated circumpolar assessment. *Global Change Biol.* 21 (4), 1434–1453. <https://doi.org/10.1111/gcb.12794>.
- Handegard, N.O., Buisson, L. Du, Brehmer, P., Chalmers, S.J., De Robertis, A., Huse, G., et al., 2013. Towards an acoustic-based coupled observation and modelling system for monitoring and predicting ecosystem dynamics of the open ocean. *Fish Fish.* 14 (4), 605–615. <https://doi.org/10.1111/j.1467-2979.2012.00480.x>.
- Harris, P.T., Macmillan-Lawler, M., Rupp, J., Baker, E.K., 2014. Geomorphology of the oceans. *Mar. Geol.* 352, 4–24. <https://doi.org/10.1016/j.margeo.2014.01.011>.
- Hill, N.A., Foster, S.D., Duhamel, G., Welsford, D., Koubbi, P., Johnson, C.R., 2017. Model-based mapping of assemblages for ecology and conservation management: a case study of demersal fish on the Kerguelen Plateau. *Divers. Distrib.* 23 (10), 1216–1230. <https://doi.org/10.1111/ddi.12613>.
- Hogg, O.T., Huvenne, V.A.I., Griffiths, H.J., Linse, K., 2018. On the ecological relevance of landscape mapping and its application in the spatial planning of very large marine protected areas. *Sci. Total Environ.* 626, 384–398. <https://doi.org/10.1016/j.scitotenv.2018.01.009>.
- Hosie, G., Fukuchi, M., Kawaguchi, S., 2003. Development of the Southern Ocean continuous plankton recorder survey. *Prog. Oceanogr.* 58 (2–4), 263–283. <https://doi.org/10.1016/j.pocean.2003.08.007>.
- Hosie, G., Mormède, S., Kitchener, J., Takahashi, K., Raymond, B., 2014. 10.3. Near-surface zooplankton communities. In: *Biogeographic atlas of the Southern Ocean* (pp. 422–430).

- Hunt, B.P., Hsieh, G.W., 2003. The Continuous Plankton Recorder in the Southern Ocean: a comparative analysis of zooplankton communities sampled by the CPR and vertical net hauls along 140 E. *J. Plankton Res.* 25 (12), 1561–1579. <https://doi.org/10.1093/plankt/fbg108>.
- Hunt, B.P.V., Hsieh, G.W., 2006a. The seasonal succession of zooplankton in the Southern Ocean south of Australia, part I: the seasonal ice zone. *Deep Sea Res.* *Oceanogr. Res. Pap.* 53 (7), 1182–1202. <https://doi.org/10.1016/j.dsr.2006.05.001>.
- Hunt, B.P.V., Hsieh, G.W., 2006b. The seasonal succession of zooplankton in the Southern Ocean south of Australia, part II: the sub-antarctic to polar frontal zones. *Deep Sea Res.* *Oceanogr. Res. Pap.* 53 (7), 1203–1223. <https://doi.org/10.1016/j.dsr.2006.05.002>.
- Hunt, B.P.V., Pakhomov, E.A., Williams, R., 2011. Comparative analysis of 1980's and 2004 macrozooplankton composition and distribution in the vicinity of Kerguelen and Heard Islands: seasonal cycles and oceanographic forcing of long-term change. *Cybiurn* 35, 79–92. <https://doi.org/10.26028/cybiurn/2011-35SP-008>.
- IPCC, 2019. In: Pörtner, H.-O., Roberts, D.C., Masson-Delmotte, V., Zhai, P., Tignor, M., Poloczanska, E., Mintenbeck, K., Alegría, A., Nicolai, M., Okem, A., Petzold, J., Rama, B., Weyer, N.M. (Eds.), *IPCC Special Report on the Ocean and Cryosphere in a Changing Climate* (in press).
- Irigoin, X., Huisman, J., Harris, R.P., 2004. Global biodiversity patterns of marine phytoplankton and zooplankton. *Nature* 429 (6994), 863–867.
- Kodinariya, T.M., Makwana, P.R., 2013. Review on determining number of Cluster in K-Means Clustering. *International Journal of Advance Research in Computer Science and Management Studies* 1 (6), 90–95.
- Koubbi, P., 1993. Influence of the frontal zones on ichthyoplankton and mesopelagic fish assemblages in the Crozet Basin (Indian sector of the Southern Ocean). *Polar Biol.* 13 (8), 557–564. <https://doi.org/10.1007/BF00236398>.
- Koubbi, P., Ozouf-Costaz, C., Goarant, A., Moteki, M., Hulley, P.-A., Causse, R., et al., 2010. Estimating the biodiversity of the east antarctic shelf and oceanic zone for ecoregionalisation: example of the ichthyofauna of the CEAMARC (collaborative east antarctic marine census) CAML surveys. *Pol. Sci.* 4 (2), 115–133. <https://doi.org/10.1016/j.polar.2010.04.012>.
- Koubbi, P., Mignard, C., Causse, R., Da Silva, O., Baudena, A., Bost, C., et al., 2016. Ecoregionalisation of the Kerguelen and Crozet islands oceanic zone. Part II: the Crozet oceanic zone. *CCAMLR Document*, WG-EMM-16/54.
- Koubbi, P., Moteki, M., Duhamel, G., Goarant, A., Hulley, P.A., O'Driscoll, R., et al., 2011. Ecoregionalization of myctophid fish in the Indian sector of the Southern Ocean: results from generalized dissimilarity models. *Deep-Sea Res. Part II Top. Stud. Oceanogr.* 58 (1–2), 170–180. <https://doi.org/10.1016/j.dsr2.2010.09.007>.
- Koubbi, P., Guinet, C., Alloncle, N., Ameziane, N., Azam, C.S., Baudena, A., et al., 2016a. Ecoregionalisation of the Kerguelen and Crozet islands oceanic zone. Part I: introduction and Kerguelen oceanic zone. *CCAMLR Document* WG-EMM-16/43.
- Lê, S., Josse, J., Husson, F., 2008. FactoMineR: an R package for multivariate analysis. *J. Stat. Software* 25 (1), 1–18.
- Lehodey, P., Conchon, A., Senina, I., Domokos, R., Calmettes, B., Jouanno, J., et al., 2015. Optimization of a micronekton model with acoustic data. *ICES (Int. Council Explor. Sea) J. Mar. Sci.* 72 (5), 1399–1412.
- Lévy, M., 2008. The modulation of biological production by oceanic mesoscale turbulence. In: *Transport and Mixing in Geophysical Flows*. Springer, Berlin, Heidelberg, pp. 219–261.
- Longhurst, A.R., 2010. *Ecological Geography of the Sea*. Elsevier.
- Machu, E., Garçon, V., 2001. Phytoplankton seasonal distribution from SeaWiFS data in the Agulhas Current system. *J. Mar. Res.* 59 (5), 795–812. <https://doi.org/10.1357/00224001762674944>.
- MacQueen, J., 1967. Some methods for classification and analysis of multivariate observations. *Proc. Fifth Berkeley Symp. Math. Statist. Prob.* 1 (14), 281–297. <https://doi.org/10.1007/s11665-016-2173-6>.
- Martin, J.H., 1990. Glacial-interglacial CO<sub>2</sub> change: the iron hypothesis. *Paleoceanography* 5 (1), 1–13.
- McClain, C.R., Signorini, S.R., Christian, J.R., 2004. Subtropical gyre variability observed by ocean-color satellites. *Deep Sea Res. Part II Top. Stud. Oceanogr.* 51 (1–3), 281–301.
- Meilland, J., Fabri-Ruiz, S., Koubbi, P., Monaco, C. Lo, Cotte, C., Hsieh, G.W., et al., 2016. Planktonic foraminiferal biogeography in the Indian sector of the Southern Ocean: contribution from CPR data. *Deep-Sea Res. Part I Oceanogr. Res. Pap.* 110, 75–89. <https://doi.org/10.1016/j.dsr.2015.12.014>.
- Morel, A., Claustre, H., Gentili, B., 2010. The most oligotrophic subtropical zones of the global ocean: similarities and differences in terms of chlorophyll and yellow substance. *Biogeosciences* 7 (10), 3139–3151. <https://doi.org/10.5194/bg-7-3139-2010>.
- Orsi, A.H., Whitworth, T., Nowlin, W.D., 1995. On the meridional extent and fronts of the Antarctic Circumpolar Current. *Deep-Sea Res. Part I* 42 (5), 641–673. [https://doi.org/10.1016/0967-0637\(95\)00021-W](https://doi.org/10.1016/0967-0637(95)00021-W).
- Oschlies, A., Garçon, V., 1998. Eddy-induced enhancement of primary production in a model of the North Atlantic Ocean. *Nature* (266). [https://doi.org/10.1038/28373\\_394\(6690\)](https://doi.org/10.1038/28373_394(6690)).
- Park, Y.H., Gambèroni, L., Charriaud, E., 1991. Frontal structure and transport of the antarctic circumpolar current in the South Indian ocean sector, 40–80°E. *Mar. Chem.* 35 (1–4), 45–62. [https://doi.org/10.1016/S0304-4203\(09\)90007-X](https://doi.org/10.1016/S0304-4203(09)90007-X).
- Park, Y.H., Gambèroni, L., Charriaud, E., 1993. Frontal structure, water masses, and circulation in the Crozet Basin. *J. Geophys. Res.* 98 (C7), 12361–12385. <https://doi.org/10.1029/93jc00938>.
- Park, Y.H., Pollard, R.T., Read, J.F., Lebour, V., 2002. A quasi-synoptic view of the frontal circulation in the Crozet Basin during the Antares-4 cruise. *Deep-Sea Res. Part II Top. Stud. Oceanogr.* 49 (9–10), 1823–1842. [https://doi.org/10.1016/S0967-0645\(02\)00014-0](https://doi.org/10.1016/S0967-0645(02)00014-0).
- Park, Y.H., Roquet, F., Durand, I., Fuda, J.L., 2008. Large-scale circulation over and around the northern Kerguelen plateau. *Deep-Sea Res. Part II Top. Stud. Oceanogr.* 55 (5–7), 566–581. <https://doi.org/10.1016/j.dsr2.2007.12.030>.
- Pitcher, T.J., Morato, T., Hart, P.J., Clark, M.R., Haggan, N., Santos, R.S. (Eds.), 2008. *Seamounts: Ecology, Fisheries and Conservation*. John Wiley & Sons.
- Pollard, R.T., Read, J.F., 2001. Circulation pathways and transports of the Southern Ocean in the vicinity of the Southwest Indian ridge. *J. Geophys. Res.: Oceans* 106 (C2), 2881–2898. <https://doi.org/10.1029/2000JC900090>.
- Pollard, R.T., Lucas, M.L., Read, J.F., 2002. Physical controls on biogeochemical zonation in the Southern Ocean. *Deep-Sea Res. Part II Top. Stud. Oceanogr.* 49 (16), 3289–3305. [https://doi.org/10.1016/S0967-0645\(02\)00084-X](https://doi.org/10.1016/S0967-0645(02)00084-X).
- Pollard, R.T., Venables, H.J., Read, J.F., Allen, J.T., 2007. Large-scale circulation around the Crozet Plateau controls an annual phytoplankton bloom in the Crozet Basin. *Deep-Sea Res. Part II Top. Stud. Oceanogr.* 54 (18–20), 1915–1929. <https://doi.org/10.1016/j.dsr2.2007.06.012>.
- Pollard, R., Sanders, R., Lucas, M., Statham, P., 2007. The Crozet natural iron bloom and export experiment (CROZEX). *Deep-Sea Res. Part II Top. Stud. Oceanogr.* 54 (18–20), 1905–1914. <https://doi.org/10.1016/j.dsr2.2007.07.023>.
- Pondaven, P., Fravallo, C., Ruiz-Pino, D., Tréguer, P., Quéguiner, B., Jeandel, C., 1998. Modelling the silica pump in the permanently open ocean zone of the Southern Ocean. *J. Mar. Syst.* 17 (1–4), 587–619.
- Pörtner, H.O., Peck, L., Somero, G., 2007. Thermal limits and adaptation in marine Antarctic ectotherms: an integrative view. *Phil. Trans. Biol. Sci.* 362 (1488), 2233–2258. <https://doi.org/10.1098/rstb.2006.1947>.
- Post, A.L., Meijers, A.J.S., Fraser, A.D., Meiners, K.M., Ayers, J., Bindoff, N., et al., 2014. Environmental setting. In: *Biogeographic Atlas of the Southern Ocean*, pp. 418–421. R Core Team, 2018. R: a language and environment for statistical computing. Retrieved from <https://www.r-project.org/>.
- Raymond, B., 2014. Pelagic regionalisation. In: *Biogeographic Atlas of the Southern Ocean*, pp. 418–421.
- Reygondaud, G., Huettmann, F., 2014. Past, present and future state of pelagic habitats in the Antarctic Ocean. *Biogeogr. Atls South. Ocean.* 397–403.
- Ropert-Coudert, Y., Hindell, M.A., Phillips, R.A., Charrassin, J.B., Trudelle, L., Raymond, B., 2014. Biogeographic patterns of birds and mammals. In: *Biogeographic Atlas of the Southern Ocean*, pp. 418–421.
- Roquet, F., Park, Y.H., Guinet, C., Baillieu, F., Charrassin, J.B., 2009. Observations of the fawn trough current over the Kerguelen plateau from instrumented elephant seals. *J. Mar. Syst.* 78 (3), 377–393. <https://doi.org/10.1016/j.jmarsys.2008.11.017>.
- Sanial, V., van Beek, P., Lansard, B., D'Ovidio, F., Kestenare, E., Souhaut, M., et al., 2014. Study of the phytoplankton plume dynamics off the Crozet Islands (Southern Ocean): a geochemical-physical coupled approach. *J. Geophys. Res.: Oceans* 119 (4), 2227–2237. <https://doi.org/10.1002/2013JC009305>.
- Sokolov, S., Rintoul, S.R., 2007. On the relationship between fronts of the Antarctic Circumpolar Current and surface chlorophyll concentrations in the Southern Ocean. *J. Geophys. Res.: Oceans* 112 (7), 1–17. <https://doi.org/10.1029/2006JC004072>.
- Sokolov, S., Rintoul, S.R., 2009. Circumpolar structure and distribution of the antarctic circumpolar current fronts: 1. Mean98 circumpolar paths. *J. Geophys. Res.: Oceans* 114 (11), 1–19. <https://doi.org/10.1029/2008JC005108>.
- Spalding, M.D., Fox, H.E., Allen, G.R., Davidson, N., Ferdana, Z.A., Finlayson, M., et al., 2007. Marine ecoregions of the world: a bioregionalization of coastal and shelf areas. *Bioscience* 57 (7), 573–583. <https://doi.org/10.1641/B570707>.
- Takahashi, K.T., Kawaguchi, S., Kobayashi, M., Hsieh, G.W., Fukuchi, M., Toda, T., 2002. Zooplankton distribution patterns in relation to the antarctic polar front zones recorded by continuous plankton recorder (CPR) during 1999/2000 kaiyo maru cruise. *Polar Biosci* 15, 97–107. <https://doi.org/10.1016/j.polar.2011.04.003>.
- Takahashi, K.T., Hsieh, G.W., Kitchener, J.A., McLeod, D.J., Odate, T., Fukuchi, M., 2010. Comparison of zooplankton distribution patterns between four seasons in the Indian Ocean sector of the Southern Ocean. *Pol. Sci.* 4 (2), 317–331. <https://doi.org/10.1016/j.polar.2010.05.002>.
- Takahashi, K.T., Hsieh, G.W., McLeod, D.J., Kitchener, J.A., 2011. Surface zooplankton distribution patterns during austral summer in the Indian sector of the Southern Ocean, south of Australia. *Pol. Sci.* 5 (2), 134–145. <https://doi.org/10.1016/j.polar.2011.04.003>.
- Turner, J., Barrard, N.E., Bracegirdle, T.J., Convey, P., Hodgson, D.A., Jarvis, M., et al., 2014. Antarctic climate change and the environment: an update. *Polar Rec.* 50 (3), 237–259. <https://doi.org/10.1017/S0032247413000296>.
- Venkataramana, V., Anilkumar, N., Naik, R.K., Mishra, R.K., Sabu, P., 2019. Temperature and phytoplankton size class biomass drives the zooplankton food web dynamics in the Indian Ocean sector of the Southern Ocean. *Polar Biol.* 42 (4), 823–829. <https://doi.org/10.1007/s00300-019-02472-w>.

# Bibliography





- Abadie, C., Lacan, F., Radic, A., Pradoux, C., and Poitrasson, F. (2017). Iron isotopes reveal distinct dissolved iron sources and pathways in the intermediate versus deep southern ocean. *Proceedings of the National Academy of Sciences*, 114(5):858–863. Publisher: National Academy of Sciences Section: Physical Sciences.
- Agostini, V., Arico, S., Briones, E., Clark, M., Cresswell, I., Gjerde, K., Grant, S., Niewijk, D., Polacheck, A., Rice, J., Roff, J., Scanlon, K., Smith, C., Spalding, M., Tong, E., Vierros, M., and Watling, L. (2009). Biogeographic classification. In *Global Open Oceans and Deep Seabed (GOODS) biogeographic classification*. UNESCO-IOC Technical Series.
- Almany, G. R., Connolly, S. R., Heath, D. D., Hogan, J. D., Jones, G. P., McCook, L. J., Mills, M., Pressey, R. L., and Williamson, D. H. (2009). Connectivity, biodiversity conservation and the design of marine reserve networks for coral reefs. *Coral Reefs*, 28(2):339–351.
- Alvain, S., Moulin, C., Dandonneau, Y., and Bréon, F. M. (2005). Remote sensing of phytoplankton groups in case 1 waters from global SeaWiFS imagery. *Deep Sea Research Part I: Oceanographic Research Papers*, 52(11):1989–2004.
- Alvain, S., Moulin, C., Dandonneau, Y., and Loisel, H. (2008). Seasonal distribution and succession of dominant phytoplankton groups in the global ocean: A satellite view. *Global Biogeochemical Cycles*, 22(3).
- Andrello, M., Mouillot, D., Somot, S., Thuiller, W., and Manel, S. (2015). Additive effects of climate change on connectivity between marine protected areas and larval supply to fished areas. *Diversity and Distributions*, 21(2):139–150.
- Andrews-Goff, V., Bestley, S., Gales, N. J., Laverick, S. M., Paton, D., Polanowski, A. M., Schmitt, N. T., and Double, M. C. (2018). Humpback whale migrations to antarctic summer foraging grounds through the southwest pacific ocean. *Scientific Reports*, 8(1):12333. Nature Publishing Group.
- Ardyna, M., Claustre, H., Sallée, J.-B., D’Ovidio, F., Gentili, B., van Dijken, G., D’Ortenzio, F., and Arrigo, K. R. (2017). Delineating environmental control of phytoplankton biomass and phenology in the southern ocean: Phytoplankton dynamics in the SO. *Geophysical Research Letters*, 44(10):5016–5024.
- Ardyna, M., Lacour, L., Sergi, S., d’Ovidio, F., Sallée, J.-B., Rembauville, M., Blain, S., Tagliabue, A., Schlitzer, R., Jeandel, C., Arrigo, K. R., and Claustre, H. (2019). Hydrothermal vents trigger massive phytoplankton blooms in the southern ocean. *Nature Communications*, 10(1):2451.
- Bakker, D. C. E., Nielsdttir, M. C., Morris, P. J., Venables, H. J., and Watson, A. J. (2007). The island mass effect and biological carbon uptake for the subantarctic crozet archipelago. *Deep Sea Research Part II: Topical Studies in Oceanography*, 54(18):2174–2190.
- Bakun, A. (1996). *Patterns in the ocean: ocean processes and marine population dynamics*. California Sea Grant, in cooperation with Centro de Investigaciones Biológicas del Noroeste, La Paz, Mexico. ISBN: 978-1-888691-01-6.
- Baudena, A., Ser-Giacomi, E., Lpez, C., Hernandez-Garca, E., and d’Ovidio, F. (2019). Crossroads of the mesoscale circulation. *Journal of Marine Systems*, 192:1–14.
- Beaulieu, S. E. and Szafranski, K. M. (2020). InterRidge global database of active submarine hydrothermal vent fields version 3.4. Publisher: PANGAEA Type: dataset.

- Bennett, S. A., Achterberg, E. P., Connelly, D. P., Statham, P. J., Fones, G. R., and German, C. R. (2008). The distribution and stabilisation of dissolved Fe in deep-sea hydrothermal plumes. *Earth and Planetary Science Letters*, 270(3):157–167.
- Benoit-Bird, K. J. and McManus, M. A. (2012). Bottom-up regulation of a pelagic community through spatial aggregations. *Biology Letters*, 8(5):813–816.
- Bergquist, B. A. and Boyle, E. A. (2006). Dissolved iron in the tropical and subtropical Atlantic ocean. *Global Biogeochemical Cycles*, 20(1).
- Bergquist, B. A., Wu, J., and Boyle, E. A. (2007). Variability in oceanic dissolved iron is dominated by the colloidal fraction. *Geochimica et Cosmochimica Acta*, 71(12):2960–2974.
- Bestley, S., Ropert-Coudert, Y., Bengtson Nash, S., Brooks, C. M., Cotté, C., Dewar, M., Friedlaender, A. S., Jackson, J. A., Labrousse, S., Lowther, A. D., McMahon, C. R., Phillips, R. A., Pistorius, P., Puskic, P. S., Reis, A. O. d. A., Reisinger, R. R., Santos, M., Tarszisz, E., Tixier, P., Trathan, P. N., Wege, M., and Wienecke, B. (2020). Marine ecosystem assessment for the southern ocean: Birds and marine mammals in a changing climate. *Frontiers in Ecology and Evolution*, 8. Publisher: Frontiers.
- Black, E. E., Kienast, S. S., Lemaitre, N., Lam, P. J., Anderson, R. F., Planquette, H., Planchon, F., and Buesseler, K. O. (2020). Ironing out Fe residence time in the dynamic upper ocean. *Global Biogeochemical Cycles*, 34(9):e2020GB006592.
- Blain, S., Quéguiner, B., Armand, L., Belviso, S., Bombled, B., Bopp, L., Bowie, A., Brunet, C., Brussaard, C., Carlotti, F., Christaki, U., Corbière, A., Durand, I., Ebersbach, F., Fuda, J.-L., Garcia, N., Gerringa, L., Griffiths, B., Guigue, C., Guillerm, C., Jacquet, S., Jeandel, C., Laan, P., Lefèvre, D., Lo Monaco, C., Malits, A., Mosseri, J., Obernosterer, I., Park, Y.-H., Picheral, M., Pondaven, P., Remenyi, T., Sandroni, V., Sarthou, G., Savoye, N., Scouarnec, L., Souhaut, M., Thuiller, D., Timmermans, K., Trull, T., Uitz, J., van Beek, P., Veldhuis, M., Vincent, D., Viollier, E., Vong, L., and Wagener, T. (2007). Effect of natural iron fertilization on carbon sequestration in the southern ocean. *Nature*, 446(7139):1070–1074. Number: 7139 Publisher: Nature Publishing Group.
- Blain, S., Tréguer, P., Belviso, S., Bucciarelli, E., Denis, M., Desabre, S., Fiala, M., Martin-Jezequel, V., Fèvre, J., Mayzaud, P., Marty, J.-C., and Razouls, S. (2001). Biogeochemical study of an island mass effect in the context of the iron hypothesis in the southern ocean. *Deep Sea Research Part I Oceanographic Research Papers*, 48:163–187.
- Bonizzoni, S., Furey, N. B., Santostasi, N. L., Eddy, L., Valavanis, V. D., and Bearzi, G. (2019). Modelling dolphin distribution within an important marine mammal area in Greece to support spatial management planning. *Aquatic Conservation: Marine and Freshwater Ecosystems*, 29(10):1665–1680.
- Borrione, I., Aumont, O., Nielsdttir, M. C., and Schlitzer, R. (2014). Sedimentary and atmospheric sources of iron around South Georgia, Southern Ocean: a modelling perspective. *Biogeosciences*, 11(7):1981–2001.
- Borrione, I. and Schlitzer, R. (2013). Distribution and recurrence of phytoplankton blooms around South Georgia, Southern Ocean. *Biogeosciences*, 10(1):217–231.
- Bossart, G. D. (2011). Marine mammals as sentinel species for oceans and human health. *Veterinary Pathology*, 48(3):676–690. Publisher: SAGE Publications Inc.

- Bost, C. A., Cotté, C., Bailleul, F., Cherel, Y., Charrassin, J. B., Guinet, C., Ainley, D. G., and Weimerskirch, H. (2009). The importance of oceanographic fronts to marine birds and mammals of the southern oceans. *Journal of Marine Systems*, 78(3):363–376.
- Bost, C. A., Cotté, C., Terray, P., Barbraud, C., Bon, C., Delord, K., Gimenez, O., Handrich, Y., Naito, Y., Guinet, C., and Weimerskirch, H. (2015). Large-scale climatic anomalies affect marine predator foraging behaviour and demography. *Nature Communications*, 6(1):8220. Publisher: Nature Publishing Group.
- Bowie, A. R., van der Merwe, P., Quéroúé, F., Trull, T., Fourquez, M., Planchon, F., Sarthou, G., Chever, F., Townsend, A. T., Obernosterer, I., Sallée, J.-B., and Blain, S. (2015). Iron budgets for three distinct biogeochemical sites around the kerguelen archipelago (southern ocean) during the natural fertilisation study, KEOPS-2. *Biogeosciences*, 12(14):4421–4445.
- Boyd, P. W., Arrigo, K. R., Strzepek, R., and Dijken, G. L. v. (2012). Mapping phytoplankton iron utilization: Insights into southern ocean supply mechanisms. *Journal of Geophysical Research: Oceans*, 117.
- Boyd, P. W. and Ellwood, M. J. (2010). The biogeochemical cycle of iron in the ocean. *Nature Geoscience*, 3(10):675–682.
- Boyd, P. W., Ellwood, M. J., Tagliabue, A., and Twining, B. S. (2017). Biotic and abiotic retention, recycling and remineralization of metals in the ocean. *Nature Geoscience*, 10(3):167–173. Publisher: Nature Publishing Group.
- Boyd, P. W., Strzepek, R. F., Ellwood, M. J., Hutchins, D. A., Nodder, S. D., Twining, B. S., and Wilhelm, S. W. (2015). Why are biotic iron pools uniform across high- and low-iron pelagic ecosystems? *Global Biogeochemical Cycles*, 29(7):1028–1043. Publisher: John Wiley & Sons, Ltd.
- Boyd, P. W., Watson, A. J., Law, C. S., Abraham, E. R., Trull, T., Murdoch, R., Bakker, D. C., Bowie, A. R., Buesseler, K. O., Chang, H., Charette, M., Croot, P., Downing, K., Frew, R., Gall, M., Hadfield, M., Hall, J., Harvey, M., Jameson, G., LaRoche, J., Liddicoat, M., Ling, R., Maldonado, M. T., McKay, R. M., Nodder, S., Pickmere, S., Pridmore, R., Rintoul, S., Safi, K., Sutton, P., Strzepek, R., Tanneberger, K., Turner, S., Waite, A., and Zeldis, J. (2000). A mesoscale phytoplankton bloom in the polar southern ocean stimulated by iron fertilization. *Nature*, 407(6805):695–702.
- Brooks, C. M. (2013). Competing values on the antarctic high seas: CCAMLR and the challenge of marine-protected areas. *The Polar Journal*, 3(2):277–300.
- Brooks, C. M., Chown, S. L., Douglass, L. L., Raymond, B. P., Shaw, J. D., Sylvester, Z. T., and Torrens, C. L. (2020a). Progress towards a representative network of southern ocean protected areas. *PLOS ONE*, 15(4):e0231361.
- Brooks, C. M., Crowder, L. B., sterblom, H., and Strong, A. L. (2020b). Reaching consensus for conserving the global commons: The case of the ross sea, antarctica. *Conservation Letters*, 13(1):e12676.
- Browning, T. J., Achterberg, E. P., Yong, J. C., Rapp, I., Utermann, C., Engel, A., and Moore, C. M. (2017). Iron limitation of microbial phosphorus acquisition in the tropical north atlantic. *Nature Communications*, 8(1):15465. Publisher: Nature Publishing Group.

- Bruland, K. W., Orians, K. J., and Cowen, J. P. (1994). Reactive trace metals in the stratified central north pacific. *Geochimica et Cosmochimica Acta*, 58(15):3171–3182.
- Bruno, J. F., Bates, A. E., Cacciapaglia, C., Pike, E. P., Amstrup, S. C., van Hooedonk, R., Henson, S. A., and Aronson, R. B. (2018). Climate change threatens the world’s marine protected areas. *Nature Climate Change*, 8(6):499–503. Publisher: Nature Publishing Group.
- Caldow, C., Monaco, M., Pittman, S., Kendall, M., Goedeke, T., Menza, C., Kinlan, B., and Costa, B. (2015). Biogeographic assessments: A framework for information synthesis in marine spatial planning. *Marine Policy*, 51:423–432.
- Camphuysen, C. J. (2006). *Top Predators in Marine Ecosystems: Their Role in Monitoring and Management*. Cambridge University Press.
- Charrassin, J.-B., Park, Y.-H., Maho, Y. L., and Bost, C.-A. (2002). Penguins as oceanographers unravel hidden mechanisms of marine productivity. *Ecology Letters*, 5(3):317–319.
- Christie, M. R., Tissot, B. N., Albins, M. A., Beets, J. P., Jia, Y., Ortiz, D. M., Thompson, S. E., and Hixon, M. A. (2010). Larval connectivity in an effective network of marine protected areas. *PLOS ONE*, 5(12):e15715. Publisher: Public Library of Science.
- Claustre, H. (2010). Bio-optical profiling floats as new observational tools for biogeochemical and ecosystem studies: Potential synergies with ocean color remote sensing. In *Proceedings of OceanObs’09: Sustained Ocean Observations and Information for Society*, pages 177–183. European Space Agency. ISBN: 978-3-86987-200-1.
- Collins, M. A., Xavier, J. C., Johnston, N. M., North, A. W., Enderlein, P., Tarling, G. A., Waluda, C. M., Hawker, E. J., and Cunningham, N. J. (2008). Patterns in the distribution of myctophid fish in the northern scotia sea ecosystem. *Polar Biology*, 31(7):837–851.
- Corrigan, C. M., Ardron, J. A., Comeros-Raynal, M. T., Hoyt, E., Sciara, G. N. D., and Carpenter, K. E. (2014). Developing important marine mammal area criteria: learning from ecologically or biologically significant areas and key biodiversity areas. *Aquatic Conservation: Marine and Freshwater Ecosystems*, 24:166–183.
- cotté, C., d’Ovidio, F., Chaigneau, A., Lévy, M., Taupier-Letage, I., Mate, B., and Guinet, C. (2011). Scale-dependent interactions of mediterranean whales with marine dynamics. *Limnology and Oceanography*, 56(1):219–232.
- Cotté, C., d’Ovidio, F., Dragon, A.-C., Guinet, C., and Lévy, M. (2015). Flexible preference of southern elephant seals for distinct mesoscale features within the antarctic circumpolar current. *Progress in Oceanography*, 131:46–58.
- Cotté, C., Park, Y.-H., Guinet, C., and Bost, C.-A. (2007). Movements of foraging king penguins through marine mesoscale eddies. *Proceedings of the Royal Society B: Biological Sciences*, 274(1624):2385–2391.
- Cowen, R. K. and Sponaugle, S. (2009). Larval dispersal and marine population connectivity. *Annual Review of Marine Science*, 1(1):443–466.
- Crain, C. M., Kroeker, K., and Halpern, B. S. (2008). Interactive and cumulative effects of multiple human stressors in marine systems. *Ecology Letters*, 11(12):1304–1315.

- Croll, D., Marinovic, B., Benson, S., Chavez, F., Black, N., Ternullo, R., and Tershy, B. (2005). From wind to whales: trophic links in a coastal upwelling system. *Marine Ecology Progress Series*, 289:117–130.
- Cullis-Suzuki, S. and Pauly, D. (2010). Failing the high seas: A global evaluation of regional fisheries management organizations. *Marine Policy*, 34(5):1036–1042.
- Cunningham, S. and Pavic, M. (2007). Surface geostrophic currents across the antarctic circumpolar current in drake passage from 1992 to 2004. *Progress in Oceanography*, 73(3):296–310.
- Cushing, D. (1989). A difference in structure between ecosystems in strongly stratified waters and in those that are only weakly stratified. *Journal of Plankton Research*, 11(1):1–13.
- Davies, T. E., Maxwell, S. M., Kaschner, K., Garilao, C., and Ban, N. C. (2017). Large marine protected areas represent biodiversity now and under climate change. *Scientific Reports*, 7(1):9569.
- de Baar, H. J. W. (2005). Synthesis of iron fertilization experiments: From the iron age in the age of enlightenment. *Journal of Geophysical Research*, 110:C09S16.
- De Broyer, C. and Danis, B. (2011). How many species in the southern ocean? towards a dynamic inventory of the antarctic marine species. *Deep Sea Research Part II: Topical Studies in Oceanography*, 58(1):5–17.
- De Broyer, C., Koubbi, P., Griffiths, H. J., Raymond, B., Udekem, C. d., Van de Putte, A., Danis, B., David, B., Grant, S., Gutt, J., Held, C., Hosie, G., Huettmann, F., Post, A., and Ropert-Coudert, Y. (2014). *Biogeographic Atlas of the Southern Ocean*. Cambridge: Scientific Committee on Antarctic Research. ISBN: 978-0-948277-28-3.
- de Jong, J., Schoemann, V., Lannuzel, D., Croot, P., de Baar, H., and Tison, J.-L. (2012). Natural iron fertilization of the atlantic sector of the southern ocean by continental shelf sources of the antarctic peninsula. *Journal of Geophysical Research*, 117.
- Deagle, B., Gales, N., and Hindell, M. (2008-05-05). Variability in foraging behaviour of chick-rearing macaroni penguins eudyptes chrysolophus and its relation to diet. *Marine Ecology Progress Series*, 359:295–309.
- Della Penna, A., De Monte, S., Kestenare, E., Guinet, C., and d’Ovidio, F. (2015). Quasi-planktonic behavior of foraging top marine predators. *Scientific Reports*, 5(1):18063. Publisher: Nature Publishing Group.
- Della Penna, A., Koubbi, P., Cotté, C., Bon, C., Bost, C.-A., and d’Ovidio, F. (2017). Lagrangian analysis of multi-satellite data in support of open ocean marine protected area design. *Deep Sea Research Part II: Topical Studies in Oceanography*, 140:212–221.
- Delord, K., Barbraud, C., Bost, C., Cherel, Y., Guinet, C., and Weimerskirch, H. (2013). Atlas of top predators from french southern territories in the southern indian ocean. Artwork Size: 252 p.
- Delord, K., Cotté, C., Terray, P., Bost, C.-A., Weimerskirch, H., and Barbraud, C. (2021). Factors affecting adult body condition in the endangered northern rockhopper penguin. *Marine Biology*, 168(3):27.

- Desbruyeres, D., Segonzac, M., Bright, M., and Decapoda, A. (2006). Handbook of deepsea hydrothermal vent fauna. *Denisia*.
- Di Lorenzo, E., Mountain, D., Batchelder, H., Bond, N., and Hofmann, E. (2013). Advances in marine ecosystem dynamics from US GLOBEC: The horizontal-advection bottom-up forcing paradigm. *Oceanography*, 26(4):22–33.
- Dias, M. P., Oppel, S., Bond, A. L., Carneiro, A. P., Cuthbert, R. J., González-Solís, J., Wanless, R. M., Glass, T., Lascelles, B., Small, C., Phillips, R. A., and Ryan, P. G. (2017). Using globally threatened pelagic birds to identify priority sites for marine conservation in the south atlantic ocean. *Biological Conservation*, 211:76–84.
- Dinerstein, E., Olson, D., Joshi, A., Vynne, C., Burgess, N. D., Wikramanayake, E., Hahn, N., Palminteri, S., Hedao, P., Noss, R., Hansen, M., Locke, H., Ellis, E. C., Jones, B., Barber, C. V., Hayes, R., Kormos, C., Martin, V., Crist, E., Sechrest, W., Price, L., Baillie, J. E. M., Weeden, D., Suckling, K., Davis, C., Sizer, N., Moore, R., Thau, D., Birch, T., Potapov, P., Turubanova, S., Tyukavina, A., de Souza, N., Pintea, L., Brito, J. C., Llewellyn, O. A., Miller, A. G., Patzelt, A., Ghazanfar, S. A., Timberlake, J., Klsler, H., Shennan-Farfn, Y., Kindt, R., Lilles, J.-P. B., van Breugel, P., Graudal, L., Voge, M., Al-Shammari, K. F., and Saleem, M. (2017). An ecoregion-based approach to protecting half the terrestrial realm. *BioScience*, 67(6):534–545.
- D’Ortenzio, F. (2009). On the trophic regimes of the mediterranean sea: a satellite analysis. *Biogeosciences*, (6):139–148.
- D’Ortenzio, F., Antoine, D., Martinez, E., and d’Alcal, M. R. (2012). Phenological changes of oceanic phytoplankton in the 1980s and 2000s as revealed by remotely sensed ocean-color observations. *Global Biogeochemical Cycles*, 26(4).
- Doty, M. S. and Oguri, M. (1956). The island mass effect. *ICES Journal of Marine Science*, 22(1):33–37.
- Douvere, F. (2008). The importance of marine spatial planning in advancing ecosystem-based sea use management. *Marine Policy*, 32(5):762–771.
- d’Ovidio, F., Della Penna, A., Trull, T. W., Nencioli, F., Pujol, M.-I., Rio, M.-H., Park, Y.-H., Cotté, C., Zhou, M., and Blain, S. (2015). The biogeochemical structuring role of horizontal stirring: Lagrangian perspectives on iron delivery downstream of the kerguelen plateau. *Biogeosciences*, 12(19):5567–5581.
- d’Ovidio, F., Fernández, V., Hernández-García, E., and López, C. (2004). Mixing structures in the mediterranean sea from finite-size lyapunov exponents. *Geophysical Research Letters*, 31(17).
- d’Ovidio, F., Monte, S. D., Alvain, S., Dandonneau, Y., and Lévy, M. (2010). Fluid dynamical niches of phytoplankton types. *Proceedings of the National Academy of Sciences*, 107(43):18366–18370. Publisher: National Academy of Sciences Section: Physical Sciences.
- Duce, R. A. and Tindale, N. W. (1991). Atmospheric transport of iron and its deposition in the ocean. *Limnology and Oceanography*, 36(8):1715–1726.
- Dunstan, P. K., Foster, S. D., King, E., Risbey, J., O’Kane, T. J., Monselesan, D., Hobday, A. J., Hartog, J. R., and Thompson, P. A. (2018). Global patterns of change and variation in sea surface temperature and chlorophyll a. *Scientific Reports*, 8(1):14624.



- Edgar, G. J., Stuart-Smith, R. D., Willis, T. J., Kininmonth, S., Baker, S. C., Banks, S., Barrett, N. S., Becerro, M. A., Bernard, A. T. F., Berkhout, J., Buxton, C. D., Campbell, S. J., Cooper, A. T., Davey, M., Edgar, S. C., Frsterra, G., Galvn, D. E., Irigoyen, A. J., Kushner, D. J., Moura, R., Parnell, P. E., Shears, N. T., Soler, G., Strain, E. M. A., and Thomson, R. J. (2014). Global conservation outcomes depend on marine protected areas with five key features. *Nature*, 506(7487):216–220.
- Estrada, M., Delgado, M., Blasco, D., Latasa, M., Cabello, A. M., Bentez-Barrios, V., Fraile-Nuez, E., Mozeti, P., and Vidal, M. (2016). Phytoplankton across tropical and subtropical regions of the atlantic, indian and pacific oceans. *PLOS ONE*, 11(3):e0151699. Publisher: Public Library of Science.
- Fauchald, P. and Tveraa, T. (2003). Using first-passage time in the analysis of area-restricted search and habitat selection. *Ecology*, 84(2):282–288.
- Feely, R. A., Lewison, M., Massoth, G. J., Robert-Baldo, G., Lavelle, J. W., Byrne, R. H., Von Damm, K. L., and Curl Jr., H. C. (1987). Composition and dissolution of black smoker particulates from active vents on the juan de fuca ridge. *Journal of Geophysical Research: Solid Earth*, 92:11347–11363.
- Firing, Y. L., Chereskin, T. K., and Mazloff, M. R. (2011). Vertical structure and transport of the antarctic circumpolar current in drake passage from direct velocity observations. *Journal of Geophysical Research: Oceans*, 116.
- Fitzsimmons, J. N., John, S. G., Marsay, C. M., Hoffman, C. L., Nicholas, S. L., Toner, B. M., German, C. R., and Sherrell, R. M. (2017). Iron persistence in a distal hydrothermal plume supported by dissolvedparticulate exchange. *Nature Geoscience*, 10(3):195–201.
- Foley, M. M., Halpern, B. S., Micheli, F., Armsby, M. H., Caldwell, M. R., Crain, C. M., Prahler, E., Rohr, N., Sivas, D., Beck, M. W., Carr, M. H., Crowder, L. B., Emmett Duffy, J., Hacker, S. D., McLeod, K. L., Palumbi, S. R., Peterson, C. H., Regan, H. M., Ruckelshaus, M. H., Sandifer, P. A., and Steneck, R. S. (2010). Guiding ecological principles for marine spatial planning. *Marine Policy*, 34(5):955–966.
- Frederiksen, M., Edwards, M., Richardson, A. J., Halliday, N. C., and Wanless, S. (2006). From plankton to top predators: bottom-up control of a marine food web across four trophic levels. *Journal of Animal Ecology*, 75(6):1259–1268.
- Gandhi, N., Ramesh, R., Laskar, A. H., Sheshshayee, M. S., Shetye, S., Anilkumar, N., Patil, S. M., and Mohan, R. (2012). Zonal variability in primary production and nitrogen uptake rates in the southwestern indian ocean and the southern ocean. *Deep Sea Research Part I: Oceanographic Research Papers*, 67:32–43.
- Garrett, C. and Kunze, E. (2007). Internal tide generation in the deep ocean. *Annual Review of Fluid Mechanics*, 39(1):57–87.
- Gattuso, J.-P., Magnan, A. K., Bopp, L., Cheung, W. W. L., Duarte, C. M., Hinkel, J., Mcleod, E., Micheli, F., Oschlies, A., Williamson, P., Billé, R., Chalastani, V. I., Gates, R. D., Irisson, J.-O., Middelburg, J. J., Prtner, H.-O., and Rau, G. H. (2018). Ocean solutions to address climate change and its effects on marine ecosystems. *Frontiers in Marine Science*, 0. Publisher: Frontiers.

- German, C. R., Campbell, A. C., and Edmond, J. M. (1991). Hydrothermal scavenging at the mid-atlantic ridge: Modification of trace element dissolved fluxes. *Earth and Planetary Science Letters*, 107(1):101–114.
- Gille, S., Metzger, J., and Tokmakian, R. (2004). Seafloor topography and ocean circulation. *Oceanography*, 17(1):47–54.
- Godet, C., Robuchon, M., Leroy, B., Cotté, C., Baudena, A., Da Silva, O., Fabri-Ruiz, S., Lo Monaco, C., Sergi, S., and Koubbi, P. (2020). Matching zooplankton abundance and environment in the south indian ocean and southern ocean. *Deep Sea Research Part I: Oceanographic Research Papers*, 163:103347.
- González, H., Graeve, M., Kattner, G., Silva, N., Castro, L., Iriarte, J., Osmn, L., Daneri, G., and Vargas, C. (2016). Carbon flow through the pelagic food web in southern chilean patagonia: relevance of euphausia vallentini as a key species. *Marine Ecology Progress Series*, 557:91–110.
- González-Wevar, C. A., Segovia, N. I., Rosenfeld, S., Noll, D., Maturana, C. S., Hne, M., Naretto, J., Grard, K., Díaz, A., Spencer, H. G., Saucède, T., Féral, J. P., Morley, S. A., Brickle, P., Wilson, N. G., and Poulin, E. (2021). Contrasting biogeographical patterns in margarella (gastropoda: Calliostomatidae: Margarellinae) across the antarctic polar front. *Molecular Phylogenetics and Evolution*, 156:107039.
- Good, S., Fiedler, E., Mao, C., Martin, M. J., Maycock, A., Reid, R., Roberts-Jones, J., Searle, T., Waters, J., While, J., and Worsfold, M. (2020). The current configuration of the OSTIA system for operational production of foundation sea surface temperature and ice concentration analyses. *Remote Sensing*, 12(4):720.
- Gouretski, V. and Koltermann, K. P. (2004). WOCE global hydrographic climatology. *Berichte des BSH*, 35:1–52.
- Graham, R. M., De Boer, A. M., van Sebille, E., Kohfeld, K. E., and Schlosser, C. (2015). Inferring source regions and supply mechanisms of iron in the southern ocean from satellite chlorophyll data. *Deep Sea Research Part I: Oceanographic Research Papers*, 104:9–25.
- Grant, R., Griffiths, H., Steinke, D., Wadley, V., and Linse, K. (2010). Antarctic DNA barcoding; a drop in the ocean? *Polar Biology*, 34:775–780.
- Green, K., Williams, R., and Green, M. G. (1998). Foraging ecology and diving behaviour of macaroni penguins eudyptes chrysolophus at heard island. *Marine Ornithology*, page 8.
- Griffiths, H. J. (2010). Antarctic marine biodiversity what do we know about the distribution of life in the southern ocean? *PLOS ONE*, 5(8):e11683. Publisher: Public Library of Science.
- Griffiths, H. J., Danis, B., and Clarke, A. (2011). Quantifying antarctic marine biodiversity: The SCAR-MarBIN data portal. *Deep Sea Research Part II: Topical Studies in Oceanography*, 58(1):18–29.
- Gruber, N., Lachkar, Z., Frenzel, H., Marchesiello, P., Mnnich, M., McWilliams, J. C., Nagai, T., and Plattner, G.-K. (2011). Eddy-induced reduction of biological production in eastern boundary upwelling systems. *Nature Geoscience*, 4(11):787–792.

- Guieu, C., Bonnet, S., Petrenko, A., Menkes, C., Chavagnac, V., Desboeufs, K., Maes, C., and Moutin, T. (2018). Iron from a submarine source impacts the productive layer of the western tropical south pacific (WTSP). *Scientific Reports*, 8(1):9075. Number: 1 Publisher: Nature Publishing Group.
- Guinehut, S., Dhomps, A.-L., Larnicol, G., and Le Traon, P.-Y. (2012). High resolution 3-d temperature and salinity fields derived from in situ and satellite observations. *Ocean Science*, 8(5):845–857.
- Guinet, C., Dubroca, L., Lea, M., Goldsworthy, S., Cherel, Y., Duhamel, G., Bonadonna, F., and Donnay, J. (2001). Spatial distribution of foraging in female antarctic fur seals *arctocephalus gazella* in relation to oceanographic variables: a scale-dependent approach using geographic information systems. *Marine Ecology Progress Series*, 219:251–264.
- Hawkes, J. A., Connelly, D. P., Rijkenberg, M. J. A., and Achterberg, E. P. (2014). The importance of shallow hydrothermal island arc systems in ocean biogeochemistry. *Geophysical Research Letters*, 41(3):942–947.
- Hays, G. C., Bailey, H., Bograd, S. J., Bowen, W. D., Campagna, C., Carmichael, R. H., Casale, P., Chiaradia, A., Costa, D. P., Cuevas, E., Nico de Bruyn, P., Dias, M. P., Duarte, C. M., Dunn, D. C., Dutton, P. H., Esteban, N., Friedlaender, A., Goetz, K. T., Godley, B. J., Halpin, P. N., Hamann, M., Hammerschlag, N., Harcourt, R., Harrison, A.-L., Hazen, E. L., Heupel, M. R., Hoyt, E., Humphries, N. E., Kot, C. Y., Lea, J. S., Marsh, H., Maxwell, S. M., McMahon, C. R., Notarbartolo di Sciara, G., Palacios, D. M., Phillips, R. A., Righton, D., Schofield, G., Seminoff, J. A., Simpfendorfer, C. A., Sims, D. W., Takahashi, A., Tetley, M. J., Thums, M., Trathan, P. N., Villegas-Amtmann, S., Wells, R. S., Whiting, S. D., Wildermann, N. E., and Sequeira, A. M. (2019). Translating marine animal tracking data into conservation policy and management. *Trends in Ecology & Evolution*, 34(5):459–473.
- Hazen, E., Suryan, R., Santora, J., Bograd, S., Watanuki, Y., and Wilson, R. (2013). Scales and mechanisms of marine hotspot formation. *Marine Ecology Progress Series*, 487:177–183.
- Heerah, K., Dias, M., Delord, K., Opper, S., Barbraud, C., Weimerskirch, H., and Bost, C. (2019). Important areas and conservation sites for a community of globally threatened marine predators of the southern indian ocean. *Biological Conservation*, 234:192–201.
- Henley, S. F., Cavan, E. L., Fawcett, S. E., Kerr, R., Monteiro, T., Sherrell, R. M., Bowie, A. R., Boyd, P. W., Barnes, D. K. A., Schloss, I. R., Marshall, T., Flynn, R., and Smith, S. (2020). Changing biogeochemistry of the southern ocean and its ecosystem implications. *Frontiers in Marine Science*, 7. Publisher: Frontiers.
- Henschke, N., Everett, J. D., Richardson, A. J., and Suthers, I. M. (2016). Rethinking the role of salps in the ocean. *Trends in Ecology & Evolution*, 31(9):720–733.
- Hindell, M. A., Reisinger, R. R., Ropert-Coudert, Y., Hekst, L. A., Trathan, P. N., Bornemann, H., Charrassin, J.-B., Chown, S. L., Costa, D. P., Danis, B., Lea, M.-A., Thompson, D., Torres, L. G., Van de Putte, A. P., Alderman, R., Andrews-Goff, V., Arthur, B., Ballard, G., Bengtson, J., Bester, M. N., Blix, A. S., Boehme, L., Bost, C.-A., Boveng, P., Cleeland, J., Constantine, R., Corney, S., Crawford, R. J. M., Dalla Rosa, L., de Bruyn, P. J. N., Delord, K., Descamps, S., Double, M., Emmerson, L., Fedak, M., Friedlaender, A., Gales, N., Goebel, M. E., Goetz, K. T., Guinet, C., Goldsworthy, S. D., Harcourt, R., Hinke, J. T., Jerosch, K., Kato, A., Kerry, K. R., Kirkwood, R., Kooyman, G. L., Kovacs, K. M., Lawton, K., Lowther, A. D., Lydersen, C.,

- Lyver, P. O., Makhado, A. B., Mrquez, M. E. I., McDonald, B. I., McMahon, C. R., Muelbert, M., Nachtsheim, D., Nicholls, K. W., Nordy, E. S., Olmastroni, S., Phillips, R. A., Pistorius, P., Pltz, J., Ptz, K., Ratchliffe, N., Ryan, P. G., Santos, M., Southwell, C., Staniland, I., Takahashi, A., Tarroux, A., Trivelpiece, W., Wakefield, E., Weimerskirch, H., Wienecke, B., Xavier, J. C., Wotherspoon, S., Jonsen, I. D., and Raymond, B. (2020). Tracking of marine predators to protect southern ocean ecosystems. *Nature*, 580(7801):87–92. Publisher: Nature Publishing Group.
- Hogg, O. T., Huvenne, V. A. I., Griffiths, H. J., and Linse, K. (2018). On the ecological relevance of landscape mapping and its application in the spatial planning of very large marine protected areas. *The Science of the Total Environment*, 626:384–398.
- Holte, J., Talley, L. D., Gilson, J., and Roemmich, D. (2017). An argo mixed layer climatology and database. *Geophysical Research Letters*, 44(11):5618–5626. Publisher: John Wiley & Sons, Ltd.
- Hunt, G. L., Drinkwater, K. F., Arrigo, K., Berge, J., Daly, K. L., Danielson, S., Daase, M., Hop, H., Isla, E., Karnovsky, N., Laidre, K., Mueter, F. J., Murphy, E. J., Renaud, P. E., Smith, W. O., Trathan, P., Turner, J., and Wolf-Gladrow, D. (2016). Advection in polar and sub-polar environments: Impacts on high latitude marine ecosystems. *Progress in Oceanography*, 149:40–81.
- Hutchings, L., Pitcher, G., Probyn, T., and Bailey, G. (1995). The chemical and biological consequences of coastal upwelling. In *Upwelling in the ocean: Modern processes and ancient records*, pages 65–81. John Wiley and Sons.
- IPBES (2019). *Global assessment report on biodiversity and ecosystem services of the Intergovernmental Science-Policy Platform on Biodiversity and Ecosystem Services*. IPBES secretariat. E. S. Brondizio, J. Settele, S. Daz, and H. T. Ngo (eds.).
- IPCC (2019). *Special Report on the Ocean and Cryosphere in a Changing Climate*. IPCC secretariat. H.-O. Portner, D.C. Roberts, V. Masson-Delmotte, P. Zhai, M. Tignor, E. Poloczanska, K. Mintenbeck, A. Alegria, M. Nicolai, A. Okem, J. Petzold, B. Rama, N.M. Weyer (eds.).
- Jasmine, P., Muraleedharan, K., Madhu, N., Asha Devi, C., Alagarsamy, R., Achuthankutty, C., Jayan, Z., Sanjeevan, V., and Sahayak, S. (2009). Hydrographic and productivity characteristics along 45e longitude in the southwestern indian ocean and southern ocean during austral summer 2004. *Marine Ecology Progress Series*, 389:97–116.
- Jena, B., Sahu, S., Avinash, K., and Swain, D. (2013). Observation of oligotrophic gyre variability in the south indian ocean: Environmental forcing and biological response. *Deep Sea Research Part I: Oceanographic Research Papers*, 80:1–10.
- Jenkins, W. J. (2020). Using excess  $^3\text{He}$  to estimate southern ocean upwelling time scales. *Geophysical Research Letters*, 47(15):e2020GL087266.
- Johnson, D. (2018). Climate change is likely to severely limit the effectiveness of deep-sea ABMTs in the north atlantic. *Marine Policy*, page 12.
- Karsten, R. H. and Marshall, J. (2002). Testing theories of the vertical stratification of the ACC against observations. *Dynamics of Atmospheres and Oceans*, 36(1):233–246.

- Kavanaugh, M. T., Oliver, M. J., Chavez, F. P., Letelier, R. M., Muller-Karger, F. E., and Doney, S. C. (2016). Seascapes as a new vernacular for pelagic ocean monitoring, management and conservation. *ICES Journal of Marine Science*, 73(7):1839–1850.
- Klinck, J. and Nowlin, W. (2001). Antarctic circumpolar current. In *Encyclopedia of Ocean Sciences*, pages 151–159. Elsevier. ISBN: 978-0-12-227430-5.
- Kock, K.-H., Reid, K., Croxall, J., and Nicol, S. (2007). Fisheries in the southern ocean: an ecosystem approach. *Philosophical Transactions of the Royal Society B: Biological Sciences*, 362(1488):2333–2349.
- Koubbi, P., C, M., Romain, C., O, D., Baudena, A., Bost, C., cotté, C., d’Ovidio, F., Penna, A., Karine, D., Fabri-Ruiz, S., Ferrieux, M., Guinet, C., Lo Monaco, C., Saucède, T., and Weimerskirch, H. (2016a). *Ecoregionalisation of the Kerguelen and Crozet islands oceanic zone. Part II: The Crozet oceanic zone*. CCAMLR-WG-EMM-16/54.
- Koubbi, P., Guinet, C., Alloncle, N., Améziane, N., Azam, C.-S., Baudena, A., Bost, C., Romain, C., Chazeau, C., Coste, G., cotté, C., F, D., Karine, D., Duhamel, G., A, F., Gasco, N., Hautecoeur, M., Lehodey, P., Lo Monaco, C., and Weimerskirch, H. (2016b). *Ecoregionalisation of the Kerguelen and Crozet islands oceanic zone. Part I: Introduction and Kerguelen oceanic zone*. CCAMLR-WG-EMM-16/43.
- Koubbi, P., Ozouf-Costaz, C., Goarant, A., Moteki, M., Hulley, P.-A., Causse, R., Dettai, A., Duhamel, G., Pruvost, P., Tavernier, E., Post, A. L., Beaman, R. J., Rintoul, S. R., Hirawake, T., Hirano, D., Ishimaru, T., Riddle, M., and Hosie, G. (2010). Estimating the biodiversity of the east antarctic shelf and oceanic zone for ecoregionalisation: Example of the ichthyofauna of the CEAMARC (collaborative east antarctic marine census) CAML surveys. *Polar Science*, 4(2):115–133.
- Lacour, L., Claustre, H., Prieur, L., and D’Ortenzio, F. (2015). Phytoplankton biomass cycles in the north atlantic subpolar gyre: A similar mechanism for two different blooms in the labrador sea. *Geophysical Research Letters*, 42(13):5403–5410.
- Lancelot, C., de Montety, A., Goosse, H., Becquevort, S., Schoemann, V., Pasquer, B., and Vancoppenolle, M. (2009). Spatial distribution of the iron supply to phytoplankton in the southern ocean: a model study. *Biogeosciences*, 6:18.
- Lascelles, B. G., Langham, G. M., Ronconi, R. A., and Reid, J. B. (2012). From hotspots to site protection: Identifying marine protected areas for seabirds around the globe. *Biological Conservation*, 156:5–14.
- Lathuiliere, C., Levy, M., and Echevin, V. (2011). Impact of eddy-driven vertical fluxes on phytoplankton abundance in the euphotic layer. *Journal of Plankton Research*, 33(5):827–831.
- Latimer, J. C. and Filippelli, G. M. (2001). Terrigenous input and paleoproductivity in the southern ocean. *Paleoceanography*, 16(6):627–643.
- Lavergne, C. d., Vic, C., Madec, G., Roquet, F., Waterhouse, A. F., Whalen, C. B., Cuypers, Y., BouruetAubertot, P., Ferron, B., and Hibiya, T. (2020). A parameterization of local and remote tidal mixing. *Journal of Advances in Modeling Earth Systems*, 12(5):e2020MS002065.

- Le Bohec, C., Durant, J. M., Gauthier-Clerc, M., Stenseth, N. C., Park, Y.-H., Pradel, R., Gremillet, D., Gendner, J.-P., and Le Maho, Y. (2008). King penguin population threatened by southern ocean warming. *Proceedings of the National Academy of Sciences*, 105(7):2493–2497.
- Lea, M., Guinet, C., Cherel, Y., Duhamel, G., Dubroca, L., Pruvost, P., and Hindell, M. (2006). Impacts of climatic anomalies on provisioning strategies of a southern ocean predator. *Marine Ecology Progress Series*, 310:77–94.
- Leathwick, J., Elith, J., Francis, M., Hastie, T., and Taylor, P. (2006). Variation in demersal fish species richness in the oceans surrounding new zealand: an analysis using boosted regression trees. *Marine Ecology Progress Series*, 321:267–281.
- Lebouvier, M. (2007). Conservation and management in the french sub-antarctic islands and surrounding seas. *Papers and Proceedings of the Royal Society of Tasmania*, pages 23–28.
- Lehahn, Y., d’Ovidio, F., and Koren, I. (2018). A satellite-based lagrangian view on phytoplankton dynamics. *Annual Review of Marine Science*, 10(1):99–119.
- Lemos, A. T., Ghisolfi, R. D. R., and Mazzini, P. L. F. (2018). Annual phytoplankton blooming using satellite-derived chlorophyll-a data around the vitria-trindade chain, southeastern brazil. *Deep Sea Research Part I: Oceanographic Research Papers*, 136:62–71.
- Lenn, Y.-D., Chereskin, T. K., Sprintall, J., and Firing, E. (2007). Mean jets, mesoscale variability and eddy momentum fluxes in the surface layer of the antarctic circumpolar current in drake passage. *Journal of Marine Research*, 65(1):27–58.
- Lester, S., Halpern, B., Grorud-Colvert, K., Lubchenco, J., Ruttenberg, B., Gaines, S., Airamé, S., and Warner, R. (2009). Biological effects within no-take marine reserves: a global synthesis. *Marine Ecology Progress Series*, 384:33–46.
- Lévy, M., Franks, P. J. S., and Smith, K. S. (2018). The role of submesoscale currents in structuring marine ecosystems. *Nature Communications*, 9(1):4758. Number: 1 Publisher: Nature Publishing Group.
- Lévy, M., Iovino, D., Resplandy, L., Klein, P., Madec, G., Tréguier, A.-M., Masson, S., and Takahashi, K. (2012). Large-scale impacts of submesoscale dynamics on phytoplankton: Local and remote effects. *Ocean Modelling*, 43-44:77–93.
- Lewison, R., Hobday, A. J., Maxwell, S., Hazen, E., Hartog, J. R., Dunn, D. C., Briscoe, D., Fossette, S., O’Keefe, C. E., Barnes, M., Abecassis, M., Bograd, S., Bethoney, N. D., Bailey, H., Wiley, D., Andrews, S., Hazen, L., and Crowder, L. B. (2015). Dynamic ocean management: Identifying the critical ingredients of dynamic approaches to ocean resource management. *BioScience*, 65(5):486–498.
- Liu, N. and Brooks, C. M. (2018). China’s changing position towards marine protected areas in the southern ocean: Implications for future antarctic governance. *Marine Policy*, 94:189–195.
- Longhurst, A. R. (2010). *Ecological Geography of the Sea*. Elsevier.
- Louise Allan, E., William Froneman, P., Durgadoo, J. V., McQuaid, C. D., Anson, I. J., and Richoux, N. B. (2013). Critical indirect effects of climate change on sub-antarctic ecosystem functioning. *Ecology and Evolution*, 3(9):2994–3004.

- Lourenço, C. R., Zardi, G. I., McQuaid, C. D., Serro, E. A., Pearson, G. A., Jacinto, R., and Nicastro, K. R. (2016). Upwelling areas as climate change refugia for the distribution and genetic diversity of a marine macroalga. *Journal of Biogeography*, 43(8):1595–1607.
- Lynam, C. P., Llope, M., Mllmann, C., Helaout, P., Bayliss-Brown, G. A., and Stenseth, N. C. (2017). Interaction between top-down and bottom-up control in marine food webs. *Proceedings of the National Academy of Sciences*, 114(8):1952–1957. Publisher: National Academy of Sciences Section: Biological Sciences.
- Machu, E., Biastoch, A., Oschlies, A., Kawamiya, M., Lutjeharms, J. R. E., and Garon, V. (2005). Phytoplankton distribution in the agulhas system from a coupled physicalbiological model. *Deep Sea Research Part I: Oceanographic Research Papers*, 52(7):1300–1318.
- Macqueen, J. (1967). *Some methods for classification and analysis of multivariate observations*, volume 1. Proceedings of the fifth Berkeley symposium on mathematical statistics and probability.
- Mahowald, N. M., Hamilton, D. S., Mackey, K. R. M., Moore, J. K., Baker, A. R., Scanza, R. A., and Zhang, Y. (2018). Aerosol trace metal leaching and impacts on marine microorganisms. *Nature Communications*, 9(1):2614. Publisher: Nature Publishing Group.
- Mahowald, N. M., Muhs, D. R., Levis, S., Rasch, P. J., Yoshioka, M., Zender, C. S., and Luo, C. (2006). Change in atmospheric mineral aerosols in response to climate: Last glacial period, preindustrial, modern, and doubled carbon dioxide climates. *Journal of Geophysical Research: Atmospheres*, 111.
- Mark Moore, C., Mills, M. M., Achterberg, E. P., Geider, R. J., LaRoche, J., Lucas, M. I., McDonagh, E. L., Pan, X., Poulton, A. J., Rijkenberg, M. J. A., Suggett, D. J., Ussher, S. J., and Woodward, E. M. S. (2009). Large-scale distribution of atlantic nitrogen fixation controlled by iron availability. *Nature Geoscience*, 2(12):867–871. Publisher: Nature Publishing Group.
- Martin, J. H. (1990). Glacial-interglacial CO<sub>2</sub> change: The iron hypothesis. *Paleoceanography*, 5(1):1–13.
- Martínez-García, A., Sigman, D. M., Ren, H., Anderson, R. F., Straub, M., Hodell, D. A., Jaccard, S. L., Eglinton, T. I., and Haug, G. H. (2014). Iron fertilization of the subantarctic ocean during the last ice age. *Science*, 343(6177):1347–1350. Publisher: American Association for the Advancement of Science Section: Report.
- Maxwell, S. M., Hazen, E. L., Lewison, R. L., Dunn, D. C., Bailey, H., Bograd, S. J., Briscoe, D. K., Fossette, S., Hobday, A. J., Bennett, M., Benson, S., Caldwell, M. R., Costa, D. P., Dewar, H., Eguchi, T., Hazen, L., Kohin, S., Sippel, T., and Crowder, L. B. (2015). Dynamic ocean management: Defining and conceptualizing real-time management of the ocean. *Marine Policy*, 58:42–50.
- Mayot, N., D’Ortenzio, F., Ribera d’Alcal, M., Lavigne, H., and Claustre, H. (2016). Interannual variability of the mediterranean trophic regimes from ocean color satellites. *Biogeosciences*, 13(6):1901–1917.
- McCormack, S. A., Melbourne-Thomas, J., Trebilco, R., Blanchard, J. L., and Constable, A. (2020). Alternative energy pathways in southern ocean food webs: Insights from a balanced model of prydz bay, antarctica. *Deep Sea Research Part II: Topical Studies in Oceanography*, 174:104613.



- McLeod, E., Salm, R., Green, A., and Almany, J. (2009). Designing marine protected area networks to address the impacts of climate change. *Frontiers in Ecology and the Environment*, 7(7):362–370.
- McMahon, C., Hindell, M., Charrassin, J.-B., Corney, S., Guinet, C., Harcourt, R., Jonsen, I., Trebilco, R., Williams, G., and Bestley, S. (2019). Finding mesopelagic prey in a changing southern ocean. *Scientific Reports*, 9:19013.
- Melet, A., Hallberg, R., Legg, S., and Nikurashin, M. (2014). Sensitivity of the ocean state to lee wavedriven mixing. *Journal of Physical Oceanography*, 44(3):900–921. Publisher: American Meteorological Society Section: Journal of Physical Oceanography.
- Merlivat, L., Boutin, J., and d’Ovidio, F. (2015). Carbon, oxygen and biological productivity in the southern ocean in and out the kerguelen plume: CARIOCA drifter results. *Biogeosciences*, 12(11):3513–3524.
- Meyssignac, B., Boyer, T., Zhao, Z., Hakuba, M. Z., Landerer, F. W., Stammer, D., Khl, A., Kato, S., L’Ecuyer, T., Ablain, M., Abraham, J. P., Blazquez, A., Cazenave, A., Church, J. A., Cowley, R., Cheng, L., Domingues, C. M., Giglio, D., Gouretski, V., Ishii, M., Johnson, G. C., Killick, R. E., Legler, D., Llovel, W., Lyman, J., Palmer, M. D., Piotrowicz, S., Purkey, S. G., Roemmich, D., Roca, R., Savita, A., Schuckmann, K. v., Speich, S., Stephens, G., Wang, G., Wijffels, S. E., and Zilberman, N. (2019). Measuring global ocean heat content to estimate the earth energy imbalance. *Frontiers in Marine Science*, 6. Publisher: Frontiers.
- Moilanen, A., Wilson, K., and Possingham, H. (2009). *Spatial Conservation Prioritization: Quantitative Methods and Computational Tools*. Oxford University Press.
- Molenaar, E. J. (2001). CCAMLR and southern ocean fisheries. *The International Journal of Marine and Coastal Law*, 16(3):465–499. Publisher: Brill Nijhoff Section: The International Journal of Marine and Coastal Law.
- Moline, M. A., Claustre, H., Frazer, T. K., Scarschofield, O., and Vernet, M. (2004). Alteration of the food web along the antarctic peninsula in response to a regional warming trend. *Global Change Biology*, page 8.
- Mongin, M., Molina, E., and Trull, T. W. (2008). Seasonality and scale of the kerguelen plateau phytoplankton bloom: A remote sensing and modeling analysis of the influence of natural iron fertilization in the southern ocean. *Deep Sea Research Part II: Topical Studies in Oceanography*, 55(5):880–892.
- Mongin, M. M., Abraham, E. R., and Trull, T. W. (2009). Winter advection of iron can explain the summer phytoplankton bloom that extends 1000 km downstream of the kerguelen plateau in the southern ocean. *Journal of Marine Research*, 67(2):225–237.
- Montégut, C. d. B., Madec, G., Fischer, A. S., Lazar, A., and Iudicone, D. (2004). Mixed layer depth over the global ocean: An examination of profile data and a profile-based climatology. *Journal of Geophysical Research: Oceans*, 109.
- Moore, C. M., Mills, M. M., Arrigo, K. R., Berman-Frank, I., Bopp, L., Boyd, P. W., Galbraith, E. D., Geider, R. J., Guieu, C., Jaccard, S. L., Jickells, T. D., La Roche, J., Lenton, T. M., Mahowald, N. M., Maran, E., Marinov, I., Moore, J. K., Nakatsuka, T., Oschlies, A., Saito, M. A., Thingstad, T. F., Tsuda, A., and Ulloa, O. (2013). Processes and patterns of oceanic nutrient limitation. *Nature Geoscience*, 6(9):701–710.

- Morato, T., Hoyle, S. D., Allain, V., and Nicol, S. J. (2010). Seamounts are hotspots of pelagic biodiversity in the open ocean. *Proceedings of the National Academy of Sciences*, 107(21):9707–9711.
- Morato, T., Varkey, D., Damaso, C., Machete, M., Santos, M., Prieto, R., Pitcher, T., and Santos, R. (2008). Evidence of a seamount effect on aggregating visitors. *Marine Ecology Progress Series*, 357:23–32.
- Morel, A., Claustre, H., and Gentili, B. (2010). The most oligotrophic subtropical zones of the global ocean: similarities and differences in terms of chlorophyll and yellow substance. *Biogeosciences*, 7(10):3139–3151.
- Morton, B. R., Taylor, G., and Turner, J. S. (1956). Turbulent gravitational convection from maintained and instantaneous sources. *Proceedings of the Royal Society of London. Series A, Mathematical and Physical Sciences*, 234(1196):1–23. Publisher: The Royal Society.
- Mottl, M. J. and McConachy, T. F. (1990). Chemical processes in buoyant hydrothermal plumes on the east pacific rise near 21n. *Geochimica et Cosmochimica Acta*, 54(7):1911–1927.
- Mulet, S., Rio, M. H., Mignot, A., Guinehut, S., and Morrow, R. (2012). A new estimate of the global 3d geostrophic ocean circulation based on satellite data and in-situ measurements. *Deep Sea Research Part II: Topical Studies in Oceanography*, 77-80:70–81.
- Nel, D., Lutjeharms, J., Pakhomov, E., Anson, I., Ryan, P., and Klages, N. (2001). Exploitation of mesoscale oceanographic features by grey-headed albatross thalassarche chrysostoma in the southern indian ocean. *Marine Ecology Progress Series*, 217:15–26.
- Norman, L., Cabanes, D., Blanco-Ameijeiras, S., Sophie, M., and Hassler, C. (2014). Iron biogeochemistry in aquatic systems: From source to bioavailability. *CHIMIA International Journal for Chemistry*, 68.
- Ohman, M., Barbeau, K., Franks, P., Goericke, R., Landry, M., and Miller, A. (2013). Ecological transitions in a coastal upwelling ecosystem. *Oceanography*, 26(3):210–219.
- O’Leary, B. C., Ban, N. C., Fernandez, M., Friedlander, A. M., Garca-Borboroglu, P., Golbuu, Y., Guidetti, P., Harris, J. M., Hawkins, J. P., Langlois, T., McCauley, D. J., Pikitch, E. K., Richmond, R. H., and Roberts, C. M. (2018). Addressing criticisms of large-scale marine protected areas. *BioScience*, 68(5):359–370.
- O’Leary, B. C., Winther-Janson, M., Bainbridge, J. M., Aitken, J., Hawkins, J. P., and Roberts, C. M. (2016). Effective coverage targets for ocean protection. *Conservation Letters*, 9(6):398–404.
- Oliveira, A. P., Coutinho, T. P., Cabeadas, G., Brogueira, M. J., Coca, J., Ramos, M., Calado, G., and Duarte, P. (2016). Primary production enhancement in a shallow seamount (gorringe northeast atlantic). *Journal of Marine Systems*, 164:13–29.
- Osterblom, H. and Folke, C. (2013). Emergence of global adaptive governance for stewardship of regional marine resources. *Ecology and Society*, 18(2). Publisher: Resilience Alliance Inc.
- O’Toole, M., Guinet, C., Lea, M., and Hindell, M. (2017). Marine predators and phytoplankton: how elephant seals use the recurrent kerguelen plume. *Marine Ecology Progress Series*, 581:215–227.

- o'Toole, M., Sergi, S., Baudena, A., Cotté, C., Bost, C., Guinet, C., Weimerskirch, H., Hindell, M. A., Koubbi, P., and d'Ovidio, F. (2018). Predator trophic hotspots in the indian sector of the subantarctic southern ocean: how do they overlap with marine protected areas? CCAMLR-WS-SM-18-07.
- Pakhomov, E. A., Henschke, N., Hunt, B. P. V., Stowasser, G., and Cherel, Y. (2019). Utility of salps as a baseline proxy for food web studies. *Journal of Plankton Research*, 41(1):3–11.
- Park, Y.-H., Park, T., Kim, T.-W., Lee, S.-H., Hong, C.-S., Lee, J.-H., Rio, M.-H., Pujol, M.-I., Ballarotta, M., Durand, I., and Provost, C. (2019). Observations of the antarctic circumpolar current over the udintsev fracture zone, the narrowest choke point in the southern ocean. *Journal of Geophysical Research: Oceans*, 124(7):4511–4528.
- Paterson, J. T., Rotella, J. J., Arrigo, K. R., and Garrott, R. A. (2015). Tight coupling of primary production and marine mammal reproduction in the southern ocean. *Proceedings of the Royal Society B: Biological Sciences*, 282(1806):20143137. Publisher: Royal Society.
- Perissinotto, R. (1992). Mesozooplankton size-selectivity and grazing impact on the phytoplankton community of the prince edward archipelago (southern ocean). *Marine Ecology Progress Series*, 79(3):243–258. Publisher: Inter-Research Science Center.
- Petrou, K., Kranz, S. A., Trimborn, S., Hassler, C. S., Ameijeiras, S. B., Sackett, O., Ralph, P. J., and Davidson, A. T. (2016). Southern ocean phytoplankton physiology in a changing climate. *Journal of Plant Physiology*, 203:135–150.
- Phillips, H. E. and Bindoff, N. L. (2014). On the nonequivalent barotropic structure of the antarctic circumpolar current: An observational perspective. *Journal of Geophysical Research: Oceans*, 119(8):5221–5243.
- Pinto, D. D. P. (2012). *Fisheries management in areas beyond national jurisdiction: The impact of ecosystem based law-making*, volume 13. Martinus Nijhoff Publishers.
- Pitcher, T. J., Morato, T., Hart, P. J. B., Clark, M. R., Haggan, N., and Santos, R. S. (2007). *Seamounts: Ecology, Fisheries & Conservation*. Blackwell Publishing Ltd.
- Pittman, S. (2018). *Seascape ecology*. ISBN: 978-1-119-08445-7 1-119-08445-8.
- Pittman, S., Kneib, R., Simenstad, C., and I, N. (2011). Seascape ecology: application of landscape ecology to the marine environment. *Marine Ecology Progress Series*, 427:187–190.
- Planquette, H., Sanders, R. R., Statham, P. J., Morris, P. J., and Fones, G. R. (2011). Fluxes of particulate iron from the upper ocean around the crozet islands: A naturally iron-fertilized environment in the southern ocean. *Global Biogeochemical Cycles*, 25(2).
- Raiswell, R., Hawkings, J. R., Benning, L. G., Baker, A. R., Death, R., Albani, S., Mahowald, N., Krom, M. D., Poulton, S. W., Wadham, J., and Tranter, M. (2016). Potentially bioavailable iron delivery by iceberg-hosted sediments and atmospheric dust to the polar oceans. *Biogeosciences*, 13(13):3887–3900.
- Raymond, B., Wotherspoon, S., Jonsen, I., and Reisinger, R. (2018). Availability: Estimating geographic space available to animals based on telemetry data. r package version 0.13.0. 2018. <https://github.com/AustralianAntarcticDataCentre/>.

- Resing, J. A., Sedwick, P. N., German, C. R., Jenkins, W. J., Moffett, J. W., Sohst, B. M., and Tagliabue, A. (2015). Basin-scale transport of hydrothermal dissolved metals across the south pacific ocean. *Nature*, 523(7559):200–203.
- Reygondeau, G., Cheung, W. W. L., Wabnitz, C. C. C., Lam, V. W. Y., Frlicher, T., and Maury, O. (2020). Climate change-induced emergence of novel biogeochemical provinces. *Frontiers in Marine Science*, 7:657.
- Reygondeau, G., Longhurst, A., Martinez, E., Beaugrand, G., Antoine, D., and Maury, O. (2013). Dynamic biogeochemical provinces in the global ocean. *Global Biogeochemical Cycles*, 27(4):1046–1058.
- Rigby, S. J., Williams, R. G., Achterberg, E. P., and Tagliabue, A. (2020). Resource availability and entrainment are driven by offsets between nutriclines and winter mixed-layer depth. *Global Biogeochemical Cycles*, 34(7):e2019GB006497.
- Rintoul, S. R. and Naveira Garabato, A. C. (2013). Chapter 18 - dynamics of the southern ocean circulation. In Siedler, G., Griffies, S. M., Gould, J., and Church, J. A., editors, *International Geophysics*, volume 103 of *Ocean Circulation and Climate*, pages 471–492. Academic Press.
- Roberts, C. M., O’Leary, B. C., McCauley, D. J., Cury, P. M., Duarte, C. M., Lubchenco, J., Pauly, D., Senz-Arroyo, A., Sumaila, U. R., Wilson, R. W., Worm, B., and Castilla, J. C. (2017). Marine reserves can mitigate and promote adaptation to climate change. *Proceedings of the National Academy of Sciences*, 114(24):6167–6175.
- Robinson, J., Popova, E. E., Srokosz, M. A., and Yool, A. (2016). A tale of three islands: Downstream natural iron fertilization in the southern ocean. *Journal of Geophysical Research: Oceans*, 121(5):3350–3371.
- Robison, B. H. (2009). Conservation of deep pelagic biodiversity. *Conservation Biology*, 23(4):847–858.
- Rogers, A. D., Yesson, C., and Gravestock, P. (2015). A biophysical and economic profile of south georgia and the south sandwich islands as potential large-scale antarctic protected areas. In *Advances in Marine Biology*, volume 70, pages 1–286. Elsevier.
- Ropert-Coudert, Y., Van de Putte, A. P., Reisinger, R. R., Bornemann, H., Charrassin, J.-B., Costa, D. P., Danis, B., Heckstet, L. A., Jonsen, I. D., Lea, M.-A., Thompson, D., Torres, L. G., Trathan, P. N., Wotherspoon, S., Ainley, D. G., Alderman, R., Andrews-Goff, V., Arthur, B., Ballard, G., Bengtson, J., Bester, M. N., Blix, A. S., Boehme, L., Bost, C.-A., Boveng, P., Clelland, J., Constantine, R., Crawford, R. J. M., Dalla Rosa, L., Nico de Bruyn, P. J., Delord, K., Descamps, S., Double, M., Emmerson, L., Fedak, M., Friedlaender, A., Gales, N., Goebel, M., Goetz, K. T., Guinet, C., Goldsworthy, S. D., Harcourt, R., Hinke, J. T., Jerosch, K., Kato, A., Kerry, K. R., Kirkwood, R., Kooyman, G. L., Kovacs, K. M., Lawton, K., Lowther, A. D., Lydersen, C., Lyver, P. O., Makhado, A. B., Mrquez, M. E. I., McDonald, B. I., McMahon, C. R., Muelbert, M., Nachtsheim, D., Nicholls, K. W., Nordy, E. S., Olmastroni, S., Phillips, R. A., Pistorius, P., Pltz, J., Ptz, K., Ratcliffe, N., Ryan, P. G., Santos, M., Southwell, C., Staniland, I., Takahashi, A., Tarroux, A., Trivelpiece, W., Wakefield, E., Weimerskirch, H., Wienecke, B., Xavier, J. C., Raymond, B., and Hindell, M. A. (2020). The retrospective analysis of antarctic tracking data project. *Scientific Data*, 7(1):94. Publisher: Nature Publishing Group.

- Rossi, V., Ser-Giacomi, E., López, C., and Hernández-García, E. (2014). Hydrodynamic provinces and oceanic connectivity from a transport network help designing marine reserves. *Geophysical Research Letters*, 41(8):2883–2891.
- Rowden, A. A., Dower, J. F., Schlacher, T. A., Consalvey, M., and Clark, M. R. (2010). Paradigms in seamount ecology: fact, fiction and future. *Marine Ecology*, 31:226–241. Publisher: John Wiley & Sons, Ltd.
- Ruckelshaus, M., Klinger, T., Knowlton, N., and DeMaster, D. P. (2008). Marine ecosystem-based management in practice: Scientific and governance challenges. *BioScience*, 58(1):53–63.
- Sallée, J.-B., Llort, J., Tagliabue, A., and Lévy, M. (2015). Characterization of distinct bloom phenology regimes in the southern ocean. *ICES Journal of Marine Science*, 72(6):1985–1998.
- Salm, R., Done, T., and Mcleod, E. (2006). Coral reefs and climate change: Science and management. *Coastal and estuarine studies.*, 61:207–221.
- Samaran, F., Stafford, K. M., Branch, T. A., Gedamke, J., Royer, J.-Y., Dziak, R. P., and Guinet, C. (2013). Seasonal and geographic variation of southern blue whale subspecies in the indian ocean. *PLOS ONE*, 8(8):e71561. Publisher: Public Library of Science.
- Sander, S. G. and Koschinsky, A. (2011). Metal flux from hydrothermal vents increased by organic complexation. *Nature Geoscience*, 4(3):145–150.
- Sanial, V., van Beek, P., Lansard, B., Souhaut, M., Kestenare, E., d’Ovidio, F., Zhou, M., and Blain, S. (2015). Use of rare isotopes to deduce rapid transfer of sediment-derived inputs off kerguelen. *Biogeosciences*, 12(5):1415–1430.
- Santora, J. A., Sydeman, W. J., Schroeder, I. D., Field, J. C., Miller, R. R., and Wells, B. K. (2017). Persistence of trophic hotspots and relation to human impacts within an upwelling marine ecosystem. *Ecological Applications*, 27(2):560–574.
- Schine, C. M. S., Alderkamp, A.-C., Dijken, G. v., Gerringa, L. J. A., Sergi, S., Laan, P., Haren, H. v., Poll, W. H. v. d., and Arrigo, K. R. (2021). Massive southern ocean phytoplankton bloom fed by iron of possible hydrothermal origin. *Nature Communications*, 12(1):1–11. Publisher: Nature Publishing Group.
- Sciara, G. N. d., Hoyt, E., Reeves, R., Ardron, J., Marsh, H., Vongraven, D., and Barr, B. (2016). Place-based approaches to marine mammal conservation. *Aquatic Conservation: Marine and Freshwater Ecosystems*, 26:85–100.
- Sergi, S., Baudena, A., Cotté, C., Ardyna, M., Blain, S., and d’Ovidio, F. (2020). Interaction of the antarctic circumpolar current with seamounts fuels moderate blooms but vast foraging grounds for multiple marine predators. *Frontiers in Marine Science*, 7. Publisher: Frontiers.
- Sergi, S., Grizaud, G., Cotté, C., and d’Ovidio, F. (2019). Unfolding the connectivity patterns along the antarctic circumpolar current in the sub-antarctic region. CCAMLR-WG-EMM-19-71.
- Shaked, Y. and Lis, H. (2012). Disassembling iron availability to phytoplankton. *Frontiers in Microbiology*, 3. Publisher: Frontiers.
- Shaw, J. D., Terauds, A., Riddle, M. J., Possingham, H. P., and Chown, S. L. (2014). Antarctica’s protected areas are inadequate, unrepresentative, and at risk. *PLOS Biology*, 12(6):e1001888.

- Shiozaki, T., Kodama, T., and Furuya, K. (2014). Large-scale impact of the island mass effect through nitrogen fixation in the western south pacific ocean. *Geophysical Research Letters*, 41(8):2907–2913.
- Signorini, S. R., Franz, B. A., and McClain, C. R. (2015). Chlorophyll variability in the oligotrophic gyres: mechanisms, seasonality and trends. *Frontiers in Marine Science*, 2. Publisher: Frontiers.
- Sohrin, Y., Iwamoto, S., Matsui, M., Obata, H., Nakayama, E., Suzuki, K., Handa, N., and Ishii, M. (2000). The distribution of Fe in the Australian sector of the southern ocean. *Deep Sea Research Part I: Oceanographic Research Papers*, 47(1):55–84.
- Sokolov, S. and Rintoul, S. R. (2007). On the relationship between fronts of the antarctic circumpolar current and surface chlorophyll concentrations in the southern ocean. *Journal of Geophysical Research*, 112:C07030.
- Sommer, U., Stibor, H., Katschek, A., Sommer, F., and Hansen, T. (2002). Pelagic food web configurations at different levels of nutrient richness and their implications for the ratio fish production. *Hydrobiologia*, 484:11–20.
- Sullivan, C. W., Arrigo, K. R., McClain, C. R., Comiso, J. C., and Firestone, J. (1993). Distributions of phytoplankton blooms in the southern ocean. *Science*, 262(5141):1832–1837. Publisher: American Association for the Advancement of Science.
- Sylvester, Z. T. and Brooks, C. M. (2020). Protecting Antarctica through co-production of actionable science: Lessons from the CCAMLR marine protected area process. *Marine Policy*, 111:103720.
- Tagliabue, A., Bopp, L., Dutay, J.-C., Bowie, A. R., Chever, F., Jean-Baptiste, P., Bucciarelli, E., Lannuzel, D., Remenyi, T., Sarthou, G., Aumont, O., Gehlen, M., and Jeandel, C. (2010). Hydrothermal contribution to the oceanic dissolved iron inventory. *Nature Geoscience*, 3(4):252–256.
- Tagliabue, A., Bowie, A. R., Boyd, P. W., Buck, K. N., Johnson, K. S., and Saito, M. A. (2017). The integral role of iron in ocean biogeochemistry. *Nature*, 543(7643):51–59. Publisher: Nature Publishing Group.
- Tagliabue, A., Bowie, A. R., DeVries, T., Ellwood, M. J., Landing, W. M., Milne, A., Ohnemus, D. C., Twining, B. S., and Boyd, P. W. (2019). The interplay between regeneration and scavenging fluxes drives ocean iron cycling. *Nature Communications*, 10(1):4960. Publisher: Nature Publishing Group.
- Tagliabue, A. and Resing, J. (2016). Impact of hydrothermalism on the ocean iron cycle. *Philosophical Transactions of the Royal Society A: Mathematical, Physical and Engineering Sciences*, 374(2081):20150291.
- Tagliabue, A., Sallée, J.-B., Bowie, A. R., Lévy, M., Swart, S., and Boyd, P. W. (2014). Surface-water iron supplies in the southern ocean sustained by deep winter mixing. *Nature Geoscience*, 7(4):314–320.
- Talley, L. D., Pickard, G. L., Emery, W. J., and Swift, J. H. (2011). Chapter 6 - data analysis concepts and observational methods. In Talley, L. D., Pickard, G. L., Emery, W. J., and Swift, J. H., editors, *Descriptive Physical Oceanography (Sixth Edition)*, pages 147–186. Academic Press.

- Tamsitt, V., Drake, H. F., Morrison, A. K., Talley, L. D., Dufour, C. O., Gray, A. R., Griffies, S. M., Mazloff, M. R., Sarmiento, J. L., Wang, J., and Weijer, W. (2017). Spiraling pathways of global deep waters to the surface of the southern ocean. *Nature Communications*, 8(1):172.
- Thiers, L., Delord, K., Bost, C.-A., Guinet, C., and Weimerskirch, H. (2017). Important marine sectors for the top predator community around kerguelen archipelago. *Polar Biology*, 40(2):365–378.
- Thomalla, S. J., Fauchereau, N., Swart, S., and Monteiro, P. M. S. (2011). Regional scale characteristics of the seasonal cycle of chlorophyll in the southern ocean. *Biogeosciences*, 8(10):2849–2866.
- Tittensor, D. P., Mora, C., Jetz, W., Lotze, H. K., Ricard, D., Berghe, E. V., and Worm, B. (2010). Global patterns and predictors of marine biodiversity across taxa. *Nature*, 466(7310):1098–1101. Publisher: Nature Publishing Group.
- Trebilco, R., Melbourne-Thomas, J., and Constable, A. J. (2020). The policy relevance of southern ocean food web structure: Implications of food web change for fisheries, conservation and carbon sequestration. *Marine Policy*, 115:103832.
- Tsukamoto, K. (2006). Spawning of eels near a seamount. *Nature*, 439(7079):929–929. Publisher: Nature Publishing Group.
- Tuerena, R. E., Williams, R. G., Mahaffey, C., Vic, C., Green, J. A. M., NaveiraGarabato, A., Forryan, A., and Sharples, J. (2019). Internal tides drive nutrient fluxes into the deep chlorophyll maximum over midocean ridges. *Global Biogeochemical Cycles*, 33(8):995–1009.
- Turner, J. S. (1979). *Buoyancy Effects in Fluids*. Cambridge University Press. ISBN: 978-0-521-29726-4.
- Turner, M. G. (2005). Landscape ecology: What is the state of the science? *Annual Review of Ecology, Evolution, and Systematics*, 36(1):319–344.
- Turner, W., Spector, S., Gardiner, N., Fladeland, M., Sterling, E., and Steininger, M. (2003). Remote sensing for biodiversity science and conservation. *Trends in Ecology & Evolution*, 18(6):306–314.
- van Gennip, S. J., Popova, E. E., Yool, A., Pecl, G. T., Hobday, A. J., and Sorte, C. J. B. (2017). Going with the flow: the role of ocean circulation in global marine ecosystems under a changing climate. *Global Change Biology*, 23(7):2602–2617.
- van Sebille, E., Griffies, S. M., Abernathey, R., Adams, T. P., Berloff, P., Biastoch, A., Blanke, B., Chassignet, E. P., Cheng, Y., Cotter, C. J., Deleersnijder, E., Ds, K., Drake, H. F., Drijfhout, S., Gary, S. F., Heemink, A. W., Kjellsson, J., Koszalka, I. M., Lange, M., Lique, C., MacGilchrist, G. A., Marsh, R., Mayorga Adame, C. G., McAdam, R., Nencioli, F., Paris, C. B., Piggott, M. D., Polton, J. A., Rhs, S., Shah, S. H. A. M., Thomas, M. D., Wang, J., Wolfram, P. J., Zanna, L., and Zika, J. D. (2018). Lagrangian ocean analysis: Fundamentals and practices. *Ocean Modelling*, 121:49–75.
- Verity, P. and Smetacek, V. (1996). Organism life cycles, predation, and the structure of marine pelagic ecosystems. *Marine Ecology Progress Series*, 130:277–293.

- Visser, A. W., Nielsen, T. G., Middelboe, M., Hyer, J. L., and Markager, S. (2015). Oceanography and the base of the pelagic food web in the southern indian ocean. *Journal of Plankton Research*, 37(3):571–583.
- Wadley, M. R., Jickells, T. D., and Heywood, K. J. (2014). The role of iron sources and transport for southern ocean productivity. *Deep Sea Research Part I: Oceanographic Research Papers*, 87:82–94.
- Weber, T. (2020). Commentary: Southern ocean upwelling and the marine iron cycle. *Geophysical Research Letters*, 47(20):e2020GL090737.
- Wessel, P., Sandel, D. T., and Kim, S.-S. (2010). The global seamount census. *Oceanography*, 23(1):24–33. Publisher: Oceanography Society.
- Wollrab, S., Diehl, S., and Roos, A. M. D. (2012). Simple rules describe bottom-up and top-down control in food webs with alternative energy pathways. *Ecology Letters*, 15(9):935–946.
- Woolley, S. N. C., Foster, S. D., Bax, N. J., Currie, J. C., Dunn, D. C., Hansen, C., Hill, N., O’Hara, T. D., Ovaskainen, O., Sayre, R., Vanhatalo, J. P., and Dunstan, P. K. (2020). Bioregions in marine environments: Combining biological and environmental data for management and scientific understanding. *BioScience*, 70(1):48–59.
- Wu, J., Wells, M. L., and Rember, R. (2011). Dissolved iron anomaly in the deep tropicalsubtropical pacific: Evidence for long-range transport of hydrothermal iron. *Geochimica et Cosmochimica Acta*, 75(2):460–468.
- Yesson, C., Clark, M. R., Taylor, M. L., and Rogers, A. D. (2011). The global distribution of seamounts based on 30 arc seconds bathymetry data. *Deep Sea Research Part I: Oceanographic Research Papers*, 58(4):442–453.
- Yücel, M., Gartman, A., Chan, C., and Luther, G. (2011). Hydrothermal vents as a kinetically stable source of iron-sulphide-bearing nanoparticles to the ocean. *Nature Geoscience*, 4:367–371.